11. STATUS OF HIGGS BOSON PHYSICS

Written November 2013 by M. Carena (Fermi National Accelerator Laboratory and the University of Chicago), C. Grojean (ICREA at IFAE, Universitat Autònoma de Barcelona), M. Kado (Laboratoire de l'Accélérateur Linéaire, LAL and CERN), and V. Sharma (University of California San Diego).

I. Introduction

The observation by ATLAS [1] and CMS [2] of a new boson with a mass of approximately 125 GeV decaying into $\gamma\gamma$, WW and ZZ bosons and the subsequent studies of the properties of this particle is a milestone in the understanding of the mechanism that breaks electroweak symmetry and generates the masses of the known elementary particles[1], one of the most fundamental problems in particle physics.

In the Standard Model, the mechanism of electroweak symmetry breaking (EWSB) [3] provides a general framework to keep untouched the structure of the gauge interactions at high energy and still generate the observed masses of the W and Z gauge bosons by means of charged and neutral Goldstone bosons that manifest themselves as the longitudinal components of the gauge bosons. The discovery of ATLAS and CMS now strongly suggests that these three Goldstone bosons combine with an extra (elementary) scalar boson to form a weak doublet.

This picture matches very well with the Standard Model (SM) [4] which describes the electroweak interactions by a gauge field theory invariant under the $\mathrm{SU}(2)_L \times \mathrm{U}(1)_Y$ symmetry group. In the SM, the EWSB mechanism posits a self-interacting complex

[1] In the case of neutrinos, it is possible that the EWSB mechanism plays only a partial role in generating the observed neutrino masses, with additional contributions at a higher scale via the so called see-saw mechanism.

doublet of scalar fields, and the renormalizable interactions are arranged such that the neutral component of the scalar doublet acquires a vacuum expectation value (VEV) $v \approx 246\,\text{GeV}$, which sets the scale of electroweak symmetry breaking.

Three massless Goldstone bosons are generated, which are absorbed to give masses to the W and Z gauge bosons. The remaining component of the complex doublet becomes the Higgs boson – a new fundamental scalar particle. The masses of all fermions are also a consequence of EWSB since the Higgs doublet is postulated to couple to the fermions through Yukawa interactions. However, the true structure behind the newly discovered boson, including the exact dynamics that triggers the Higgs VEV, and the corresponding ultraviolet completion is still unsolved.

Even if the discovered boson has weak couplings to all known SM degrees of freedom, it is not impossible that it is part of an extended symmetry structure or that it emerges from a light resonance of a strongly coupled sector. It needs to be established whether the Higgs boson is solitary or whether other states populate the EWSB sector.

Without the Higgs boson, the calculability of the SM would have been spoiled. In particular, perturbative unitarity [5,6] would be lost at high energies as the longitudinal W/Z boson scattering amplitude would grow as the centre-of-mass energy increases. Moreover, the radiative corrections to the self-energies of the gauge boson pertaining their longitudinal components would exhibit dangerous logarithmic divergences. With the discovery of the Higgs boson, it has been experimentally established that the SM is based on a gauge theory that could a priori be consistently extrapolated to the Planck scale. The Higgs boson must have couplings to W/Z gauge bosons and fermions precisely as those in the SM to maintain the consistency of the theory at high energies, hence, formally there is no need for new physics at the EW scale. However, the SM Higgs boson is a scalar particle, therefore without a symmetry to protect its mass, at the quantum level it has sensitivity to the physics in the ultraviolet. Quite generally, the Higgs mass parameter may be affected by the presence of heavy particles. Specifically, apart from terms proportional to m^2 itself, which are corrected by the Higgs field anomalous dimension, if there are fermion and boson particles with squared masses $m^2_{F,B}+\lambda^2_{F,B}\phi^2/2$,

$$m^2(Q) = m^2(\mu) + \delta m^2, \tag{11.1}$$

$$\delta m^2 = \sum_{B,F} g_{B,F}(-1)^{2S}\frac{\lambda^2_{B,F}m^2_{B,F}}{32\pi^2}\log(\frac{Q^2}{\mu^2}), \tag{11.2}$$

where $g_{B,F}$ and S correspond to the number of degrees of freedom and the spin of the boson and fermion particles, respectively. Therefore, particles that couple to the Higgs and have a large mass parameter $m^2_{B,F}$ would induce very large corrections to the Higgs mass parameter, demanding a large fine tuning to explain why m^2 remains small. Hence, in general, light scalars like the Higgs boson cannot naturally survive in the presence of heavy states at the grand-unification, string or Planck scales. This is known as the hierarchy or naturalness problem [7]. In the Standard Model where there are no other explicit mass parameter than the Higgs one, all corrections are proportional to the Higgs mass parameter itself.

There are two possible preferred solutions to the naturalness problem: one is based on a new fermion-boson symmetry in nature called supersymmetry (SUSY) [8–10]. This is a weakly coupled approach to EWSB, and in this case, the Higgs boson remains elementary and the corrections to its mass are cut at the scale at which SUSY is broken and remain insensitive to the details of the physics at higher scales. These theories predict at least one charged and three neutral Higgs particles[2] [12], and one of the neutral Higgs bosons, most often the lightest *CP*-even Higgs, has properties that resemble those of the SM Higgs boson. It will be referred to as a SM-like Higgs boson, meaning that its VEV is predominantly responsible for EWSB, and hence has SM-like couplings to the W and Z gauge bosons.

The other approach invokes the existence of strong interactions at a scale of the order of a TeV or above and induces strong breaking of the electroweak symmetry [13]. In the original incarnation of this second approach, dubbed technicolor, the strong interactions themselves trigger EWSB without the need of a Higgs boson. Another possibility, more compatible with the ATLAS and CMS discovery, is that the strong interactions produce 4 light resonances identified with the Higgs doublet and EWSB proceeds through vacuum misalignment [14].

Both approaches can have important effects on the phenomenology of the Higgs boson associated with EWSB. Also, in each case the Higgs role in unitarization is shared by other particles: additional Higgs bosons in supersymmetry, or new particles in the strong sector.

A third option has also been considered in the literature. It is also a variation of technicolor or Higgsless models [13,15]. In light of the Higgs boson discovery these models are ruled out. However, there still exists the possibility that the Higgs discovered at the LHC is in fact the Goldstone boson of the spontaneous breaking of scale invariance at a scale f [16,17]. Given the good agreement of the coupling measurements with the SM predictions, this scenario now requires rather involved model-building engineering.

The naturalness problem has been the prime argument for new physics at the TeV scale. But the absence of any direct signal of new dynamics and the apparent agreement of the Higgs couplings with the SM predictions, together with the strong bounds inherited from precision electroweak and flavor data leaves open the possibility that the Higgs boson may very well be elementary, weakly coupled and solitary till the Planck scale. Such a scenario, would force physicists to rethink the basic concepts of high energy physics.

In this review, some of the most interesting models proposed in the above two categories will be discussed in detail. Extensions of the SM Higgs sector without low-energy supersymmetry will also be discussed. These type of models do not address the naturalness problem in a specific manner, but provide grounds to explore new Higgs boson signals in a more model-independent way, with different types of coupling structure

[2] Except in exotic SUSY scenarios where the Higgs boson is identified as a sneutrino, the scalar partner of a neutrino [11], in which case the gauge anomalies cancel without the need for a second Higgs doublet

to fermions and gauge bosons. Extended Higgs sectors are usually quite restricted by experimental constraints from precision electroweak measurements as well as constraints from flavor changing neutral and charged current effects.

Section II is a review of the Higgs boson of the Standard Model, discussing its properties and the production mechanisms and decay rates. In Section III, the SM Higgs boson analysis channels are described. In Section IV, a general theoretical framework to describe the deviations of the Higgs couplings from the SM predictions is introduced and the experimental measurements of these Higgs couplings is reviewed together with the analysis establishing the spin and *CP*-properties of the Higgs boson. Section V presents, in detail, some of the most interesting models proposed for Higgs extensions of the SM and considers their experimental signatures. Section VI provides a brief outlook.

II. The Standard Model and the Mechanism of Electroweak Symmetry Breaking

As mentioned above, in the SM [4], the mechanism of electroweak symmetry breaking [3] is responsible for generating mass for the W and Z gauge bosons rendering the weak interactions short range. The SM scalar potential reads:

$$V(\Phi) = m^2\Phi^\dagger\Phi + \lambda(\Phi^\dagger\Phi)^2 \tag{11.3}$$

with the Higgs field Φ being a self-interacting SU(2) complex doublet (four real degrees of freedom) with weak hypercharge $Y{=}1$ (the hypercharge is normalized such that $Q = T_{3L} + Y/2$):

$$\Phi = \frac{1}{\sqrt{2}}\begin{pmatrix}\sqrt{2}\phi^+\\ \phi^0 + ia^0\end{pmatrix}. \tag{11.4}$$

$V(\Phi)$ is the most general renormalizable scalar potential and if the quadratic term is negative the neutral component of the scalar doublet acquires a non-zero vacuum expectation value (VEV)

$$\langle\Phi\rangle = \frac{1}{\sqrt{2}}\begin{pmatrix}0\\ v\end{pmatrix}, \tag{11.5}$$

defining $\phi^0 = H + v$, inducing the spontaneous breaking of the SM gauge symmetry $\mathrm{SU(3)}_C \times \mathrm{SU(2)}_L \times \mathrm{U(1)}_Y$ into $\mathrm{SU(3)}_C \times \mathrm{U(1)}_{\mathrm{em}}$. The global minimum of the theory defines the ground state, and spontaneous symmetry breaking implies that there is a symmetry of the system (Lagrangian) that is not respected by the ground state. The Higgs field permeates the entire universe and through its self-interactions can cause spontaneous electroweak symmetry-breaking (EWSB) in the vacuum. From the 4 generators of the $\mathrm{SU(2)}_L \times \mathrm{U(1)}_Y$ gauge group, three are spontaneously broken, implying that they lead to non-trivial transformations of the ground state and indicate the existence of three massless Goldstone bosons identified with three of the four Higgs field degrees of freedom. The Higgs field couples to the W_μ and B_μ gauge fields associated with the $\mathrm{SU(2)}_L \times \mathrm{U(1)}_Y$ local symmetry, respectively, through the covariant derivative, $D_\mu\Phi = (\partial_\mu + ig\sigma^a W^a_\mu/2 + ig'YB_\mu/2)\Phi$ (g and g' are the SU(2) and U(1) gauge couplings

and $\sigma^a, a = 1, 2, 3$ are the usual Pauli matrices) appearing in the kinetic term of the Higgs Lagrangian

$$\mathcal{L}_{\rm Higgs} = (D_\mu \Phi)^\dagger (D^\mu \Phi) - V(\Phi)\,. \tag{11.6}$$

As a result, the neutral and the two charged massless Goldstone degrees of freedom mix with the gauge fields corresponding to the broken generators of $\mathrm{SU}(2)_L \times \mathrm{U}(1)_Y$ and become the longitudinal components of the Z and W physical gauge bosons, respectively. The fourth generator remains unbroken since it is the one associated to the conserved $\mathrm{U}(1)_{\rm em}$ gauge symmetry, and its corresponding gauge field, the photon, remains massless. Similarly the eight color gauge bosons, the gluons, corresponding to the conserved $\mathrm{SU}(3)_C$ gauge symmetry with 8 unbroken generators, also remain massless. Hence, from the initial four degrees of freedom of the Higgs field, two are absorbed by the $W^\pm$ gauge bosons and one by the Z gauge boson that become massive:

$$M_W^2 = \frac{g^2 v^2}{4} \quad M_Z^2 = \frac{(g'^2 + g^2) v^2}{4}. \tag{11.7}$$

There is one remaining degree of freedom, H, that is the physical Higgs boson — a new scalar particle. The Higgs boson is neutral under the electromagnetic interactions and transforms as a singlet under $\mathrm{SU}(3)_C$ and hence does not couple at tree level to the massless photons and gluons.

The fermions of the SM acquire mass through a new type of renormalizable interactions between the Higgs field and the fermions: the Yukawa interactions,

$$\mathcal{L}_{\rm Yukawa} = -\hat{h}_{d_{ij}} \bar{q}_{L_i} \Phi\, d_{R_j} - \hat{h}_{u_{ij}} \bar{q}_{L_i} \tilde{\Phi} u_{R_j} - \hat{h}_{l_{ij}} \bar{l}_{L_i} \Phi\, e_{R_j} + h.c., \tag{11.8}$$

that respect the symmetries of the SM but generate fermion masses once EWSB occurs. In the above, $\tilde{\Phi} = i\sigma_2 \Phi^*$ and q_L (l_L) and u_R, d_R (e_R) are the quark (lepton) $\mathrm{SU}(2)_L$ doublets and singlets, respectively, while each term is parametrized by a 3×3 matrix in family space. The mass term for neutrinos is omitted, but could be added in an analogous manner to the up type quarks when right-handed neutrinos are supplementing the SM particle content. Once the Higgs acquires a VEV, and after rotation to the fermion mass eigenstate basis that also diagonalize the Higgs-fermion interactions, $\hat{h}_{f_{ij}} \to h_f \mathbf{1_{3\times 3}}$, all fermions acquire a mass given by $m_f = h_f v/\sqrt{2}$. It should be noted that the EWSB mechanism provides no additional insight on possible underlying reasons for the large variety of masses of the fermions, often referred to as the flavor hierarchy. The fermion masses, accounting for a large number of the free parameters of the SM are simply translated in terms of Yukawa couplings h_f.

II.1. The SM Higgs boson mass, couplings and quantum numbers

The SM Higgs boson is a *CP*-even scalar of spin 0. Its mass is given by $m_H = \sqrt{2\lambda}\, v$, where λ is the Higgs self-coupling parameter in $V(\Phi)$. The expectation value of the Higgs field, $v = (\sqrt{2} G_F)^{-1/2} \approx 246\,\mathrm{GeV}$, is fixed by the Fermi coupling G_F, which is determined with a precision of 0.6 ppm from muon decay measurements [18]. The quartic coupling

λ, instead, is a free parameter in the SM, and hence there is, a priori, no prediction for the Higgs mass. Moreover the sign of the mass parameter $m^2 = -\lambda v^2$ is crucial for the EW symmetry breaking to take place, but it is not specified in the SM. Therefore, if the newly discovered particle is indeed the SM Higgs boson with $m_H \simeq$125 GeV, it implies that $\lambda \simeq 0.13$ and $|m| \simeq 88.8$ GeV. It is interesting to observe that in the SM one needs to assume that the mass term in the potential is negative in order to trigger EWSB. In other theories beyond the SM (BSM), such as supersymmetry, the analogue of the Higgs mass parameter can be made negative dynamically.

The Higgs boson couplings to the fundamental particles are set by their masses. This is a new type of interaction, very weak for ordinary particles, such as up and down quarks, and electrons, but strong for heavy particles such as the W and Z bosons and the top quark. More precisely, the SM Higgs couplings to fundamental fermions are linearly proportional to the fermion masses, whereas the couplings to bosons are proportional to the square of the boson masses. The SM Higgs boson couplings to gauge bosons, Higgs bosons and fermions are summarized in the following Lagrangian:

$$\begin{aligned}\mathcal{L} = &- g_{Hff}\bar{f}fH + \frac{g_{HHH}}{6}H^3 + \frac{g_{HHHH}}{24}H^4 \\ &+ \delta_V V_\mu V^\mu \left(g_{HVV}H + \frac{g_{HHVV}}{2}H^2\right)\end{aligned} \tag{11.9}$$

with

$$g_{Hf\bar{f}} = \frac{m_f}{v}, \quad g_{HVV} = \frac{2m_V^2}{v}, \quad g_{HHVV} = \frac{2m_V^2}{v^2} \tag{11.10}$$

$$g_{HHH} = \frac{3m_H^2}{v}, \quad g_{HHHH} = \frac{3m_H^2}{v^2} \tag{11.11}$$

where $V = \mathrm{W}^\pm$ or Z and $\delta_W = 1, \delta_Z = 1/2$. As a result, the dominant mechanisms for Higgs boson production and decay involve the coupling of H to W, Z and/or the third generation quarks and leptons. The Higgs boson coupling to gluons [19,20], is induced at leading order by a one-loop graph in which H couples to a virtual $t\bar{t}$ pair. Likewise, the Higgs boson coupling to photons is also generated via loops, although in this case the one-loop graph with a virtual W^+W^- pair provides the dominant contribution [12] and the one involving a virtual $t\bar{t}$ pair is subdominant.

II.2. The SM custodial symmetry

The SM Higgs Lagrangian, $\mathcal{L}_{\text{Higgs}}$ of Eq. (11.6), is, by construction, $\mathrm{SU}(2)_L \times \mathrm{U}(1)_Y$ gauge invariant, but it also has an approximate global symmetry. In the limit $g' \to 0$ and $h_f \to 0$, the Higgs sector has a global $\mathrm{SU}(2)_R$ symmetry, and hence in such limit it is invariant under a global $\mathrm{SU}(2)_L \times \mathrm{SU}(2)_R$ symmetry, with $\mathrm{SU}(2)_L$ just being the global variant of the SM chiral gauge symmetry. This symmetry is preserved for non-vanishing Yukawa couplings, provided $h_u = h_d$. Once the Higgs acquires a VEV, both the $\mathrm{SU}(2)_L$ and $\mathrm{SU}(2)_R$ symmetry groups are broken but the subgroup $\mathrm{SU}(2)_{L+R}$ remains unbroken and is the subgroup that defines the custodial symmetry of the SM [21].

In the limit $g' \to 0$ ($\sin^2\theta_W \to 0$), the W and Z gauge bosons have equal mass and form a triplet of the $SU(2)_{L+R}$ unbroken global symmetry. The ρ parameter characterizes the breaking of the custodial symmetry, which manifest itself in the equality of the three tree-level SU(2)-gauge boson masses, even when $g' \neq 0$. Using the expressions for the W and Z gauge boson masses in term of the gauge couplings, one obtains

$$\frac{M_W^2}{M_Z^2} = \frac{g^2}{g'^2 + g^2} = \cos^2\theta_W \quad \text{or} \quad \rho = \frac{M_W^2}{M_Z^2 \cos^2\theta_W} = 1 \tag{11.12}$$

at tree level. The custodial symmetry protects the above relation between the W and Z masses under radiative corrections. All corrections to the ρ parameter are therefore proportional to terms that break the custodial symmetry. For instance, radiative corrections involving the Higgs are proportional to g'^2. Since $m_t \neq m_b$, there are also relevant radiative corrections generated by massive fermions. They are proportional to $m_t^2 + m_b^2 - 2(m_t^2 m_b^2)\,\log(m_t^2/m_b^2)/(m_t^2 - m_b^2)$ [22].

One can conceive BSM theories in which the Higgs is a pseudo Nambu–Goldstone boson of a strongly interacting sector [23], and/or where there are additional degrees of freedom that may contribute to the W and Z mass via virtual loops, but in as much as the electroweak sector has a manifest custodial symmetry, the theory is protected from large radiative corrections. Precision measurement of the electroweak observables are powerful in constraining such large radiative corrections. The custodial isospin symmetry is a powerful probe of BSM physics. For a pedagogical discussion, see Ref. [24].

II.3. Stability of the Higgs potential

The discovery of a scalar particle with mass $m_H \approx 125\,\text{GeV}$ has far reaching consequences within the SM framework. Such a low value of the Higgs boson mass is in perfect agreement with the upper bound on the Higgs boson mass from perturbative unitarity constraints [5,6], thereby rendering the SM a consistent, calculable theory. Moreover, the precise value of m_H determines the value of the quartic coupling λ at the electroweak scale and makes it possible to investigate its behavior up to high energy scales. A larger value of m_H would have implied that the Higgs self-coupling would become non-perturbative at some scale Λ that could be well below the Planck scale. From the measured values of the Higgs mass, the top quark mass, the W and Z boson masses, and the strong gauge coupling, all within their experimental uncertainties, it follows that, similar to the SM gauge and Yukawa couplings, the Higgs quartic coupling remains perturbative all the way up to M_{Planck} [25].

The recently measured Higgs mass, however, generates an EW Higgs potential in which the vacuum state is at the edge between being stable and metastable. Indeed, for $m_H = 125.7 \pm 0.3\,\text{GeV}$ and allowing all relevant SM observables to fluctuate within their experimental and theoretical uncertainties, the metastability condition seems to be favored [26]. The high energy evolution of λ shows that it becomes negative at energies $\Lambda = \mathcal{O}(10^{10} - 10^{12})\,\text{GeV}$, with a broader range if a 3σ fluctuation in the top quark mass value is allowed, as shown in Fig. 11.1 [26]. When this occurs, the SM Higgs potential develops an instability and the long term existence of the EW vacuum is challenged. This

behavior may call for new physics at an intermediate scale before the instability develops, i.e., below M_{Planck} or, otherwise, the electroweak vacuum remains metastable [27]. Therefore, within the SM framework, the relevant question is related to the lifetime of the EW metastable vacuum that is determined by the rate of quantum tunneling from this vacuum into the true vacuum of the theory. The running of the Higgs self coupling slows down at high energies with a cancellation of its β-function at energies just one to two orders of magnitude below the Planck scale [28,26]. This slow evolution of the quartic coupling is responsible for saving the EW vacuum from premature collapse allowing it to survive much longer times than those relevant from astrophysical considerations. It might help the Higgs boson to play the role of an inflaton [30] (see, however, Ref. [31] and references therein for potential issues with this Higgs-as-inflaton idea).

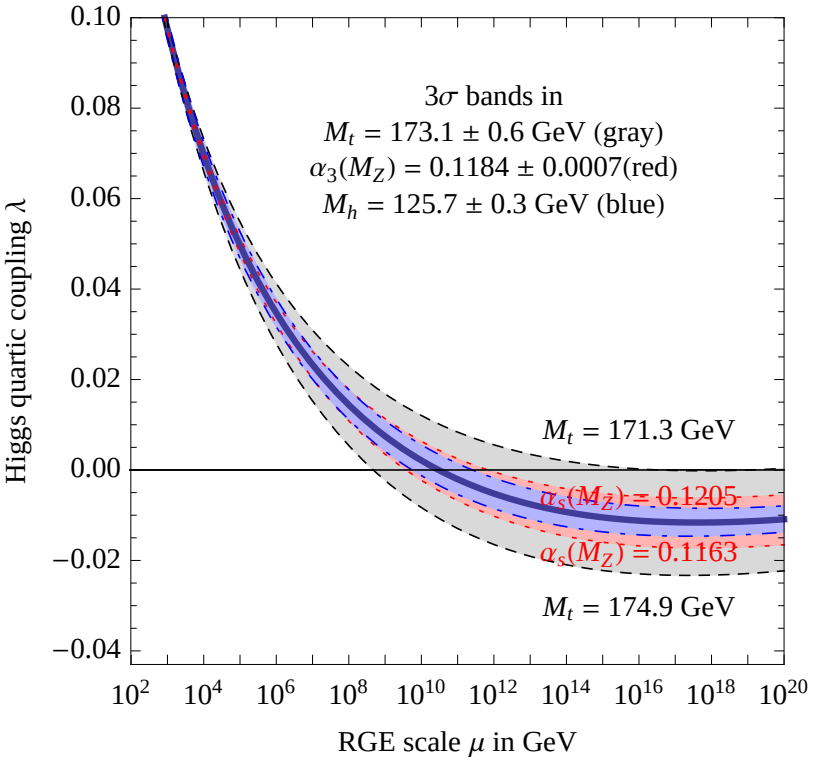

Figure 11.1: Renormalization group evolution of the Higgs self coupling λ, for the central values of $m_H = 125.7\,\text{GeV}$, $m_t = 173.4\,\text{GeV}$ and $\alpha_S(M_Z) = 0.1184$ (solid curve), and variation of these central values by $\pm$ 3 σ for the blue, gray and red, dashed curves, respectively. For negative values of λ, the lifetime of the SM vacuum due to quantum tunneling at zero temperature is longer than the age of the universe. From Ref. [26].

The peculiar behavior of the quartic coupling does not exclude the possibility that the SM might be all what is there up to the quantum gravity scale [29] or it could be the result of a special dynamics or a new symmetry at high energies, such as supersymmetry

with possible flat directions. Still, physics at lower energies is desirable to solve other mysteries of the universe such as dark matter or the matter-antimatter asymmetry. The Higgs boson discovery at the LHC leaves all these options open.

II.4. Higgs production and decay mechanisms

Reviews of the SM Higgs boson's properties and phenomenology, with an emphasis on the impact of loop corrections to the Higgs boson decay rates and cross sections, can be found in Refs. [32–38].

II.4.1. Production mechanisms at hadron colliders

The main production mechanisms at the Tevatron and the LHC are gluon fusion, weak-boson fusion, associated production with a gauge boson and associated production with top quarks. Figure 11.2 depicts representative diagrams for these dominant Higgs production processes.

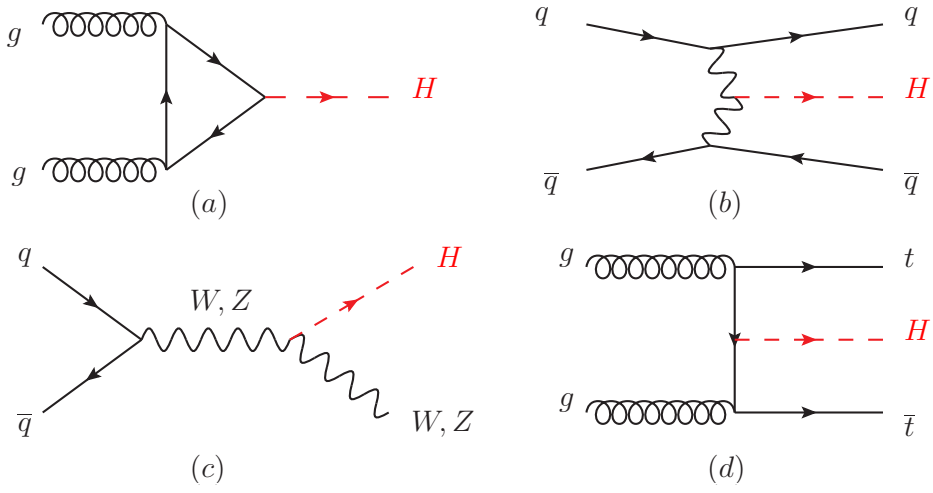

Figure 11.2: Generic Feynman diagrams contributing to the Higgs production in (a) gluon fusion, (b) weak-boson fusion, (c) Higgs-strahlung (or associated production with a gauge boson) and (d) associated production with top quarks.

The cross sections for the production of a SM Higgs boson as a function of $\sqrt{s}$, the center of mass energy, for pp collisions, including bands indicating the theoretical uncertainties, are summarized in Fig. 11.3 [39]. A detailed discussion, including uncertainties in the theoretical calculations due to missing higher order effects and experimental uncertainties on the determination of SM parameters involved in the calculations can be found in Refs. [36–38]. These references also contain state of the art discussions on the impact of PDF's uncertainties, QCD scale uncertainties and uncertainties due to different matching procedures when including higher order corrections matched to parton shower simulations as well as uncertainties due to hadronization and parton-shower events.

Table 11.1, from Refs. [36,38], summarizes the Higgs boson production cross sections and relative uncertainties for a Higgs mass of 125 GeV, for $\sqrt{s} = 7$, 8 and 14 TeV.

Table 11.1: The SM Higgs boson production cross sections or $m_H = 125\,\text{GeV}$ in pp collisions, as a function of the center of mass energy, $\sqrt{s}$. The predictions for the LHC energies are taken from Refs. [36,38], the ones for the Tevatron energy are from Ref. [40].

$\sqrt{s}$ (TeV)	Production cross section (in pb) for $m_H = 125\,\text{GeV}$					
	ggF	VBF	WH	ZH	$t\bar{t}H$	total
.96	$0.95^{+17\%}_{-17\%}$	$0.065^{+8\%}_{-7\%}$	$0.13^{+8\%}_{-8\%}$	$0.079^{+8\%}_{-8\%}$	$0.004^{+10\%}_{-10\%}$	1.23
	$15.1^{+15\%}_{-15\%}$	$1.22^{+3\%}_{-2\%}$	$0.58^{+4\%}_{-4\%}$	$0.33^{+6\%}_{-6\%}$	$0.09^{+12\%}_{-18\%}$	17.4
	$19.3^{+15\%}_{-15\%}$	$1.58^{+3\%}_{-2\%}$	$0.70^{+4\%}_{-5\%}$	$0.41^{+6\%}_{-6\%}$	$0.13^{+12\%}_{-18\%}$	22.1
4	$49.8^{+20\%}_{-15\%}$	$4.18^{+3\%}_{-3\%}$	$1.50^{+4\%}_{-4\%}$	$0.88^{+6\%}_{-5\%}$	$0.61^{+15\%}_{-28\%}$	57.0

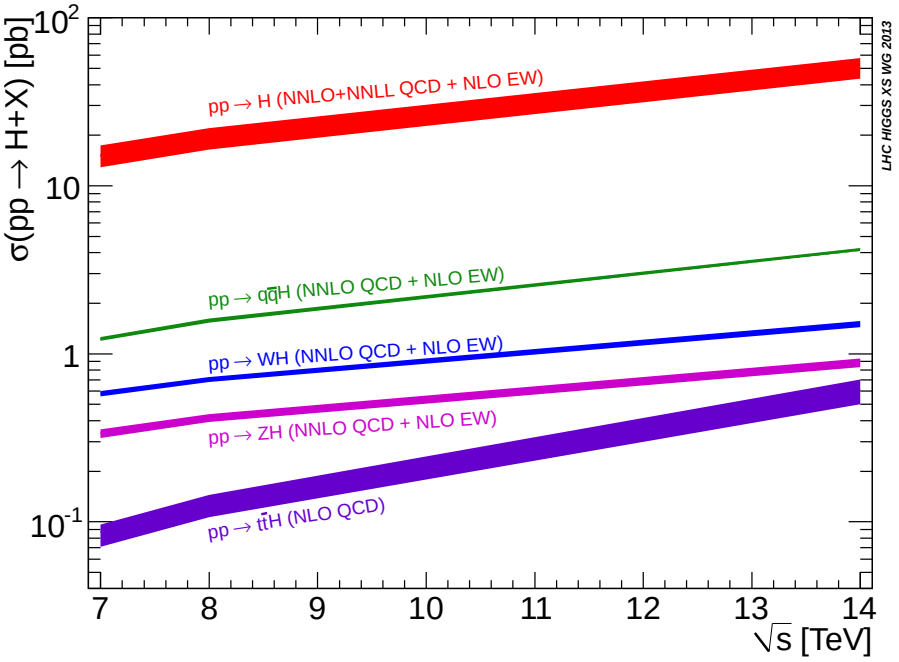

Figure 11.3: The SM Higgs boson production cross sections as a function of the center of mass energy, $\sqrt{s}$, for pp collisions. The theoretical uncertainties [39] are indicated as a band.

(i) Gluon fusion production mechanism

At high-energy hadron colliders, the Higgs boson production mechanism with the largest cross section is the gluon-fusion process, $gg \to H + X$, mediated by the exchange of a virtual, heavy top quark [41]. Contributions from lighter quarks propagating in the loop are suppressed proportional to m_q^2. QCD radiative corrections to the gluon-fusion

process are very important and have been studied in detail. Including the full dependence on the quark and Higgs boson masses, the cross section has been calculated at the next-to-leading order (NLO) in α_s [42,43]. To a very good approximation, the leading top-quark contribution can be evaluated in the limit $m_t \to \infty$ by matching the Standard Model to an effective theory. The gluon-fusion amplitude is then evaluated from an effective Lagrangian containing a local $HG^a_{\mu\nu}G^{a\,\mu\nu}$ operator [19,20]. In this approximation the cross section is known at NLO [44] and at next-to-next-to-leading order (NNLO) [45], and a strong effort is under way to extend the calculations to NNNLO. The validity of the large top-quark mass approximation in NNLO calculations has been established at the percent level by means of approximate calculations of the m_t dependence based on asymptotic expansions [46].

The NLO QCD corrections increase the leading-order prediction for the cross section by about 80%, and the NNLO corrections further enhance the cross section by approximately 20% (at $\mu_f = \mu_r = m_H$). The convergence of the perturbation series can be improved by lowering the factorization and renormalization scales. Electroweak radiative corrections have been computed at NLO and increase the cross section by about 5% for $m_H \simeq 125\,\text{GeV}$ [47]. Mixed QCD-electroweak corrections of $O(\alpha\alpha_s)$ have been calculated in Ref. [48].

The NLO and NNLO fixed-order QCD predictions for the gluon-fusion cross section have been improved by resumming the soft-gluon contributions to the cross section at next-to-next-to-leading logarithmic (NNLL) and partial NNNLL accuracy [49]. The convergence of the perturbation series can be improved significantly by systematically resumming a subset of enhanced corrections contained in the time-like gluon form factor, using methods of soft-collinear effective theory [50]. Up-to-date predictions for the gluon-fusion cross section for different Higgs boson masses and LHC energies, and including detailed error budgets, have been obtained by combining the NNLO fixed-order QCD results with soft-gluon resummation at NNLL or NNNLL accuracy and two-loop electroweak corrections, and using the most recent sets of parton distribution functions [48,51].

Besides considering the inclusive Higgs boson production cross section at the LHC, it is important to study differential distributions in order to probe the properties of the Higgs boson in a detailed way. A more exclusive account of Higgs production is also required because experimental analyses often impose cuts on the final states in order to improve the signal-to-background ratio. To this end, it is useful to define benchmark cuts and compare the differential distributions obtained at various levels of theoretical accuracy (i.e., at NLO or NNLO) and with Monte Carlo generators. Many search modes for the Higgs boson are carried out by separating the events according to the number of jets or the transverse momentum and rapidity of the Higgs boson. For $p_T < 30\,\text{GeV}$, predictions for the transverse-momentum distribution can only be trusted after large logarithms of the form $\alpha_s^n \ln^{2n-1}(m_H/p_T)$ have been resummed to all orders in perturbation theory [52]. This has been accomplished with NNLL accuracy [53], and the results have been matched onto the fixed-order prediction at NNLO [54]. Electroweak corrections, and in particular the effect of the non-zero b-quark mass, on the p_T spectrum have been studied in Refs. [55,56]. Recently, there has been much activity in computing Higgs plus

jet(s) production processes at NLO (see e.g. Refs. [57] and [58] for associated production with one and two jets, respectively), and even at NNLO [59]. In addition, efforts to improve the calculation of the Higgs production cross section with a jet veto (the "0-jet bin") by resumming large logarithms of the form $\alpha_s^n \ln^{2n-1}(m_H/p_T^{\rm veto})$ at NNLL order and beyond [60] have been made. Accurate predictions for the jet-veto cross section are required, e.g., to suppress the background in the $H \to WW$ channel.

(ii) Vector boson fusion production mechanism

The SM Higgs production mode with the second-largest cross section at the LHC is the vector boson fusion (VBF). At the Tevatron, VBF also occurs, but for $m_H = 125\,\text{GeV}$ exhibits a smaller cross section than Higgs production in association with a W or Z boson. Higgs production via VBF, $qq \to qqH$, proceeds by the scattering of two (anti-)quarks, mediated by t- or u-channel exchange of a W or Z boson, with the Higgs boson radiated off the weak-boson propagator. The scattered quarks give rise to two hard jets in the forward and backward regions of the detector.[3] Because of the color-singlet nature of the weak-gauge boson exchange, gluon radiation from the central-rapidity regions is strongly suppressed [63]. These characteristic features of VBF processes can be exploited to distinguish them from a priori overwhelming QCD backgrounds, including gluon-fusion induced Higgs + 2 jet production, and from s-channel WH or ZH production with a hadronically decaying weak boson. After the application of specific selection cuts, the VBF channel provides a particularly clean environment not only for Higgs searches but also for the determination of Higgs boson couplings at the LHC [64].

Computations for total cross sections and differential distributions to Higgs production via VBF including NLO QCD and EW corrections have been presented in Refs. [33,65] and are available in the form of flexible parton-level Monte-Carlo generators. Parton-shower effects have been considered in Ref. [66]. Parts of the NNLO QCD corrections have been presented in Refs. [67,68]. The NNLO QCD corrections of Ref. [67] reduce the residual scale uncertainties on the inclusive cross section to approximately 2%. The uncertainties due to parton distributions are estimated to be at the same level.

(iii) WH and ZH associated production mechanism

The next most relevant Higgs boson production mechanisms after gluon fusion and VBF at the LHC, and the most relevant ones after gluon fusion at the Tevatron, are associated production with W and Z gauge bosons. The cross sections for the associated production processes, $pp \to VH + X$, with $V = W^\pm, Z$ receive contributions at NLO given by NLO QCD corrections to the Drell–Yan cross section [69,70,71] and from NLO EW corrections. The latter, unlike the QCD corrections, do not respect the factorization into Drell–Yan production since there are irreducible box contributions already at one loop [72]. At NNLO, the Drell-Yan-like corrections to WH production also give the bulk of the corrections to ZH production [73]. For ZH production there are, however, gluon-gluon induced contributions that do not involve a virtual Z gauge boson but are

[3] The production of a Higgs boson with two additional jets has been computed in Refs. [61] and [62].

such that the Z gauge boson and H boson couple to gluons via top quark loops [74]. In addition, WH and ZH production receive non Drell–Yan-like corrections in the $q\bar{q}'$ and $q\overline{q}$ initiated channels, respectively, at the NNLO level, where the Higgs is radiated off top quark loops [75]. The full QCD corrections up to NNLO order, the NLO EW corrections and the NLO corrections to the gluon-gluon channel are available in a public program [76].

As neither the Higgs boson nor the weak gauge bosons are stable particles, their decays also have to be taken into account. Providing full kinematical information for the decay products can furthermore help in the suppression of large QCD backgrounds. Differential distributions for the processes $pp \to WH \to \nu_\ell \ell H$ and $pp \to ZH \to \ell^+\ell^- H \to \nu_\ell \bar{\nu}_\ell H$, including NLO QCD and EW corrections, have been presented in Ref. [77]. The NNLO QCD corrections to differential observables for WH production at the LHC, including the leptonic decays of the W boson and the decay of the Higgs boson into a $b\bar{b}$ pair, are presented in Ref. [78]. The WH and ZH production modes, together with Higgs production in association with a top quark pair, provide a relatively clean environment for studying the decay of the Higgs boson into bottom quarks.

(iv) Higgs production in association with $t\bar{t}$

Higgs radiation off top quarks, $pp \to Ht\bar{t}$, can provide important information on the the top-Higgs Yukawa coupling and gives access to the Higgs decay into bottom quarks. The LO cross section for this production process was computed in Ref. [79]. Later, the NLO QCD corrections [80] were evaluated yielding a moderate increase in the total cross section of at most 20%, but reducing significantly the scale dependence of the inclusive cross section. The total theoretical errors, estimated by combining the uncertainties from factorization and renormalization scales, strong gauge coupling, and parton distributions, amount to 10–15% of the corresponding inclusive cross section. Interfaces between NLO QCD calculations for $Ht\bar{t}$ production with parton-shower Monte Carlo programs have been provided in Ref. [81]. These programs provide the most flexible tools to date for the computation of differential distributions, including experimental selection cuts and vetoes on the final-state particles and their decay products.

(v) Subleading Higgs production mechanisms at the LHC

The Higgs boson production in association with bottom quarks is known at NNLO in the case of five quark flavors [82–84]. The coupling of the Higgs boson to a b quark is suppressed in the SM by the bottom quark mass over the Higgs VEV, m_b/v, implying that associated production of a SM Higgs boson with b quarks is very small at the LHC. In a two Higgs doublet model or a supersymmetric model, which will be discussed in Section V, this coupling is proportional to the ratio of neutral Higgs boson vacuum expectation values, $\tan\beta$, and can be significantly enhanced for large values of this ratio.

II.4.2. Production mechanisms at e^+e^- colliders

The main Higgs boson production cross sections at an e^+e^- collider are the Higgs-strahlung process $e^+e^- \to ZH$ [6,19,85], and the WW fusion process [86] $e^+e^- \to \bar{\nu}_e\nu_e W^*W^* \to \bar{\nu}_e\nu_e H$. As the center-of-mass energy $\sqrt{s}$ is increased, the cross-section for the Higgs-strahlung process decreases as s^{-1} and is dominant at low energies,

while the cross-section for the WW fusion process grows as $\ln(s/m_H^2)$ and dominates at high energies [87–89]. The ZZ fusion mechanism, $e^+e^- \to e^+e^-Z^*Z^* \to e^+e^-H$, also contributes to Higgs boson production, with a cross-section suppressed by an order of magnitude with respect to that of WW fusion. The process $e^+e^- \to t\bar{t}H$ [90,91] becomes relevant for large $\sqrt{s} \geq 500\,\text{GeV}$. For a more detailed discussion of Higgs production properties at lepton colliders see for example Refs. [34,35,92,93] and references therein.

II.4.3. SM Higgs branching ratios and total width

For the understanding and interpretation of the experimental results, the computation of all relevant Higgs decay widths is essential, including an estimate of their uncertainties and, when appropriate, the effects of Higgs decays into off-shell particles with successive decays into lighter SM ones. A Higgs mass of about 125 GeV provides an excellent opportunity to explore the Higgs couplings to many SM particles. In particular the dominant decay modes are $H \to b\bar{b}$ and $H \to WW^*$, followed by $H \to gg$, $H \to \tau^+\tau^-$, $H \to c\bar{c}$ and $H \to ZZ^*$. With much smaller rates follow the Higgs decays into $H \to \gamma\gamma$, $H \to \gamma Z$ and $H \to \mu^+\mu^-$. Since the decays into gluons, diphotons and $Z\gamma$ are loop induced, they provide indirect information on the Higgs to WW, ZZ and $t\bar{t}$ couplings in different combinations. The Higgs decays into WW^* and ZZ^* effectively need to be studied considering the decays of the gauge bosons into four fermions, i.e., the leptonic, semi-leptonic and full hadronic final states. The uncertainties in the branching ratios include the missing higher order corrections in the theoretical calculations as well as the errors in the SM input parameters, in particular fermions masses and gauge couplings, involved in the calculations. In the following the state of the art of the theoretical calculations will be discussed and the reader is referred to Refs. [36,37,94] for further details.

The evaluation of radiative corrections of fermionic decays of the SM Higgs at different levels of accuracy are implemented in HDECAY [95]. The decays $H \to b\bar{b}$ and $H \to c\bar{c}$ are computed including the complete massless QCD corrections up to and including NNNNLO, with a corresponding scale dependence of about 0.1% [96]. Both the electroweak corrections to $H \to b\bar{b}$, $c\bar{c}$ as well as $H \to \tau^+\tau^-$ are known at NLO [97] providing predictions with an overall accuracy of about 1-2% for $m_H \simeq 125\,\text{GeV}$.

The loop induced decays of the SM Higgs are known at NLO and partially beyond that approximation. For $H \to gg$, the QCD corrections are known up to NNNLO in the limit of heavy top quarks [98,43] and the uncertainty from the scale dependence is about 3%. For the $H \to \gamma\gamma$, the full NLO QCD corrections are available [43,99]. The NLO electroweak corrections to $H \to gg$ and $H \to \gamma\gamma$ have been computed in Ref. [100]. Missing higher orders corrections are estimated to be below 1%. All these corrections are implemented in HDECAY. In addition the contribution of the $H \to \gamma e^+e^-$ decay via virtual photon conversion has been computed in Ref. [101]. The partial decay width $H \to Z\gamma$ is only implemented at LO in HDECAY, including the virtual W, top, bottom, and τ loop contributions. The QCD corrections have been calculated and are at the percent level [102], The theoretical uncertainty due to unknown electroweak corrections is estimated to be less than 5%, an accuracy that will be hard to achieve in measurements at the LHC.

The decays $H \to WW/ZZ \to 4f$ can be simulated with the Monte-Carlo generator of Ref. [103] that includes complete NLO QCD and EW corrections for Higgs decays into any possible four-fermion final state. All calculations are consistently performed with off-shell gauge bosons, without any on-shell approximation. For the SM Higgs boson the missing higher-order corrections are estimated to roughly 0.5%. Such uncertainties will have to be combined with the parametric uncertainties, in particular those associated to the bottom quark mass and the strong gauge coupling, to arrive at the full theory uncertainties. A detailed treatment of the differential distributions for a Higgs decay with four charged leptons in the final state is presented in Refs. [104,38].

The branching ratios for the most relevant decay modes of the SM Higgs boson as functions of m_H, including the most recent theoretical uncertainties, are shown in Fig. 11.4 and listed for $m_H = 125\,\text{GeV}$ in Table 11.2. The total width of a 125 GeV SM Higgs boson is $\Gamma_H = 4.07 \times 10^{-3}\,\text{GeV}$, with a relative uncertainty of $^{+4.0\%}_{-3.9\%}$. Further details of these calculations can be found in Refs. [94,105] and in the reviews [33–38].

Table 11.2: The branching ratios and the relative uncertainty [38] for a SM Higgs boson with $m_H = 125\,\text{GeV}$.

Decay channel	Branching ratio	Rel. uncertainty
$H \to \gamma\gamma$	2.28×10^{-3}	$^{+5.0\%}_{-4.9\%}$
$H \to ZZ$	2.64×10^{-2}	$^{+4.3\%}_{-4.1\%}$
$H \to W^+W^-$	2.15×10^{-1}	$^{+4.3\%}_{-4.2\%}$
$H \to \tau^+\tau^-$	6.32×10^{-2}	$^{+5.7\%}_{-5.7\%}$
$H \to b\bar{b}$	5.77×10^{-1}	$^{+3.2\%}_{-3.3\%}$
$H \to Z\gamma$	1.54×10^{-3}	$^{+9.0\%}_{-8.9\%}$
$H \to \mu^+\mu^-$	2.19×10^{-4}	$^{+6.0\%}_{-5.9\%}$

III. The discovery of a Higgs boson

Indirect experimental bounds on the SM Higgs boson mass are obtained from a global fit of precision electroweak measurements of electroweak observables, by comparing them with theory predictions which account for M_H effects at higher orders (see the electroweak model and constraints on new physics in this review for more details). This global fit to the precision electroweak data accumulated in the last two decades at LEP, SLC, the Tevatron, and elsewhere, suggests $m_H = 89^{+22}_{-18}\,\text{GeV}$, or $m_H < 127\,\text{GeV}$ at 90% confidence level [106].

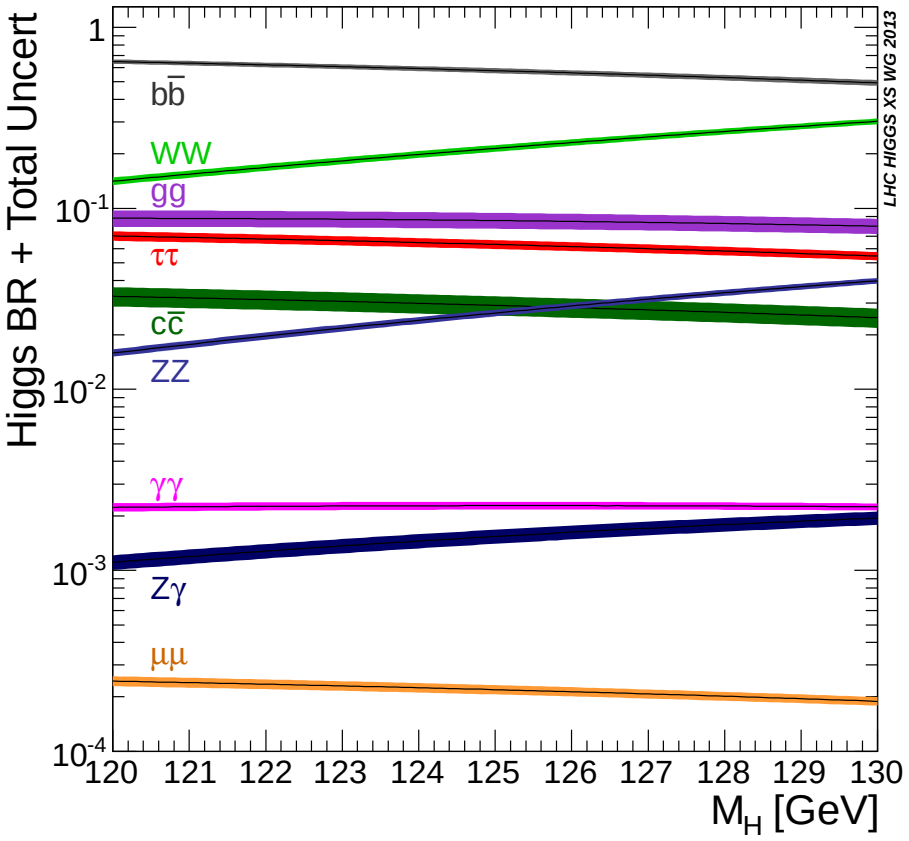

Figure 11.4: The branching ratios for the main decays of the SM Higgs boson near $m_H = 125\,\text{GeV}$. The theoretical uncertainties [38] are indicated as a band.

Direct and model-independent searches for the Higgs boson were conducted by the ALEPH, DELPHI, L3, and OPAL experiments at the LEP e^+e^- collider. The combination of LEP data collected near the Z resonance and at centre-of-mass energies of up to 209 GeV yielded a 95% Confidence level (CL) lower bound [107] of 114.4 GeV for the mass of the SM Higgs boson.

Following the shutdown of the LEP collider in 2000, the direct search for the Higgs boson continued at Fermilab's Tevatron $p\overline{p}$ collider. The combined results [108] from approximately $10\,\text{fb}^{-1}$ recorded by the CDF and D0 experiments excluded two ranges in m_H: between 90 GeV and 109 GeV, and between 149 GeV and 182 GeV. In addition, a broad excess in data was seen in the mass range $115\,\text{GeV} < m_H < 140\,\text{GeV}$ with a local significance[4] of 3 standard deviations at $m_H = 125\,\text{GeV}$. The commissioning in 2010 and the high intensity running of the LHC pp collider at CERN at $\sqrt{s}$ =7 TeV in 2011 followed by an energy boost to $\sqrt{s}$ =8 TeV in 2012 opened up a new landscape where the Higgs boson could be searched for, quickly and effectively, in the 110–1000 GeV mass

[4] In this review, we use the phrase "local significance" to indicate a calculation of the significance not corrected for the look-elsewhere effect [109].

range.

The announcement on July 4, 2012 of the observation [1,2] at the LHC of a narrow resonance with a mass of about 125 GeV has provided an important new direction in the decades-long search for the SM Higgs boson. The analyzed data corresponded to integrated luminosities of up to 4.8 (5.1) fb^{-1} at $\sqrt{s} = 7\,\text{TeV}$ in 2011 and 5.9 (5.3) at $\sqrt{s} = 8\,\text{TeV}$ in 2012 recorded by the ATLAS and CMS experiments, respectively. The observed decay channels indicated that the new particle is a boson. The evidence was strong that the new particle decays to $\gamma\gamma$ and ZZ with rates consistent with those predicted for the Standard Model (SM) Higgs boson. There were indications that the new particle also decays to W^+W^-. Although the experiments searched for decays to $b\bar{b}$ and $\tau^+\tau^-$, no statistically significant signal was found. The significance of these observations are quantified by a p-value [110], the probability for a background only experiment to give a result at least as signal-like as that observed in the data. For example, a p-value of 2.87×10^{-7} corresponds to a five-standard-deviation excess over the background-only prediction. ATLAS observed the largest excess with a local significance of 5.9σ at a mass $m_H = 126.5\,\text{GeV}$, to be compared with an expected significance of 4.6σ if a SM Higgs boson were present at such a mass. CMS observed an excess with a local significance of 4.9σ at a mass of 125.5 GeV, to be compared with an expected significance of 5.9σ in this dataset.

Even as this discovery was being announced, ATLAS and CMS continued to accumulate pp collision data at $\sqrt{s} = 8\,\text{TeV}$ recording a total of about $20\,\text{fb}^{-1}$ each at this energy. Figure 11.5 shows four snapshots of the evolution of the p-value and the signal significance near 125 GeV with increasing datasets analyzed by the two experiments.

In the remainder of this section the focus will be on the recent major results. Unless explicitly mentioned, all measurements are based on the full dataset of about $10\,\text{fb}^{-1}$ recorded by the Tevatron experiments and about $25\,\text{fb}^{-1}$ recorded by the LHC experiments. An extensive review of the searches for the Higgs boson from LEP to the LHC can be found in Ref [111].

III.1. The discovery channels

For a given m_H the sensitivity of a search channel depends on the production cross section of the Higgs bosons, its decay branching fraction, reconstructed mass resolution, selection efficiency and the level of background in the final state. For a low mass Higgs boson ($110 < m_H < 150\,\text{GeV}$) where the natural width of the Higgs boson is only a few MeV, the five decay channels that play an important role at the LHC are listed in Table 11.3. In the $H \to \gamma\gamma$ and $H \to ZZ \to 4\ell$ channels, all final state particles can be very precisely measured and the reconstructed m_H resolution is excellent. While the $H \to W^+W^- \to \ell^+\nu_\ell\ell'^-\bar{\nu}_{\ell'}$ channel has relatively large branching fraction, the m_H resolution is poor due to the presence of neutrinos. The $H \to b\bar{b}$ and the $H \to \tau^+\tau^-$ channels suffer from large backgrounds and a poor mass resolution. For $m_H > 150\,\text{GeV}$, the sensitive channels are $H \to WW$ and $H \to ZZ$ where the W or Z boson decays into a variety of leptonic and hadronic final states.

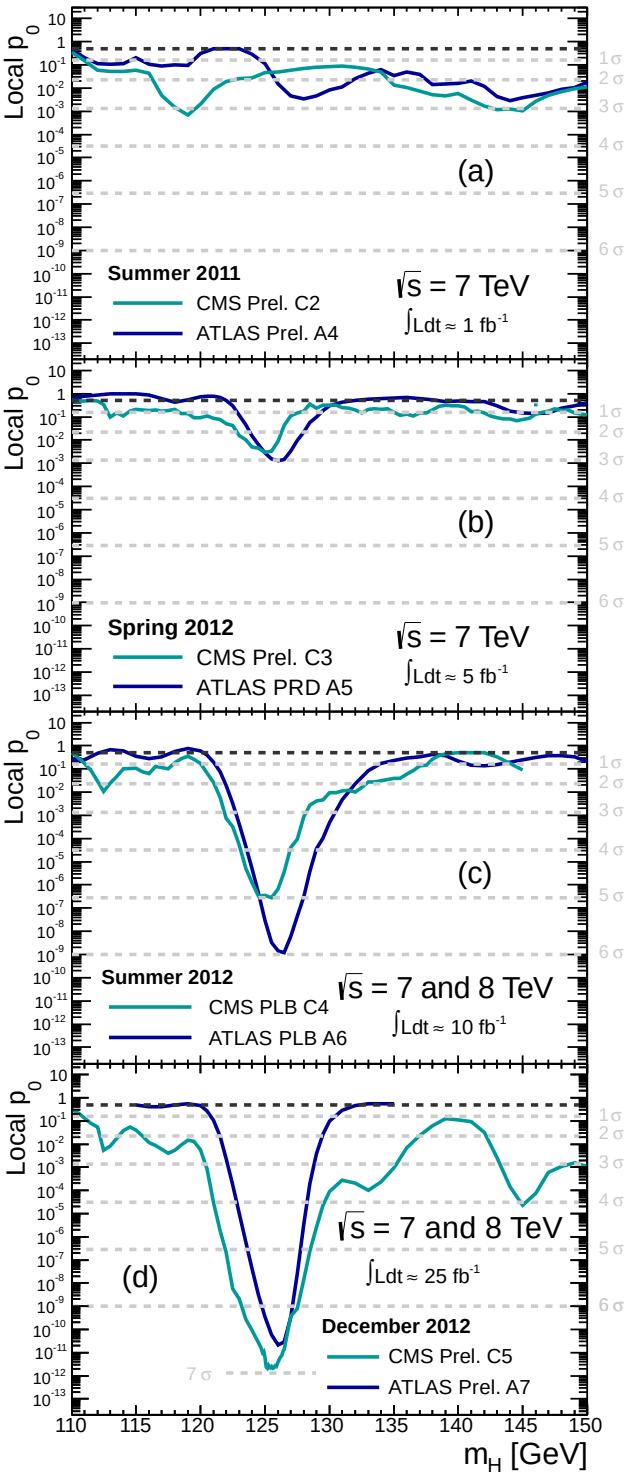

Figure 11.5: Evolution of the p-value and the signal significance observed by the ATLAS and CMS experiments with increasingly larger datasets: (a) Summer 2011 ($\approx 1\,\text{fb}^{-1}$/expt) for ATLAS A4 [112] and CMS C4 [113], (b) Spring 2012 ($\approx 5\,\text{fb}^{-1}$/expt) for ATLAS A5 [114] and CMS C3 [115], (c) Summer 2012 ($\approx 10\,\text{fb}^{-1}$/expt) for ATLAS A6 [1] and CMS C4 [2], and (d) December 2012 ($\approx 25\,\text{fb}^{-1}$/expt) for ATLAS A7 [116] and CMS C4 [117].

Table 11.3: The five sensitive channels for low mass SM Higgs boson searches at the LHC. The numbers reported are for $m_H = 125\,\text{GeV}$.

Decay channel	Mass resolution
$H \to \gamma\gamma$	1-2%
$H \to ZZ \to \ell^+\ell^-\ell'^+\ell'^-$	1-2%
$H \to W^+W^- \to \ell^+\nu_\ell\ell'^-\bar{\nu}_{\ell'}$	20%
$H \to b\bar{b}$	10%
$H \to \tau^+\tau^-$	15%

In order to distinguish between different production modes, the LHC experiments usually split the Higgs boson candidates into several mutually exclusive categories (or tags) based on the topological and/or kinematics features present in the event. These categories contain an admixture of various signal production modes. For example, a typical VBF category contains Higgs boson candidates accompanied by two energetic jets ($\geq 30\,\text{GeV}$) with a large dijet mass ($\geq 400\,\text{GeV}$) and separated by a large pseudorapidity ($\Delta\eta_{jj} \geq 3.5$). While such a category is enriched in Higgs boson produced via VBF, the contamination from the dominant gluon fusion production mechanism can be significant. Hence a measurement of the Higgs boson production cross section in the VBF category does not imply a measurement of VBF production cross-section. Simulations are used to determine the relative contributions of the various Higgs production modes in a particular category.

III.1.1. $H \to \gamma\gamma$

In the $H \to \gamma\gamma$ channel a search is performed for a narrow peak over a smoothly falling background in the invariant mass distribution of two high p_T photons. The background in this channel is high and stems from prompt $\gamma\gamma$, γ+jet and dijet processes. In order to optimize search sensitivity and also to separate the various Higgs production modes, ATLAS and CMS experiments split events into several mutually exclusive categories. Diphoton events containing a high p_T muon, electron, dijets or missing energy (E_T^{miss}) consistent with the decay of a W or Z boson are tagged in the VH production category, those containing energetic dijets with a large mass and pseudorapidity difference are assigned to the VBF production category and the remaining events ($\approx 99\%$ of the total) are considered in the gluon fusion production category. While the VH category is relatively pure, the VBF category has significant contamination from the gluon fusion process. ATLAS uses the diphoton transverse momentum orthogonal to the diphoton thrust axis in the transverse plane (p_{Tt}) [118] to differentiate between Higgs boson produced via gluon fusion and the VBF/VH production modes.

Untagged events are further categorized according to their expected $m_{\gamma\gamma}$ resolution and signal-to-background ratio. Categories with good m_H resolution and larger signal-to-background ratio contribute most to the sensitivity of the search.

In each category, $Z \to e^+e^-$ and $Z \to \mu^+\mu^-\gamma$ events from data are used to construct a parametric signal model. The functional form of the background is determined by a fit

to the full $m_{\gamma\gamma}$ distribution in each category. All categories are fitted simultaneously to determine the signal yield at a particular mass. In the full dataset, the $m_{\gamma\gamma}$ distribution after combining all categories are shown for the ATLAS experiment in Fig. 11.6 and for the CMS experiment in Fig. 11.7. ATLAS observes [119] its largest excess over background at $m_H = 126.8\,\text{GeV}$ with a significance of 7.4σ compared with 4.3σ expected for SM Higgs boson at that mass. CMS observes [120] its largest excess at $m_H = 125.4\,\text{GeV}$ with a significance of 3.2σ compared with 4.2σ expected for SM Higgs boson of that mass.

The signal strength $\mu = (\sigma \cdot \mathcal{B})_{\text{obs}}/(\sigma \cdot \mathcal{B})_{\text{SM}}$ which is the observed product of the Higgs boson production cross section (σ) and its branching ratio ($\mathcal{B}$) in units of the corresponding SM values, is $1.65^{+0.34}_{-0.30}$ for ATLAS and 0.78 ± 0.27 for CMS at $m_H = 125.5$ and 125 GeV respectively.

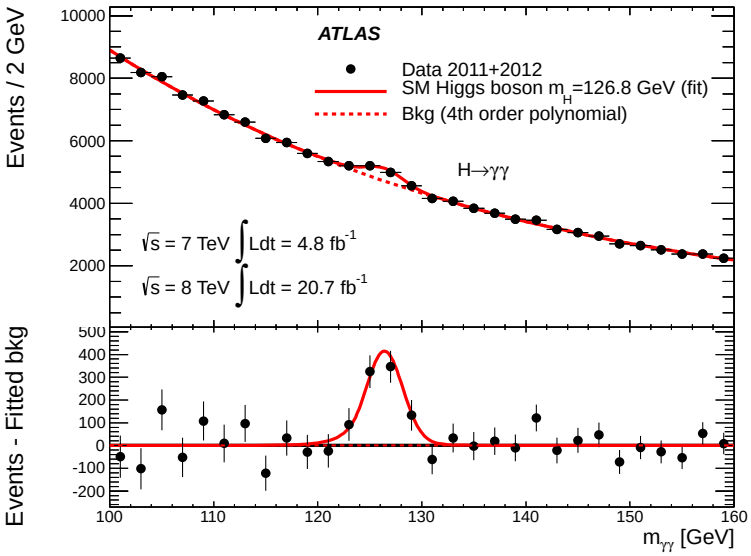

Figure 11.6: The combined invariant mass distribution of diphoton candidates observed by ATLAS [119]. The residuals of the data with respect to the fitted background are displayed in the lower panel.

III.1.2. $H \to ZZ^{(*)} \to \ell^+\ell^-\ell'^+\ell'^-$, $(\ell, \ell' = e, \mu)$

In the $H \to ZZ^{(*)} \to \ell^+\ell^-\ell'^+\ell'^-$ channel a search is performed for a narrow mass peak over a small continuous background dominated by non-resonant $ZZ^{(*)}$ production from $q\overline{q}$ annihilation and gg fusion processes. The contribution and the shape of this background is taken from simulated events. The subdominant and reducible backgrounds stem from $Z + b\bar{b}$, $t\overline{t}$ and $Z +$ jets events. Their contribution is suppressed by requirements on lepton isolation and lepton impact parameter and their yield is estimated from control samples in data.

To help distinguish the Higgs signal from the dominant non-resonant $ZZ^{(*)}$ background, CMS uses a matrix element likelihood approach [2] to construct a kinematic

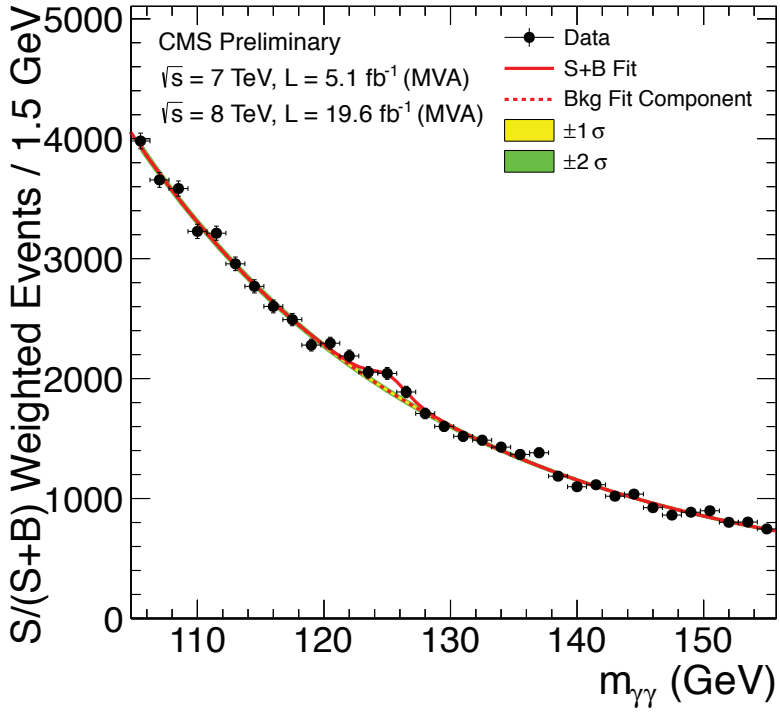

Figure 11.7: The combined CMS $M_{\gamma\gamma}$ distribution with each event weighted by the ratio of signal-to-background in each event category [120].

discriminant built for each 4ℓ event based on the ratio of complete leading-order matrix elements $|\mathcal{M}_{sig}{}^2/\mathcal{M}_{bkg}{}^2|$ for the signal ($gg \to H \to 4\ell$) and background($q\overline{q} \to ZZ \to 4\ell$) hypotheses. The signal matrix element $\mathcal{M}_{sig}$ is computed assuming $m_H = m_{4\ell}$.

To enhance the sensitivity to VBF and VH production processes, the ATLAS and CMS experiment divide 4ℓ events into mutually exclusive categories. Events containing dijets with a large mass and pseudorapidity difference populate the VBF category. ATLAS requires presence of an additional lepton in the VH category. In events with less than two jets, CMS uses the $p_T^{4\ell}$ to distinguish between production via the gluon fusion and the VH/VBF processes.

Since the $m_{4\ell}$ resolutions and the reducible background levels are different in the 4μ, $4e$ and $2e2\mu$ sub-channels, they are analyzed separately and the results are then combined.

The combined ATLAS $m_{4\ell}$ distribution is shown in Fig. 11.8. The largest deviation from the SM background-only expectation is observed [119] at $m_H = 124.3\,\text{GeV}$ where the significance of the observed peak is 6.7σ in the full 7 and 8 TeV data. The expected significance for the SM Higgs boson at that mass is 4.4σ. As shown in Fig. 11.9, the CMS experiment observes [121] its largest excess at $m_H = 125.8\,\text{GeV}$ with a observed significance of 6.7σ to be compared with an expected significance of 7.2σ at that mass. Both experiments also observe a clear peak at $m_{4\ell} = 91\,\text{GeV}$ from Z/γ^* production at the expected SM rate [122].

The signal strength μ for the inclusive $H \to 4\ell$ production measured by the ATLAS and CMS experiments are $1.43^{+0.40}_{-0.35}$ at $m_H = 125.5\,\text{GeV}$ and $0.91^{+0.30}_{-0.24}$ at $m_H = 125.8\,\text{GeV}$ respectively.

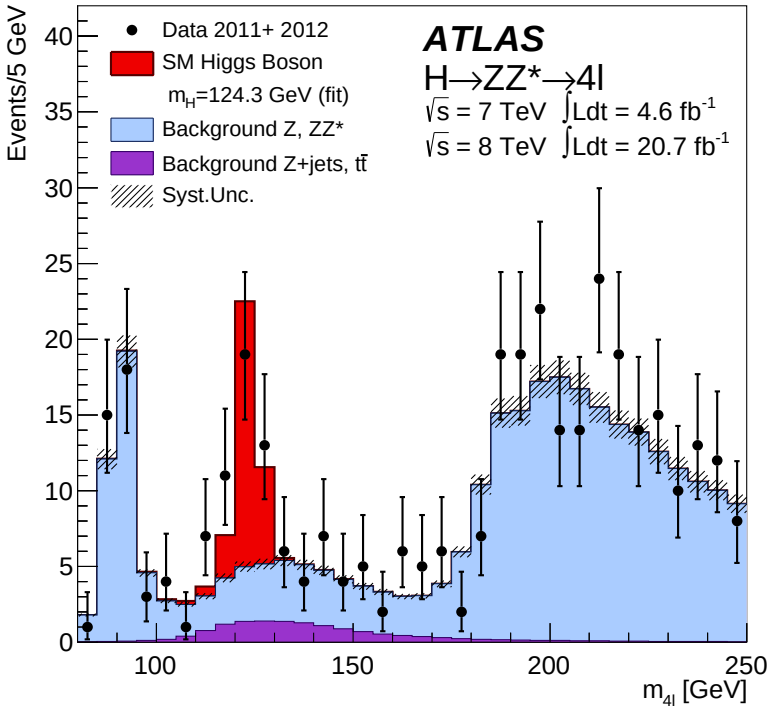

Figure 11.8: The combined $m_{4\ell}$ distribution from ATLAS [119].

III.2. Mass and width measurements

In order to measure the mass of the observed state, the ATLAS and CMS experiments combine the measurements from the $\gamma\gamma$ and ZZ channels which have excellent mass resolution and where excesses with large significance are observed. For a model-independent mass measurement, the signal strengths in the $\gamma\gamma$ and ZZ channels are assumed to be independent and not constrained to the expected rate ($\mu = 1$) for the SM Higgs boson. The combined mass measured by ATLAS [119] and CMS [124] are $125.5 \pm 0.2(\text{stat.})\ ^{+0.5}_{-0.6}(\text{syst.})\,\text{GeV}$ and $125.7 \pm 0.3(\text{stat.}) \pm 0.3(\text{syst.})\,\text{GeV}$ respectively. In both experiments the systematic uncertainty is dominated by the imprecision in the knowledge of the photon energy and the lepton momentum scale. The significance of the difference between the measurements of the masses in the $\gamma\gamma$ and ZZ channels by the ATLAS experiment is 2.4σ [119]. Fig. 11.10 summarizes these measurements and our combination of the ATLAS and CMS results assuming uncorrelated systematic uncertainties between the two experiments.

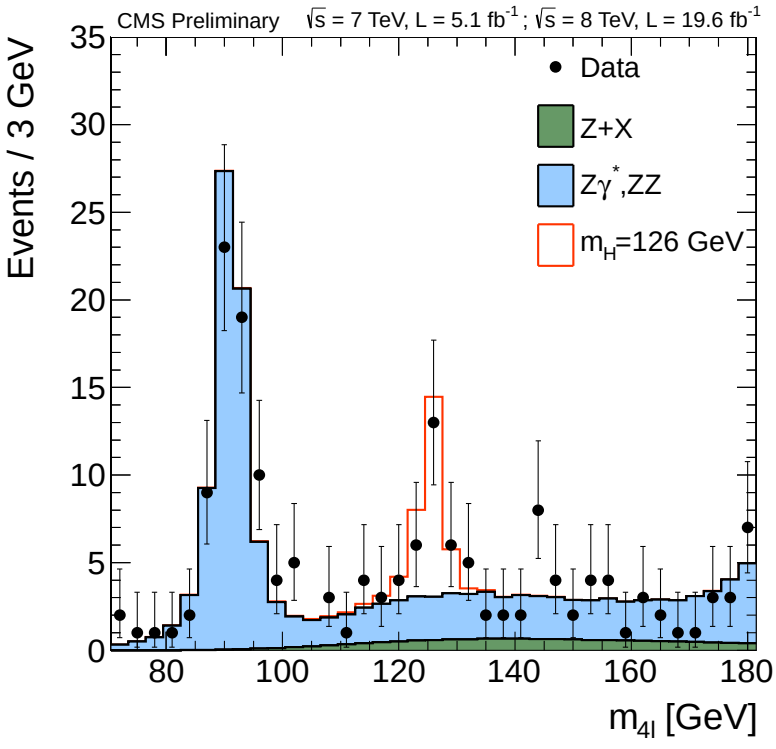

Figure 11.9: The combined $m_{4\ell}$ distribution from CMS [121].

The natural width of a SM Higgs boson with a mass of 125 GeV is about 4 MeV, much smaller than the instrumental mass resolution in the $\gamma\gamma$ and ZZ channels. CMS has placed 95% CL bound [123] on the natural width of the observed boson of $\Gamma_H < 3.4\,\text{GeV}$.

III.3. $H \to W^+W^- \to \ell^+\nu\ell^-\bar{\nu}$

While the production rate in the $H \to W^+W^- \to \ell^+\nu\ell^-\bar{\nu}$ channel is large, due to the presence of two neutrinos in the decay, the m_H resolution is quite poor ($\approx 20\%\ m_H$) so the search is reduced to a counting experiment of the event yield in broad bins in m_H.

Experiments search for an excess of events with two leptons of opposite charge accompanied by missing energy and up to two jets. Events are divided into several categories depending on the lepton flavor combination (e^+e^-, $\mu^+\mu^-$and $e^\pm\mu^\mp$) and the number of accompanying jets ($N_{jet} = 0, 1, \geq 2$). The $N_{jet} \geq 2$ category is optimized for VBF production process by selecting two leading jets with a large pseudorapidity difference and with a large mass ($m_{jj} > 500\,\text{GeV}$). Backgrounds contributing to this channel are numerous and vary by the category of selected events. Reducing them and accurately estimating the remainder is major challenge in this analysis. For events with opposite flavor lepton and no accompanying high p_T jets, the dominant background stems from non-resonant WW production. Events with same-flavor leptons suffer from large Drell–Yan contamination. The $t\bar{t}$, Wt and $W+$jets (with the jet misidentified as a lepton) events contaminate all categories. Non-resonant WZ, ZZ and $W\gamma$ processes also

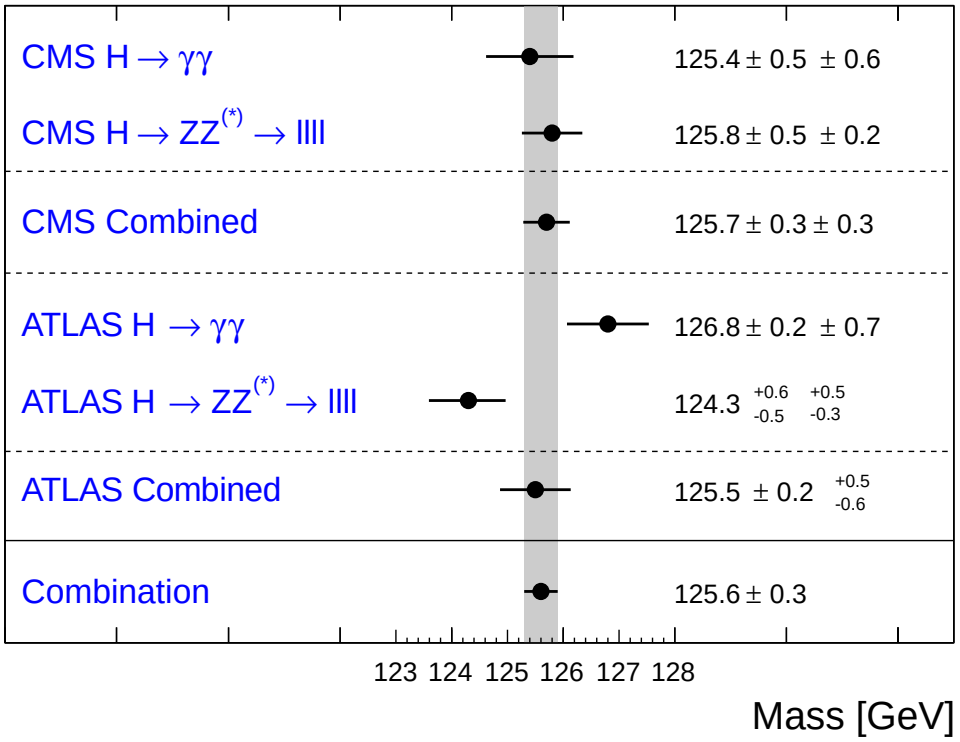

Figure 11.10: A compilation of the CMS and ATLAS mass measurements in the $\gamma\gamma$ and ZZ channels, the combined result from each experiment and our average of the combinations.

contribute to the background at a sub-leading level.

A requirement of large missing transverse energy ($E_T^{\rm miss}$) is used to reduce the Drell–Yan and multi-jet backgrounds. In the e^+e^- and $\mu^+\mu^-$ categories, events with $m_{\ell\ell}$ consistent with the Z mass are vetoed. The $t\bar{t}$ background is suppressed by a veto against identified b-jets or low p_T muons (assumed to be coming from semileptonic b-hadron decays within jets) and tight isolation requirements diminish the W+jets background. The scalarity of the Higgs boson and the $V-A$ nature of the W boson decay implies that the two charged leptons in the final state are emitted at small angles with respect to each other. Therefore the dilepton invariant mass ($m_{\ell\ell}$) and the azimuthal angle difference between the leptons ($\Delta\phi_{\ell\ell}$) are used to discriminate between the signal and non-resonant WW events. The transverse mass constructed from the dilepton p_T ($p_T^{\ell\ell}$) , $E_T^{\rm miss}$ and the azimuthal angle between $E_T^{\rm miss}$ and $p_T^{\ell\ell}$ and defined as $m_T = \sqrt{2p_T^{\ell\ell}E_T^{\rm miss}(1-\cos\Delta\phi_{E_T^{\rm miss}\ell\ell})}$ serves as an effective discriminant against backgrounds. The transverse mass variable also tracks the Higgs boson mass but with a poor mass resolution. All residual background rates except for the small contributions from non-resonant WZ, ZZ and $W\gamma$ are evaluated from control samples devised from data.

The m_T distributions of selected events is shown in Fig. 11.11 and Fig. 11.12 for

the ATLAS and CMS experiments respectively. The 0-jet category is dominated by non-resonant WW background while $t\bar{t}$ dominates the 1 and 2 jet categories. Both experiments see a clear excess over background expectation in the 0 and 1 jet categories. ATLAS fits the m_T distributions and observes [119,126] the most significant excess for $m_H = 140\,\text{GeV}$. The significance of the observed excess for $m_H = 125.5\,\text{GeV}$ is 3.8σ, the same as expected. The measured inclusive signal strength $\mu = 1.01 \pm 0.31$ at $m_H = 125\,\text{GeV}$. In the VBF category an excess with a significance of 2.5σ corresponding to a signal strength of $\mu = 1.66 \pm 0.67 \pm 0.43$ is observed for $m_H = 125\,\text{GeV}$. The CMS analysis of 0 and 1 jet categories, using all lepton flavor combinations, shows [127] an excess with an observed significance of 4σ consistent with the expected significance of 5.1σ for a 125 GeV Higgs boson. A separate analysis optimized for the VBF production mode reports [128] no significant excess and sets a 95% CL upper limit of $\mu < 1.7$ for $m_H = 125\,\text{GeV}$.

The ATLAS and CMS experiments have also performed dedicated searches for the associated Higgs boson production (VH) in this channel. The signal consists of three (WH) or four (ZH) high p_T isolated leptons with missing transverse energy and low hadronic activity. The major backgrounds stem from triboson and diboson production where each boson decays leptonically. The 95% CL limits on μ of 7.2 [129] and 5.0 [130] have been set by ATLAS and CMS respectively for a $m_H = 125\,\text{GeV}$.

III.4. Decays to fermions

As described in Section III.1, significant signals for the decay of the observed boson in the the $\gamma\gamma$, ZZ and W^+W^- channels have been measured by the ATLAS and CMS experiments. The measured signal strengths in these channels are consistent with this boson playing a role in electroweak symmetry breaking. However the nature of its interaction with fermions and whether this boson serves also as a source of mass generation for quarks and leptons via Yukawa interactions is a topic of active investigation[5].

At the hadron colliders, the most promising channel for probing the coupling of the Higgs field to the quarks and leptons are $H \to b\bar{b}$ and $H \to \tau^+\tau^-$ respectively. For a Higgs boson with $m_H \approx 125\,\text{GeV}$, the branching fraction to $b\bar{b}$ is about 57% and to $\tau^+\tau^-$ is about 6%. Nevertheless the presence of very large backgrounds makes the isolation of a Higgs boson signal in these channels quite challenging.

III.4.1. $H \to \tau^+\tau^-$

In the $H \to \tau\tau$ search, τ leptons decaying to electrons (τ_e), muons (τ_μ) and hadrons (τ_{had}) are considered. The $\tau^+\tau^-$ invariant mass ($m_{\tau\tau}$) is reconstructed from a kinematic fit of the visible products from the two τ leptons and the missing energy observed in the event. Due to the presence of missing neutrinos, the $m_{\tau^+\tau^-}$ resolution is poor ($\approx 15\%$). As a result, a broad excess over the expected background in the $m_{\tau\tau}$ distribution is

[5] We note here that the Higgs boson production via gluon fusion as observed in the $\gamma\gamma$, ZZ and W^+W^- channels provides indirect measurement of the Higgs boson coupling to the top quark at approximately the expected rate.

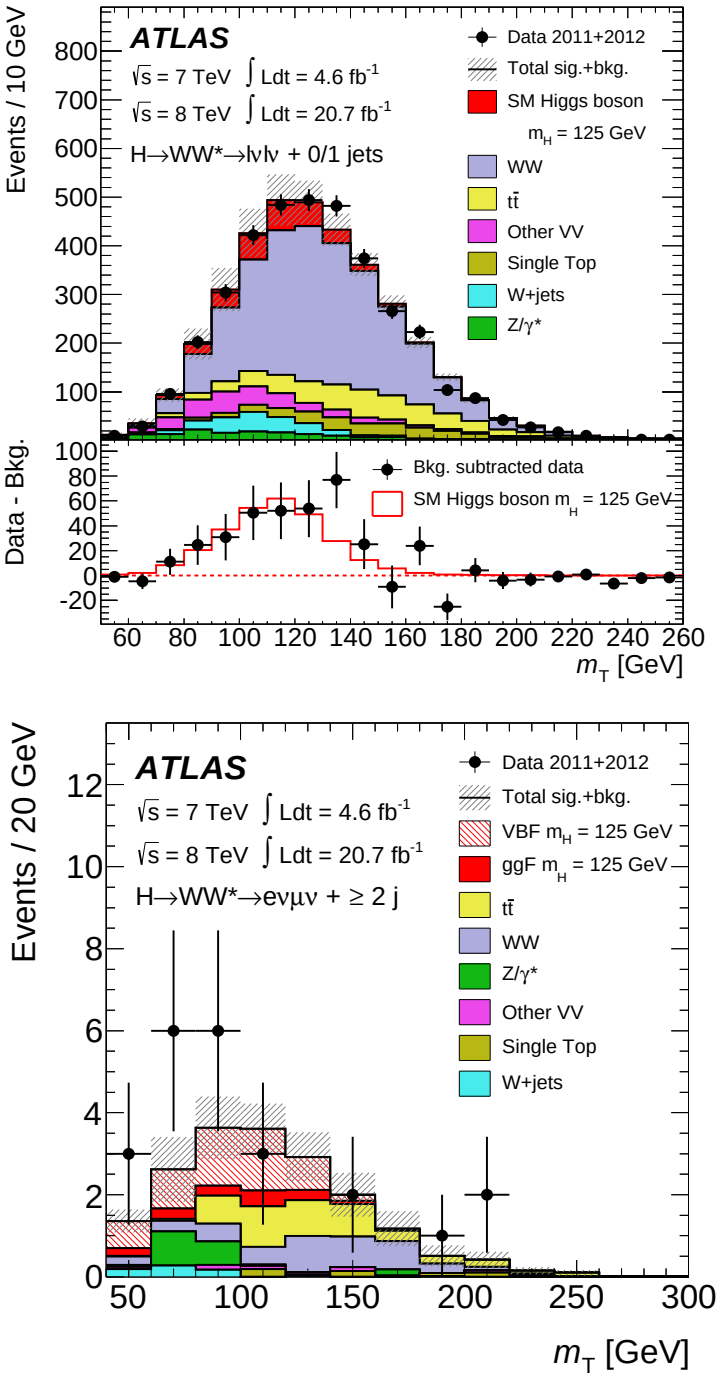

Figure 11.11: (Top) The m_T distribution for selected events summed over all lepton flavors and with ≤ 1 associated jets. The observed excess over the estimated SM background and the expectation from a SM Higgs boson with $m_H = 125\,\text{GeV}$ are shown in the lower panel. (Bottom) The m_T distribution for selected $e^{\pm}\mu^{\mp}$ events and with ≥ 2 associated jets [119].

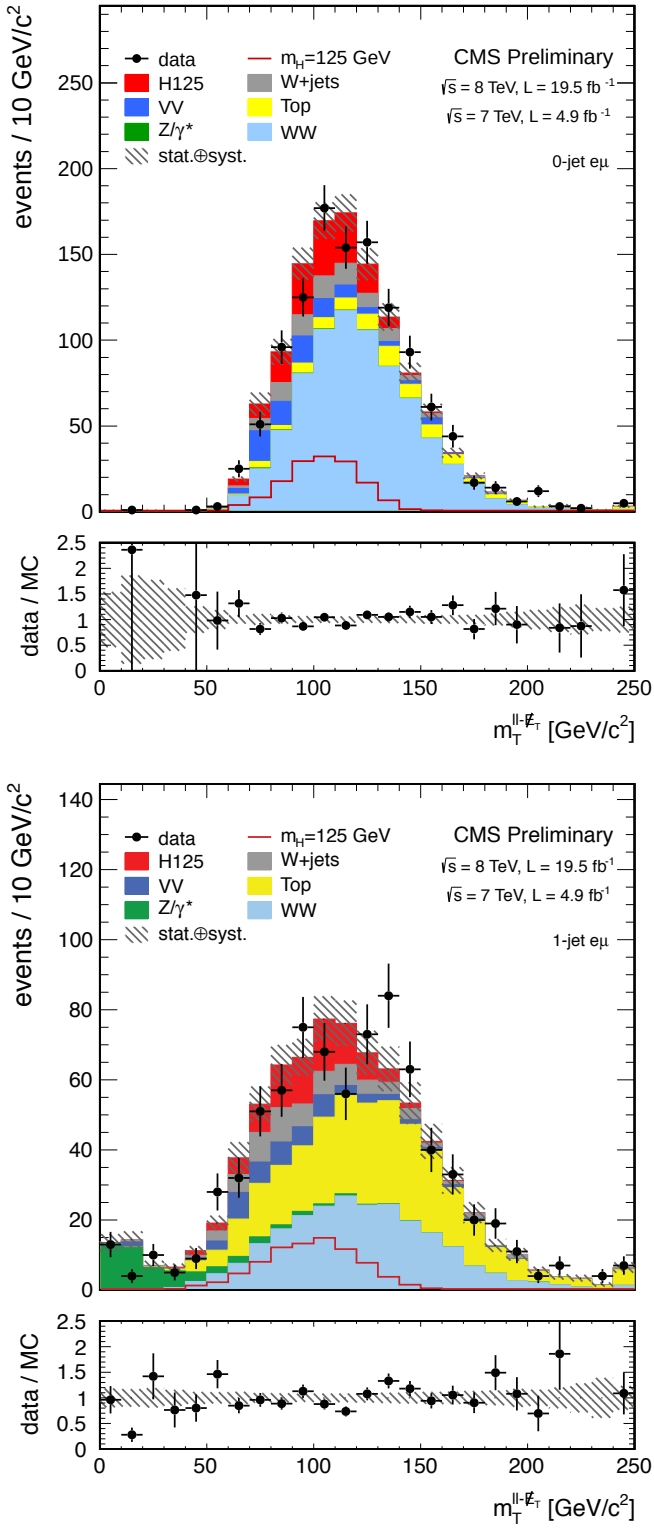

Figure 11.12: The m_T distribution for events, selected with a cut-based analysis, summed over all lepton flavors and with zero accompanying reconstructed jets (Top) and 1-jet (Bottom). The contributions of all SM background sources and a SM Higgs with m_H=125 GeV are stacked together [127].

searched for. The major sources of background stem from Drell–Yan $Z \to \tau^+\tau^-$ and $Z \to e^+e^-$, W+jets, $t\bar{t}$ and multijet production. Events in all sub-channels are divided into categories based on the number and kinematic properties of additional energetic jets in the event. The sensitivity of the search is generally higher for categories with one or more additional jets. The VBF category, consisting of a $\tau\tau$ pair with two energetic jets separated by a large pseudorapidity, has the best signal-to-background and search sensitivity followed by the $\tau^+\tau^-$+1 jet category. The signal to background discrimination relies in part on $m_{\tau\tau}$ resolution which improves with the boost of the Higgs boson, the non-VBF categories are further subdivided according to the observed boost of the $\tau^+\tau^-$ system. The 0-jet category which has the poorest signal/background ratio is used to constrain the background yields, the reconstruction efficiencies, and the energy scales. The CMS experiment uses the reconstructed mass as discriminating variable [131,132] while the ATLAS experiment combines various kinematic properties of each event categories with multivariate techniques to build a discriminant [133].

$H \to \tau^+\tau^-$ decays in the VH production mode are searched for in final states where the W or Z boson decays into leptons or into two jets (in [134] but currently not in the latest ATLAS results [133]) . While the decays to tau pairs are the dominant Higgs boson signal contribution, the final states used can additionally be produced by the decay of the Higgs boson into a pair of W bosons that both decay to leptons. The irreducible background in this search arises from non-resonant WZ and ZZ diboson production. The reducible backgrounds originate from W, Z, and $t\bar{t}$ events that contain at least one fake lepton in the final state due to a misidentified jet. The shape and yield of the major backgrounds in each category is estimated from control samples in data. Contributions from non-resonant WZ and ZZ diboson production is estimated from simulations but corrected for reconstruction efficiency using control samples formed from observed data.

Figure 11.13 shows the CMS [131] $m_{\tau\tau}$ distributions combining all non-VH categories, weighing the distributions in each category of each sub-channel by the ratio between the expected signal and background yields for that category. The inset plot shows the difference between the observed data and expected background distributions, together with the expected distribution for a SM Higgs boson signal with $m_H = 125\,\text{GeV}$. The significance of the observed excess at $m_H = 125\,\text{GeV}$ is 2.85 standard deviations and corresponds to a signal strength of $\mu = 1.10 \pm 0.41$. The result in this channel has been updated with an optimized analysis [132] yielding an observed excess of 3.4 standard deviations at $m_H = 125\,\text{GeV}$ corresponding to a signal strength of $\mu = 0.87 \pm 0.29$. It has not yet been included in the combination of all low mass Higgs boson searches.

The ATLAS results [133] are based on the full 8 TeV data sample of $20.3\,\text{fb}^{-1}$. At $m_H = 125\,\text{GeV}$, the observed (expected) deviation from the background-only hypothesis corresponds to a local significance of 4.1 (3.2) standard deviations and the best fit value of the signal strength $\mu = 1.4^{+0.5}_{-0.4}$. This result does not include the aforementioned leptonic VH modes. These results are summarized in Table 11.4.

Both ATLAS and CMS measurements provide substantial evidence of the coupling of the Higgs boson to leptons.

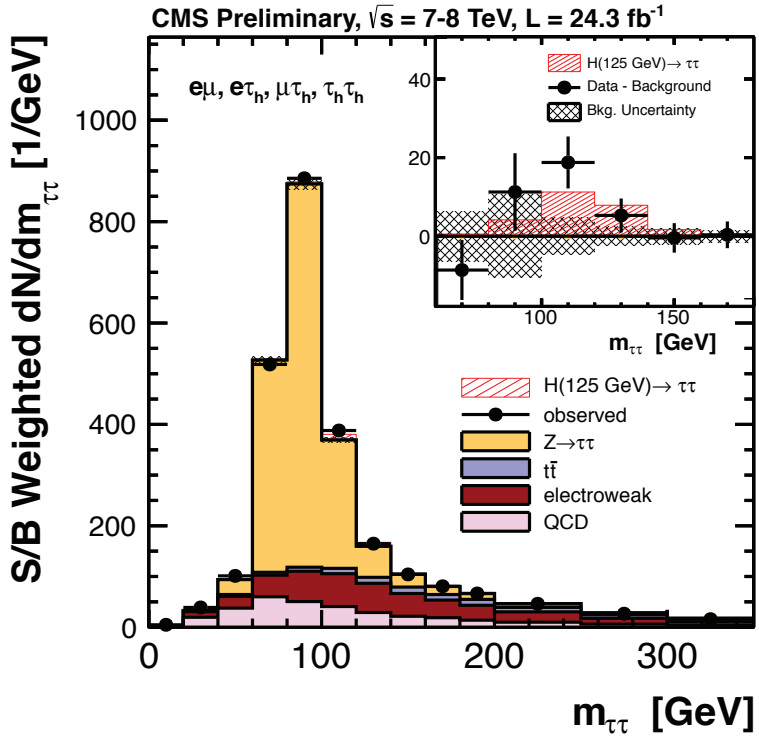

Figure 11.13: CMS results : The combined observed and expected $m_{\tau\tau}$ distributions for all sub-channels combined. The insert shows the difference between the observed data and the expected background distributions, together with the expected signal distribution for a SM Higgs signal at $m_H = 125\,\text{GeV}$ [131].

III.4.2. $H \to b\bar{b}$

The dominant production mode $gg \to H$ with $H \to b\bar{b}$ is overwhelmed by the background from the inclusive production of $p\bar{p} \to b\bar{b} + X$ via the strong interaction. The associated production modes WH and ZH (collectively termed VH modes) allow use of the leptonic W and Z decays to purify the signal and reject QCD backgrounds. The W bosons are reconstructed via their leptonic decay $W \to \ell\bar{\nu}_\ell$ where $\ell = e, \mu$ or τ. The Z boson is reconstructed via their decay into $e^+e^-, \mu^+\mu^-$or $\nu\bar{\nu}$. The Higgs boson candidate mass is reconstructed from two b-tagged jets in the event. Backgrounds arise from production of W and Z bosons in association with gluon, light and heavy-flavored jets (V+jets), $t\bar{t}$, non-resonant diboson (ZZ and WZ with $Z \to b\bar{b}$) and QCD multijet processes. Due to the limited $m_{b\bar{b}}$ mass resolution, a SM Higgs boson signal is expected to appear as a broad enhancement in the reconstructed dijet mass distribution. The crucial elements in this search are b-jet tagging with high efficiency and low fake rate, accurate estimate of b-jet momentum and estimate of backgrounds from various signal depleted control samples constructed from data.

At the Tevatron, the $H \to b\bar{b}$ channel contributes the majority of the Higgs boson search sensitivity below $m_H = 130\,\text{GeV}$. The CDF and D0 experiments use multivariate

analysis (MVA) techniques that combine several discriminating variables into a single final discriminant used to separate signal from background. Each channel is divided into exclusive sub-channels according to various lepton, jet multiplicity, and b-tagging characteristics in order to group events with similar signal-to-background ratio and thus optimize the overall search sensitivity. The combined CDF and D0 data show [135,108] an excess of events with respect to the predicted background in the 115-140 GeV mass range in the most sensitive bins of the discriminant distributions suggesting the presence of a signal. At $m_H = 125\,\text{GeV}$ the local significance of the excess is 3.0 standard deviations. At that mass, the observed signal strength $\mu = 1.59^{+0.69}_{-0.72}$. Figure 11.14 shows the best-fit cross section times branching ratio $(\sigma_{\text{WH}} + \sigma_{\text{ZH}}) \times \text{B}(H \to b\bar{b})$ as well as the SM prediction as a function of m_H.

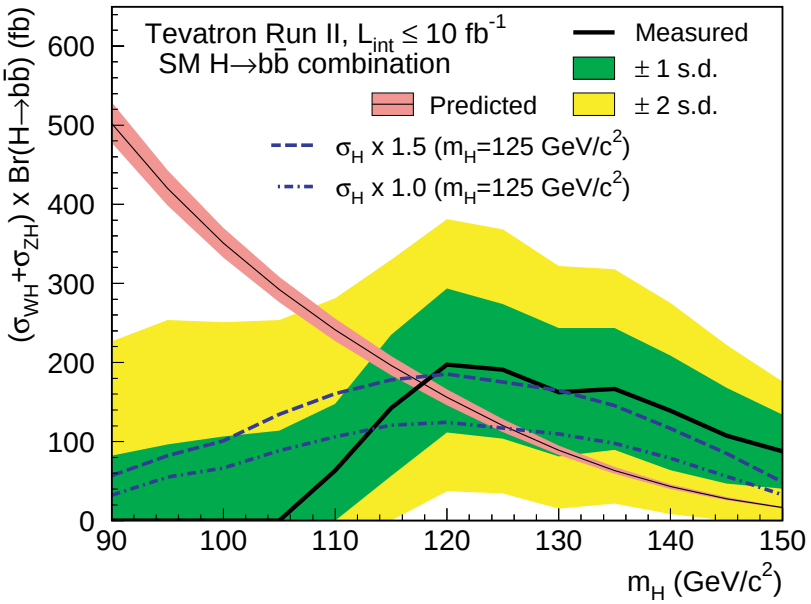

Figure 11.14: The combined CDF and D0 results on the best-fit cross section times branching ratio $(\sigma_{\text{WH}} + \sigma_{\text{ZH}}) \times \text{B}(H \to b\bar{b})$ as well as the SM prediction as a function of m_H [108].

To reduce the dominant V+jets background, following Ref. [136], the LHC experiments select a region in VH production phase space where the vector boson is significantly boosted and recoils from the $H \to b\bar{b}$ candidate with a large azimuthal angle $\Delta\phi_{\text{VH}}$. For each channel, events are categorized into different $p_T(\text{V})$ regions with varying signal/background ratios. Events with higher $p_T(\text{V})$ have smaller backgrounds and better $m_{b\bar{b}}$ resolution. CMS uses [137] MVA classifiers based on kinematic, topological and quality of b-jet tagging and trained on different values of m_H to separate Higgs boson signal in each category from backgrounds. The MVA outputs for all categories are then fit simultaneously. Figure 11.15 (Top) shows the combined MVA output of all channels where events are gathered in bins of similar expected signal-to-background ratios as predicted by the MVA discriminants. The excess of events observed in bins with the

largest signal-to-background ratios is consistent with the production of a 125 GeV SM Higgs boson with a significance of 2.1 standard deviations. The observed signal strength at 125 GeV is $\mu = 1.0 \pm 0.5$. Figure 11.15 (Bottom) shows the $m_{b\bar{b}}$ distribution for all categories combined, weighted by the signal-to-background ratio in each category, with all backgrounds except dibosons subtracted. The data show the clear presence of a diboson ($W/Z + \mathrm{Z} \to b\bar{b}$) signal, with a rate consistent with the Standard Model prediction, together with an excess that agrees with that expected from the production of a 125 GeV SM Higgs boson.

ATLAS performs a cut based analysis [138], with selected events divided into a large number of categories in $p_T(\mathrm{V})$. The discriminating variable used is $m_{b\bar{b}}$, and customized control samples devised from data are used to constrain the contributions of the dominant background processes. No significant excess is observed. The signal strength for $m_H = 125$ GeV is measured to be $\mu = 0.2 \pm 0.5(\mathrm{stat.}) \pm 0.4(\mathrm{syst.})$.

III.5. Observed signal strengths

The μ value obtained by ATLAS [119] and CMS [124] in the five channels and the combined best fit value are displayed in Fig. 11.16. The μ value for each channel and the combination is calculated for the best fit mass of 125.5 and 125.7 GeV by ATLAS and CMS respectively. The ATLAS combination used only the $\gamma\gamma$, WW and ZZ channels for which the full 7 and 8 TeV data were analyzed. Table 11.4 summarizes the measurements from the Tevatron and the LHC. All measurements are consistent with the expectation from the SM Higgs boson with a mass of 125 GeV.

III.6. Higgs Production in association with top quarks

As discussed in Section II, the coupling of the Higgs particle to top quarks plays a special role in the electroweak breaking mechanism and in its possible extensions. Substantial indirect evidence of this coupling is provided by the compatibility of observed rates of the Higgs boson in the main discovery channels as one of the main production processes, the gluon fusion, is dominated by a top quark loop. Direct evidence of this coupling at the LHC and the future e^+e^- colliders will be mainly available through the $t\bar{t}H$ final state. The analyses channels for such complex final states can be separated in four classes according to the decays of the Higgs boson. In each of these classes, most of the decay final states of the top quarks are considered. The topologies related to the decays of the top quarks are denoted 0L, 1L and 2L, for the fully hadronic, semi-leptonic and dilepton final states of the $t\bar{t}$ pair respectively.

The first in this set is the search for $t\bar{t}H$ production in the $H \to \gamma\gamma$ channel. This analysis relies on the search of a narrow mass peak in the $m_{\gamma\gamma}$ distribution. The background is estimated from the $m_{\gamma\gamma}$ sidebands. The sensitivity in this channel is mostly limited by the available statistics. This search was done in all three 0L and 1L final states by the ATLAS and CMS collaborations with the full 8 TeV datasets [139,140].

The second is the search in the $H \to b\bar{b}$ channel. This search is extremely intricate due to the large backgrounds, both physical and combinatorial in resolving the $b\bar{b}$ system related to the Higgs particle, in events with six jets and four b-tagged jets which are

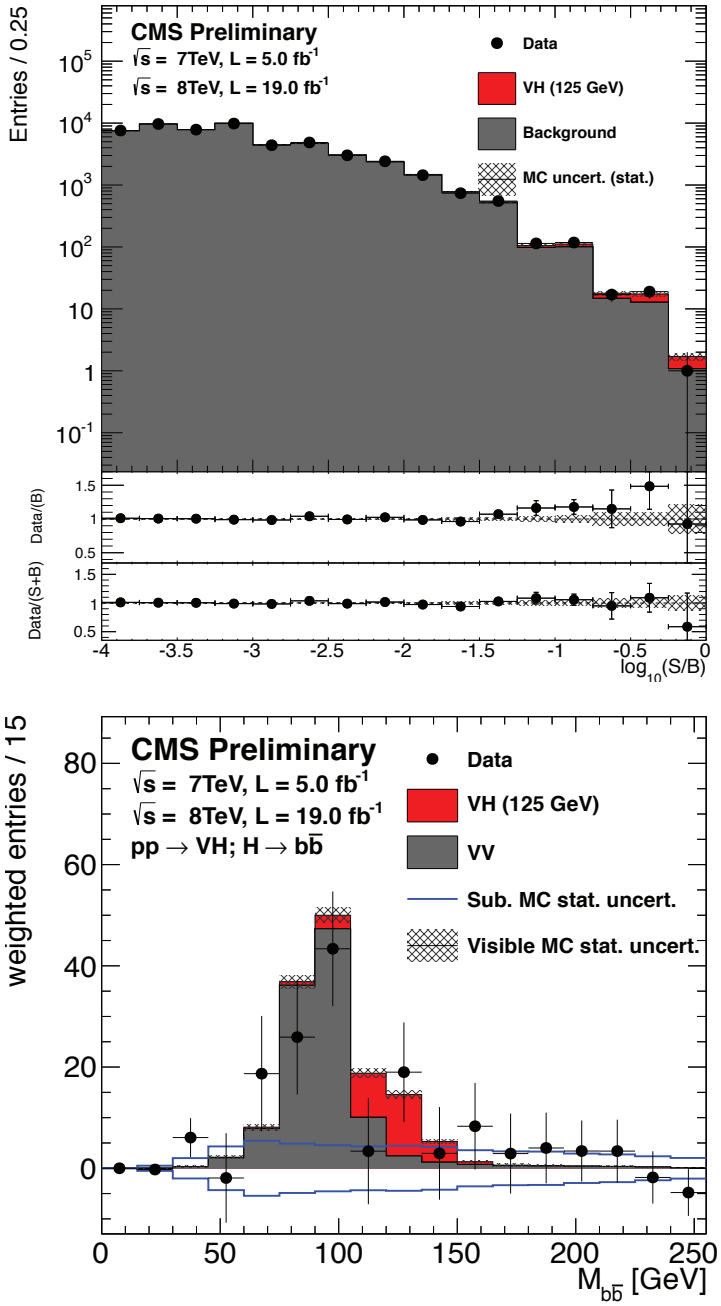

Figure 11.15: CMS results: (Top) The combination of all channels into a single distribution. The two bottom panels show the ratio of the data to the background-only prediction (above) and to the predicted sum of background and SM Higgs boson signal with a mass of 125 GeV (below). (Bottom) The $m_{b\bar{b}}$ distribution with all backgrounds, except dibosons, subtracted. The solid histograms for the backgrounds and the signal are summed cumulatively. The line histogram for signal and for VV backgrounds are also shown superimposed [137].

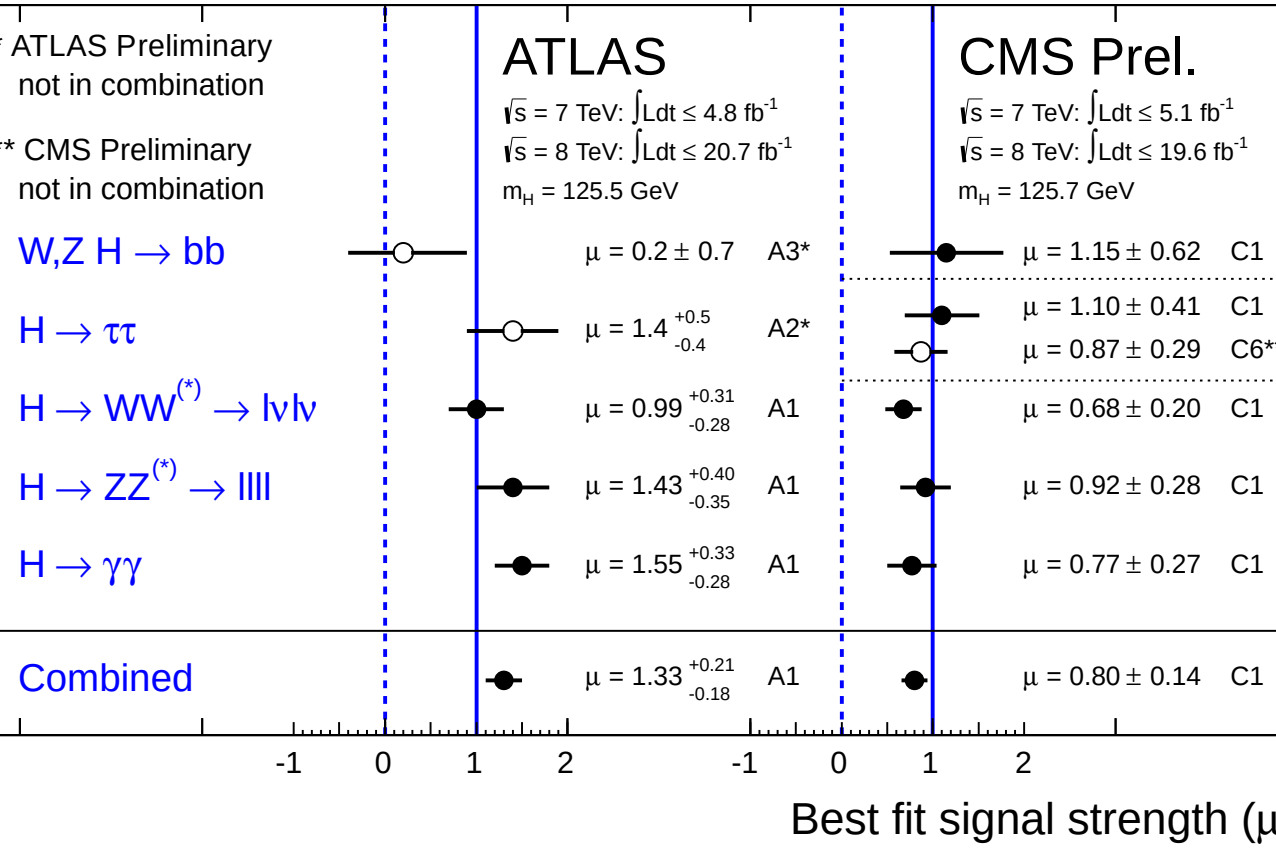

Figure 11.16: The signal strengths μ measured by the ATLAS experiment from Refs. A1 [119], A2 [133] and A3 [138], and CMS experiment from Ref. C1 [124] and C6 [132] in the five principal channels and their combination. It should be noted that the ATLAS combination only includes the bosonic $\gamma\gamma$, ZZ and WW channels.

very hard to simulate. With the current dataset, the sensitivity of this analysis is already limited by the systematic uncertainties on the background predictions. The ATLAS search was done in the 1L channel with the 7 TeV dataset only [141]. The CMS collaboration after having published first results with the full 7 TeV dataset [142,143], has complemented this result with a full 8 TeV analysis [144] with the 1L and 2L channels.

The third channel is a specific search for $\tau^+\tau^-$ where the two taus decay to hadrons and in the 1L channel only performed by CMS with the full 8 TeV dataset [144].

Finally, both W^+W^- and $\tau^+\tau^-$ final states are searched for inclusively by CMS in the full 8 TeV dataset in multilepton topologies [145]. The corresponding $t\bar{t}H$ modes can be simply decomposed in terms of the decays of the Higgs boson and those of the top quarks as having four W bosons in the final state (or two W and two taus) and two b-quarks. Three resulting distinctive topologies with leptonic decays of the W bosons or the taus have been investigate by CMS [145] with the full 8 TeV dataset: (i) the same

Table 11.4: Summary of the results in the five low mass Higgs channels measured at the LHC and the Tevatron. It should be noted that the ATLAS combined signal strength measurement only includes the bosonic $\gamma\gamma$, ZZ and WW channels. The latest result of the CMS experiment in the $H \to \tau^+\tau^-$ final state [132] is reported and denoted by (*).

	$\gamma\gamma$	ZZ (4ℓ)	WW ($\ell\nu\ell\nu$)	$\tau\tau$	W/Z(bb)	Combin
GeV)	$1.55^{+0.33}_{-0.28}$	$1.43^{+0.40}_{-0.35}$	$0.99^{+0.31}_{-0.28}$	$1.4^{+0.5}_{-0.4}$	0.2±0.7	1.3
	4.1	4.4	3.8	4.1	1.4	
	7.4	6.6	3.8	3.2	0.3	
)	126.8±0.2±0.7	124.3±0.5±0.5	–	–	–	125.5±0.2
	[119]	[119]	[119]	[133]	[138]	
GeV)	0.77±0.27	0.92±0.28	0.68±0.20	1.10±0.41	1.15±0.62	0.80±
				0.87±0.29*		
	3.9	7.1	5.3	2.6 (3.6*)	2.2	
	3.2	6.7	3.9	2.8 (3.4*)	2.0	
)	125.4±0.5±0.6	125.8±0.5±0.2				125.7±0.3
	[120]	[121]	[127]	[131,132]	[137]	
eV)	$6.0^{+3.4}_{-3.1}$	–	0.9±0.8	$1.7^{+2.3}_{-1.7}$	1.6±0.7	1.4
	[108]		[108]	[108]	[108]	

sign dileptons, (ii) the trileptons and (iii) the four leptons.

The results of all aforementioned analyses are reported in Table 11.5. CMS has performed a combination of all their channels [146] yielding an upper limit on the signal strength at the 95% CL of 4.3, while having an expected sensitivity of 1.8. This difference is due to an excess of events observed in various sensitive channels. The measured combined signal strength is $\mu = 2.5^{+1.1}_{-1.0}$, yielding first hints of the presence of a signal in this channel.

III.7. Searches for rare decays of the Higgs boson

III.7.1. $H \to Z\gamma$

The search for $H \to Z\gamma$ is performed in the final states where the Z boson decays into opposite sign and same flavor leptons ($\ell^+\ell^-$), ℓ here refers to e or μ. While the branching fraction for $H \to Z\gamma$ is comparable to $H \to \gamma\gamma$ (about 10^{-3}) at $m_H = 125\,\text{GeV}$, the observable signal yield is brought down by the small branching

Table 11.5: Summary of the results of searches for a Higgs boson in association with a top quark pair by the ATLAS and CMS collaborations. The results are given in terms of upper limits at the 95% CL on the signal strength, the expected limits are given in parentheses. For the results of the CMS searches, the measured signal strengths in each channel are also given. The ATLAS results indicated by ‡ are with the 7 TeV dataset only, and the results indicate by * are combining the full 7 TeV and 8 TeV datasets. The unmarked results are with the full 8 TeV dataset.

	ATLAS limits	CMS limits	CMS sig. strengths
$t\bar{t}(H \to \gamma\gamma)$	<5.3 (6.4)	<5.4 (5.5)	$\mu = -0.2^{+2.4}_{-1.9}$
$t\bar{t}(H \to b\bar{b})$	<13.1 (10.5)‡	<4.5 (3.7)*	$\mu = 1.0^{+1.9}_{-2.0}$
$t\bar{t}(H \to 4\ell)$	–	<6.8 (8.8)	$\mu = -4.8^{+5.0}_{-1.2}$
$t\bar{t}(H \to 3\ell)$	–	<6.7 (3.8)	$\mu = 2.7^{+2.2}_{-1.8}$
$t\bar{t}(H \to SS2\ell)$	–	<9.1 (3.4)	$\mu = 5.3^{+2.2}_{-1.8}$
$t\bar{t}(H \to \tau^+\tau^-)$	–	<12.9 (14.2)	$\mu = -1.4^{+6.3}_{-5.5}$
Combination	–	<4.3 (1.8)	$\mu = 2.5\ ^{+1.1}_{-1.0}$

ratio of $Z \to (e^+e^- + \mu^+\mu^-) = 6.7 \times 10^{-2}$. In these channels, the $m_{\ell\ell\gamma}$ mass resolution is excellent (1-3%) so the analyses search for a narrow mass peak over a continuous background. The major backgrounds arise from the $Z + \gamma$, final state radiation in Drell–Yan decays and $Z +$ jets process where a jet is misidentified as a photon.

Events are divided into mutually exclusive categories on basis of the expected $m_{Z\gamma}$ resolution and the signal-to-background ratio. A VBF category is formed for $H \to Z\gamma$ candidates which are accompanied by two energetic jets separated by a large pseudorapidity. While this category contains only about 2% of the total event count, the signal-to-noise is about an order of magnitude higher. The search for a Higgs boson is conducted independently in each category and the results from all categories are then combined.

No excess of events is observed. The expected and observed 95% CL upper limits [147] on the signal strength μ are 10 and 9.5 respectively for $m_H = 125\,\text{GeV}$. The ATLAS expected and observed upper limits [148] on μ are 13.5 and 18.2 respectively at that mass.

III.7.2. $H \to \mu^+\mu^-$

$H \to \mu^+\mu^-$ is the only channel where the Higgs coupling to second generation fermions can be measured at the LHC. The branching fraction in this channel for a 125 GeV SM Higgs boson is 2.2×10^{-4}, about ten times smaller than that for $H \to \gamma\gamma$. The dominant and irreducible background arises from the $Z/\gamma^* \to \mu^+\mu^-$ process which has a rate several orders of magnitude larger than that from the SM Higgs boson signal. Due to the precise muon momentum measurement achieved by ATLAS and CMS, the $m_{\mu^+\mu^-}$

mass resolution is excellent ($\approx 2-3\%$) but rendered marginally asymmetric due to final state radiation from the muons. A search is performed for a narrow peak over a large but smoothly falling background. For optimal search sensitivity, events are divided into several categories. To take advantage of the superior muon momentum measurement in the central region, the two experiments subdivide events by the pseudorapidity of the muons. To suppress the Drell–Yan background, ATLAS requires $p_T^{\mu^+\mu^-} > 15\,\text{GeV}$ while CMS separates them into two $p_T^{\mu^+\mu^-}$ based categories. CMS further categorizes events by the number and the topology of additional energetic jets in the event.

No excess in the $m_{\mu^+\mu^-}$ spectrum is observed near 125 GeV. From an analysis of $21\,\text{fb}^{-1}$ data at 8 TeV, ATLAS sets [149] a 95% CL upper limit on the signal strength $\mu < 9.8$. The CMS analysis [150] of their 7 and 8 TeV data sets a limit of $\mu < 7.4$.

III.7.3. Rare modes outlook

Rare decays such as those described in the above sections are clearly limited by statistics. They however already deliver a remarkable message. If the coupling of the Higgs boson was as strong in the dimuon channel as it is for the top quark, this mode would have been observed already with large significance. Thus it leads to the conclusion that, contrary to gauge bosons, the observed Higgs boson couples in a non-universal way to the different families of the SM fermions.

These searches play an increasingly important role in the characterization of the couplings of the Higgs particle. New channels such as those related to charm decays [151] and exclusive quarkonia final states such as $J/\Psi\gamma$ [152] are also of great interest.

III.8. Non-standard decay channels

The main decay and production properties of H are consistent with a standard model Higgs boson. It may however have other decay channels beyond those predicted by the Standard Model. Among these and of great interest are those invisible decays into stable particles that do not interact with the detector. The other non-standard decay channels that have been investigated are the decays of the Higgs particle to hidden valley or dark particles.

III.8.1. Invisible Higgs boson decays

The discovery of the Higgs particle has immediately raised the question of its couplings to dark matter and how it could be used to further try to reveal its existence at colliders, using the Higgs boson as a portal to dark matter, see Ref. [153] and references therein. If kinematically accessible and with a sufficiently large coupling to the Higgs boson, dark matter particles, such as, e.g., neutralinos in SUSY models or heavy neutrinos in the context of fourth generation of fermions models, would manifest themselves as invisible decays of the Higgs boson, thus strongly motivating searches for invisible decays of the Higgs boson.

Searches for invisible decays of the Higgs particle have been carried out in the following channels, taking advantage of the VBF and associated production with a vector boson

Table 11.6: Summary of the results of searches for invisible decays of the Higgs particle H. Results can be interpreted in terms of 95% CL limit on the invisible branching fraction for a Standard Model production cross section or as the ratio of the product of the ZH production cross section times the Higgs invisible branching fraction its SM expectation. The results in parentheses are the expected exclusions.

	ATLAS	CMS
$W, Z \to$ fatjet, $H \to$ inv.	1.6 (2.2)	–
$Z \to \ell^+\ell^-$, $H \to$ inv.	65% (84%)	75% (91%)
$Z \to b\overline{b}$, $H \to$ inv.	–	1.8 (2.0)
VBF $H \to$ inv.	–	69% (53%)

signatures: (i) the search for high transverse momentum mono-vector boson production by the ALTAS collaboration [154] using fat-jet substructure techniques; (ii) the associated production with a vector boson subsequently decaying either to a pair of leptons by the ATLAS [155] and the CMS [156] collaborations or a pair of b-quarks by CMS [157]; (iii) in the VBF production process by the CMS experiment [158]. An independent reinterpretation of the monojet search results by the ATLAS and CMS collaborations was also done in Ref. [153]. The results of these searches are reported in Table 11.6.

A combination of the VH and VBF channels by the CMS collaboration yields an upper limit on the invisible branching fraction of the Higgs boson, assuming SM production cross sections, of 54% at the 95% CL, while the expected sensitivity is 46% at 95% CL [156].

III.8.2. Exotic Higgs boson decays

The discovered Higgs particle not only serves as a probe for potential dark matter candidates, but also to search for other exotic particles arising from fields associated with a low-mass hidden sector. Such hidden sectors are composed of fields that are singlets under the SM group SU(3) $\times$ SU(2) $\times$ $U(1)$. These models are referred to as hidden valley models [159,160]. Since a light Higgs boson is a particle with a narrow width, even modest couplings to new states can give rise to a significant modification of Higgs phenomenology through exotic decays. Simple hidden valley models exist in which the Higgs boson decays to an invisible fundamental particle, which has a long lifetime to decay back to SM particles through small mixings with the SM Higgs boson; Ref. [160] describes an example. The Higgs boson may also decay to a pair of hidden valley "v-quarks," which subsequently hadronize in the hidden sector, forming "v-mesons." These mesons often prefer to decay to the heaviest state kinematically available, so that a possible signature is $h \to 4b$. Some of the v-mesons may be stable, implying a mixed missing energy plus heavy flavor final state. In other cases, the v-mesons may decay to leptons, implying the presence of low mass lepton resonances in high H_T events [161]. Other scenarios have been studied [162] in which Higgs bosons decay predominantly into light hidden sector particles, either directly, or through light SUSY states, and with subsequent cascades that increase the multiplicity of hidden sector particles. In such scenarios, the high multiplicity hidden sector particles, after decaying back into the Standard Model,

appear in the detector as clusters of collimated leptons known as lepton jets.

A variety of models have been investigated searching for final states involving dark photons and hidden valley scalars. The resulting topologies searched for are prompt electron jets in the WH production process [163], displaced muonic jets [164], the four muons final state where and the search for long lived weakly interacting particles [165]. The latter occur not only in hidden valley scenarios, but also in gauge-mediated extensions of the Minimal Supersymmetric Standard Model (MSSM), the MSSM with R-parity violation, and inelastic dark matter [166]. Finally the CMS collaboration has performed a search for pair production of light bosons [167]. Such a scenario can occur in supersymmetric models with additional hidden (or dark) valleys.

IV. Properties and nature of the new bosonic resonance

As discussed in Section II, within the SM, all the Higgs couplings are fixed unambiguously once all the particle masses are known. Any deviation in the measurement of the couplings of the recently discovered Higgs boson could thus signal the presence of new physics beyond the Standard Model.

Measuring the Higgs couplings without relying on the SM assumption requires a general framework treating deviations from the SM coherently at the quantum level in order to provide theoretical predictions for relevant observables to be confronted with experimental data. The effective Lagrangian approach offers such a coherent framework. It assumes that the new physics degrees of freedom are sufficiently heavy to be integrated out and simply give rise to effective interactions among the light SM particles. By construction these effective Lagrangians cannot account for deviations in Higgs physics induced by light degrees of freedom, unless they are added themselves as extra fields in the effective Lagrangians. In Section V, several examples of models with light degrees of freedom affecting Higgs production and decay rates will be presented.

IV.1. Theoretical framework

IV.1.1. Effective Lagrangian formalism

The most general $\mathrm{SU}(3)_C \times \mathrm{SU}(2)_L \times \mathrm{U}(1)_Y$-invariant Lagrangian for a weak doublet Φ at the level of dimension-6 operators was first classified in a systematic way in Ref. [168]. Subsequent analyses pointed out the presence of redundant operators, and a minimal and complete list of operators was finally provided in Ref. [169]. For a single family of fermions, there are 59 independent ways to deform the SM. With the 3 families of fermions of the SM, a flavor index can be added to these 59 operators. Furthermore, new operator structures, that have been dismissed by means of Fierz transformations in the single family case, have to be considered. Of particular interest are the 18 CP-invariant[6]

[6] When the 3 fermion families are considered, there is a nineteenth operator involving different families of leptons, $(\bar{L}^i\gamma^\mu\sigma^a L^i)(\bar{L}^j\gamma^\mu\sigma^a L^j)$, that alters the Fermi constant and hence indirectly affects the predictions of the Higgs rates. The coefficient of this operator is actually constrained by the fit of EW precision data and thus cannot give any observable deviation in Higgs physics.

and the 4 CP-breaking[7] deformation-directions, in addition to 8 dipole operators, that affect, at tree-level, the Higgs production and decay rates [170,171,172].

A convenient basis of these operators relevant for Higgs physics, assuming that the Higgs is a CP-even weak doublet and the baryon and lepton numbers are conserved, is the following:

$$\mathcal{L} = \mathcal{L}_{SM} + \sum_i \bar{c}_i \mathcal{O}_i \,, \tag{11.13}$$

where the operators are listed in Table 11.7, Table 11.8 and Table 11.9. When the operator $\mathcal{O}_i$ is not hermitian, like $\mathcal{O}_{t,b,\tau,Htb}$ and the dipole operators, it is understood that the hermitian-conjugated operator is added to the Lagrangian. The factor multiplying each operator in the effective Lagrangian has been conveniently defined such that the new physics dependence is fully encoded in the dimensionless coefficients $\bar{c}_i$ which will all have to be smaller than 1 to ensure the consistency of the expansion in terms of higher dimensional operators. The SM gauge couplings are denoted by g', g, g_S while $y_{t,b,\tau}$ are the SM Yukawa couplings (in the mass eigenstate basis that diagonalizes the general Yukawa coupling matrices $Y_{u,d,l}$), λ is the SM Higgs quartic coupling and v denotes the weak scale defined through the Fermi constant at tree-level $v \equiv 1/(\sqrt{2}G_F)^{1/2} \approx 246.2\,\text{GeV}$. $i\Phi^\dagger \overleftrightarrow{D}^\mu \Phi$ denotes the Hermitian derivative $i\Phi^\dagger(D^\mu\Phi) - i(D^\mu\Phi)^\dagger\Phi$, and $\sigma^{\mu\nu} \equiv i[\gamma^\mu, \gamma^\nu]/2$ and Φ^c is the Higgs charge-conjugate doublet: $\Phi^c = i\sigma^2\Phi^*$. Each operator $\mathcal{O}_{t,b,\tau}$ is further assumed to be flavor-aligned with the corresponding fermion mass term, as required in order to avoid large Flavor-Changing Neutral Currents (FCNC) mediated by the tree-level exchange of the Higgs boson. This implies one coefficient for the up-type quarks ($\bar{c}_t$), one for down-type quarks ($\bar{c}_b$), and one for the charged leptons ($\bar{c}_\tau$), i.e. the $\bar{c}_{t,b,\tau}$ matrices should be proportional to the identity matrix in flavor space. Requiring that the only source of flavor violation in the new physics sector are proportional to the SM Yukawa interactions, the so-called minimal flavor violation assumption, imposes the presence of the $y_u y_d$ factor in the $\mathcal{O}_{Hud}$ operator,and the Yukawa dependence in the 8 dipole operators, while all the other operators are flavor universal up to corrections like $Y_u Y_u^\dagger$ or $Y_d Y_d^\dagger$.

The choice of the basis of operators is not unique and using the equations of motion, i.e., performing field redefinitions, different dimension-6 operators can be obtained as linear combinations of the operators in the previous tables and of four-fermion operators. In particular, two other standard bases [173,169] involve the two extra bosonic operators

$$\begin{aligned} \mathcal{O}_{WW} &\equiv \frac{g^2}{4m_W^2}\,\Phi^\dagger\Phi\, W^i_{\mu\nu} W^{i\,\mu\nu} \\ &= \mathcal{O}_W - \mathcal{O}_B + \mathcal{O}_{HB} - \mathcal{O}_{HW} + \frac{1}{4}\,\mathcal{O}_{BB} \\ \mathcal{O}_{WB} &\equiv \frac{gg'}{4m_W^2}\,\Phi^\dagger\sigma^i\Phi\, W^i_{\mu\nu} B^{\mu\nu} = \mathcal{O}_B - \mathcal{O}_{HB} - \frac{1}{4}\,\mathcal{O}_{BB}\,. \end{aligned} \tag{11.14}$$

[7] In this counting, non-hermitian operators with fermions that could have complex Wilson coefficients and would also break the CP-invariance are not included.

Table 11.7: List of 9 CP-even and 4 CP-odd bosonic operators affecting Higgs production and decay rates. The 4 CP-odd operators involve the dual field strengths defined as $\tilde{F}_{\mu\nu} = 1/2\,\epsilon_{\mu\nu\rho\sigma}F^{\rho\sigma}$ for $F = W, B, G$ (ϵ is the totally antisymmetric tensor normalized to $\epsilon_{0123} = 1$). See text for notations.

Operators involving bosons only
$\mathcal{O}_H = 1/(2v^2)\left(\partial^\mu\left(\Phi^\dagger\Phi\right)\right)^2$
$\mathcal{O}_T = 1/(2v^2)\left(\Phi^\dagger \overleftrightarrow{D}^\mu \Phi\right)^2$
$\mathcal{O}_6 = -\lambda/(v^2)\left(\Phi^\dagger\Phi\right)^3$
$\mathcal{O}_B = (ig')/(2m_W^2)\left(\Phi^\dagger \overleftrightarrow{D}^\mu \Phi\right)(\partial^\nu B_{\mu\nu})$
$\mathcal{O}_W = (ig)/(2m_W^2)\left(\Phi^\dagger\sigma^i \overleftrightarrow{D}^\mu \Phi\right)(D^\nu W_{\mu\nu})^i$
$\mathcal{O}_{HB} = (ig')/m_W^2\,(D^\mu\Phi)^\dagger(D^\nu\Phi)B_{\mu\nu}$
$\mathcal{O}_{HW} = (ig)/m_W^2\,(D^\mu\Phi)^\dagger\sigma^i(D^\nu\Phi)W^i_{\mu\nu}$
$\mathcal{O}_{BB} = g'^2/m_W^2\,\Phi^\dagger\Phi\,B_{\mu\nu}B^{\mu\nu}$
$\mathcal{O}_{GG} = g_S^2/m_W^2\,\Phi^\dagger\Phi\,G^A_{\mu\nu}G^{A\mu\nu}$
$\mathcal{O}_{H\tilde{B}} = (ig')/m_W^2\,(D^\mu\Phi)^\dagger(D^\nu\Phi)\tilde{B}_{\mu\nu}$
$\mathcal{O}_{H\tilde{W}} = (ig)/m_W^2\,(D^\mu\Phi)^\dagger\sigma^i(D^\nu\Phi)\tilde{W}^i_{\mu\nu}$
$\mathcal{O}_{B\tilde{B}} = g'^2/m_W^2\,\Phi^\dagger\Phi\,B_{\mu\nu}\tilde{B}^{\mu\nu}$
$\mathcal{O}_{G\tilde{G}} = g_S^2/m_W^2\,\Phi^\dagger\Phi\,G^A_{\mu\nu}\tilde{G}^{A\mu\nu}$

Table 11.8: List of 9 operators with bosons and fermions affecting Higgs production and decay rates. See text for notations.

Ops. involving bosons and fermions
$\mathcal{O}_t = y_t/v^2\,(\Phi^\dagger\Phi)\,(\bar{q}_L\Phi^c t_R)$
$\mathcal{O}_b = y_b/v^2\,(\Phi^\dagger\Phi)\,(\bar{q}_L\Phi b_R)$
$\mathcal{O}_\tau = y_\tau/v^2\,(\Phi^\dagger\Phi)\,(\bar{L}_L\Phi\tau_R)$
$\mathcal{O}_{Hq} = i/v^2\,\left(\bar{q}_L\gamma^\mu q_L\right)\left(\Phi^\dagger\overleftrightarrow{D}_\mu\Phi\right)$
$\mathcal{O}^{(3)}_{Hq} = i/v^2\,\left(\bar{q}_L\gamma^\mu\sigma^i q_L\right)\left(\Phi^\dagger\sigma^i\overleftrightarrow{D}_\mu\Phi\right)$
$\mathcal{O}_{Hu} = i/v^2\,\left(\bar{u}_R\gamma^\mu u_R\right)\left(\Phi^\dagger\overleftrightarrow{D}_\mu\Phi\right)$
$\mathcal{O}_{Hd} = i/v^2\,\left(\bar{d}_R\gamma^\mu d_R\right)\left(\Phi^\dagger\overleftrightarrow{D}_\mu\Phi\right)$
$\mathcal{O}_{Hud} = i\,y_u y_d/v^2\,\left(\bar{u}_R\gamma^\mu d_R\right)\left(\Phi^{c\,\dagger}\overleftrightarrow{D}_\mu\Phi\right)$
$\mathcal{O}_{Hl} = i/v^2\,\left(\bar{l}_R\gamma^\mu l_R\right)\left(\Phi^\dagger\overleftrightarrow{D}_\mu\Phi\right)$

Table 11.9: List of 8 dipoles operators. See text for notations.

Ops. involving bosons and fermions
$\mathcal{O}_{uB} = (g'\, y_u)/m_W^2\, (\bar{q}_L \Phi^c \sigma^{\mu\nu} u_R)\, B_{\mu\nu}$
$\mathcal{O}_{uW} = (g\, y_u)/m_W^2\, (\bar{q}_L \sigma^i \Phi^c \sigma^{\mu\nu} u_R)\, W^i_{\mu\nu}$
$\mathcal{O}_{uG} = (g_S\, y_u)/m_W^2\, (\bar{q}_L \Phi^c \sigma^{\mu\nu} t^A u_R)\, G^A_{\mu\nu} R$
$\mathcal{O}_{dB} = (g'\, y_d)/m_W^2\, (\bar{q}_L \Phi \sigma^{\mu\nu} d_R)\, B_{\mu\nu}$
$\mathcal{O}_{dW} = (g\, y_d)/m_W^2\, (\bar{q}_L \sigma^i \Phi \sigma^{\mu\nu} d_R)\, W^i_{\mu\nu}$
$\mathcal{O}_{dG} = (g_S\, y_d)/m_W^2\, (\bar{q}_L \Phi \sigma^{\mu\nu} t^A d_R)\, G^A_{\mu\nu}$
$\mathcal{O}_{lB} = (g'\, y_l)/m_W^2\, (\bar{L}_L \Phi \sigma^{\mu\nu} l_R)\, B_{\mu\nu}$
$\mathcal{O}_{lW} = (g\, y_l)/m_W^2\, (\bar{L}_L \sigma^i \Phi \sigma^{\mu\nu} l_R)\, W^i_{\mu\nu}$

IV.1.2. Constraints on Higgs physics from other measurements

Among the 30 operators affecting Higgs physics, some of them were already severely constrained before the Higgs discovery and result in deviations of the Higgs couplings that remain below the LHC sensitivity. This is obviously the case of the operators giving rise to some oblique corrections

$$\Delta\epsilon_1 \equiv \Delta\rho \equiv \Delta\hat{T} = \bar{c}_T, \quad \Delta\epsilon_3 \equiv \Delta\hat{S} = \bar{c}_W + \bar{c}_B. \tag{11.15}$$

Electroweak precision data from LEP-I physics at the Z-pole constrain these oblique parameters and restrict the deviations of the couplings of the Z to e_R, u_L, u_R, d_L and d_R, leaving the following intervals for the values of the Wilson coefficients with 95% probability [171,174]

$$\begin{aligned}
-1.5 \times 10^{-3} < \bar{c}_T < 2.2 \times 10^{-3}\,, \\
-1.4 \times 10^{-3} < \bar{c}_W + \bar{c}_B < 1.9 \times 10^{-3}\,, \\
-5 \times 10^{-3} < \bar{c}_{Hl} < 0 \times 10^{-3}\,, \\
-1 \times 10^{-3} < \bar{c}_{Hq} < 2 \times 10^{-3}\,, \\
-8 \times 10^{-3} < \bar{c}_{Hu} < 0 \times 10^{-3}\,, \\
-53 \times 10^{-3} < \bar{c}_{Hd} < 1 \times 10^{-3}\,, \\
-7 \times 10^{-3} < \bar{c}^{(3)}_{Hq} < 4 \times 10^{-3}\,.
\end{aligned} \tag{11.16}$$

Two other linear combinations of the operators are constrained by the bounds on the anomalous triple gauge boson self-couplings [174]

$$\begin{aligned}
-8.8 \times 10^{-2} < \bar{c}_W - \bar{c}_B + \bar{c}_{HW} - \bar{c}_{HB} < 13.2 \times 10^{-2}\,, \\
-2.2 \times 10^{-2} < \bar{c}_{HW} + \bar{c}_{HB} < 1.9 \times 10^{-2}\,.
\end{aligned} \tag{11.17}$$

Notice, that there is one linear combination of the four bosonic operators $\mathcal{O}_B, \mathcal{O}_W, \mathcal{O}_{HB}$ and $\mathcal{O}_{HW}$ that remains unconstrained. This direction, $\bar{c}_B = -\bar{c}_W = -\bar{c}_{HB} = \bar{c}_{HW}$, induces a deviation of the $H \to Z\gamma$ decay rate that can thus only be constrained directly from the Higgs data. This free direction is a simple linear combination of $\mathcal{O}_{WW}$ and $\mathcal{O}_{BB}$.

The minimal flavor violation assumption imposes Yukawa dependences in the 8 dipole operators and in the $\mathcal{O}_{Hud}$ operator. For the light generations of fermions, this dependence lowers the induced deviations in the Higgs rates below the experimental sensitivity reachable in any foreseeable future. The corresponding operators in the top sector are not suppressed but they are already constrained by the limit of the top dipole operators imposed by the bounds on the neutron electric dipole moment, on the $b \to s\gamma$ and $b \to s\ell^+\ell^-$ rates and on the $t\bar{t}$ cross section [175,171].

Finally, in the CP-even sector, only 8 operators can potentially induce sizable deviations of the Higgs rates and can only be constrained, at tree-level, by Higgs data. These 8 operators correspond to $\{\mathcal{O}_H, \mathcal{O}_6, \mathcal{O}_{BB}, \mathcal{O}_{GG}, \mathcal{O}_{WW}, \mathcal{O}_t, \mathcal{O}_b, \mathcal{O}_\tau\}$, where by $\mathcal{O}_{WW}$ is the linear combination defined in Eq. (11.14). Section IV.2 illustrates how the Higgs data accumulated at the LHC can (partially) constrain the Wilson coefficients of these 8 directions. Automatic tools [171,176] are being developed to analyze the experimental data within an effective field theory framework.

IV.2. Experimental results

IV.2.1. Introduction

As described in Section II, there are five main production modes of a Standard Model Higgs boson at the LHC. In the current dataset corresponding to an integrated luminosity of approximately 20 fb^{-1} of pp collisions at 8 TeV, and approximately 5 fb^{-1} of collisions at 7 TeV, the predicted numbers of SM Higgs bosons produced per experiment are 0.5 million, 40,000, 20,000 and 3,000 events produced in the gluon fusion, vector boson fusion, the associated WH or ZH, and the associated $t\bar{t}H$ production modes respectively. The typical number of events selected eventually in each decay channel is then much smaller ranging from O(10) to O(100) events per experiment. For each main decay mode, exclusive categories according to production modes have been designed to maximize the sensitivity of the analyses to the presence of a signal and using known discriminating features of these modes. These categories can also be used to further separate production modes for each decay channel. Similarly at the Tevatron where the CDF and DØ experiments have gathered approximately 10 fb^{-1} of data at 1.96 TeV, the predicted numbers of SM Higgs boson events produced per experiment are approximately 10000 and 2000 events in the gluon fusion and VH associated production, respectively.

At the LHC or the Tevatron, in none of the production modes is the total cross section measurable. As a consequence, neither absolute branching fractions nor the total natural width of the Higgs boson can be directly measured. However a combined measurement of the large variety of categories described in Section III, with different sensitivities to various production and decay modes permits a wide variety of measurements of the

production, decay or in general coupling properties. These measurements require in general a limited but nevertheless restrictive number of assumptions.

IV.2.2. Measuring the signal in categories

For each category of a given channel the number of signal events yield can be measured and be converted to signal strengths per categories μ_c. These categories signal strengths can be expressed as follows in terms of the number of signal events fitted in a given category c:

$$n^c_{signal} = \mu_c(\sum_i \sigma_{i,SM} \times A^c_{if} \times \varepsilon^c_{if}) \times B_{f,SM} \times \mathcal{L} \tag{11.18}$$

where A represents the detector acceptance, ε the reconstruction efficiency and $\mathcal{L}$ the integrated luminosity. μ_c can be interpreted as the ratio of the number of signal events n^c_{signal} fitted in category c divided by the expected number of events in that category. The production index $i \in \{ggH, VBF, VH, ttH\}$ and the decay index $f \in \{\gamma\gamma, WW, ZZ, b\bar{b}, \tau\tau\}$. Typically a given category covers mainly one decay mode, but possibly various production modes. Table 11.10 summarizes the individual categories signal strengths for the main categories considered by the two experiments ATLAS [119] and CMS [177] in their combined measurement of the coupling properties of the H. It should be noted that the ATLAS combination does not include the $b\bar{b}$ [178] and $\tau^+\tau^-$ channels [179]. The results of these two individual channels are nonetheless reported in Table 11.10. It should also be noted that the CMS combination includes the search for a Higgs boson in the $b\bar{b}$ decay channel and produced in association to a pair of top quarks [180].

From the categories individual signal strengths, an already quite coherent picture emerges with a good consistency of the observation in each of the channels categories with the expectation for a Standard Model Higgs boson. The errors on the measurements reported in Table 11.10 reflect both statistical and systematic uncertainties.

IV.2.3. Characterization of the main production modes

Coupling properties can be measured via a combined fit of all categories simultaneously with a parametrization of the number of signal events per categories defined as follows.

$$n^c_{signal} = (\sum_i \mu_i \sigma_{i,SM} \times A^c_{if} \times \varepsilon^c_{if}) \times \mu_f \times B_{f,SM} \times \mathcal{L}\,, \tag{11.19}$$

where μ_i and μ_f are the main parameters of interest. It is manifest in the above equation that production mode (μ_i) and decay mode (μ_f) signal strengths cannot be determined simultaneously. However given that in the main channels the decay mode strength parameters factorize, for each decay mode individually, the products of the $\mu_i \times \mu_f$, where f is fixed can be measured simultaneously. The results of such fits in the $H \to \gamma\gamma$, $H \to W^{(*)}W^{(*)} \to \ell\nu\ell\nu$ and $H \to Z^{(*)}Z^{(*)} \to 4\ell$ channels are shown in Fig. 11.17, illustrating a probe of the main production modes, where the small $t\bar{t}H$ mode component is assumed to scale as the gluon fusion mode ($\mu_{ggH+ttH} = \mu_{ggH} = \mu_{ttH}$). Similarly the VBF and VH production modes are scaled simultaneously ($\mu_{VBF+VH} = \mu_{VBF} = \mu_{VH}$).

Table 11.10: Summary of the individual categories signal strengths for the main analysis channels of ATLAS (A) and CMS (C). It should be noted that the expected number of SM signal events in each category is typically composed of various production modes. * denotes those results which are are not in the combination. ‡ denotes the $H \to \tau^+\tau^-$ ATLAS analysis which is the only measurement not based on the full dataset, but the full 2011 7 TeV dataset and a partial 2012 8 TeV set of pp collision events, corresponding to an integrated luminosity of approximately 13 fb^{-1}.

	$\gamma\gamma$	ZZ (4ℓ)	WW ($\ell\nu\ell\nu$)	$\tau^+\tau^-$	b
tagged	0.7 ± 0.3 (C)	$1.6^{+0.5}_{-0.4}$ (A)	—	—	–
w ptT	$1.6^{+0.5}_{-0.4}$ (A)	—	—	—	–
gh ptT	$1.7^{+0.7}_{-0.6}$ (A)	—	—	—	–
1-jet tag	—	0.9 ± 0.3 (C)	$0.82^{+0.33}_{-0.32}$ (A)	—	–
	—	—	0.7 ± 0.2 (C)	0.8 ± 0.6 (C)	–
BF tag	$1.9^{+0.8}_{-0.6}$ (A)	$1.2^{+1.6}_{-0.9}$ (A)	$1.4^{+0.7}_{-0.6}$ (A)	—	
	$1.0^{+0.6}_{-0.5}$ (C)	$1.2^{+0.6}_{-0.9}$ (C)	$0.6^{+0.6}_{-0.5}$ (C)	$1.4^{+0.7}_{-0.6}$ (C)	$1.3^{+0.7}_{-0.6}$ (C
H tag	$1.3^{+1.2}_{-1.1}$ (A)	—	—		0.2 ± 0.7 (A*
	$0.6^{+1.3}_{-1.1}$ (C)	—	$0.5^{+1.3}_{-0.9}$ (C)	$1.0^{+1.7}_{-1.5}$ (C)	$1.4^{+0.7}_{-0.6}$ (C*
H tag	—	—	—	—	$0.1^{+2.8}_{-2.9}$ (C
verall	1.5 ± 0.3 (A)	1.4 ± 0.4 (A)	1.0 ± 0.3 (A)	0.7 ± 0.7 (A*)	0.2 ± 0.7 (A*
	0.8 ± 0.3 (C)	0.9 ± 0.3 (C)	0.7 ± 0.2 (C)	1.1 ± 0.4 (C)	1.1 ± 0.6 (C

The SM expectation correspond to the (1,1) coordinates. The aspect ratio of the contours of Fig. 11.17 also shows the relative strength of the gluon fusion and the VBF+VH the observations for each individual channel.

IV.2.4. Evidence for VBF production

To cancel the dependence on the branching fractions, a measure of the presence of a VBF or VBF+VH signal is given by the ratio of the productions times decay signal strength parameters.

$$\rho_{VBF+VH,ggH+ttH} = \frac{\mu_{VBF+VH}\mu_f}{\mu_{ggF+ttH}\mu_f} = \frac{\mu_{VBF+VH}}{\mu_{ggF+ttH}} \tag{11.20}$$

For the VBF-only ratio $\rho_{VBF,ggH+ttH}$, the VH production mode is independently determined from the fit, thus needing at least one exclusive category to be sensitive enough to VH in order to remove the degeneracy with the VBF signal. The measured

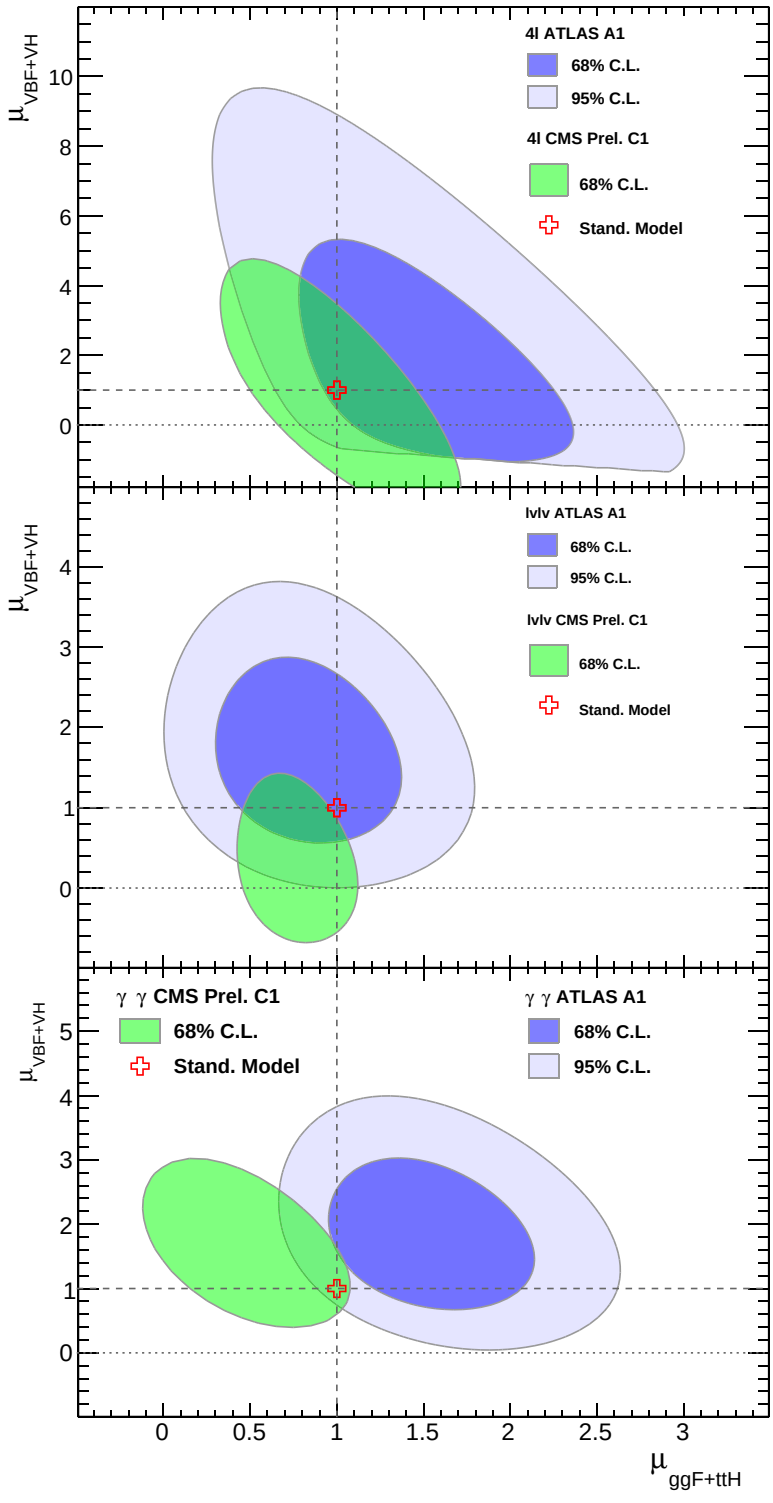

Figure 11.17: Likelihood contours for individual production mode signal strengths ($ggF + ttH$ versus $VBF + VH$) for various decay modes for the ATLAS experiment A1 [119] and the CMS experiment C1 [120] results.

values of these parameters by the ATLAS (A) and CMS (C) experiments are the following:

$$\begin{aligned} \rho_{VBF,ggH+ttH} &= 1.1^{+0.4}_{-0.3} \ (A) \\ \rho_{VBF+VH,ggH+ttH} &= 1.1^{+0.4}_{-0.3} \ (A) \\ \rho_{VBF+VH,ggH+ttH} &= 1.7^{+0.7}_{-0.5} \ (C) \end{aligned} \tag{11.21}$$

The observation by ATLAS excludes a value of the $\rho_{VBF,ggH+ttH} = 0$ at more than 3σ, thus providing a quantitative evidence for VBF production. The observations by ATLAS and CMS exclude a value of $\rho_{VBF+VH,ggH+ttH} = 0$ at an even greater level of confidence.

IV.2.5. Measurement of the coupling properties of H

(i) From effective Lagrangians to Higgs observables

All 8 operators of the effective Lagrangian Eq. (11.13) that were unconstrained before the Higgs data induce, at tree-level, deviations in the Higgs couplings that respect the Lorentz structure of the SM interactions, or generate simple new interactions of the Higgs boson to the W and Z field strengths, or induce some contact interactions of the Higgs boson to photons (and to a photon and a Z boson) and gluons that take the form of the ones that are generated by integrating out the top quark. In other words, the Higgs couplings are described, in the unitary gauge, by the following effective Lagrangian [181,38]

$$\begin{aligned} \mathcal{L} = & \kappa_3 \frac{m_H^2}{2v} H^3 + \kappa_Z \frac{m_Z^2}{v} Z_\mu Z^\mu H + \kappa_W \frac{2m_W^2}{v} W^+_\mu W^{-\mu} H \\ & + \kappa_g \frac{\alpha_s}{12\pi v} G^a_{\mu\nu} G^{a\mu\nu} H + \kappa_\gamma \frac{\alpha}{2\pi v} A_{\mu\nu} A^{\mu\nu} H + \kappa_{Z\gamma} \frac{\alpha}{\pi v} A_{\mu\nu} Z^{\mu\nu} H \\ & + \kappa_{VV} \frac{\alpha}{2\pi v} \left(\cos^2\theta_W Z_{\mu\nu} Z^{\mu\nu} + 2\, W^+_{\mu\nu} W^{-\mu\nu} \right) H \\ & - \left(\kappa_t \sum_{f=u,c,t} \frac{m_f}{v} f\overline{f} + \kappa_b \sum_{f=d,s,b} \frac{m_f}{v} f\overline{f} + \kappa_\tau \sum_{f=e,\mu,\tau} \frac{m_f}{v} f\overline{f} \right) H. \end{aligned} \tag{11.22}$$

The correspondence between the Wilson coefficients of the dimension-6 operators and the κ's is given in Table 11.11. In the SM, the Higgs boson does not couple to massless gauge bosons at tree level, hence $\kappa_g = \kappa_\gamma = \kappa_{Z\gamma} = 0$. Nonetheless, the contact operators are generated radiatively by SM particles loops. In particular, the top quark gives a contribution to the 3 coefficients $\kappa_g, \kappa_\gamma, \kappa_{Z\gamma}$ that does not decouple in the infinite top mass limit. For instance, in that limit $\kappa_\gamma = \kappa_g = 1$ [19,20,182] (the contribution of the top quark to $\kappa_{Z\gamma}$ can be found in Ref. [182]).

The coefficient for the contact interactions of the Higgs boson to the W and Z field strengths is not independent but obeys the relation

$$(1 - \cos^4\theta_W)\kappa_{VV} = \sin 2\theta_W \kappa_{Z\gamma} + \sin^2\theta_W \kappa_{\gamma\gamma}. \tag{11.23}$$

Table 11.11: Correspondence between the κ's and the Wilson coefficients of the dimension-6 operators of the Higgs EFT Lagrangian constrained only by Higgs physics.

Coupling modifier	Wilson coefficient dependence
κ_3	$1 + \bar{c}_6 - 3\bar{c}_H/2$
κ_V	$1 - \bar{c}_H/2$
κ_f	$1 - \bar{c}_f - \bar{c}_H/2$
κ_γ	$(2\pi/\alpha)\, \sin^2\theta_W\, (4\bar{c}_{BB} + \bar{c}_{WW})$
$\kappa_{Z\gamma}$	$(\pi/\alpha)\, \sin 2\theta_W\, \bar{c}_{WW}$
κ_{VV}	$(\pi/\alpha)\, \bar{c}_{WW}$
κ_g	$(48\pi/\alpha)\, \sin^2\theta_W\, \bar{c}_{GG}$

This relation is a general consequence of the custodial symmetry [171]. When the Higgs boson is part of an $SU(2)_L$ doublet, the custodial symmetry could only be broken by the $\mathcal{O}_T$ operator at the level of dimension-6 operators and it is accidentally realized among the interactions with four derivatives, like the contact interactions considered.

The coefficient κ_3 can be accessed only through double Higgs production processes, hence it will remain largely unconstrained at the LHC. The LHC will also have a limited sensitivity on the coefficient κ_τ since the lepton contribution to the Higgs production cross section remains subdominant and the only way to access the Higgs coupling is via the $H \to \tau^+\tau^-$ and possibly $H \to \mu^+\mu^-$ channels. Until the associated production of a Higgs with a pair of top quarks is observed, the Higgs coupling to the top quark is only probed indirectly via the one-loop gluon fusion production or the radiative decay into two photons. However, these two processes are only sensitive to the two combinations $(\kappa_t + \kappa_g)$ and $(\kappa_t + \kappa_\gamma)$ and a deviation in the Higgs coupling to the top quark can in principle always be masked by new contact interactions to photons and gluons.

The operators already bounded by EW precision data and the limits on anomalous gauge couplings modify in general the Lorentz structure of the Higgs couplings and hence induce some modifications of the kinematical differential distributions [183,174]. A promising way to have a direct access to the Wilson coefficients of these operators in Higgs physics is to study the VH associated production with a W or a Z at large invariant mass [183,184]. It has not been estimated yet whether the sensitivity on the determination of the Wilson coefficients in these measurements can compete with the one derived for the study of anomalous gauge couplings. In any case, these differential distributions could also be a way to directly test the hypothesis that the Higgs boson belongs to a $SU(2)_L$ doublet together with the longitudinal components of the massive electroweak gauge bosons.

(ii) Interpretations of the experimental data

To further interpret the observations in the analysis categories, a global approach can be adopted where the μ_i and μ_f categories signal strength parameters are further interpreted in terms of modifiers of the SM couplings κ_k where $k \in \{Z, W, f, g, \gamma, Z\gamma\}$ as

in Eq. (11.22). These coupling modifiers κ are motivated as leading order coupling scale factors defined such that the cross sections σ_j and the partial decay widths Γ_j associated with the SM particle j scale with the factor κ_j^2 when compared to the corresponding SM prediction. The number of signal events per category for the various production modes are typically estimated at higher orders in the analyses but are scaled by these single LO-inspired factors, thus not taking into account possible intricacies and correlations of these parameters through the higher order corrections. This approximation is valid within the level of precision of current results and their compatibility with the SM expectation.

The κ_g, κ_γ and $\kappa_{Z\gamma}$, can be treated effectively as free parameters in the fit or in terms of the know SM field content and as a function of the SM coupling modifiers, in the following way:

$$\begin{aligned}\kappa_g^2(\kappa_t,\kappa_b) &= 1.06\cdot\kappa_t^2 - 0.07\cdot\kappa_t\kappa_b + 0.01\cdot\kappa_b^2\\ \kappa_\gamma^2(\kappa_F,\kappa_V) &= 1.59\cdot\kappa_V^2 - 0.66\cdot\kappa_V\kappa_F + 0.07\cdot\kappa_F^2\\ \kappa_{Z\gamma}^2(\kappa_F,\kappa_V) &= 1.12\cdot\kappa_V^2 - 0.15\cdot\kappa_V\kappa_F + 0.03\cdot\kappa_F^2\end{aligned} \tag{11.24}$$

These parametrizations are given for a Higgs boson mass hypothesis of 125 GeV. It can be noted from the expression of κ_γ that the coupling of the Higgs boson to photons is dominated by the loop of W bosons, and it is affected by the top quark loop mostly through its interference with the W loop. The sensitivity of the current measurements to the relative sign of the fermion and vector boson couplings to the Higgs boson is due to this large negative interference term. The κ_g parameter is expressed in terms of the scaling of production cross sections and therefore also depends on the pp collisions centre-of-mass energy. The parametrizations of κ_γ and $\kappa_{Z\gamma}$ are obtained from the scaling of partial widths and are only dependent on the Higgs boson mass hypothesis. Experiments use a more complete parametrization with the contributions from the b-quarks, τ-leptons in the loop [181,38].

The global fit is then performed expressing the μ_i and μ_f parameters in terms of a limited number of κ_k parameters or their ratios, under various assumptions. The parametrization for the production modes are: $\mu_{ggF} = \kappa_g^2$ for the gluon fusion; $\mu_{VBF,VH} = \kappa_V^2$ for the VBF and VH processes when the W and Z couplings are assumed to scale equally, and the following expression for the VBF production mode is used:

$$\kappa_{VBF}^2(\kappa_W,\kappa_Z) = \frac{\kappa_W^2\sigma_{WWH} + \kappa_Z^2\sigma_{ZZH}}{\sigma_{WWH}+\sigma_{ZZH}} \tag{11.25}$$

when the couplings to the W and Z bosons are varied independently (σ_{WWH} and σ_{ZZH} denote the VBF cross sections via the fusion of a W and a Z boson respectively, the small interference term is neglected); $\mu_{ttH} = \kappa_t^2$ for the $t\bar{t}$H production mode. The decay mode signal strengths are parametrized as $\mu_k = \kappa_k^2/\kappa_H^2$ where $k \in \{Z, W, f, g, \gamma, Z\gamma\}$ denotes the decay mode and κ_H the overall modifier of the total width. Similarly to κ_g, κ_γ, and $\kappa_{Z\gamma}$, κ_H can be treated as an effective parameter or expressed in terms of the coupling modifiers to the SM field content.

Beyond this approximation two further assumptions are implicitly made: (i) the signals observed in the different search channels originate from a single narrow resonance with a

mass of 125 GeV. The width of the assumed Higgs boson is neglected, both in the fitted signal model (for both approaches) and in the zero-width approximation (in the second case to allow the decomposition of signal yields); (ii) the tensor structure of the couplings is assumed to be the same as that of a SM Higgs boson. This means in particular that the observed state is assumed to be a CP-even scalar as in the SM.

A global fit to the data is then performed to specifically test three aspects of the coupling properties of the H under different assumptions: (i) the relative couplings of the Higgs boson to fermions and bosons; (ii) the relative couplings of the Higgs boson to the W and the Z, and (iii) the potential impact of the presence of new particles beyond the SM either in the loops or both in the loops and the decay of the H.

(iii) Relative couplings to bosons and fermions

In this benchmark only SM particles are assumed to contribute to the gluon fusion and the diphoton loops, all fermion couplings modifiers are required to scale simultaneously with a unique factor κ_F and all vector boson couplings modifiers must scale simultaneously with a unique factor κ_V. The global fit is then performed under both the assumption that no new particles affect the direct decays or the loops, and without assumptions on the total width.

In the first scenario it is a two parameters fit with κ_V and κ_F as parameters of interest. The contours from the two LHC experiments and the Tevatron combination are shown in Fig. 11.18.

The global fit is only sensitive to the relative sign of κ_V and κ_F. By convention negative values of κ_F are considered. Such values are not excluded a priori, but would imply the existence of new physics at a light scale and would also raise questions about the stability of such a vacuum [185]. Among the five low mass Higgs channels, only the $\gamma\gamma$ is sensitive to the sign of κ_F through the interference of the W and t loops as shown in Eq. (11.24). The current global fit disfavors a negative value of κ_F at more than two standard deviations. A specific analysis for the Higgs boson production in association with a single top quark has been proposed [186,187] in order to more directly probe the sign of κ_F. All available experimental data show a fair agreement of the SM prediction of the couplings of the Higgs boson to fermions and gauge bosons. These results yield an indirect evidence for the coupling of the H to fermions.

In the second scenario the number of signal events per categories are parametrized using the two following parameters $\lambda_{FV} = \kappa_F/\kappa_V$ and $\lambda_{VV} = \kappa_V^2/\kappa_H$ where no assumption is made on the total width. It should be noted that this scenario corresponds to a model where the total width can vary but the field content that might modify the width should not sizably affect the loops.

The results for these two scenarios are reported in Table 11.12.

(iv) Probing the ratio of couplings to the W and Z bosons

The ratio of the couplings of the Higgs boson to W and Z bosons is an important probe of the EWSB mechanism as it is directly related to the tree level prediction $\rho = 1$ and the custodial symmetry. The W to Z couplings are probed in various production

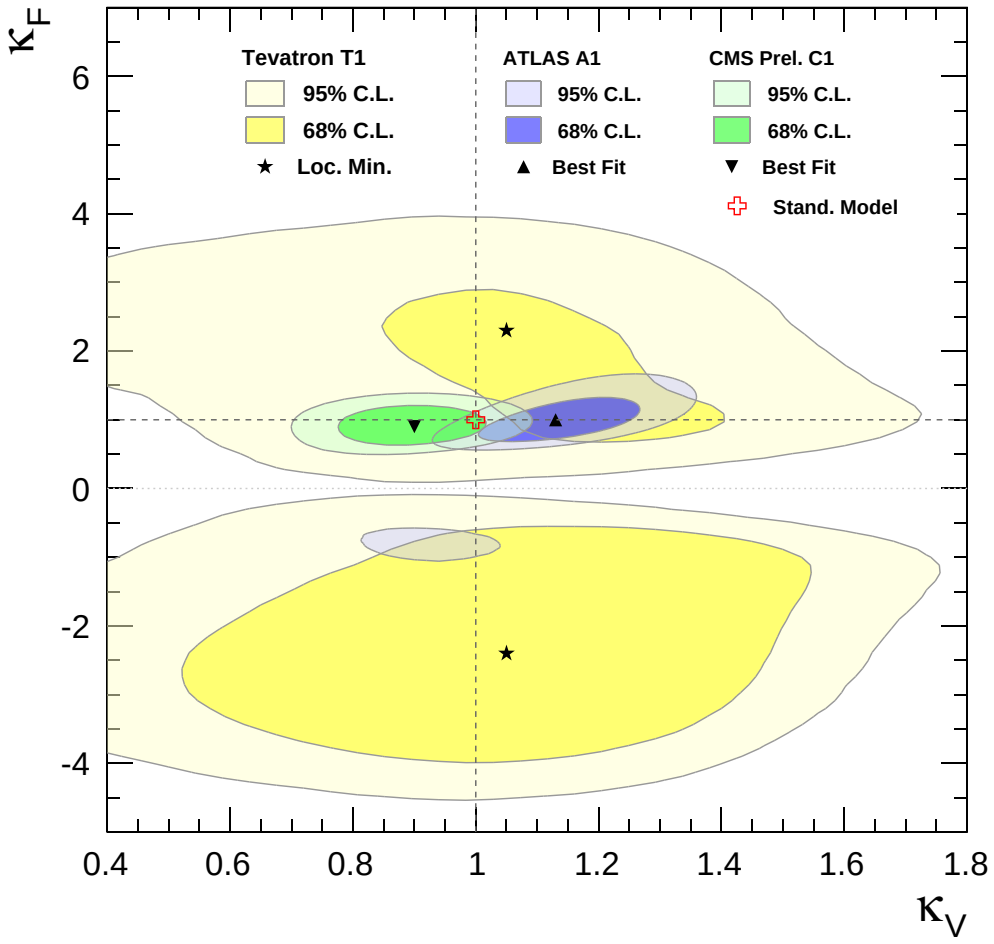

Figure 11.18: Likelihood contours of the global fit in the (κ_F, κ_V) plane for the ATLAS A1 [119], the CMS C1 [120] and the D0 and CDF combined T1 [108] results.

processes and decay modes of the Higgs boson. The ratio $\lambda_{WZ} = \kappa_W/\kappa_Z$ can therefore be probed under a large number of conditions.

The first requires that all fermion couplings scale with a single coupling modifier κ_F and the total width is allowed to vary, embedded in a single factor κ_{ZZ}. Both the ATLAS and CMS experiments have performed the a global fit using this model. Similarly to the λ_{FV} ratio, no assumption is made on the total width but the loops assume exclusively a SM content.

In order to be less dependent on loops, which in the case of the diphoton decay channel are dominated by the coupling to the W boson, and to the yet to be fully established coupling to fermions, since the main channels in the direct fermion decay channels rely on production processes dominated by gauge boson couplings (VH and VBF), additional models are used. In the first, performed by CMS only and denoted λ^*_{WZ} in Table 11.12,

only the $H \to W^{(*)}W^{(*)} \to \ell\nu\ell\nu$ and $H \to Z^{(*)}Z^{(*)} \to 4\ell$ channels are used in the fit. The second, similar to the latter and performed by the ATLAS collaboration only, consists in a fit of the ratio of categories signal strengths:

$$(\lambda^{\circ}_{WZ})^2 = \frac{\mu_{H\to WW^*}}{\mu_{H\to ZZ^*}} \tag{11.26}$$

The other parameters of this model are the $\mu_{ggF+ttH} \times \mu_{H\to ZZ^*}$ and the ratio $\mu_{VBF+VH}/\mu_{ggF+ttH}$ which are fitted independently.

In the third, performed by ATLAS, the coupling to photons is taken as effective in the fit, thus decoupling the observation in the diphoton channel. The latter is denoted $\lambda^{\ddagger}_{WZ}$.

The results of all models are reported in Table 11.12. For all models probed the measured ratios λ_{WZ} are compatible with the SM expectation. Although these measurements are not the most precise tests of the custodial symmetry it is of fundamental check of the nature of the electroweak symmetry breaking mechanism to see that the ratio of the couplings of the H to the W and Z bosons are compatible with what is expected from the SM Higgs sector.

(v) Probing new physics in loops and in the decay

In the models described above the assumption is that no new fields sizably distort the loop contributions in the couplings of the H to gluons and photons and its couplings to known SM particles are probed. Assuming that the couplings of the H are equal to their SM expectation, the effective coupling of the H to photons and gluons can be used to probe new physics beyond the SM through the loops. These assumptions can be simply expressed as $\kappa_F = \kappa_V = 1$ and the κ_g and κ_γ couplings modifiers are free in the fit. A first approach is to probe for new physics beyond the SM in the loops and not in the decay. The total width is then defined as a function of the two effective coupling modifiers (for a Higgs boson mass hypothesis of $m_H = 125\,\text{GeV}$) as follows.

$$\kappa^2_H = 0.085 \cdot \kappa^2_g + 0.0023 \cdot \kappa^2_\gamma + 0.91. \tag{11.27}$$

The results of the combined fits performed by the ATLAS and CMS experiments are given in Table 11.12 and the contours of the combined likelihood in the $(\kappa_\gamma, \kappa_g)$ plane are shown in Fig. 11.19.

In the second approach, new physics is considered also in the decay thus affecting the total width of the H through decays to particles which are either "invisible" in that they escape detection in the experiments, or "undetected" in that they are not distinctive enough to be seen in the current analyses. This contribution is parametrized as an invisible and undetected branching fraction $Br_{inv,und}$ which is fitted in addition to the κ_γ and κ_g parameters. The ATLAS result on $Br_{inv,und}$ is from the preliminary combination including the fermion modes [116]. The results of this fit are also reported in Table 11.12. This indirect approach, can be combined with direct invisible decay searches.

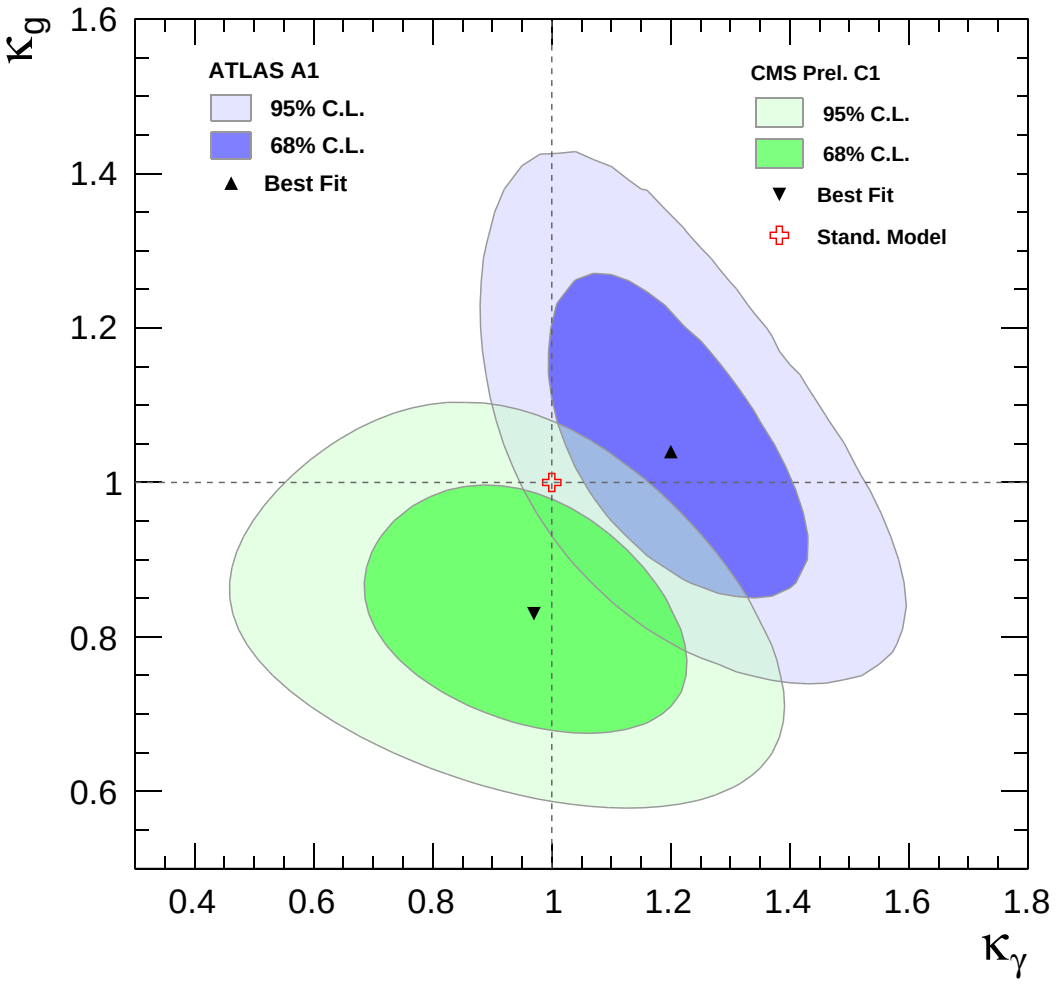

Figure 11.19: Likelihood contours of the global fit in the $(\kappa_g, \kappa_\gamma)$ plane for the ATLAS experiment A1 [119] and the CMS experiment C1 [120] results.

(vi) Generic measurement of the H couplings to fermions and gauge bosons

A more generic model testing the couplings of the H to the W and Z bosons through a single coupling modifier parameter κ_V and the couplings to the third generation fermions are tested separatedly κ_b, κ_τ and κ_t. In this model the effective couplings to photons and gluons take into account possible loop induced contributions in the κ_γ and κ_g modifiers, respectively. The assumption is that no additional contribution affect the total width and that the couplings to the fermions of the first and second generation are equal to those of the third (separating charged leptons, and up and down type quarks).

The results of this global fit are reported in Table 11.12. It illustrates the good agreement of the measured coupling modifiers with the SM Higgs boson couplings, in particular with its dependence in mass as described in Section II.

Table 11.12: Summary of the coupling properties measurements in terms of 68% confidence intervals. The ATLAS limit on the invisible or undetected branching fraction denoted by (*) is from the preliminary combination reported in Ref. [116].

	ATLAS	CMS
κ_F	$[0.76, 1.18]$	$[0.71, 1.11]$
κ_V	$[1.05, 1.22]$	$[0.81, 0.97]$
λ_{FV}	$[0.70, 1.01]$	–
λ_{WZ}	$[0.67, 0.97]$	$[0.73, 1.00]$
λ^{*}_{WZ}	–	$[0.75, 1.13]$
λ°_{WZ}	$[0.66, 0.97]$	–
$\lambda^{\ddagger}_{WZ}$	$[0.61, 1.04]$	–
κ_g	$[0.90, 1.18]$	$[0.73, 0.94]$
κ_γ	$[1.05, 1.35]$	$[0.79, 1.14]$
$\mathrm{BR}_{inv,und}$	$< 60\%^{*}$ at 95% CL	$< 64\%$ at 95% CL
κ_V	–	$[0.84, 1.23]$
κ_b	–	$[0.61, 1.69]$
κ_τ	–	$[0.82, 1.45]$
κ_t	–	$[0.00, 2.03]$
κ_g	–	$[0.65, 1.15]$
κ_γ	–	$[0.77, 1.27]$

IV.2.6. Differential cross sections

To further characterize the production and decay properties of H, first measurements of fiducial and differential cross sections have been carried out by the ATLAS collaboration [188], with the 8 TeV dataset of pp collision at LHC, corresponding to an integrated luminosity of 20.3 fb^{-1}, in the diphoton channel. The selection criteria to define the fiducial volume are the following: the two highest transverse momentum (E_T), isolated final state photons, within $|\eta| < 2.37$ and with $105\,\mathrm{GeV} < M_{\gamma\gamma} < 160\,\mathrm{GeV}$ are selected (the transition region between the barrel and endcap calorimeters is not removed); after the pair is selected, the same cut on $E_T/M_{\gamma\gamma}$ as in the event selection *i.e.* in excess of 0.35 (0.25) for the two photons is applied. Several observables have been studied: the transverse momentum rapidity of the diphoton system, the production angle in the Collins–Soper frame, the jet multiplicity, the jet veto fractions for a given jet multiplicity, and the transverse momentum distribution of the leading jet. The following additional observables: the difference in azimuthal angle between the leading and the

subleading jets, and the transverse component of the vector sum of the momenta of the Higgs boson and dijet system, have also been measured in two jet events. To minimize the model dependence the differential cross sections are given within a specific fiducial region of the two photons. The observables were chosen to probe the production properties and the spin and parity of the H. The differential cross section in H transverse momentum is given in Fig. 11.20.

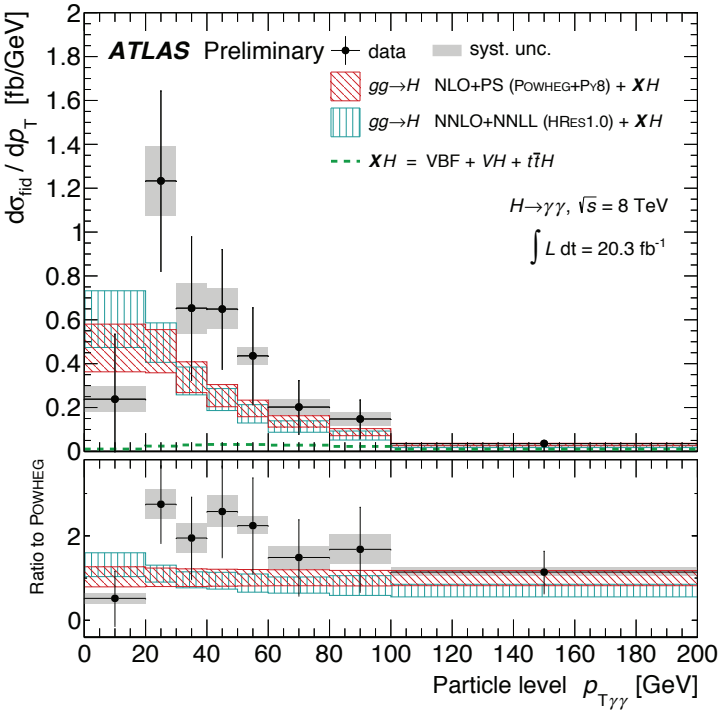

Figure 11.20: Observed differential cross sections in transverse momentum of the H in the diphoton channel, compared to the prediction of the ggH process [188].

IV.3. Main quantum numbers J^{PC}

The measurements of the signal event yields of the observed new state in all the channels discussed above and their compatibility with the Standard Model Higgs boson predictions, gives qualitative, but nonetheless compelling evidence of its nature. This qualitative picture is further complemented by the implications of the observation of the particle in the diphoton channel. According to the Landau–Yang theorem [189], the observation made in the diphoton channel excludes the spin 1 hypothesis and restricts possibilities for the spin of the observed particle to 0 or 2.

However, the Landau–Yang theorem does not apply if the observed state is not decaying to a pair of photons but to a pair of scalars subsequently decaying to two very collimated pairs of photons (as for example in the case of $H \to a_1 a_1 \to 4\gamma$). This possibility has not been rigorously tested but it is not experimentally favored as tight

selection criteria are applied on the electromagnetic shower shapes of the reconstructed photons. A more systematic analysis of shower shapes and the fraction of conversions could be performed to further discriminate between the single prompt photon and the two overlapping photons hypotheses. There are also potential theoretical loopholes concerning the applicability of the Landau–Yang theorem, such as off-shell vector boson decays.

For the observed particle not to be of spin 0 and +1 parity would require an improbable conspiracy of effects. It is nevertheless very important that this hypothesis be independently tested.

IV.3.1. Charge conjugation C

The charge conjugation quantum number is multiplicative, therefore given that the Higgs-like particle is observed in the $H \to \gamma\gamma$ channel, and given that photons are C-odd eigenstates, assuming C conservation, the observed neutral particle should be C-even.

IV.3.2. General framework

To further assess the spin and parity quantum numbers of the discovered particle, a systematic analysis of its production and decay processes is performed. These analyses have been designed to be as independent as possible from the event yields measured in each exclusive categories, relying instead on the production and the decay angles, and on the threshold distributions, of the produced particle.

This leads to test hypotheses which are typically disfavored by the analysis of the rates, such as a pseudoscalar particle decaying to a pair of W or Z bosons which requires, decays through loops or to test spin 2 hypotheses for which no renormalizable model exist. The sizable interaction of the observed state with electroweak gauge bosons, if it were pseudoscalar, would imply low scale physics in the loops and therefore would be ruled out by the absence of direct observation of such states.

To define, generate and test the newly observed state without theoretical prejudice, the most general tensor structure is used for the three possible spin hypotheses of spin 0, spin 1 and spin 2. The most general spin-0 interaction amplitude with two gauge bosons can be written as follows [190,191]

$$\begin{aligned} A^{(0)} =& v^{-1}\left(g_1^{(0)} m_V^2 \varepsilon_1^* \varepsilon_2^* + g_2^{(0)} f^{*(1)}_{\mu\nu} f^{*(2),\mu\nu}\right. \\ &\left. + g_3^{(0)} f^{*(1),\mu\nu} f^{*(2)}_{\mu\alpha} \frac{q_\nu q_\alpha}{\Lambda^2} + g_4^{(0)} f^{*(1)}_{\mu\nu} \tilde{f}^{*(2),\mu\nu}\right) , \end{aligned} \tag{11.28}$$

where the ε denotes the polarization vector of a spin 1 boson, q the momentum of the a vector boson, $f^{(i),\mu\nu} = \varepsilon_i^\mu q_i^\nu - \varepsilon_i^\nu q_i^\mu$ is the field strength tensor of a gauge boson with momentum q_i and polarization ε_i, and Λ is the new physics mass scale. The $g_j^{(0)}$ are dimensionless and momentum dependent complex form factors.

The first term corresponds to the Standard Model case 0^{++} where

$$\mathcal{L} \supset g_1^{(0)} H Z_\mu Z^\mu \tag{11.29}$$

The second (CP conserving if H^0 is 0^+) and fourth (CP violating) terms correspond to 5 dimensional operator couplings through loops of the type

$$\mathcal{L} \supset g_2^{(0)} H Z_{\mu\nu} Z^{\mu\nu} + g_4^{(0)} H Z_{\mu\nu} \tilde{Z}^{\mu\nu} \tag{11.30}$$

The third term corresponds to a dimension-7 operator involving new physics possibly appearing at a scale Λ.

Analogously the most general spin 1 interaction amplitude with two gauge bosons can be expressed as follows

$$A^{(1)} = g_1^{(1)} \left[(\varepsilon_1^* q)(\varepsilon_2^* \varepsilon_X) \right] + g_2^{(1)} \epsilon_{\alpha\beta\mu\nu} \varepsilon_X^{\alpha} \varepsilon_1^{*,\mu} \varepsilon_2^{*,\nu} \tilde{q}^{\beta} \tag{11.31}$$

Finally the general spin 2 case can be expressed as follows [190]

$$\begin{aligned} A^{(2)} = \frac{1}{\Lambda} \Bigg[& 2 g_1^{(2)} t_{\mu\nu} f^{*1,\mu\alpha} f^{*2,\nu\alpha} + 2 g_2^{(2)} t_{\mu\nu} \frac{q_\alpha q_\beta}{\Lambda^2} f^{*1,\mu\alpha} f^{*2,\nu\beta} \\ & + g_3^{(2)} \frac{\tilde{q}^\beta \tilde{q}^\alpha}{\Lambda^2} t_{\beta\nu} (f^{*1,\mu\nu} f^{*2}_{\nu\alpha} + f^{*2,\mu\nu} f^{*1}_{\nu\alpha}) \\ & + g_4^{(2)} \frac{\tilde{q}^\mu \tilde{q}^\nu}{\Lambda^2} t_{\mu\nu} f^{*1,\alpha\beta} f^{*2}_{\alpha\beta} + 2 g_5^{(2)} m_V^2 t_{\mu\nu} \varepsilon_1^{*\mu} \varepsilon_2^{*\nu} \\ & + 2 g_6^{(2)} m_V^2 \frac{\tilde{q}^\mu \tilde{q}^\nu}{\Lambda^2} t_{\mu\nu} (\varepsilon_1^{*\nu} \varepsilon_2^{*\alpha} - \varepsilon_1^{*\alpha} \varepsilon_2^{*\nu}) + g_7^{(2)} m_V^2 \frac{\tilde{q}^\mu \tilde{q}^\nu}{\Lambda^2} t_{\mu\nu} \varepsilon_1^* \varepsilon_2^* \\ & + g_8^{(2)} \frac{\tilde{q}^\mu \tilde{q}^\nu}{\Lambda^2} t_{\mu\nu} f^{*1,\alpha\beta} \tilde{f}^{*2}_{\alpha\beta} + g_9^{(2)} t_{\mu\alpha} \tilde{q}^\alpha \epsilon_{\mu\nu\rho\sigma} \varepsilon_1^{*\nu} \varepsilon_2^{*\rho} q^\sigma \\ & + g_{10}^{(2)} \frac{t_{\mu\alpha} \tilde{q}^\alpha}{\Lambda^2} \epsilon_{\mu\nu\rho\sigma} q^\rho \tilde{q}^\sigma (\varepsilon_1^{*\nu} (q \varepsilon_2^*) + \varepsilon_2^{*\nu} (q \varepsilon_1^*)) \Bigg] \end{aligned} \tag{11.32}$$

where $t_{\mu\nu}$ is a symmetric traceless tensor, transverse to the momentum of the spin 2 state $t_{\mu\nu} q^\nu = 0$ [190]. As in the general spin 0 case $g_1^{(1),(2)}$ are dimensionless and momentum dependent complex form factors are effective and dimensionless. Similar amplitudes are derived in the case of fermion couplings, as reported in Ref. [36]. Studies of the spin and CP properties of the discovered state can either use an effective Lagrangian approach or generic scattering amplitudes. The two are equivalent at leading order. However the effective Lagrangian is typically used to generate specific hypotheses and the scattering amplitudes are used in analyses.

The JHU generator [190,192] has been used to define benchmark scenarios for exotic hypotheses of the nature of the observed state according to the general couplings of the observed new particle to gluons and quarks in production and to vector bosons in decay and includes all spin correlations and interferences of all contributing amplitudes. The models which have been investigated by experiments are reported in Table 11.13. It should be noted that while the 0^+_m has a very detailed simulation at NLO in QCD, the alternative hypotheses do not.

Table 11.13: Benchmark scenarios for the analysis of the production and decay of the observed state with J^P quantum numbers. The subscripts refer to the specificities of the couplings of the observed state, where m denotes minimal couplings and h denotes couplings with higher dimension operators. For each scenarios only the non vanishing coupling constants are reported in this table. 0_h^+ denotes a scalar with higher orer (HO) couplings.

Scenario	Production	Decay	Scenario
0_m^+	$gg \to X$	$g_1^{(0)} = 2$	SM Higgs bosons
0_h^+	$gg \to X$	$g_2^{(0)} \neq 0$	HO scalar
0^-	$gg \to X$	$g_4^{(0)} \neq 0$	PSeudo scalar
1^+	$qq \to X$	$g_2^{(1)} \neq 0$	Pseudo vector
1^-	$qq \to X$	$g_a^{(1)} \neq 0$	Vector
2_m^+	$g_1^{(2)} \neq 0$	$g_1^{(2)} = g_5^{(2)} \neq 0$	Graviton tensor MC
2_h^+	$g_4^{(2)} \neq 0$	$g_4^{(2)} \neq 0$	Graviton tensor HD op.
2^-	$g_8^{(2)} \neq 0$	$g_8^{(2)} \neq 0$	Pseudo tensor

The 2_m^+ scenario is investigated in different production modes according to the fraction of $q\overline{q}$ versus gg initiated processes. Results were derived by experiments for various fractions. These results will be reported for the two extreme cases where the observed state is fully produced in one or the other processes and will be denoted 2_{gg}^+ and 2_{qq}^+.

IV.3.3. Statistical procedure

Discriminant distributions are used to define the likelihood functions for a given J^P hypothesis and the background $\mathcal{L}_{J^P}$. The test statistic used to probe a given model is defined as $q = -2\ln \mathcal{L}_{J^P}/\mathcal{L}_{0^+}$. This test statistic is kept as independent as possible independent of the measured signal strength, which is left as a free parameter. To measure the compatibility of the observation with one or the other hypotheses, distributions of this test statistic are derived under a signal J^P and under the 0_m^+ hypotheses. It is important to note that to generate these distributions the number of signal events used is the number of signal events fitted on the data under the given hypothesis. Consequently the number of signal events generated under a given null hypothesis can be different from that of the alternative hypothesis. For the 0_m^+ hypothesis in some cases the SM signal normalization has been used. The two numbers characterizing the observation are: (i) the compatibility with the 0_m^+ hypothesis and (ii) the level of confidence of the exclusion of the hypothesis J^P. An example of distributions is illustrated in Fig. 11.22.

To quantify the compatibility of an observation with test statistic q_{obs} with the 0_m^+ hypothesis the cumulative probability $P_{0^+} = P(q > q_{obs}|0_m^+)$ is used. A perfect compatibility is obtained for a P_{0^+} value close to 50%. For a given analysis the observed P_{0^+} can change depending on which alternative hypothesis is tested.

To quantify the exclusion of an alternative hypothesis J^P, a probability $P_{J^P} = P(q > q_{obs}|J^P)$ is defined. The level of confidence at which the J^P is excluded is given by the CL_S criterion [193]

$$CL_S = \frac{P_{J^P}}{1 - P_{0^+}} \tag{11.33}$$

IV.3.4. J^P determination

At the LHC, the determination of the spin and CP properties of the discovered state is done independently from the rates observed, from a global angular helicity analysis, derived from the general scattering amplitude expressed in Section IV.3.2 and when applicable in the threshold effects in the decay. The channels used for this analysis, the $H \to \gamma\gamma$, $H \to W^{(*)}W^{(*)} \to \ell\nu\ell\nu$ and $H \to Z^{(*)}Z^{(*)} \to 4\ell$, are those where a the observation of a signal is established.

At the Tevatron, an analysis using the threshold distribution of the production of the discovered state [194] in the associated production mode VH with subsequent decay to a pair of b-quarks was performed by the D0 collaboration.

(i) The VH production at D0

The mass of the VH system is a very powerful discriminant to distinguish a $J^P = 0^+_m$, with a threshold behavior in $d\sigma/dM^2 \sim \beta$ from 0^- or 2^+ with threshold behaviors respectively in $\sim \beta^3$ and $\sim \beta^5$ (for a graviton like spin 2) [194]. The VH mass observable, is not only strongly discriminating signal hypotheses, but also have an increased separation of the 0^- and 2^+ hypotheses with respect to the backgrounds, thus allowing, with a small and not yet significant signal, to exclude that the observed state is 0^- at 98% CL [195] and 2^+ at the 99.9% CL [196].

(ii) The $\gamma\gamma$ channel at LHC

In the $H \to \gamma\gamma$ channel, the analysis is performed by ATLAS inclusively using the production angle $\cos\theta^*_{CS}$ as discriminant [197]. The definition chosen for the polar angle in the rest frame is the Collins–Soper frame, which is defined as the bisector axis of the momenta of the incoming protons in the diphoton rest frame. The 0^+_m signal distribution is expected to be uniform with a cutoff due to the lower selection requirements on the photons transverse momentum. The $H \to \gamma\gamma$ channel is mostly sensitive to the gluon-initiated production scenario 2^+_{gg}, which yields a $\cos\theta^*_{CS}$ distribution peaking at values close to 1. It is much less so for the quark-initiated scenarios 2^+_{qq}. The results are derived from a fit of the signal in bins of $\cos\theta^*_{CS}$ and are summarized in Table 11.14. The data shows a good compatibility with the SM 0^+_m hypothesis. ATLAS excludes the alternative hypotheses 2^+_{gg} and 2^+_{qq} at the 99% CL and 95% CL.

(iii) The $H \to W^{(*)}W^{(*)} \to \ell\nu\ell\nu$ channel at LHC

The $H \to W^{(*)}W^{(*)} \to \ell\nu\ell\nu$ the production and decay angles cannot be easily reconstructed due to the neutrinos in the final state, however an important feature is the V-A structure of the decay of the W bosons. A scalar state thus yields a clear

spin correlation pattern that implies that the charged leptons e or μ from the decays of the W bosons are produced close to one another in the transverse plane. In the main analysis this feature is used to gain sensitivity, in this case the initial selection need to be reappraised in order not to discriminate specific J^P hypotheses. This feature, which immediately impacts observables such as the azimuthal angle between the two leptons $\Delta\Phi_{\ell\ell}$ or their invariant mass $M_{\ell\ell}$ in addition of the threshold behavior of the decay which is used in kinematic variables such as the transverse mass defined in Section III, can be used to discriminate spin and parity hypotheses. The approach adopted by ATLAS is a multivariate discriminant, whereas CMS uses a 2D-fit of the dilepton mass and the transverse mass. The results of the $H \to W^{(*)}W^{(*)} \to \ell\nu\ell\nu$ analyses are summarized in Table 11.14. The hypotheses tested by this approach are the 1^+ and 1^- by the ATLAS experiment and the 2^+ by ATLAS and CMS. A good compatibility of the observation with the 0^+_m hypothesis is observed in the discrimination of all hypotheses. ATLAS excludes the 1^+ and 1^- hypotheses at the 98% CL and 99% CL respectively. When discriminating the 2^+ hypothesis, the $H \to W^{(*)}W^{(*)} \to \ell\nu\ell\nu$ analysis is more sensitive to the quark-initiated production mode and is therefore complementary to the $H \to \gamma\gamma$ channel. ATLAS [197] and CMS [198] disfavor the 2^+_{gg} and 2^+_{qq} at different levels of confidence. The strongest observed exclusion is obtained by ATLAS excluding the 2^+_{gg} and 2^+_{qq} at the 98% CL and 99% CL respectively.

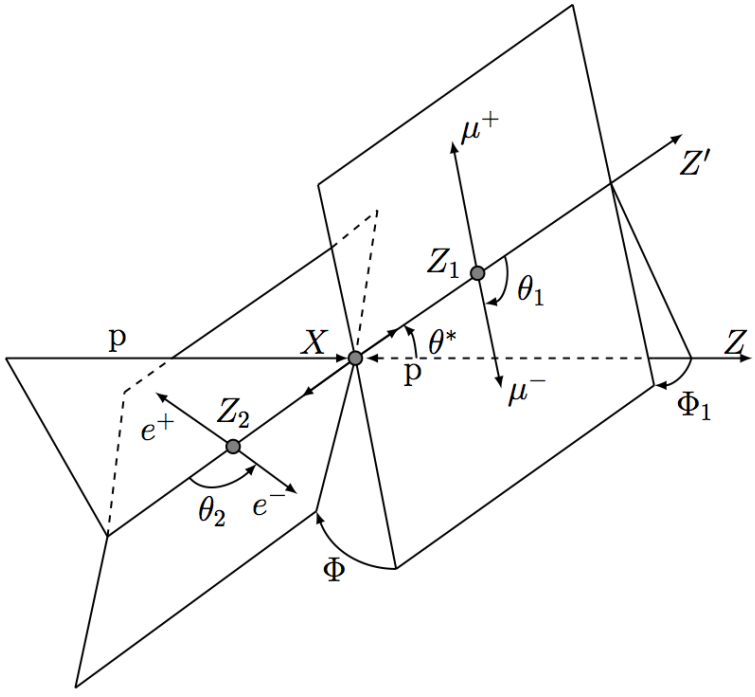

Figure 11.21: Definition of the production and decay angles defined for the $H \to Z^{(*)}Z^{(*)} \to 4\ell$ final state [199].

(iv) The $H \to Z^{(*)}Z^{(*)} \to 4\ell$ channel at LHC

The main $H \to Z^{(*)}Z^{(*)} \to 4\ell$ coupling analysis, as described in Section III, also uses a discriminant based on the 0^+_m nature of the Higgs boson to further discriminate the signal from the background. In this analysis this feature is used to discriminate between signal hypotheses. The observables sensitive to the spin and parity are the masses of the two Z bosons [191](due to the threshold dependence of the mass of the off-shell Z boson), two production angle θ^* and ϕ_1, and three decay angles, ϕ, θ_1 and θ_2. The production and decay angles defined as:

– θ_1 and θ_2, the angles between the negative final state lepton and the direction of flight of Z_1 and Z_2 in the rest frame.

– ϕ, the angle between the decay planes of the four final state leptons expressed in the four lepton rest frame.

– ϕ_1, the angle defined between the decay plane of the leading lepton pair and a plane defined by the vector of the Z_1 in the four lepton rest frame and the positive direction of the proton axis.

– θ^*, the production angle of the Z_1 defined in the four lepton rest frame with respect to the proton axis.

These angles are illustrated in Fig. 11.21. There are two approaches to this analysis. The first, used by CMS, is a matrix element likelihood approach where a kinematic discriminant is defined based on the ratio of the signal and background probabilities. These probabilities are defined using the leading-order matrix elements. A similar approach is also performed by ATLAS as a cross check of their main result. The main approach adopted by ATLAS is the combination of sensitive variables in a boosted decision tree. These analyses are sensitive to various J^P hypotheses and in particular to discriminate the 0^+_m hypothesis from the 0^-. In all scenarios investigated and for both the ATLAS and CMS experiments the data are compatible with the 0^+_m hypothesis. ATLAS [197] and CMS [199] exclude a pseudo scalar nature of the H^0 at CL_S levels of 98% and 99.8%. The distribution of the test statistic q defined in Section IV.3.3 is illustrated in Fig. 11.22 for the 0^+_m and 0^- hypotheses. All benchmark scenarios results are summarized in Table 11.14.

IV.3.5. Probing CP mixing

The most general decay amplitude for spin-0 state decaying to a pair of gauge bosons described in Section IV.3.2 can be expressed in a more compact form [190]

$$\begin{aligned} A^{(0)} =& \frac{\varepsilon_1^{*\mu}\varepsilon_2^{*\nu}}{v}(a_1\, m_H^2\, g_{\mu\nu} + a_2\, q_\mu q_\nu + a_3\, \epsilon_{\mu\nu\alpha\beta}\, q_1^\alpha q_2^\beta) \\ =& A_1 + A_2 + A_3\,, \end{aligned} \tag{11.34}$$

where q_i and ε_i are the momenta and polarization vectors of the two gauge bosons, and $q = q_1 + q_2$ is the four-momentum of the spin 0 boson.

The SM Higgs boson is dominated by the A_1 amplitude, while a 0^- state is dominated by A_3. The CMS collaboration has performed an analysis of the ratio

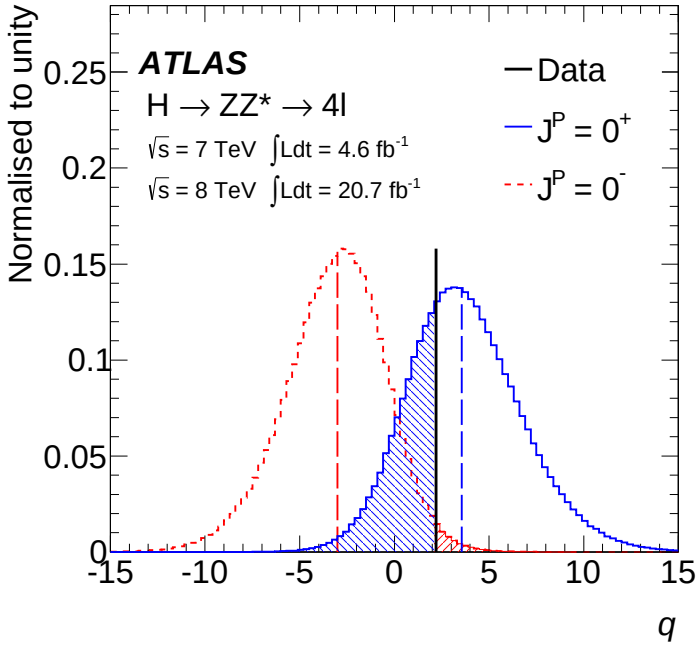

Figure 11.22: Expected distributions of q, for the Standard Model 0^+ (blue/solid line distribution) or 0^- (red/dashed line distribution) signals [197]. The observed value is indicated by the vertical solid line and the expected medians by the dashed lines. The colored areas correspond to the integrals of the expected distributions up to the observed value and are used to compute the p_0-values for the rejection of each hypothesis.

$f_{a_3} = |A_3|^2/(|A_1|^2 + |A_3|^2)$ in the $H \to Z^{(*)}Z^{(*)} \to 4\ell$ channel [199], where the presence of the A_2 term is neglected. This second term corresponds to higher order couplings of the 0^+ state. The two extreme cases $f_{a_3} = 0, 1$ correspond approximately to the 0^+ and 0^- cases respectively. Other values of f_{a_3} would be an indication of CP-violation. The analysis uses a kinematic discriminant defined similarly to the cases discussed in Section IV.3.4 taking the dependence with f_{a_3} into account. Using the full dataset corresponding to an integrated luminosity of approximately $25\,\text{pb}^{-1}$ of pp collisions at 7 TeV and 8 TeV, CMS measures $f_{a_3} = 0.00 \pm 0.23$ corresponding to a limit of $f_{a_3} < 0.58$ at 95% CL. It should be noted that an indication of CP-violation from f_{a_3} would not yield a measure of the mixing of opposite parity states.

V. New physics models of EWSB in the light of the Higgs boson discovery

A main theoretical motivation to add a Higgs boson to the Standard Model is that, without it, the longitudinal components of the massive EW gauge bosons would form a strongly coupled system as their scattering amplitude would have grown with their energy,

Table 11.14: Results in all benchmark scenarios for the analysis of the production and decay of the observed state with J^P quantum numbers, for the ATLAS (A) and CMS (C) experiments. The upper part of the table gives the compatibility of the observation with the SM 0_m^+ hypothesis. The lower part of the table gives the CL_S observed exclusion and in parenthesis the sensitivity of the given alternative model.

J^P	ZZ	WW	$\gamma\gamma$	Combined
0^-	31% A	–	–	–
	31% C	–	–	–
0_h^+	50% C	–	–	–
1^+	55% A	70% A	–	62% A
	4.5% C	–	–	–
1^-	15% A	66% A	–	33% A
	8.1% C	–	–	–
$2^+_{q\overline{q}}$	96% A	54% A	80% A	81% A
	3.6% C	–	–	–
2^+_{gg}	53% A	73% A	59% A	63% A
	82% C	33% C	–	63% C
0^-	2.2% (0.4%) A	–	–	–
	0.2% (0.5%) C	–	–	–
0_h^+	8.1% (4.5%) C	–	–	–
1^+	0.2% (0.2%) A	8.0% (8.0%) A	–	<0.1% (<0.1%) A
	<0.1% (1.1%) C	–	–	–
1^-	6.0% (0.4%) A	1.7% (2.0%) A	–	0.3% (<0.1%) A
	<0.1% (0.3%) C	–	–	–
$2^+_{q\overline{q}}$	2.6% (8.2%) A	<0.1% (<0.1%) A	12.4% (13.5%) A	<0.1% (<0.1%) A
	<0.1% (4.0%) C	–	–	–
2^+_{gg}	16.9% (9.2%) A	4.8% (5.4%) A	0.7% (0.5%) A	<0.1% (<0.1%) A
	1.4% (5.5%) C	14.0% (5.5%) C	–	0.6% (1.1%) C

destroying all the predictive power of the model above $4\pi v \sim 3\,\text{TeV}$. The discovery of a light scalar with couplings to gauge bosons and fermions that are apparently consistent with SM predictions and the slow running of the Higgs self-coupling at high energies allows one to consider the SM as a valid perturbative description of nature all the way to the Planck scale. This picture is admittedly very attractive, but it posits that the Higgs boson is an elementary scalar field, which comes with an intrinsic instability of its mass under radiative corrections. This Higgs naturalness problem calls for new physics around the TeV scale. Supersymmetric models are the most elegant solution to maintain the perturbativity of the SM while alleviating the instability issue. Another possibility

is that the Higgs boson itself has a finite size and is composite and thus never feels the UV degrees of freedom that would drag its mass to much higher scales. Both classes of models predict specific modifications from the SM Higgs properties. In this section, these possible deviations will be discussed in detail.

The realization of supersymmetry at low energies has many good qualities that render it attractive as a model of new physics. First of all since for every fermion there is a boson of equal mass and effective coupling to the SM-like Higgs, in the case of exact supersymmetry it yields an automatic cancellation of loop corrections to the Higgs mass parameter: (analogous to Eq. (11.2)) $\delta m^2 = 0$ [8,10]. In practice, it is known that SUSY must be broken in nature since no superpartners of the SM particles have been observed so far. Taking into account the fact that the fermion and boson couplings to the Higgs and the number of degrees of freedom of the SM particles and their superpartners are the same, the Higgs mass correction simply writes

$$\delta m^2 = \sum_F g_F \lambda_F^2 \frac{(m_B^2 - m_F^2)}{32\pi^2} \log \frac{Q^2}{\mu^2}, \tag{11.35}$$

where the sum is over all fermion fields of mass m_F and includes implicitly their superpartners with a squared mass m_B^2. The mass difference between the boson and fermion degrees of freedom is governed by the soft supersymmetry breaking parameters. Therefore, independently of how large m_B^2 and m_F^2 are, all corrections are proportional to M_{SUSY}^2. Hence, provided that $M_{SUSY} \simeq \mathcal{O}(1\text{–few})$ TeV, the fine-tuning problem is solved, in the sense that the low energy mass parameters become insensitive to physics at the GUT or Planck scale. Another interesting feature of SUSY theories is related to the dynamical generation of EWSB [201]. In the SM a negative Higgs mass parameter, m^2, needs to be inserted by hand to induce EWSB. In SUSY, instead, even if the relevant Higgs mass parameter is positive in the ultraviolet, it may become negative and induce electroweak symmetry breaking radiatively through the strong effect of the top quark-Higgs coupling in its renormalization group evolution. Moreover, supersymmetry with a supersymmetry breaking scale of order 1 TeV allows for grand unification of the electroweak and strong gauge interactions in a consistent way, strongly supported by the prediction of the electroweak mixing angle at low energy scales, with an accuracy at the percent level [202,203]. In addition, supersymmetry theories can provide a suitable dark matter candidate [204] and even a low energy physics explanation of baryogenesis [205], all of this compatible with existing precision data.

In the following discussion, the Higgs sector will be explored in specific SUSY models. In all of them there is one neutral Higgs boson with properties that resemble those of the SM Higgs boson whereas additional neutral and charged Higgs bosons are also predicted and are intensively being sought for at the LHC (see Section V.9). In the simplest SUSY model the lightest Higgs boson mass, that usually plays the role of the SM-like Higgs, is predicted to be less than 135 GeV for stops in the TeV to few TeV range [206–220], whereas, larger values of the SM-like Higgs boson mass – up to about 250 GeV – can be obtained in non-minimal SUSY extensions of the SM [344,221–227]. In general, accommodating a SM-like Higgs boson with mass of 125 GeV results in constraints on the supersymmetric parameter space of specific SUSY models, as discussed below.

The more and more constraining bounds on the SUSY parameter space do not preclude a solution to the naturalness problem but they require either heavier SUSY partners or some specific engineering to hide any SUSY signal from the optimized searches conducted at the LHC. In their most commonly studied incarnations, SUSY models distinguish themselves from the background by a substantial amount of missing transverse energy (MET) taken away by the stable lightest supersymmetric particle (LSP), and by a large activity associated with the superpartners around the TeV scale. Nonetheless, light SUSY is still allowed by current LHC limits if these two characteristic features of the generic SUSY signals are softened. Compressing the SUSY spectrum [228] reduces the amount of available energy transferred to the visible particles at the end of the cascade decays of the heavy superpartners. Also the LSP's tend to be produced back-to-back, minimizing the amount of missing energy along the transverse direction. A compressed spectrum can be obtained if the gluino happens to be lighter than the other gauginos at the high scale in gravity mediated or gauge mediated SUSY breaking scenarios. Another approach, dubbed as stealth supersymmetry [229], is designed to reduce the SUSY signals by introducing a new light and approximately supersymmetric multiplet that is complementary to the MSSM matter content. The heavy MSSM particles will chain-decay to the R-odd particle of this new multiplet but the small mass splitting within this multiplet kinematically limits the amount of MET finally taken away by the LSP. Dedicated experimental searches have already been designed to probe such scenarios.

A more radical solution to reduce the amount of MET in the final state is to revoke the R-parity assumption that is usually imposed to save the proton from a fast decay and also to guarantee the existence of a stable particle with a relic abundance compatible with what is expected to form the dark matter component of the Universe. R-parity is however not a necessity. For instance if the 96 new complex parameters of the R-parity violating MSSM [230] are arranged to follow a minimal flavor violation pattern [231], the proton lifetime will exceed the current bounds. Such scenarios predict either multilepton or multijet final states that are already the target of ongoing LHC searches.

While naturalness dictates relatively light stops and gluinos, the first and second generation of squarks and sleptons couple weakly to the Higgs sector and may be heavy. Moreover, small values of the μ parameter and therefore light Higgsinos would be a signature of a natural realization of electroweak symmetry breaking. Such SUSY spectra, consisting of light stops and light Higgsinos, have been under intense scrutiny by the experimental collaborations [232] in order to derive model-independent bounds on the stop masses and to understand if such natural SUSY scenarios endure [233] and can explain why the Higgs boson remains light.

In the context of weakly coupled models of EWSB one can also consider multiple Higgs $\mathrm{SU}(2)_L$ doublets as well as additional Higgs singlets, triplets or even more complicated multiplet structures, with or without low energy supersymmetry. In general for such models one needs to take into account experimental constraints from precision measurements and flavor changing neutral currents. The LHC signatures of such extended Higgs sectors are largely shaped by the role of the exotic scalar fields in EWSB.

The idea that the Higgs boson itself could be a composite bound state emerging from a new strongly-coupled sector has regained some interest. The composite Higgs idea is an

interesting incarnation of EWSB via strong dynamics that smoothly interpolates between the standard Technicolor approach and the true SM limit. To avoid the usual conflict with EW data, it is sufficient if not necessary that a mass gap separates the Higgs resonance from the other resonances of the strong sector. Such a mass gap can naturally follow from dynamics if the strongly-interacting sector exhibits a global symmetry, G, broken dynamically to a subgroup H at the scale f, such that, in addition to the three Nambu–Goldstone bosons of SO(4)/SO(3) that describe the longitudinal components of the massive W and Z, the coset G/H contains, a fourth Nambu–Goldstone boson that can be identified with the physical Higgs boson. Simple examples of such a coset are SU(3)/SU(2) or SO(5)/SO(4), the latter being favored since it is invariant under the custodial symmetry (it is also possible to have non-minimal custodial cosets with extra Goldstone bosons, see for instance Ref. [234]). Attempts to construct composite Higgs models in 4D have been made by Georgi and Kaplan (see for instance Ref. [235]) and modern incarnations have been recently investigated in the framework of 5D warped models where, according to the principles of the AdS/CFT correspondence, the holographic composite Higgs boson then originates from a component of a gauge field along the 5th dimension with appropriate boundary conditions.

A last crucial ingredient in the construction of viable composite Higgs models is the concept of partial compositeness [236], i.e., the idea that there are only linear mass mixings between elementary fields and composite states[8]. After diagonalization of the mass matrices, the SM particles, fermions and gauge bosons, are admixtures of elementary and composite states and thus they interact with the strong sector, and in particular with the Higgs boson, through their composite component. This setup has important consequences on the flavor properties, chiefly the suppression of large flavor changing neutral currents involving light fermions. It also plays an important role in dynamically generating a potential for the would-be Goldstone bosons. Partial compositeness also links the properties of the Higgs boson to the spectrum of the fermionic resonances, i.e. the partners of the top quark. As in the MSSM, these top partners are really the agents that trigger the EWSB and also generate the mass of the Higgs boson that otherwise would remain an exact Goldstone boson and hence massless. The bounds from the direct searches for the top partners in addition to the usual constraints from EW precision data force the minimal composite Higgs models into some rather unnatural corners of their parameter spaces [238].

V.1. Higgs bosons in the Minimal Supersymmetric Standard Model (MSSM)

The particle masses and interactions in a supersymmetric theory are uniquely defined as a function of the superpotential and the Kähler potential [200]. A fundamental theory of supersymmetry breaking, however, is unknown at this time. Nevertheless, one can parameterize the low-energy theory in terms of the most general set of soft supersymmetry-breaking operators [239]. The simplest realistic model of low-energy supersymmetry is the Minimal Supersymmetric extension of the Standard Model (MSSM) [10,200], that associates a supersymmetric partner to each gauge boson and

[8] For a pedagogical introduction to models of partial compositeness, see Ref. [237].

chiral fermion of the SM, and provides a realistic model of physics at the weak scale. However, even in this minimal model with the most general set of soft supersymmetry-breaking terms, more than 100 new parameters are introduced [240]. Fortunately, only a subset of these parameters impact the Higgs phenomenology through tree-level and quantum effects. Reviews of the properties and phenomenology of the Higgs bosons of the MSSM can be found for example in Refs. [34,200,241].

The MSSM contains the particle spectrum of a two-Higgs-doublet model (2HDM) extension of the SM and the corresponding supersymmetric partners. Two Higgs doublets,

$$\Phi_1 = \frac{1}{\sqrt{2}} \begin{pmatrix} \phi_1^0 + i a_1^0 \\ \sqrt{2}\phi_1^- \end{pmatrix}, \tag{11.36}$$

$$\Phi_2 = \frac{1}{\sqrt{2}} \begin{pmatrix} \sqrt{2}\phi_2^+ \\ \phi_2^0 + i a_2^0 \end{pmatrix}, \tag{11.37}$$

with $Y = -1$ and $Y = 1$, respectively, are required to ensure an anomaly-free SUSY extension of the SM and to generate mass for both up-type and down-type quarks and charged leptons [12]. In our notation $\Phi_{1(2)}$ gives mass to the down(up) type fermions. The Higgs potential reads

$$\begin{aligned} V = {} & m_1^2 \Phi_1^\dagger \Phi_1 + m_2^2 \Phi_2^\dagger \Phi_2 - m_3^2 (\Phi_1^T i\sigma_2 \Phi_2 + \text{h.c.}) \\ & + \frac{1}{2}\lambda_1 (\Phi_1^\dagger \Phi_1)^2 + \frac{1}{2}\lambda_2 (\Phi_2^\dagger \Phi_2)^2 + \lambda_3 (\Phi_1^\dagger \Phi_1)(\Phi_2^\dagger \Phi_2) \\ & + \lambda_4 |\Phi_1^T i\sigma_2 \Phi_2|^2 + \frac{1}{2}\lambda_5 [(\Phi_1^T i\sigma_2 \Phi_2)^2 + \text{h.c.}] \\ & + [[\lambda_6 (\Phi_1^\dagger \Phi_1) + \lambda_7 (\Phi_2^\dagger \Phi_2)] \Phi_1^T i\sigma_2 \Phi_2 + \text{h.c.}] \end{aligned} \tag{11.38}$$

where $m_i^2 = \mu^2 + m_{H_i}^2$, with μ being the supersymmetric Higgsino mass parameter and m_{H_i} (for $i = 1, 2$) the Higgs doublet soft supersymmetric breaking mass parameters; $m_3^2 \equiv B\mu$ is associated to the B-term soft SUSY breaking parameter; and λ_i, for $i = 1$ to 7, are all the Higgs quartic couplings. After the spontaneous breaking of the electroweak symmetry, five physical Higgs particles are left in the spectrum: one charged Higgs pair, $H^\pm$, one CP-odd scalar, A, and two CP-even states, H and h.

$$\begin{aligned} H^\pm &= \sin\beta \phi_1^\pm + \cos\beta \phi_2^\pm \,, \\ A &= \sin\beta \ \text{Im}\phi_1^0 + \cos\beta \ \text{Im}\phi_2^0 \,, \\ H &= \cos\alpha (\text{Re}(\phi_1^0) - v_1) + \sin\alpha (\text{Re}(\phi_2^0) - v_2), \\ h &= -\sin\alpha (\text{Re}(\phi_1^0) - v_1) + \cos\alpha (\text{Re}(\phi_2^0) - v_2), \end{aligned} \tag{11.39}$$

where $\langle \phi_i^0 \rangle = v_i$ for i=1,2 and $v_1^2 + v_2^2 \approx (246\,\text{GeV})^2$. The angle α diagonalizes the CP-even Higgs squared-mass matrix, while β diagonalizes both the CP-odd and charged

Higgs sectors with $\tan\beta = v_2/v_1$. The h and H denote the lightest and heaviest *CP*-even Higgs bosons, respectively.[9]

V.1.1. The MSSM Higgs boson masses

Quite generally for any two Higgs doublet model, including the MSSM, the phenomenology depends strongly on the size of the mixing angle α and therefore on the quartic couplings,

$$\sin\alpha = \frac{\mathcal{M}_{12}^2}{\sqrt{(\mathcal{M}_{12}^2)^2 + \left(\mathcal{M}_{11}^2 - m_h^2\right)^2}}, \tag{11.40}$$

where

$$\begin{aligned}\mathcal{M}_{12}^2 &= -\left(m_A^2 - (\lambda_3+\lambda_4)v^2\right)\sin\beta\cos\beta + \lambda_7 v^2\sin^2\beta \\ &\quad + \lambda_6 v^2\cos^2\beta, \\ \mathcal{M}_{11}^2 &= \left(m_A^2 + \lambda_5 v^2\right)\sin^2\beta + \lambda_1 v^2\cos^2\beta \\ &\quad + 2\lambda_6 v^2\cos\beta\sin\beta.\end{aligned} \tag{11.41}$$

The spectrum is given by

$$m_{h,H}^2 = \frac{\mathcal{M}_{11}^2 + \mathcal{M}_{22}^2 \mp \sqrt{\left(\mathcal{M}_{11}^2 - \mathcal{M}_{22}^2\right)^2 + 4(\mathcal{M}_{12}^2)^2}}{2}, \tag{11.42}$$

with

$$\mathcal{M}_{22}^2 = \left(m_A^2 + \lambda_5 v^2\right)\cos^2\beta + \lambda_2 v^2\sin^2\beta + 2\lambda_7 v^2\cos\beta\sin\beta\ . \tag{11.43}$$

The charged Higgs boson mass is given by

$$m_{H^\pm}^2 = m_A^2 + (\lambda_5 - \lambda_4)\frac{v^2}{2}. \tag{11.44}$$

The supersymmetric structure of the theory imposes constraints on the Higgs sector of the model. In particular, at tree level, the parameters of the Higgs self-interaction, $\lambda_{1,\ldots,4}$, are defined in terms of the electroweak gauge coupling constants,

$$\lambda_1 = \lambda_2 = g_2^2/4,\ \ \lambda_3 = -(g_1^2 - g_2^2)/4,\ \ \lambda_4 = -g_2^2/2, \tag{11.45}$$

and $\lambda_{5,6,7} = 0$. As a result, the Higgs sector at tree level is determined by only two free parameters: $\tan\beta$ and one Higgs boson mass, conventionally chosen to be the *CP*-odd Higgs boson mass, m_A. The other tree-level Higgs boson masses are then given in terms

[9] Observe that in the SM sections of this review, H denotes the SM Higgs, whereas in the sections about SUSY and more generally extensions of the SM with two Higgs doublets, H is used for the heaviest *CP*-even Higgs boson, since this is the standard notation in the literature.

of these parameters. In the large $m_A \gg M_Z$ limit, also called the decoupling limit [242], $\sin\alpha \to -\cos\beta$, $\cos\alpha \to \sin\beta$, hence, $\cos(\beta-\alpha) \to 0$ and this implies that the lightest CP-even Higgs h behaves as the SM Higgs. The condition $\cos(\beta-\alpha) \to 0$ is also obtained if the quartic couplings are such that $\mathcal{M}_{12}^2 \sin\beta = -(\mathcal{M}_{11}^2 - m_h^2)\cos\beta$ [243–245], independent of the value of m_A. The limit $\cos(\beta-\alpha) \to 0$ is called the alignment limit. As will be discussed below, in the MSSM the alignment limit can only occur once quantum corrections to the quartic couplings have been included.

The tree level value of m_h is maximized not only for $m_A \gg M_Z$ but also for $\tan\beta \gg 1$. In the large m_A limit, one finds $m_h^2 \simeq (M_Z \cos 2\beta)^2$ and $m_A \simeq m_H \simeq m_{H^\pm}$, up to corrections of $\mathcal{O}({M_Z}^2/m_A)$. Below the scale m_A, the Higgs sector of the effective low-energy theory consists only of h, which behaves as the SM Higgs boson. This scenario would have been excluded already by LEP and would not accommodate the recently discovered Higgs boson. However, radiative corrections have a significant impact on the values of Higgs boson masses and couplings in the MSSM. In particular, m_h can be lifted to agree with present LHC measurements.

The dominant radiative effects to the SM-like Higgs mass arise from the incomplete cancellation between top and scalar-top (stop) loops and at large $\tan\beta$ also from sbottom and stau loops. The loop contributions to the tree level quartic couplings depend on the SUSY spectrum, and render $\lambda_{5,6,7}$ non zero. The stop, sbottom and stau masses and mixing angles depend on the supersymmetric Higgsino mass parameter μ and on the soft-supersymmetry-breaking parameters [10,200]: M_Q, M_U, M_D, M_L, M_E, and A_t, A_b A_τ. The first three of these are the left-chiral and the two right-chiral top and bottom scalar quark mass parameters. The next two are the left-chiral stau/sneutrino and the right-chiral stau mass parameters, and the last three are the trilinear parameters that enter in the off-diagonal squark/slepton mixing elements: $X_t \equiv A_t - \mu\cot\beta$ and $X_{b,\tau} \equiv A_{b,\tau} - \mu\tan\beta$. The corrections affecting the Higgs boson masses, production, and decay properties depend on all of these parameters in various ways. At the two-loop level, the masses of the gluino and the electroweak gaugino also enter in the calculations. For simplicity, it is initially assumed that A_t, A_b, A_τ, μ, and the gluino and electroweak gaugino masses are real parameters. The impact of complex phases on MSSM parameters, which will induce CP-violation in the Higgs sector, is addressed below.

Radiative corrections to the Higgs boson masses have been computed using a number of techniques, with a variety of approximations; see Refs. [206–219,246]. The radiative corrections to m_h depend quartically on the top quark mass, quadratically and quartically on stop mixing parameter, and there is also a logarithmic dependence on the stop masses. For large $\tan\beta$, the stau/sbottom mixing parameters and masses are also relevant. In the large m_A (decoupling) limit and for $\tan\beta \gg 1$, which maximizes m_h at tree level, the m_h value can be maximized at loop level for $X_t \simeq \sqrt{6} M_{\rm SUSY}$ [10] where $M_{\rm SUSY} \simeq M_Q \simeq M_U \simeq M_D$ is an assumed common value of the soft SUSY-breaking

[10] The parameters X_t and $M_{\rm SUSY}$ depend on the renormalization scheme. The radiative corrections to the Higgs masses computed in the Feynman diagrammatic approach have been obtained in the on-shell (OS) renormalization scheme, whereas those based on the Renormalization Group approach have been calculated using the $\overline{MS}$ scheme. A detailed

squark mass parameters. This choice of X_t is called the "maximal-mixing scenario". For fixed X_t, the value of m_h can vary by several GeV by varying $M_{\rm SUSY}$ within a few TeV or by varying m_t within its experimental uncertainty, as well as by varying SUSY particle parameters that enter only beyond the one- loop order. Moreover, in the large $\tan\beta$ regime light staus and/or sbottoms with sizable mixing, governed by the μ parameter, yield negative radiative corrections to the mass of the lightest Higgs boson, and can lower it by several GeV [215,247]. Allowing for experimental and theoretical uncertainties, one finds that for $M_{\rm SUSY} \lesssim 2\,\text{TeV}$, large m_A, $\tan\beta \gg 1$ and for $X_t \simeq \sqrt{6} M_{\rm SUSY}$, the maximal value for the lightest Higgs mass is $m_h^{\rm max} = 135\,\text{GeV}$ [220,248–250]. Interestingly, the upper bound on the lightest neutral scalar boson is a prediction for both the CP-conserving (CPC) and CP-violating (CPV) MSSM scenarios [251,252].

The newly discovered SM-like Higgs boson, if interpreted as the lightest MSSM Higgs with a mass of about 125 GeV, provides information on the possible MSSM parameter space. In particular a sizable mixing in the stop sector is required ($|X_t/M_{\rm SUSY}| \geq 1.5$) for values of $M_{\rm SUSY} \simeq M_Q \simeq M_U \simeq M_D \simeq 1$ to a few TeV [247–258]. See for example Fig. 11.23 and Fig. 11.24. On the other hand, as shown in Fig. 11.25, considering the third generation soft SUSY breaking parameters as independent inputs, $M_Q \neq M_U \neq M_D$, one observes that $m_h \simeq$125 GeV can be obtained for one stop that is as light as can be experimentally allowed [259]- - i.e. in the few hundred GeV mass range- and the other one with a mass of the order of the stop mixing parameter. It is also possible to consider both stops significantly above a few TeV by varying/lowering the values of X_t and $\tan\beta$, in that case the impact of higher loops in the computation of the Higgs mass becomes relevant [246].

For a given CP-odd Higgs mass m_A, the masses of the other two Higgs bosons, H and $H^\pm$, also receive radiative corrections (for a summary, see for instance Ref. [241]) , but in the absence of additional CP-violating phases, and for m_A larger than $m_h \simeq 125\,\text{GeV}$, they are all similar, and at most about a few tens of GeV apart. Instead, for smaller values of m_A, the heavy Higgs is the SM one, $m_H \simeq 125\,\text{GeV}$ and $m_h \simeq m_A$, but this scenario is strongly challenged by present data [248]. For a more detailed discussion of the effect of radiative corrections on the heavy Higgs masses see for example Refs. [34] and [241].

V.1.2. MSSM Higgs boson couplings

The phenomenology of the Higgs sector depends on the couplings of the Higgs bosons to gauge bosons and fermions. The couplings of the two CP-even Higgs bosons to W and Z bosons are given in terms of the angles α and β

$$g_{hVV} = g_V m_V \sin(\beta-\alpha), \quad g_{HVV} = g_V m_V \cos(\beta-\alpha), \tag{11.46}$$

where $g_V \equiv 2m_V/v$, for $V = \text{W}^\pm$ or Z ($g_V m_V$ is the SM hVV coupling). There are no tree-level couplings of A or $H^\pm$ to VV. The couplings of the Z boson to two neutral Higgs

comparison of the results in the two schemes is presented in Refs. [218,214]. In particular, the lightest Higgs mass is maximized for $X_t^{\bar{M}S} \simeq \sqrt{6} M_{\rm SUSY}$ or equivalently $X_t^{OS} \simeq 2M_{\rm SUSY}$.

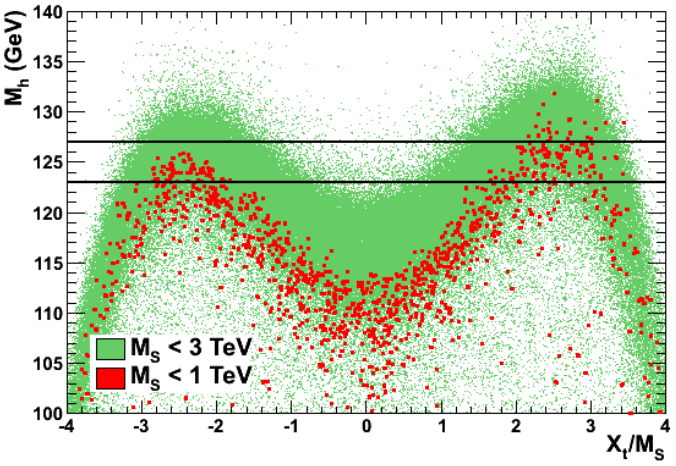

Figure 11.23: The maximal value of m_h as a function of $X_t/M_{\rm SUSY}$ ($M_{\rm SUSY} \equiv M_S$) in the pMSSM when all other soft SUSY-breaking parameters and $\tan\beta$ are scanned as defined in Ref. [253].

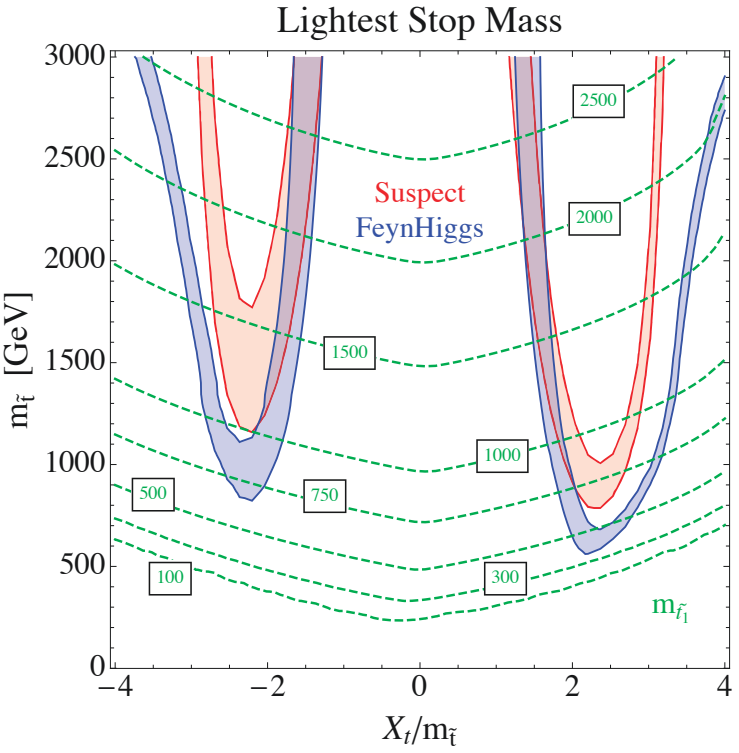

Figure 11.24: Contours of m_h in the MSSM as a function of $m_{\tilde{t}}$, a common stop mass $M_Q = M_U$, and the stop mixing parameter X_t for $\tan\beta = 20$. The red/blue bands show the result from Suspect/FeynHiggs for m_h in the range 124-126 GeV. The contours of constant lightest stop mass are shown in green Ref. [254].

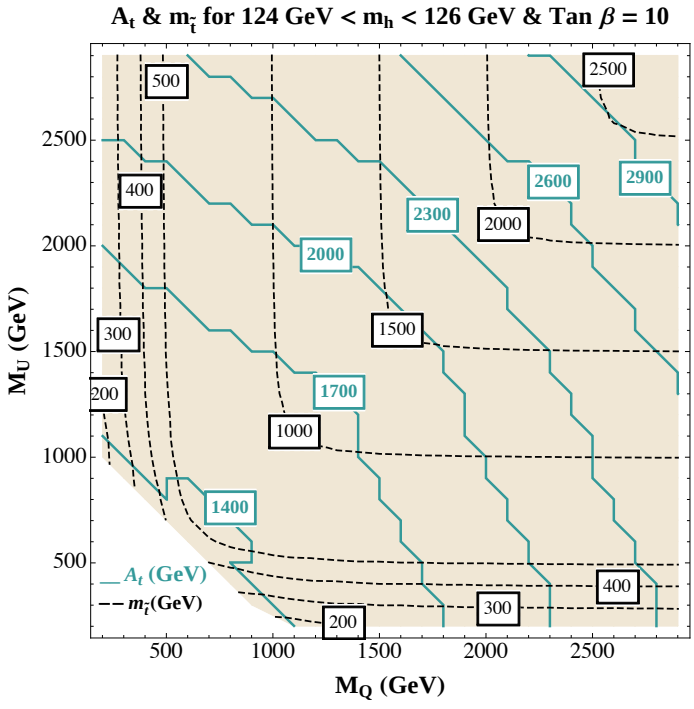

Figure 11.25: Contours of the stop mixing parameter, A_t, necessary for m_h to be in the 124–126 GeV range, given in the plane of the left- and right-handed stop soft supersymmetry-breaking mass parameters, M_Q and M_U, respectively. Other relevant parameters are fixed to be: $\mu = 650\,\text{GeV}$, $m_A = 1500\,\text{GeV}$, $A_\tau = 500\,\text{GeV}$ and $\tan\beta = 10$. From Ref. [247].

bosons, which must have opposite CP-quantum numbers, are given by $g_{\phi AZ}(p_\phi - p_A)$, where $\phi = H$ or h, the momenta p_ϕ and p_A point into the vertex, and

$$g_{hAZ} = g_Z \cos(\beta-\alpha)/2, \quad g_{HAZ} = -g_Z \sin(\beta-\alpha)/2\,. \tag{11.47}$$

Charged Higgs-W boson couplings to neutral Higgs bosons and four-point couplings of vector bosons and Higgs bosons can be found in Ref. [12].

The tree-level Higgs couplings to fermions obey the following property: the neutral components of one Higgs doublet, Φ_1, couple exclusively to down-type fermion pairs while the neutral components of the other doublet, Φ_2, couple exclusively to up-type fermion pairs [12]. This Higgs-fermion coupling structure defines the Type-II 2HDM [260]. In the MSSM, fermion masses are generated when both neutral Higgs components acquire vacuum expectation values, and the relations between Yukawa couplings and fermion masses are (in third-generation notation)

$$h_b = \sqrt{2}\, m_b/(v\cos\beta), \qquad h_t = \sqrt{2}\, m_t/(v\sin\beta)\,. \tag{11.48}$$

Similarly, one can define the Yukawa coupling of the Higgs boson to τ-leptons (the latter is a down-type fermion).

The couplings of the neutral Higgs bosons to $f\bar{f}$ relative to the SM value, $gm_f/2M_W$, are given by

$$\begin{aligned} hb\bar{b} &: -\sin\alpha/\cos\beta = \sin(\beta-\alpha) - \tan\beta\cos(\beta-\alpha)\,, \\ ht\bar{t} &: \cos\alpha/\sin\beta = \sin(\beta-\alpha) + \cot\beta\cos(\beta-\alpha)\,, \\ Hb\bar{b} &: \cos\alpha/\cos\beta = \cos(\beta-\alpha) + \tan\beta\sin(\beta-\alpha)\,, \\ Ht\bar{t} &: \sin\alpha/\sin\beta = \cos(\beta-\alpha) - \cot\beta\sin(\beta-\alpha)\,, \\ Ab\bar{b} &: \gamma_5\tan\beta\,, \\ At\bar{t} &: \gamma_5\cot\beta\,, \end{aligned} \tag{11.49}$$

where the γ_5 indicates a pseudoscalar coupling. In each relation above, the factor listed for $b\bar{b}$ also pertains to $\tau^+\tau^-$. The charged Higgs boson couplings to fermion pairs are given by

$$\begin{aligned} g_{H^-t\bar{b}} &= \frac{g}{\sqrt{2}M_W}\left[m_t\cot\beta\frac{1+\gamma_5}{2} + m_b\tan\beta\frac{1-\gamma_5}{2}\right], \\ g_{H^-\tau^+\nu} &= \frac{g}{\sqrt{2}M_W}\left[m_\tau\tan\beta\frac{1-\gamma_5}{2}\right]. \end{aligned} \tag{11.50}$$

The non-standard neutral Higgs bosons have significantly enhanced couplings to down-type fermions at sizeable $\tan\beta$. From the above equations it is clear that this occurs near the alignment limit: $\cos(\beta-\alpha) \ll 1$, where in the mass eigenbasis only one Higgs acquires a VEV [244,245]. In this case the lightest Higgs boson behaves like the SM one and H, A have $\tan\beta$ enhanced couplings to down type fermions, and analogous enhanced couplings are in place for the charged Higgs.

Quite in general, radiative corrections can modify significantly the values of the Higgs boson couplings to fermion pairs and to vector boson pairs. In a first approximation, when radiative corrections to the quartic couplings are computed, the diagonalizing angle α is shifted from its tree-level value, and hence one may compute a "radiatively-corrected" value for $\cos(\beta-\alpha)$. This shift provides an important source of the radiative corrections to the Higgs couplings [217,247]. The radiative corrections to the angle α can enable the alignment without decoupling for sizeable values of the Higgs mass parameter $\mu \geq M_{\rm SUSY}$ and sizeable $\tan\beta$. Additional contributions from the one-loop vertex corrections to tree-level Higgs couplings must also be considered [211,261–268]. These contributions alter significantly the Higgs-fermion Yukawa couplings at large $\tan\beta$, both in the neutral and charged Higgs sector. Moreover, these radiative corrections can modify the basic relationship $g_{h,H,Ab\bar{b}}/g_{h,H,A\tau^+\tau^-} \propto m_b/m_\tau$, and change the main features of MSSM Higgs phenomenology.

V.1.3. Decay properties of MSSM Higgs bosons

In the MSSM, one must consider the decay properties of three neutral Higgs bosons and one charged Higgs pair. The mass, *CP* properties, decay and production properties of one of the neutral Higgs bosons should agree with Higgs data. Given that present data allows only for moderate departures from the SM predictions, it implies that some degree

of alignment is necessary. In this subsection possible *CP*-violating effects are neglected, and will be commented upon later.

For heavy SUSY particles and sufficiently heavy non-SM-like Higgs bosons, the alignment is triggered by decoupling and departures of the lightest MSSM Higgs boson couplings to gauge bosons and fermions from those predicted in the SM would be minimal. If m_A is below a few hundred GeV, instead, departures from alignment depend on the radiative corrections to the mixing angle α that are proportional to ratios of mass parameters associated to the SUSY particles, and hence do not decouple for heavy SUSY spectra. The main effects occur in departures from the $h \to b\bar{b}$ decay rate, hence also in its total width and, thus, in all branching ratios. As mentioned before, additional effects induced through SUSY-QCD radiative corrections to the $hb\bar{b}$ coupling may also be relevant even in the presence of heavy SUSY particles.

The SM-like branching ratios of h can be modified if decays into supersymmetric particles are kinematically allowed, and, in particular, decays into a pair of the lightest supersymmetric particles - i.e. lightest neutralinos - can become dominant and would be invisible if R-parity is conserved [269–271], Moreover, if light superpartners exist that couple to photons and/or gluons, the h loop-induced coupling to gg and $\gamma\gamma$ could deviate sizeably from the corresponding SM predictions [247,272–275]. Light staus close to 100 GeV with large mixing can enhance the Higgs decay rate into diphotons by up to 40% with respect to the SM, without being in conflict with the stability of the Higgs potential [276]. Light charginos, close to the LEP limit, can also induce up to 10% variations in the Higgs to diphoton decay rate for small values of $\tan\beta \simeq 4$, and hence heavy stops with masses in the 10 TeV range [277]. Given the smallness of the Higgs to diphoton rate, and hence its negligible contribution to the total Higgs decay width, both light staus and charginos have the possibility of altering $BR(h \to \gamma\gamma)$ without altering any other decay rates. Light stops and light sbottoms could contribute to the Higgs-diphoton rate, but in practice they are strongly constrained by the fact that they would at the same time yield a much larger contribution to gluon fusion Higgs production. The Higgs to digluon decay rate and gluon fusion Higgs production can be suppressed due to sbottom effects at large $\tan\beta$ and large μ, but in practice such effects are very small for masses above 500 GeV as presently preferred by LHC searches [278]. Light stops, could give relevant contributions to the Higgs digluon rate and gluon fusion Higgs production, which depending on the value of the stop mixing and the stop masses could yield both suppression or enhancement with respect to the SM. In practice, due to the m_h constrains on the stop sector, light stops can only moderately vary the effective gluon-Higgs coupling and correspondingly the gluon fusion-Higgs production rate [56,38,279].

Given that some degree of alignment is necessary to agree with data, for the heavier Higgs states there are two possibilities to be considered: i) Alignment triggered by decoupling, hence $m_A \geq$ several hundred GeV: The HWW and HZZ couplings are very small. The dominant decay branching ratios strongly depend on $\tan\beta$. After incorporating the leading radiative corrections to Higgs couplings, the following decay features are relevant in the MSSM. The decay modes $H, A \to b\bar{b}$, $\tau^+\tau^-$ dominate when $\tan\beta$ is large (this holds even away from decoupling). For small $\tan\beta$, the $t\bar{t}$ decay mode dominates above its kinematic threshold. In contrast to the lightest SM-like Higgs boson,

the vector boson decay modes of H are strongly suppressed due to the suppressed HVV couplings in the decoupling limit. For the charged Higgs boson, $H^+ \to t\bar{b}$ dominates. ii) Alignment without decoupling, hence $m_A \leq$ a few hundred GeV. The main difference with the previous case is that in the low $\tan\beta$ regime ($\tan\beta \leq 5$) additional decay channels may be allowed which involve decays into the lightest SM-like Higgs boson. For A and H, besides the $H, A \to b\bar{b}$, $\tau^+\tau^-$ decay modes, also $A \to Zh$, $H \to hh$ as well as $H \to WW/ZZ$ decay modes are available. For the charged Higgs boson, $H^+ \to \tau^+\nu_\tau$ dominates below the $t\bar{b}$ threshold, and also $H^\pm \to W^\pm h$ may be searched for. Both in i) and ii), the heavier Higgs states, H, A and $H^\pm$, are roughly mass degenerate (with masses $\pm$ 20 GeV or less apart).

In the case of sufficiently light SUSY particles, the heavy Higgs boson decays into charginos, neutralinos and third-generation squarks and sleptons can be important if they are kinematically allowed [269]. An interesting possibility is a significant branching ratio for the decay of a neutral Higgs boson to the invisible mode $\tilde{\chi}_1^0\tilde{\chi}_1^0$ (where the lightest neutralino $\tilde{\chi}_1^0$ is the lightest supersymmetric particle) [270], which poses a challenge at hadron colliders.

V.1.4. Production mechanisms of MSSM Higgs bosons

The production mechanisms for the SM Higgs boson at e^+e^- and hadron colliders can also be relevant for the production of the MSSM neutral Higgs bosons. However, one must take into account the possibility of enhanced or suppressed couplings with respect to those of the Standard Model, as previously discussed. The SUSY-QCD corrections due to the exchange of virtual squarks and gluinos may modify the cross sections depending on the values of these supersymmetric particle masses. At both lepton and hadron colliders there are new mechanisms that produce two neutral Higgs bosons, as well as processes that produce charged Higgs bosons singly or in pairs. In the following discussion, the main processes for MSSM Higgs boson production are summarized. For more detailed discussions see Refs. [34,241], and for the state-of-the-art calculations of higher order corrections as well as estimates of uncertainties at hadron colliders see Refs. [36–38] and references therein.

The main production mechanisms for the neutral MSSM Higgs bosons at e^+e^- colliders are Higgs-strahlung ($e^+e^- \to Zh, ZH$), vector boson fusion ($e^+e^- \to \nu\bar{\nu}h, \nu\bar{\nu}H$) – with W^+W^- fusion about an order of magnitude larger than ZZ fusion – and s-channel Z boson exchange ($e^+e^- \to Ah, AH$) [280]. For the Higgs-strahlung process [281], it is possible to reconstruct the mass and momentum of the Higgs boson recoiling against the particles from the Z boson decay, and hence sensitive searches for Higgs bosons decaying even to invisible final states are possible.

The main charged Higgs boson production process at e^+e^- colliders is via s-channel γ or Z boson exchange ($e^+e^- \to H^+H^-$). Charged Higgs bosons can also be produced in top quark decays via $t \to b + H^+$ if $m_H^\pm < m_t - m_b$ or via the one-loop process $e^+e^- \to W^\pm H^\mp$ [282,283], which allows the production of a charged Higgs boson with $m_H^\pm > \sqrt{s}/2$, even when H^+H^- production is kinematically forbidden. Other single charged Higgs production mechanisms include $t\bar{b}H^-/\,\bar{t}bH^+$ production [90],

$\tau^+\nu H^-/\,\tau^-\bar{\nu}H^+$ production [284], and a variety of processes in which $H^\pm$ is produced in association with a one or two other gauge and/or Higgs bosons [285].

At hadron colliders, the dominant neutral Higgs production mechanism over the majority of the MSSM parameter space is gluon fusion, mediated by loops containing heavy top and bottom quarks and the corresponding supersymmetric partners [286]. The effect of light stops that may contribute to the gluon fusion production will be partially cancelled by the fact that they need to have sizeable mixing, while light sbottoms that could suppress gluon fusion through mixing effects are disfavored by data. Higgs boson radiation off bottom quarks becomes important for large $\tan\beta$, where at least two of the three neutral Higgs bosons have enhanced couplings to bottom-type fermions [287,288]. In the search for non-standard neutral Higgs bosons, A and H, the production can be via either of the above channels in the final inclusive ditau mode and via radiation off bottom quarks in the 4b's final mode. The total production rates of bottom quarks and τ pairs mediated by the production of a CP-odd Higgs boson in the large $\tan\beta$ regime are approximately given by

$$\begin{aligned}\sigma_{b\bar{b}A}\times \mathrm{BR}(A\to b\bar{b}) &\simeq \sigma^{\mathrm{SM}}_{b\bar{b}A}\;\frac{\tan^2\beta}{(1+\Delta_b)^2}\frac{9}{(1+\Delta_b)^2+9},\\ \sigma_{gg\to A,b\bar{b}A}\times \mathrm{BR}(A\to \tau^+\tau^-) &\simeq \sigma^{\mathrm{SM}}_{gg\to A,b\bar{b}A}\;\frac{\tan^2\beta}{(1+\Delta_b)^2+9},\end{aligned} \tag{11.51}$$

where $\sigma^{\mathrm{SM}}_{b\bar{b}A}$ and $\sigma^{\mathrm{SM}}_{gg\to A,b\bar{b}A}$ denote the values of the corresponding SM Higgs boson cross sections for a SM Higgs boson mass equal to m_A. For high $\tan\beta$, the function Δ_b includes the dominant effects of the SUSY radiative corrections affecting the relation between the bottom quark mass and the bottom Yukawa coupling [211,217,265–267,249], and it depends strongly on $\tan\beta$ and on the SUSY mass parameters. As a result of the Δ_b dependence shown in Eq. (11.51), it follows that the $b\bar{b}A$ channel is more sensitive to the specific SUSY scenario, while the inclusive $\tau^+\tau^-$ channel is rather robust under variations of the SUSY spectra. The production and decay rates of H, for m_A larger m_h^{max}, are governed by formulas similar to the ones presented above, and given that A and H are nearly degenerate in mass, the total signal cross section is increased by roughly a factor of two. Detailed discussions of the impact of radiative corrections in these search modes are presented in Refs. [249,289].

The vector boson fusion and Higgs-strahlung production of the CP-even Higgs bosons as well as the associated production of neutral Higgs bosons with top quark pairs have lower production cross sections by at least an order of magnitude with respect to the dominant ones, depending on the precise region of MSSM parameter space [36]. Higgs pair production of non-standard MSSM Higgs bosons has been studied in Ref. [290].

Charged Higgs bosons can be produced in several different modes at hadron colliders. If $m_{H^\pm} < m_t - m_b$, the charged Higgs boson can be produced in decays of the top quark via the decay $t\to bH^+$, which would compete with the SM process $t\to bW^+$. Relevant radiative corrections to $\mathrm{BR}(t\to H^+b)$ have been computed in Refs. [291–294]. For values of $m_{H^\pm}$ near m_t, width effects are important. In addition, the full $2\to 3$ processes

$pp/p\bar{p} \to H^+\bar{t}b + X$ and $pp/p\bar{p} \to H^-t\bar{b} + X$ must be considered. If $m_{H^\pm} > m_t - m_b$, then charged Higgs boson production occurs mainly through radiation from a third generation quark. Charged Higgs bosons may also be produced singly in association with a top quark via the $2 \to 3$ partonic processes gg, $q\bar{q} \to t\bar{b}H^-$ (and the charge conjugate final states). Charged Higgs bosons can also be produced via associated production with $W^\pm$ bosons through $b\overline{b}$ annihilation and gg-fusion [295]. They can also be produced in pairs via $q\overline{q}$ annihilation [296]. The inclusive H^+H^- cross section is less than the cross section for single charged Higgs associated production [296,297]. For a more extensive discussion of charged Higgs boson production at LHC see Refs. [10,298,36].

V.1.5. Benchmark scenarios in the MSSM for a 125 GeV light Higgs

The experimental uncertainties on the measurements of the production cross sections times branching ratios are at present rather large, and a Higgs sector that differs significantly from the SM case can still fit the data. Hence it is important to explore scenarios where the lightest Higgs agrees with present data but still allows for novel new physics features, and to consider the implications of such scenarios in the search for the remaining MSSM Higgs bosons. The additional Higgs bosons are sought for mainly via the channels

$$\begin{aligned}
&pp \to A/H \to \tau^+\tau^- \ \text{(inclusive)},\\
&b\bar{b}A/H, A/H \to \tau^+\tau^- \ \text{(with } b\text{−tag)},\\
&b\bar{b}A/H, A/H \to b\bar{b} \ \text{(with } b\text{−tag)},\\
&pp \to t\bar{t} \to H^\pm W^\mp b\bar{b}, \ \ H^\pm \to \tau\nu_\tau \ ,\\
&gb \to H^-t \quad \text{or} \quad g\bar{b} \to H^+\bar{t}, \ \ H^\pm \to \tau\nu_\tau \ .
\end{aligned} \tag{11.52}$$

The non-observation of any additional state in these production and decay modes puts by now stringent constraints on the MSSM parameter space, in particular on the values of the tree level parameters m_A and $\tan\beta$. Similarly, the non-observation of supersymmetric particles puts constraints on masses of stops and sbottoms as well as gluinos and electroweak gauginos that are relevant for the Higgs sector. Assuming $m_h \simeq$ 125 GeV, it is possible to do a scan of the MSSM parameters considering a simplified structure of the Higgs radiative corrections [299], or varying a restricted number of the most relevant parameters [300], and obtain a best fit to the various, measured rates of cross sections and branching ratios. However, due to the large number of free parameters that are relevant for the Higgs sector, a complete scan of the MSSM parameter space is impractical in experimental analyses and phenomenological studies. In the past, for LEP, the Tevatron and the LHC it has been useful to define a set of benchmark scenarios to highlight interesting conditions for MSSM Higgs searches [248,249]. After the Higgs boson discovery, updated MSSM benchmarks scenarios have been defined, that over a wide range of parameter space are compatible with both the mass and the detected production and decay rates of the observed signal [248,38]. They include: i) an updated version of the maximal mixing scenario with a larger value of the gluino mass compatible with LHC bounds. This scenario was originally defined to consider values of the stop mixing to maximize the m_h value and, as a result, only a small region of parameter space is compatible with $m_h \approx 125\,\text{GeV}$; ii) a moderate mixing scenario in which the

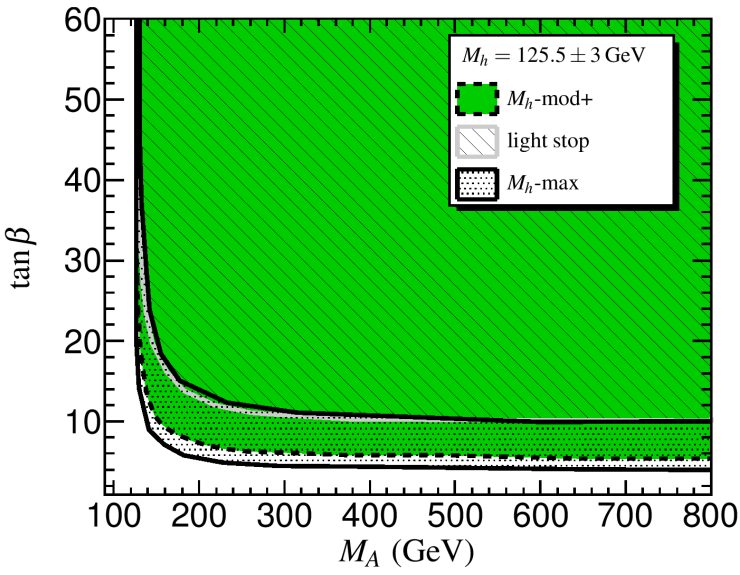

Figure 11.26: Allowed regions in the $(m_A, \tan\beta)$ plane, compatible with the lightest Higgs boson mass, $m_h = 125.5 \pm 3\,\text{GeV}$, for the maximal mixing scenario (hatched black region), the moderate stop mixing benchmark scenario (green shaded region) and the light stop scenario (blue hatched region), as defined in Ref. [248].

light *CP*-even Higgs boson can be interpreted as the newly discovered state within almost the whole parameter space of the $m_A - \tan\beta$ plane that is un-excluded by limits from Higgs searches at LEP and the LHC; iii) a light stop scenario with stop masses in the few to several hundred GeV range that can give contributions to gluon fusion Higgs production; iv) a light stau scenario where the light stau can enhance the SM branching ratio into diphotons for large $\tan\beta$ and v) a tau-phobic scenario that exhibits variations of $BR(h \to b\bar{b})$ and $BR(h \to \tau^+\tau^-)$ with respect to their SM values.

The above benchmarks are just examples that interpret the LHC signal as the lightest *CP*-even MSSM Higgs boson. In Fig. 11.26 the regions in the $(m_A, \tan\beta)$ plane that are compatible with a light *CP* even Higgs mass, $m_h = (125.5 \pm 3)\,\text{GeV}$, are shown for the above benchmarks scenarios. The parameter space allowed by cases ii, iv and v is overlapping, hence only the moderate mixing scenario is shown in the figure. In the light stop and light stau scenarios the lightest Higgs properties would deviate from those of the SM Higgs in all of the allowed parameter space due to loop effects, irrespective of the precise value of m_A. In the maximal mixing and moderate mixing scenarios, h tends to behave as a SM-like Higgs as the theory approaches the decoupling limit. In the tau-phobic scenario, h behaves SM-like due to alignment for specific regions of $\tan\beta$ and large μ, irrespective of the value of m_A. The above benchmarks also have different behavior for the properties of the heavy Higgs bosons. In particular, in the light stau scenario, the decay of $A/H \to \tilde{\tau}_1^+\tilde{\tau}_1^-$ becomes relevant. In the above benchmarks it is also possible to have decays of $H \to hh$ in regions of moderate m_A and moderate $\tan\beta$ as far as one is away from alignment. Also for the previous benchmarks, under the assumption of gaugino mass unification: $M_1 \simeq M_2/2$, and considering the traditional $A/H \to \tau^+\tau^-$

search channel, one would observe variations in the LHC reach depending on the values of μ and M_2. If both parameters are small, as in the maximal and moderate mixing scenarios, then the decays of heavy neutral Higgs bosons into electroweakinos become competitive for small to moderate $\tan\beta$ and m_A. On the contrary, if at least one of the two parameters becomes larger, as in the rest of the benchmark scenarios, then the decay of heavy neutral Higgs bosons into electroweakinos closes up and the reach in $A/H \to \tau^+\tau^-$ is significantly enhanced for the same regions of $\tan\beta$ and m_A. Lastly, varying the parameter μ in both sign and magnitude induces relevant variations in the possible discovery reach through the $4b$'s channel, and to a lesser extent through the inclusive ditau channel. Future precision measurements of the Higgs boson couplings to fermions and gauge bosons together with information on heavy Higgs searches will provide powerful information on the SUSY parameter space [245,299]. If no other new states beyond the current Higgs candidate are discovered at the LHC, it becomes mandatory to understand what would be the required precision of the Higgs rate measurements to distinguish the MSSM from the SM.

V.2. Indirect constraints on additional states

Interpreting the lightest Higgs as the observed Higgs with a mass of about 125 GeV, improvements in our understanding of B-physics observables put indirect constraints on additional Higgs bosons in mass ranges that would be accessible in direct LHC searches. In particular, $\mathrm{BR}(B_s \to \mu^+\mu^-)$, $\mathrm{BR}(b \to s\gamma)$, and $\mathrm{BR}(B_u \to \tau\nu)$ play an important role within minimal flavor-violating (MFV) models [301], in which flavor effects proportional to the CKM matrix elements are induced, as in the SM. For example, see Refs. [302–309]. The supersymmetric contributions to these observables come both at the tree and loop level, and have a different parametric dependence, but share the property that they become significant for large values of $\tan\beta$, which is also the regime in which searches for non-standard MSSM Higgs bosons at hadron colliders are the most powerful.

In the SM, the relevant contributions to the rare decay $B_s \to \mu^+\mu^-$ come through the Z-penguin and the W-box diagrams [310]. In supersymmetry with large $\tan\beta$, there are also significant contributions from Higgs-mediated neutral currents [311–314], which depend on the SUSY spectra, and grow with the sixth power of $\tan\beta$ and decrease with the fourth power of the CP-odd Higgs boson mass m_A. Therefore, measurements at the LHC experiments [315] put strong restrictions on possible flavor-changing neutral currents (FCNC) in the MSSM at large $\tan\beta$ [302,309,316].

Further constraints are obtained from the rare decay $b \to s\gamma$. The SM rate is known up to NNLO corrections [317,318] and is in good agreement with measurements [319]. In the Type-II 2HDM and in the absence of other sources of new physics at the electroweak scale, a bound on $m_{H^\pm} > 380\,\mathrm{GeV}$ can be derived [320]. Although this indirect bound appears much stronger than the results from direct charged Higgs searches, it can be invalidated by new physics contributions, such as those which can be present in the MSSM. In the minimal flavor-violating MSSM, there are new contributions from charged Higgs as well as chargino-stop and gluino-sbottom diagrams. The charged Higgs boson's contribution is enhanced for small values of its mass and can be partially canceled by the chargino and gluino contributions or by higher-order $\tan\beta$-enhanced loop effects.

The branching ratio $B_u \to \tau\nu$, measured by the Belle [321] and BaBar [322] collaborations is in good agreement with the SM prediction [323], but still leaves room for new physics In the MSSM, there is an extra tree-level contribution from the charged Higgs which interferes destructively with the SM contribution, and which increases for small values of the charged Higgs boson mass and large values of $\tan\beta$ [324]. Closely related decay modes that are also sensitive to charged Higgs effects are the $B \to D\tau\nu$ and $B \to D^*\tau\nu$ decays [325]. While predictions of the corresponding branching ratios suffer from large hadronic uncertainties coming from the $B \to D$ and $B \to D^*$ form factors, the ratios $\mathrm{BR}(B \to D\tau\nu)/\mathrm{BR}(B \to D\ell\nu)$ and $\mathrm{BR}(B \to D^*\tau\nu)/\mathrm{BR}(B \to D^*\ell\nu)$, where $\ell = e$ or μ, can be predicted with reasonable accuracy in the SM. Interestingly, recent results from BaBar [326] on these ratios are around 2σ above the SM predictions in both decay modes. Older results from Belle [327] give similar central values but with much larger uncertainties. The tensions in $B \to D\tau\nu$ and $B \to D^*\tau\nu$ cannot be addressed in the context of the MSSM with MFV [309] but would require more radical approaches. These observables constrain in an important way the parameter space for small values of the charged Higgs boson mass and sizeable values of $\tan\beta$ and are only mildly dependent on the SUSY spectra.

Several recent studies [307–309,302] show that, in extended regions of parameter space, the combined B-physics measurements impose strong constraints on minimally flavor-violating MSSM models to which Higgs boson searches at the LHC are sensitive. Consequently, the observation of a non-SM Higgs boson at the LHC would point to a rather narrow, well-defined region of MSSM parameter space or to something beyond the minimal flavor violation framework.

Another indirect constraint on the Higgs sector comes from the search for dark matter. Assuming a standard cosmological model, the proper thermal relic density is naturally obtained in particle physics models in which dark matter particles are weakly interacting and with masses of the order of the weak scale. In particular, the lightest supersymmetric particle, typically the lightest neutralino, is an excellent dark matter particle candidate [204]. Within the MSSM, the measured relic density places constraints in the parameter space, which in turn - for specific SUSY low energy spectra- have implications for Higgs searches at colliders, and also for experiments looking for direct evidence of dark matter particles in elastic scattering with atomic nuclei. Large values of $\tan\beta$ and small m_A are relevant for the $b\bar{b}A/H$ and $A/H \to \tau^+\tau^-$ searches at the LHC, and also provide a significant contribution from the CP-even Higgs H exchange to the spin-independent cross sections for direct detection experiments such as LUX, CDMS or Xenon, for example. Consequently, a signal at colliders would raise prospects for a signal in direct detection experiments and vice-versa, see for example Refs [302,307–309,328–334]. Theoretical uncertainties in the calculation of dark matter scattering cross sections, and in the precise value of the local dark matter density and velocity distributions, may dilute these model-dependent correlations.

V.3. Higgs Bosons in singlet extensions of the MSSM

In the MSSM, the Higgs mass parameter μ is a supersymmetric parameter, and as such, it should naturally be of order M_{GUT} or M_{Planck}. However, in order to enable

electroweak symmetry breaking, μ should be of the order of the SUSY breaking scale, that for naturalness we argue should be reasonably close to the electroweak scale. The fact that phenomenologically it is required that μ be at the electroweak/TeV scale is known as the μ problem [335]. Supersymmetric models with additional singlets can provide a solution to the μ problem [335], by promoting the μ parameter to a dynamical singlet superfield S that only interacts with the MSSM Higgs doublets through a coupling λ_S at the level of the superpotential. An effective μ is generated when the real scalar component of S acquires a vacuum expectation value $\langle S \rangle$

$$\mu_{eff} = \lambda_S \langle S \rangle. \tag{11.53}$$

After the minimization of the Higgs potential the vacuum state relates the vacuum expectation values of the three *CP*-even neutral scalars, ϕ_1^0, ϕ_2^0 and S, to their soft supersymmetry breaking masses, hence, one expects that these VEVs should all be of order $M_{\rm SUSY}$ and therefore the μ problem is solved.

The solution of the μ problem through the addition of a singlet superfield to the MSSM comes along with the existence of an extra global U(1) symmetry, known as the Peccei–Quinn (PQ) symmetry [336]. Once the PQ symmetry is spontaneously broken by the Higgs VEVs, a pseudo-Nambu–Goldstone boson, the PQ axion appears in the theory. For values of λ_S of order one the lack of detection of such an axion rules out the theory. Making λ_S very small ($\leq 10^{-6}$) would decouple the axion and render things compatible with experimental results, but then one would be trading the μ problem by a λ_S problem, since there is no explanation to why λ_S should be so small. Promoting the PQ symmetry to a local symmetry involving additional gauge bosons and matter fields could be a viable option that has been explored in the literature. Alternatively there is the possibility to break the PQ symmetry explicitly. For that purpose one can consider a discrete Z_3 symmetry that allows the existence of a PQ odd S^3 term in the superpotential. This model extension has been called the Next-to-Minimal Supersymmetric SM (NMSSM) [337]. It is known however that discrete symmetries may come along with the existence of domain wall structures that imply that our universe would consist of disconnected domains with different ground states, creating unacceptably large anisotropies in the cosmic microwave background [338]. To avoid the problem of domain walls one can consider the existence of non-renormalizable operators that would lead to the preferred vacuum state. However, the same operators in turn may generate quadratically divergent tadpole contributions [339] that could shift the VEV of S to be much larger, order M_{GUT}, and ruin the singlet solution to the μ problem. To cure the problem of destabilizing tadpoles, discrete R-symmetries have been proposed that secure that tadpoles would only appear at very high order loops and be safely suppressed. Depending on the symmetries imposed on the theory, different models with singlet extensions of the MSSM (xMSSM) have been proposed. In Table 11.15 we show the most studied examples: the NMSSM, the Nearly-Minimal Supersymmetric SM (nMSSM) [340], and the U(1)′-extended MSSM (UMSSM) [341], specifying the new parameters appearing in the superpotential and the respective symmetries. A Secluded U(1)′-extended MSSM (sMSSM) [342] contains three singlets in addition to the standard UMSSM Higgs singlet; this model is equivalent to the nMSSM in the limit that the additional singlet VEV's are large, and the trilinear singlet coupling, λ_S, is small [343].

Table 11.15: Symmetries associated to various models with singlet extensions, the corresponding terms in the superpotential that only involve Higgs and singlet fields, and the number of neutral states in the Higgs sector for the case of CP conservation.

Model	MSSM	NMSSM	nMSSM	UMSSM
Symmetry	-	Z_3	Z_5^R, Z_7^R	$U(1)'$
Superpotential	$\mu\Phi_2\cdot\Phi_1$	$\lambda_S S\Phi_2\cdot\Phi_1+\frac{\kappa}{3}S^3$	$\lambda_S S\Phi_2\cdot\Phi_1+t_F S$	$\lambda_S S\Phi_2\cdot\Phi_1$
H_i^0	2	3	3	3
A_i^0	1	2	2	1

Based on the extended models defined in Table 11.15, we write the most generic supersymmetric and soft supersymmetry breaking scalar potentials for the three scalar fields: Φ_1, Φ_2 and S:

$$\begin{aligned} V_{xMSSM} = &\left|\lambda_S\Phi_2\cdot\Phi_1+t_F+\kappa S^2\right|^2+|\lambda_S S|^2\left(|\Phi_1|^2+|\Phi_2|^2\right)\\ &+\frac{g'^2+g^2}{8}\left(|\Phi_1|^2-|\Phi_2|^2\right)^2\\ &+\frac{g^2}{2}\left(|\Phi_1|^2|\Phi_2|^2-|\Phi_2\cdot\Phi_1|^2\right)\\ &+\frac{g_1'^2}{2}\left(Q_{\Phi_1}|\Phi_1|^2+Q_{\Phi_2}|\Phi_2|^2+Q_S|S|^2\right)^2 \end{aligned} \tag{11.54}$$

$$\begin{aligned} V_{\rm soft} = &\, m_{H_1}^2|\Phi_1|^2+m_{H_2}^2|\Phi_2|^2+m_s^2|S|^2\\ &+\left(A_s\lambda_S S H_u\cdot H_d+\frac{\kappa}{3}A_\kappa S^3+t_S S+h.c.\right). \end{aligned} \tag{11.55}$$

where $\Phi_2\cdot\Phi_1=\epsilon_{ij}\Phi_2^i\Phi_1^j$ and the couplings g', g, and g_1' are associated to the $U(1)_Y$, $SU(2)_L$, and $U(1)'$ gauge symmetries, respectively. t_F and t_S are supersymmetric and SUSY breaking tadpole terms, respectively, m_s is a SUSY breaking mass term for the scalar component of the field S, and A_s and A_κ are the trilinear soft SUSY breaking mass parameters associated with the new terms $\lambda_S S\Phi_2\cdot\Phi_1$ and $\kappa S^3/3$ in the superpotential, with the B-term of the MSSM expressed as $B\mu\equiv A_s\mu_{eff}$. In particular, κ and A_κ are the parameters for the NMSSM model, while t_F and t_S are those of the nMSSM. The UMSSM depends on the new coupling g_1' as well as on the $U(1)'$ charges of the Higgs fields, Q_{Φ_1}, Q_{Φ_2} and Q_S, that are free parameters with the restriction that they have to add to zero for the superpotential $\lambda_3 S\Phi_2\Phi_1$ to be gauge invariant. In a given $U(1)'$ construction the charges are specified. The addition of the singlet scalar field(s) imply that additional *CP*-even and *CP*-odd Higgs bosons will appear in the spectra, whereas the charged Higgs sector remains the same as in the MSSM given that the number of Higgs doublets remains unchanged. The mixing with the extra scalar S alters the masses and properties of the physical Higgs bosons, that in general can differ significantly from the SM or the MSSM. A detailed discussion of typical mass spectra and decay properties in these models can be found for example in Refs. [344,343]. Moreover, these models have

extra neutralinos and in some cases extra neutral gauge bosons, Z'. The extra gauge boson sector is constrained by experimental data through direct Z' searches as well as the $Z - Z'$ mixing angle $\alpha_{ZZ'}$ constrained to be less that $\mathcal{O}(10^{-3})$ by precision electroweak data .

An interesting feature of models with a singlet extension of the MSSM is that they can easily lead to a strong first order phase transition that enables the possibility of baryogenesis at the electroweak scale [345]. In these models, the strong first order phase transition, necessary to preserve the baryon asymmetry created at the EW scale, is connected to the existence of the cubic soft SUSY breaking term A_S connecting the singlet scalar field with the two Higgs doublets, and does not require a too light SM like Higgs boson mass as it occurs in the MSSM. On the other hand, in SUSY models with extended singlets there is the possibility of additional *CP*-violating phases that may allow to generate the baryon asymmetry and are much less restricted by present electric dipole moments (EDM's) data than those in the MSSM.

V.3.1. The xMSSM Higgs boson masses and phenomenology

In singlet extensions of the MSSM the lightest *CP*-even Higgs mass at tree level, $m_{H_1}^{tree}$ receives a contribution from the singlet scalar that renders it larger than the MSSM value, in particular for small values of $\tan\beta$. The tree level upper bound reads[11]

$$m_{H_1}^{tree} \leq M_Z^2 \cos^2 2\beta + \frac{1}{2}\lambda_S^2 v^2 \sin^2 2\beta \,. \tag{11.56}$$

At the one-loop level, the top and stop loops (sbottom and stau loops for large $\tan\beta$) are the dominant contributions, that are common to the MSSM and to all the singlet extensions. Gauge couplings in the UMSSM are small compared to the top quark Yukawa coupling, hence the one-loop gauge contributions are negligible. Corrections exclusive to the NMSSM and the nMSSM enter only at the two loop level. Therefore, there are no significant model-dependent contributions at one loop order, and as a result, for large $\tan\beta$ the lightest *CP*-even Higgs mass does not differ in any significant way from the MSSM one. Fig. 11.27 shows the mass ranges for the lightest *CP*-even Higgs boson in the MSSM, NMSSM, nMSSM and UMSSM for a scan over parameters as defined in Ref. [343]. The value of $M_{\rm SUSY}$ is fixed to 1 TeV and the radiative corrections are computed only at one loop level. The upper bounds in Fig. 11.27 are indicative, since two loop corrections, as has been shown for the MSSM, can be rather relevant and have not been included. A value of the lightest SM Higgs mass of about 125 GeV is achievable in all these MSSM extensions, and this remains the case even after higher order corrections are implemented.

A singlet extended supersymmetric Higgs sector opens new avenues for discovery. Since the singlet pseudoscalar particle may be identified as the pseudo-Goldstone boson of a spontaneously broken Peccei–Quinn symmetry, it may become naturally light [346,347]. Generally, there is mixing of the singlet sector with the MSSM Higgs sector, and with

[11] Additional gauge interactions contribute to this increase with a term of $\mathcal{O}(g_1'^2 v^2 (Q_{\phi_2}^2 \cos^2 Q_{\phi_1}^2 \sin^2\beta))$ in the UMSSM.

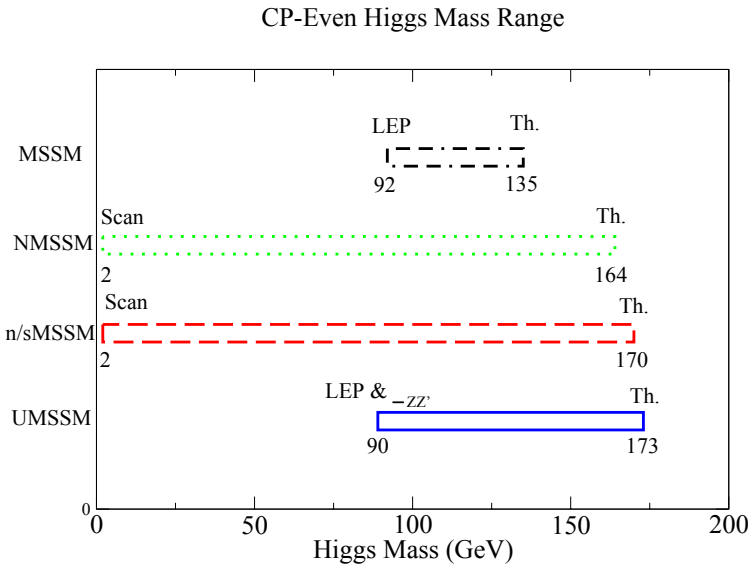

Figure 11.27: Mass ranges for the lightest *CP*-even Higgs boson in each extended MSSM scenario discussed in the text, and in the MSSM, for comparison. The value of $M_{\rm SUSY}$ is fixed to 1 TeV and the rest of parameters are scanned as defined in Ref. [343]. The radiative corrections are computed only at one loop level.

a sufficiently light, singlet dominated scalar or pseudoscalar, H_1^0 or A_1^0, respectively, the SM-like Higgs boson H_2^0 may decay to pairs of H_1^0 or A_1^0. The light scalar and/or pseudoscalar may subsequently decay to $\tau\tau$ or $b\bar{b}$ pairs [348]. Such cascade decays are more difficult to detect than standard searches due to the potentially soft decay products. In addition, the light singlet scenario in the NMSSM or nMSSM is typically associated with a light singlino-dominated neutralino. The recently discovered SM-like Higgs boson can then decay to pairs of this neutralino [349,343], opening an invisible decay mode that is not excluded by present data. In the case of a heavy singlet dominated scalar, its detection would be more challenging than for a SM-like Higgs of similar mass due to the reduced couplings.

An indirect probe of an extended Higgs sector is through precision Higgs production and decay rate measurements of the recently discovered Higgs boson at the LHC. In models with extended singlets, at low $\tan\beta$ it is possible to trade the requirement of a large stop mixing by a sizeable trilinear Higgs-Higgs singlet coupling λ_S, rendering more freedom on the requirements for gluon fusion production. Similar to the MSSM, mixing in the Higgs sector -additionally triggered by the extra new parameter λ_S - can produce variations in the Higgs-$b\bar{b}$ and Higgs-$\tau^-\tau^+$ couplings that can alter the Higgs to ZZ/WW and diphoton rates. Light charginos at low $\tan\beta$ can independently contribute to enhance the di-photon rate, without altering any other of the Higgs decay rates [275,350]

V.4. Supersymmetry with extended gauge sectors

In the MSSM, the tree-level value of the lightest *CP*-even Higgs mass originates from the D-term dependence of the scalar potential that comes from the supersymmetric kinetic

terms in the Kähler potential. The D-terms lead to tree-level quartic couplings which are governed by the squares of the gauge couplings of the weak interactions, under which the Higgs has non-trivial charges and hence the lightest Higgs mass is bounded to be smaller than M_Z. If new gauge interactions were present at the TeV scale, and the Higgs bosons would have non-trivial charges under them, there would be new D-term contributions that would lead to an enhancement of the tree-level Higgs mass value. Since the low energy gauge interactions reduce to the known $SU(3)_c \times SU(2)_L \times U(1)_Y$ ones, in order for this mechanism to work, the extended gauge and Higgs sectors should be integrated out in a non-supersymmetric way. This means that there must be supersymmetry breaking terms that are of the order or larger than the new gauge boson masses. The tree-level quartic couplings would then be enhanced through their dependence on the square of the gauge couplings of the extended Higgs sector. This effect will be suppressed when the heavy gauge boson masses are larger than the supersymmetry breaking scale and will acquire its full potential only for large values of this scale.

One of the simplest possibilities is to extend the weak interactions to a $SU(2)_1 \times SU(2)_2$ sector, such that the known weak interactions are obtained after the spontaneous breaking of these groups to $SU(2)_L$ [223]. This may be achieved by introducing a bi-doublet Σ under the two SU(2) gauge groups, which acquires a non-trivial vacuum expectation value u in the diagonal direction. The heavy gauge boson masses are therefore given by $M^2_{W'} = (g_1^2 + g_2^2)u^2/2$, and the weak coupling $g^2 = g_1^2 g_2^2/(g_1^2 + g_2^2)$. To obtain a new tree-level contribution to the Higgs potential, the Higgs bosons must be charged under the new gauge interactions. One possibility is to assume that the third generation quarks and leptons as well as the Higgs doublets have charges under the $SU(2)_1$ group, while the second and third generations have charges under $SU(2)_2$. This provides a natural explanation of the largeness of the third generation couplings compared to the first and second generation ones.

Under the above conditions, the D-term contributions to the neutral Higgs effective potential are given by

$$V_D = \frac{g^2\Delta + g'^2}{8}\left(|H_2^0|^2 - |H_1^0|^2\right)^2 \tag{11.57}$$

with

$$\Delta = \left(1 + \frac{4m_\Sigma^2}{g_2^2 u^2}\right)\left(1 + \frac{4m_\Sigma^2}{(g_1^2 + g_2^2)u^2}\right)^{-1}, \tag{11.58}$$

where m_Σ is the supersymmetry breaking term associated with the bi-doublet Σ. It is easy to see that while the MSSM D-term is recovered when $m_\Sigma \to 0$, it is replaced by the $SU(2)_1 \times U(1)_Y$ D-term when m_Σ becomes much larger than $M_{W'}$. The tree-level mass now reads

$$m_h^2|_{\rm tree} = \frac{g^2\Delta + g'^2}{4} v^2 \cos^2 2\beta, \tag{11.59}$$

and reduces to the MSSM value, $M_Z^2 \cos^2 2\beta$, for $\Delta = 1$.

Assuming $g_1 \simeq g_2$, values of $g_{1,2}$ of order one are necessary to obtain the proper value of the weak gauge coupling. In addition, if values of m_Σ of order $M_{W'}$ are assumed,

enhancements of order 50 percent of the MSSM D-term contribution to the Higgs mass may be obtained. Such enhancements are sufficient to obtain the measured Higgs mass value without the need of very heavy stops or large stop mixing parameters.

The gauge extension described above leads to new, heavy gauge and Higgs bosons, as well as new neutralinos and charginos. Constraints from precision measurements put bounds of the order of a few TeV on the mass of these gauge bosons, which may be probed at the higher energy run of the LHC collider. If the new gaugino supersymmetry breaking masses are smaller than the gauge boson masses, the new electroweakinos will have masses of the order of a few TeV and therefore the weak scale phenomenology reduces to the MSSM one.

Although a particular gauge extension of the MSSM was taken as an example, the results are rather general. Provided that the MSSM Higgs bosons are charged under the extended gauge group and that the supersymmetry breaking parameters associated with the new spontaneously broken gauge sector are large compared to the new gauge boson masses, non-decoupled D-terms for the Higgs fields are generated, leading to a modification of the tree-level Higgs mass prediction. Similar gauge extensions, including also new abelian gauge groups have been considered, for instance, in Ref. [351].

Gauge extensions of the MSSM can also lead to an enhancement of the Higgs mass value by modifying the renormalization group evolution of the Higgs quartic coupling to low energies. In the MSSM, the evolution of the quartic coupling is governed by the top-quark Yukawa interactions and depends on the fourth power of the top-quark Yukawa coupling. The neutralino and chargino contributions, which depend on the fourth power of the weak gauge couplings, are small due to the smallness of these couplings. Depending on the values of the soft supersymmetry breaking parameters in the gaugino and Higgsino sectors, the $\mathrm{SU}(2)_1$ gauginos may become light, with masses of the order of the weak scale. Since the $\mathrm{SU}(2)_1$ coupling may be significantly larger than the $\mathrm{SU}(2)_L$ one, for small values of the Higgsino mass parameter μ, the associated charginos and neutralinos may modify the evolution of the quartic coupling in a significant way [352]. This may lead to a significant increase of the lightest *CP*-even Higgs mass, even for small values of $\tan\beta \simeq 1$ for which the D-term contributions become small. In addition, under these conditions, light charginos may lead to a significant modification of the Higgs diphoton decay rate, which may be as large as 50% of the SM [352–356].

V.5. Effects of CP violation

In the Standard Model, *CP*-violation (*CPV*) is induced by phases in the Yukawa couplings of the quarks to the Higgs field, which results in one non-trivial phase in the CKM mixing matrix. SUSY scenarios with new *CPV* phases are theoretically appealing, since additional *CPV* beyond that observed in the K, D, and B meson systems is required to explain the observed cosmic matter-antimatter asymmetry [357]. In the MSSM *CP*-violation effects in the Higgs sector appear at the quantum level and are mostly determined by *CP* phases active in the third generation squark soft SUSY breaking trilinear mass parameters as well as in the gaugino/gluino masses. In extensions of the MSSM such as singlet extensions *CP* violation effects can be effective already at tree

level and due to the larger number of new parameters there are many more sources of *CP* violation. In general *CP* violation effects in the Higgs sector are importantly constrained from electric dipole moments data [358].

V.5.1. Effects of CP violation on the MSSM Higgs spectrum

In the MSSM, there are additional sources of *CPV* from phases in the various mass parameters. In particular, the gaugino mass parameters ($M_{1,2,3}$), the Higgsino mass parameter, μ, the bilinear Higgs squared-mass parameter, m_{12}^2, and the trilinear couplings of the squark and slepton fields to the Higgs fields, A_f, may carry non-trivial phases. The two parameter combinations $\arg[\mu A_f (m_{12}^2)^*]$ and $\arg[\mu M_i (m_{12}^2)^*]$ are invariant under phase redefinitions of the MSSM fields [359,252]. Therefore, if one of these quantities is non-zero, there would be new sources of *CP*-violation, which affects the MSSM Higgs sector through radiative corrections [251,252,360–364]. The mixing of the neutral *CP*-odd and *CP*-even Higgs boson states is no longer forbidden. Hence, m_A is no longer a physical parameter. However, the charged Higgs boson mass $m_{H^\pm}$ is still physical and can be used as an input for the computation of the neutral Higgs spectrum of the theory.

For large values of $m_{H^\pm}$, corresponding to the decoupling limit, the properties of the lightest neutral Higgs boson state approach those of the SM Higgs boson. That is, for $m_{H^\pm} \gg M_W$, the lightest neutral Higgs boson is approximately a *CP*-even state, with *CPV* couplings that are suppressed by terms of $\mathcal{O}(m_W^2/m_{H^\pm}^2)$. In particular, the upper bound on the lightest neutral Higgs boson mass, takes the same value as in the *CP*-conserving case [252]. Nevertheless, there still can be significant mixing between the two heavier neutral mass eigenstates. For a detailed study of the Higgs boson mass spectrum and parametric dependence of the associated radiative corrections, see Refs. [360,363].

Major variations to the MSSM Higgs phenomenology occur in the presence of explicit *CPV* phases. In the *CPV* case, vector boson pairs couple to all three neutral Higgs boson mass eigenstates, H_i $(i = 1, 2, 3)$, with couplings

$$g_{H_i VV} = \cos\beta \mathcal{O}_{1i} + \sin\beta \mathcal{O}_{2i} \,, \tag{11.60}$$

$$\begin{aligned} g_{H_i H_j Z} =& \mathcal{O}_{3i} \left(\cos\beta \mathcal{O}_{2j} - \sin\beta \mathcal{O}_{1j}\right) \\ & - \mathcal{O}_{3j} \left(\cos\beta \mathcal{O}_{2i} - \sin\beta \mathcal{O}_{1i}\right) \,, \end{aligned} \tag{11.61}$$

where the $g_{H_i VV}$ couplings are normalized to the analogous SM coupling and the $g_{H_i H_j Z}$ have been normalized to $g_Z^{\rm SM}/2$. The orthogoanl matrix $\mathcal{O}_{ij}$ is relating the weak eigenstates to the mass eigenstates. It has non-zero off-diagonal entries mixing the *CP*-even and *CP*-odd components of the weak eigenstates. The above couplings obey the relations

$$\sum_{i=1}^{3} g_{H_i ZZ}^2 = 1 \quad \text{and} \quad g_{H_k ZZ} = \varepsilon_{ijk}\, g_{H_i H_j Z} \,, \tag{11.62}$$

where ε_{ijk} is the Levi-Civita symbol.

Another consequence of *CPV* effects in the scalar sector is that all neutral Higgs bosons can couple to both scalar and pseudoscalar fermion bilinear densities. The couplings of the mass eigenstates H_i to fermions depend on the loop-corrected fermion Yukawa couplings (similarly to the *CPC* case), on $\tan\beta$ and on the $\mathcal{O}_{ji}$. The resulting expressions for the scalar and pseudoscalar components of the neutral Higgs boson mass eigenstates to fermions and the charged Higgs boson to fermions are given in Refs. [360,365].

The production processes of neutral MSSM Higgs bosons in the *CPV* scenario are similar to those in the *CPC* scenario, except for the fact that in any process, the *CP* eigenstates h, H, and A can be replaced by any of the three neutral Higgs mass eigenstates H_i. This is the case, since, in the presence of *CP* violation, the H_i's do not have well-defined *CP* quantum numbers. Regarding the decay properties, the lightest mass eigenstate, H_1, predominantly decays to $b\overline{b}$ if kinematically allowed, with a smaller fraction decaying to $\tau^+\tau^-$, similar to the *CPC* case. If kinematically allowed, a SM-like neutral Higgs boson, H_2 or H_3 can decay predominantly to H_1H_1 leading to many new interesting signals both at lepton and hadron colliders; otherwise it will decay preferentially to $b\overline{b}$.

The discovery of a 125 GeV Higgs boson has put strong constraints on the realization of the *CPV* scenario within the MSSM. This is partly due to the fact that the observed Higgs rates are close to the SM values, and a large *CP*-violating component would necessary induce a large variation in the rate of the SM-like Higgs decay into the weak gauge bosons $W^\pm$ and Z. The measured Higgs mass imposes an additional constraint on the realization of this scenario. The *CP*-violating effects are enhanced for values of the modulus of X_t larger than the ones leading to maximal mixing, $|X_t| > \sqrt{6}M_S$. Such large values of $|X_t|$, however, lead to a decrease of the radiative corrections to the Higgs mass, and for sufficiently large $|X_t|$, the SM-like Higgs mass falls below the experimentally allowed range. This effect is increased by the fact that larger mixings in the Higgs sector lead to a reduction of the smaller mass eigenvalue. Once these effects are considered, the lightest Higgs component on the would be *CP*-odd Higgs A tends to be smaller than about 10 percent, and therefore difficult to test at the LHC. The Higgs mass constraints can be alleviated in more general two Higgs doublet models, or in the NMSSM, where the Higgs mass can be fixed in a way independent of the stop mass parameters.

CP-violating effects can still be significant in the heavy Higgs sector. For instance, the Higgs bosons H_2 and H_3 may be admixtures of *CP*-even and *CP*-odd scalars, and therefore both may be able to decay into pairs of weak gauge bosons. Although the observation of this effect would be a clear signal of *CP*-violation, the proximity of the masses of H_2 and H_3 within the MSSM makes the measurement of such effects quite challenging. In generic two Higgs doublet models, the mass splitting between the two heavy mass eigenstates may become larger, which could facilitate the detection of *CP*-violating effects at collider experiments.

V.6. Non-supersymmetric extensions of the Higgs sector

There are many ways to extend the minimal Higgs sector of the Standard Model. In the preceding sections the phenomenology of SUSY Higgs sectors is considered, which

at tree level implies a constrained type-II 2HDM (with restrictions on the Higgs boson masses and couplings). In the following discussion, more generic 2HDM's [12,260,243,366] are presented. These models are theoretically less compelling since they do not provide an explanation for the SM Higgs naturalness problem, but can lead to different patterns of Higgs-fermion couplings, hence, to different phenomenology. It is also possible to consider models with a SM Higgs boson and one or more additional scalar SU(2) doublets that acquire no VEV and hence play no role in the EWSB mechanism. These models are dubbed Inert Higgs Doublet Models (IHD) [367]. Due to the lack of a VEV, the inert Higgs bosons cannot decay into a pair of gauge bosons. And imposing a Z_2 symmetry that prevents them from coupling to the fermions, it follows that, if the lightest inert Higgs boson is neutral, it becomes a good dark matter candidate with interesting associated collider signals. Recent studies of IHD models in the light of a 125 GeV Higgs have been performed [368], showing that there can be non-negligible enhancement or suppression of Higgs to diphotons or Higgs to $Z\gamma$. This may be due to the presence of a light charged Higgs, as light as 100 GeV, that is not in conflict with collider or flavor constraints, because it has no couplings to fermions. It is interesting to study the interplay between collider and direct dark matter detection signals in these models.

Other extensions of the Higgs sector can include [344,369] multiple copies of $SU(2)_L$ doublets, additional Higgs singlets [370], triplets or more complicated combinations of Higgs multiplets. It is also possible to enlarge the gauge symmetry beyond $SU(2)_L \times U(1)_Y$ along with the necessary Higgs structure to generate gauge boson and fermion masses. There are two main experimental constraints on these extensions: *(i)* precision measurements which constrain $\rho = m_W^2/(m_Z^2 \cos^2\theta_W)$ to be very close to 1 and *(ii)* flavor changing neutral current (FCNC) effects. In electroweak models based on the SM gauge group, the tree-level value of ρ is determined by the Higgs multiplet structure. By suitable choices for the hypercharges, and in some cases the mass splitting between the charged and neutral Higgs sector or the vacuum expectation values of the Higgs fields, it is possible to obtain a richer combination of singlets, doublets, triplets and higher multiplets compatible with precision measurements [371]. Concerning the constraints coming from FCNC effects, the Glashow–Weinberg (GW) criterion [372] states that, in the presence of multiple Higgs doublets the tree-level FCNC's mediated by neutral Higgs bosons will be absent if all fermions of a given electric charge couple to no more than one Higgs doublet. An alternative way of suppressing FCNC in a two Higgs doublet model has been considered in Ref. [373], where it is shown that it is possible to have tree level FCNC completely fixed by the CKM matrix, as a result of an abelian symmetry.

V.6.1. Two-Higgs-doublet models

Supersymmetry demands the existence of two Higgs doublets such that one doublet couples to up-type quarks and the other to down-type quarks and charged leptons. This Higgs-fermion coupling structure is the one identified as type-II 2HDM [260] and assures that masses for both up and down-type quarks can be generated in a supersymmetric and gauge invariant way. Two Higgs doublet models [243], however, can have a more diverse Higgs-fermion coupling structure and can be viewed as a simple extension of

the SM to realize the spontaneous breakdown of $\mathrm{SU}(2)_L \times \mathrm{U}(1)_Y$ to $\mathrm{U}(1)_{\mathrm{em}}$. Quite generally, if the two Higgs doublets contain opposite hypercharges, the scalar potential will contain mixing mass parameters of the kind $m_{12}^2 \Phi_1^T i\sigma_2 \Phi_2 + h.c.$. In the presence of such terms, both Higgs doublets will acquire vacuum expectation values, $v_1/\sqrt{2}$ and $v_2/\sqrt{2}$, respectively, and the gauge boson masses will keep their SM expressions with the Higgs vacuum expectation value v replaced by $v = \sqrt{v_1^2 + v_2^2}$. Apart from the mass terms, the most generic renormalizable and gauge invariant scalar potential contains seven quartic couplings, which are defined in Eq. (11.38).

Considering two doublets with hypercharges, with $Y_{\Phi_1} = -1$ and $Y_{\Phi_2} = 1$ as in Eqs. (11.36) and (11.37), and the most general, renormalizable Higgs potential will be given by Eq. (11.38). The same as in the MSSM case, after electroweak symmetry breaking and in the absence of *CP*-violation, the physical spectrum contains a pair of charged Higgs bosons $H^\pm$, a *CP*-odd Higgs boson A and two neutral *CP*-even Higgs bosons, h and H. The angles α and β diagonalize the *CP*-even, and the *CP*-odd and Charged Higgs sectors, respectively

The complete 2HDM is defined only after considering the interactions of the Higgs fields to fermions. Yukawa couplings of the generic from

$$-h_{ij}^a \bar{\Psi}_L^i H_a \Psi_R^j + h.c. \tag{11.63}$$

may be added to the renormalizable Lagrangian of the theory. Contrary to the SM, the two Higgs doublet structure does not ensure the alignment of the fermion mass terms $m_{ij} = h_{ij}^a v_a/\sqrt{2}$ with the Yukawa couplings h_{ij}^a. This implies that quite generally, the neutral Higgs boson will mediate flavor changing interactions between the different mass eigenstates of the fermion fields. Such flavor changing interactions should be suppressed in order to describe properly the Kaon, D and B meson phenomenology. Based on the Glashow–Weinberg criterion, it is clear that the simplest way of avoiding such transitions is to assume the existence of a symmetry that ensures the couplings of the fermions of each given quantum number (up-type and down-type quarks, charged and neutral leptons) to only one of the two Higgs doublets. Different models may be defined depending on which of these fermion fields couple to a given Higgs boson, see Table 11.16. Models of type-I [366] are those in which all SM fermions couple to a single Higgs field. In type-II models [260] down-type quarks and charged leptons couple to a common Higgs field, while the up-type quarks and neutral leptons couple to the other. In models of type-III (lepton-specific) quarks couple to one of the Higgs bosons, while leptons couple to the other. Finally, in models of type-IV (flipped), up-type quarks and charged leptons couple to one of the Higgs fields while down-quarks and neutral leptons couple to the other.

The two Higgs doublet model phenomenology depends strongly on the size of the mixing angle α and therefore on the quartic couplings. For large values of m_A, $\sin\alpha \to -\cos\beta$, $\cos\alpha \to \sin\beta$, $\cos(\beta-\alpha) \to 0$, and the lightest *CP*-even Higgs h behaves as the SM Higgs. The same behavior is obtained if the quartic couplings are such that $\mathcal{M}_{12}^2 \sin\beta = -(\mathcal{M}_{11}^2 - m_h^2)\cos\beta$. The latter condition represents a situation in which the coupling of h to fermions and weak gauge bosons become the same as in the SM, without decoupling the rest of the non-standard scalars and it is of particular interest due to the

Table 11.16: Higgs boson couplings to up, down and charged lepton-type $SU(2)_L$ singlet fermions in the four discrete types of 2HDM models that satisfy the Glashow–Weinberg criterion, from Ref. [374].

Model	2HDM I	2HDM II	2HDM III	2HDM IV
u	Φ_2	Φ_2	Φ_2	Φ_2
d	Φ_2	Φ_1	Φ_2	Φ_1
e	Φ_2	Φ_1	Φ_1	Φ_2

fact that the recently discovered Higgs boson has SM-like properties. This situation will be referred to as alignment, as in the MSSM case.

In type-II Higgs doublet models, at large values of $\tan\beta$ and moderate values of m_A, the non-standard Higgs bosons H, A and $H^\pm$ couple strongly to bottom quarks and τ leptons. Hence the decay modes of the non-standard Higgs bosons tend to be dominated by b-quark and tau-lepton modes, including top quarks or neutrinos in the case of the charged Higgs. However, for large and negative values of λ_4, the charged Higgs boson mass may be sufficiently heavy to allow on-shell decays

$$\begin{aligned} H^\pm &\to W^\pm + (H, A), \\ g_{H^\pm W^\mp H,A} &\simeq \frac{M_W}{v}\sin(\beta-\alpha)(p_{H^+} - p_{H,A})\,, \end{aligned} \tag{11.64}$$

where p_{H^+} and $p_{H,A}$ are the charged and neutral scalar Higgs momenta pointing into the vertex. On the other hand, for large and positive values of λ_5, the above charged Higgs decay into a $W^\pm$ and the *CP*-odd Higgs boson may be allowed, but the heavy Higgs H may be sufficiently heavy to decay into a *CP*-odd Higgs boson and an on-shell Z.

$$H \to Z + A, \quad g_{HZA} \simeq \frac{M_Z}{v}\sin(\beta-\alpha)(p_H - p_A). \tag{11.65}$$

The decay $H^\pm \to W^\pm + H$, on the other hand may be allowed only if $\lambda_4 < -\lambda_5$. The couplings controlling all the above decay modes are proportional to $\sin(\beta-\alpha)$ and therefore they are unsuppressed in the alignment limit. Moreover, these could still be the dominant decay modes at moderate values of $\tan\beta$, offering a way to evade the current bounds obtained assuming a dominant decay into bottom quarks or τ leptons.

The quartic couplings are restricted by the condition of stability of the effective potential as well as by the restriction of obtaining the proper value of the lightest *CP*-even Higgs mass. Close to the alignment limit, the lightest *CP*-even Higgs mass becomes, approximately independent of m_A and is given by

$$\begin{aligned} m_h^2 \simeq& v^2(\lambda_1\cos^4\beta + \lambda_2\sin^4\beta + 2\tilde{\lambda}_3 v^2\cos^2\beta\sin^2\beta) \\ &+ v^2(4\lambda_6\cos^3\beta\sin\beta + 4\lambda_7\sin^3\beta\cos\beta)\,, \end{aligned} \tag{11.66}$$

where $\tilde{\lambda}_3 = \lambda_3 + \lambda_4 + \lambda_5$.

The stability conditions imply the positiveness of all masses, as well as the avoidance of run-away solutions to large negative values of the fields in the scalar potential. These conditions imply

$$\begin{aligned} &\lambda_1 \geq 0, \quad \lambda_2 \geq 0, \quad \lambda_3 + \lambda_4 - |\lambda_5| \geq -\sqrt{\lambda_1 \lambda_2}, \\ &\lambda_3 \geq -\sqrt{\lambda_1 \lambda_2}, \quad 2|\lambda_6 + \lambda_7| < \frac{\lambda_1 + \lambda_2}{2} + \tilde{\lambda}_3, \end{aligned} \tag{11.67}$$

where the first four are necessary and sufficient conditions in the case of $\lambda_6 = \lambda_7 = 0$, while the last one is a necessary condition in the case all couplings are non-zero. Therefore, to obtain the conditions that allow the decays $H^\pm \to W^\pm H, A$ and $H \to ZA$, λ_3 should take large positive values in order to compensate for the effects of λ_4 and λ_5. For recent detailed discussions about 2HDM phenomenology see Refs. [369,375–378,245].

V.6.2. Higgs Triplets

Electroweak triplet scalars are the simplest non-doublet extension of the SM that can participate in the spontaneous breakdown of $\mathrm{SU}(2)_L \times \mathrm{U}(1)_Y$ to $\mathrm{U}(1)_{\mathrm{em}}$. Two types of model have been developed in enough detail to make a meaningful comparison to LHC data: the Higgs triplet model (HTM) [379,380] and the Georgi–Machacek model (GM) [381–384].

The Higgs triplet model extends the SM by the addition of a complex $\mathrm{SU}(2)_L$ triplet scalar field Δ with hypercharge $Y = 2$, and a general gauge-invariant renormalizable potential $V(\Phi, \Delta)$ for Δ and the SM Higgs doublet Φ. The components of the triplet field can be parameterized as

$$\Delta = \frac{1}{\sqrt{2}} \begin{pmatrix} \Delta^+ & \sqrt{2}\Delta^{++} \\ v_\Delta + \delta + i\xi & -\Delta^+ \end{pmatrix}. \tag{11.68}$$

where Δ^+ is a singly-charged field, Δ^{++} is a doubly-charged field, δ is a neutral *CP*-even scalar, ξ is a neutral *CP*-odd scalar, and v_Δ is the triplet VEV. The general scalar potential mixes the doublet and triplet components. After electroweak symmetry breaking there are seven physical mass eigenstates, denoted $H^{\pm\pm}$, $H^\pm$, A, H, and h.

A distinguishing feature of the HTM is that it violates the custodial symmetry of the SM; thus the ρ parameter deviates from 1 even at tree level. Letting x denote the ratio of triplet and doublet VEVs, the tree level expression [385] is:

$$\rho = \frac{1 + 2x^2}{1 + 4x^2}\,. \tag{11.69}$$

The measured value of the ρ parameter then limits [386] the triplet VEV to be quite small, $x \lesssim 0.03$, or $v_\Delta < 8\,\mathrm{GeV}$. This constraint severely limits the role of the triplet scalar in the EWSB mechanism.

The small VEV of the Higgs triplet in the HTM is a virtue from the point of view of generating neutrino masses without the necessity for introducing right-handed neutrino fields. The gauge invariant dimension four interaction

$$h_{\nu_{ij}}\, \ell_i^T C^{-1} i\sigma_2\, \Delta\, \ell_j\,, \tag{11.70}$$

where ℓ_i are the lepton doublets, C is the charge conjugation matrix, and $h_{\nu_{ij}}$ is a complex symmetric coupling matrix, generates a Majorana mass matrix for the neutrinos:

$$m_{\nu_{ij}} = \sqrt{2} h_{\nu_{ij}} v_\Delta \ . \tag{11.71}$$

This can be combined with the usual neutrino seesaw to produce what is known as the type-II seesaw [387].

The HTM suggests the exciting possibility of measuring parameters of the neutrino mass matrix at the LHC. If the doubly-charged Higgs is light enough and/or its couplings to W^+W^+ are sufficiently suppressed, then its primary decay is into same-sign lepton pairs: $H^{++} \to \ell_i^+ \ell_j^+$; from Eq. (11.70) and Eq. (11.71) it is apparent that these decays are in general lepton-flavor violating with branchings proportional to elements of the neutrino mass matrix [388].

Precision electroweak data constrain the mass spectrum as well as the triplet VEV of the HTM [389,385,390]. As described in Ref. [390], these constraints favor a spectrum where H^{++} is the lightest of the exotic bosons, and where the mass difference between H^+ and H^{++} is a few hundred GeV. The favored triplet VEV is a few GeV, which also favors H^{++} decays into W^+W^+ over same-sign dileptons.

The Georgi–Machacek model addresses the ρ parameter constraint directly by building in custodial symmetry. Writing the complex doublet scalar of the SM as a $(2,2)$ under $\mathrm{SU}(2)_L \times \mathrm{SU}(2)_R$, it is obvious that the next simplest construction respecting custodial symmetry is a scalar transforming like a $(3,3)$ [391]. These nine real degrees of freedom correspond to a complex electroweak triplet combined with a real triplet, with the scalar potential required to be invariant under $\mathrm{SU}(2)_R$. Under the custodial $\mathrm{SU}(2)_{L+R}$, they transform as $1 \oplus 3 \oplus 5$, with a *CP*-even neutral scalar as the custodial singlet (thus matching the SM Higgs boson), a *CP*-odd neutral scalar in the custodial triplet, and another *CP*-even neutral scalar in the custodial 5-plet.

The scalar components can be decomposed as [392]:

$$\Xi = \begin{pmatrix} \chi_3^* & \xi_1 & \chi_1 \\ -\chi_2^* & \xi_2 & \chi_2 \\ \chi_1^* & -\xi_1^* & \chi_3 \end{pmatrix}, \tag{11.72}$$

where ξ_2 is a real scalar and the others are complex scalars. Linear combinations of these account for the neutral custodial singlet, a neutral and singly-charged field making up the custodial triplet, and neutral, singly-charged, and doubly-charged fields making up the custodial 5-plet.

When combined with the usual SM doublet field Φ, the electroweak scale v is now related to the doublet and triplet VEVs by

$$v^2 = v_\Phi^2 + 8 v_\Xi^2 \ . \tag{11.73}$$

Note that the GM triplets by themselves are sufficient to explain electroweak symmetry breaking and the existence of a 125 GeV neutral boson along with a custodial triplet of

Goldstone bosons; the complex doublet field in the GM model is required to generate fermion masses via the usual dimension four Yukawa couplings. This raises the question of whether one can rule out the possibility that the 125 GeV boson is the neutral member of a custodial 5-plet rather than a custodial singlet, without invoking decays to fermions. A conclusive answer is given by observing that the ratio of the branching fractions to W versus Z bosons is completely determined by the custodial symmetry properties of the boson. For a custodial 5-plet, the ratio of the signal strength to WW over that to ZZ is predicted to be 1/4 that of a SM Higgs boson [391,393], and thus already ruled out by the experimental results shown in Table 11.12 of Section IV.2.5.

Another interesting general feature of Higgs triplet models is that, after mixing, the SM-like neutral boson can have stronger couplings to WW and ZZ than predicted by the SM [384,394]; this is in contrast to mixing with additional doublets and singlet, which can only reduce the WW and ZZ couplings versus the SM. This has interesting implications for trying to extract the total width of the 125 GeV boson without making theoretical assumptions [181,395].

Because of the built-in custodial symmetry, the triplet VEV in the GM model can be large compared to the doublet VEV. The custodial singlet neutral boson from the triplets mixes with the neutral boson from the doublet. Two interesting special cases are (i) the triplet VEV is small and the 125 GeV boson is SM-like except for small deviations, and (ii) the 125 GeV boson is mostly the custodial singlet neutral boson from the electroweak triplets. The phenomenology of the doubly-charged and singly-charged bosons is similar to that of the HTM. The constraints on the GM model from precision electroweak data, LEP data, and current LHC data are described in Refs. [392,396–399].

V.7. Composite Higgs models

Within the SM, EWSB is posited but has no dynamical origin. Furthermore, the Higgs boson appears to be unnaturally light. A scenario that remedies these two catches is to consider the Higgs boson as a bound state of new dynamics becoming strong around the weak scale. The Higgs boson can be made significantly lighter than the other resonances of the strong sector if it appears as a pseudo-Nambu–Goldstone boson.

V.7.1. Little Higgs models

The idea behind the Little Higgs models [400,401] is to identify the Higgs doublet as a (pseudo) Nambu–Goldstone boson while keeping some sizable non-derivative interactions. By analogy with QCD where the pions $\pi^{\pm,0}$ appear as Nambu–Goldstone bosons associated to the breaking of the chiral symmetry $\mathrm{SU}(2)_\mathrm{L} \times \mathrm{SU}(2)_\mathrm{R}/\mathrm{SU}(2)$, switching on some interactions that break explicitly the global symmetry will generate masses for the would-be massless Nambu–Goldstone bosons of the order of $g\Lambda_{G/H}/(4\pi)$, where g is the coupling of the symmetry breaking interaction and $\Lambda_{G/H} = 4\pi f_{G/H}$ is the dynamical scale of the global symmetry breaking G/H. In the case of the Higgs boson, the top Yukawa interaction or the gauge interactions themselves will certainly break explicitly (part of) the global symmetry since they act non-linearly on the Higgs boson. Therefore, obtaining a Higgs mass around 100 GeV would demand a dynamical scale $\Lambda_{G/H}$ of the

order of 1 TeV, which is known to lead to too large oblique corrections. Raising the strong dynamical scale by at least one order of magnitude requires an additional selection rule to ensure that a Higgs mass is generated at the 2-loop level only

$$m_H^2 = \frac{g^2}{16\pi^2}\Lambda_{G/H}^2 \to m_H^2 = \frac{g_1^2 g_2^2}{(16\pi^2)^2}\Lambda_{G/H}^2 \tag{11.74}$$

The way to enforce this selection rule is through a "collective breaking" of the global symmetry:

$$\mathcal{L} = \mathcal{L}_{G/H} + g_1\mathcal{L}_1 + g_2\mathcal{L}_2. \tag{11.75}$$

Each interaction $\mathcal{L}_1$ or $\mathcal{L}_2$ individually preserves a subset of the global symmetry such that the Higgs remains an exact Nambu–Goldstone boson whenever either g_1 or g_2 is vanishing. A mass term for the Higgs boson can be generated only by diagrams involving simultaneously both interactions. At one-loop, there is no such diagram that would be quadratically divergent. Explicitly, the cancellation of the SM quadratic divergences is achieved by a set of new particles around the Fermi scale: gauge bosons, vector-like quarks, and extra massive scalars, which are related, by the original global symmetry, to the SM particles with the same spin. Contrary to supersymmetry, the cancellation of the quadratic divergences is achieved by same-spin particles. These new particles, with definite couplings to SM particles as dictated by the global symmetries of the theory, are perfect goals for the LHC.

The simplest incarnation of the collective breaking idea, the so-called littlest Higgs model, is based on a non-linear σ-model describing the spontaneous breaking SU(5) down to SO(5). A subgroup $\mathrm{SU}(2)_1 \times \mathrm{U}(1)_1 \times \mathrm{SU}(2)_2 \times \mathrm{U}(1)_2$ is weakly gauged. This model contains a weak doublet, that is identified with the Higgs doublet, and a complex weak triplet whose mass is not protected by collective breaking. Other popular little Higgs models are based on different coset spaces: minimal moose $(\mathrm{SU}(3)^2/\mathrm{SU}(3))$ [402], the simplest little Higgs $(\mathrm{SU}(3)^2/\mathrm{SU}(2)^2)$ [403], the bestest little Higgs $(\mathrm{SO}(6)^2/\mathrm{SO}(6))$ [404] *etc.* For comprehensive reviews, see Refs. [405,406].

Generically, oblique corrections in Little Higgs models are reduced either by increasing the coupling of one of the gauge groups (in the case of product group models) or by increasing the masses of the W and Z partners, leading ultimately to a fine-tuning of the order of a few percents, i.e., improving only marginally the situation of the MSSM (see for instance Ref. [407] and references therein). The compatibility of Little Higgs models with experimental data is significantly improved when the global symmetry involves a custodial symmetry as well as a T-parity [408] under which, in analogy with R-parity in SUSY models, the SM particles are even and their partners are odd. Such Little Higgs models would therefore appear in colliders as jet(s) with missing transverse energy [409] and the ATLAS and CMS searches for squarks and gluinos [410] can be recast to obtain limits on the masses of the heavy vector-like quarks. The T-even top partner, with an expected mass below 1 TeV to cancel the top loop quadratic divergence without too much fine-tuning, would decay dominantly into a $t + Z$ pair or into a $b + W$ pair or even into $t + H$. The latest CMS and ATLAS direct searches [411] for vector-like top partners put a lower bound around 700 GeV on their mass, excluding the most natural region of the parameter space of these models.

Table 11.17: Global symmetry breaking patterns and the corresponding Goldstone boson contents of the SM, the minimal composite Higgs model, the next to minimal composite Higgs model, and the minimal composite two Higgs doublet model. Note that the SU(3) model does not have a custodial invariance. a denotes a *CP*-odd scalar while h and H are *CP*-even scalars.

Model	Symmetry Pattern	Goldstone's
SM	SO(4)/SO(3)	W_L, Z_L
–	SU(3)/SU(2)×U(1)	W_L, Z_L, H
MCHM	SO(5)/SO(4)×U(1)	W_L, Z_L, H
NMCHM	SO(6)/SO(5)×U(1)	W_L, Z_L, H, a
MC2HM	SO(6)/SO(4)×SO(2) ×U(1)	$W_L, Z_L, h, H, H^{\pm}, a$

The motivation for Little Higgs models is to solve the little hierarchy problem, i.e., to push the need for new physics (responsible for the stability of the weak scale) up to around 10 TeV. Per se, Little Higgs models are effective theories valid up to their cutoff scale $\Lambda_{G/H}$. Their UV completions could either be weakly or strongly coupled.

V.7.2. Models of partial compositeness

The Higgs boson is a special object. Even in composite models, it cannot appear as a regular resonance of the strong sector without endangering the viability of the setup when confronted to data. The way out is that the Higgs appears as a pseudo Nambu–Goldstone boson: the new strongly coupled sector is supposed to be invariant under a global symmetry G spontaneously broken to a subgroup H at the scale f. To avoid conflict with EW precision measurements, it is better to avoid the strong interactions themselves to break the EW symmetry, hence the SM gauge symmetry itself should be contained in H. See Table 11.17 for a few examples of coset spaces.

The SM (light) fermions and gauge bosons cannot be part of the strong sector itself since LEP data have already put stringent bounds on the compositeness scale of these particles far above the TeV scale. The gauge bosons couple to the strong sector by a weak gauging of an SU(2)×U(1) subgroup of the global symmetry G. Inspiration for the construction of such models comes from the AdS/CFT correspondence: the components of a gauge field along extra warped space dimension can be interpreted as the Goldstone boson resulting from the breaking of global symmetry of the strong sector, see Fig. 11.28. The couplings of the SM fermions to the strong sector could a priori take two different forms: (i) a bilinear coupling of two SM fermions to a composite scalar operator, $\mathcal{O}$, of the form $\mathcal{L} = y\,\bar{q}_L u_R \mathcal{O} + \text{hc}$ in simple analogy with the SM Yukawa interactions. This is the way fermion masses were introduced in Technicolor theories and it generically comes with severe flavor problems and calls for extended model building gymnastics [412] to circumvent them; (ii) a linear mass mixing with fermionic vector-like operators: $\mathcal{L} = \lambda_L\,\bar{q}_L \mathcal{Q}_R + \lambda_R \bar{\mathcal{U}}_L u_R$. $\mathcal{Q}$ and $\mathcal{U}$ are two fermionic composite operators of mass M_Q and M_U. Being part of the composite sector, they can have a direct coupling of generic order Y_* to the Higgs boson. In analogy with the photon-rho mixing in QCD, once the linear mixings are diagonalized, the physical states are a linear combination of elementary

and composite fields. Effective Yukawa couplings are generated and read for instance for the up-type quark

$$y = Y_* \sin\theta_L \sin\theta_R \tag{11.76}$$

where $\sin\theta_i = \lambda_i/\sqrt{M_U^2+\lambda_i^2}$, $i = L, R$, measure the amount of compositeness of the SM left- and right-handed up-type quark. If the strong sector is flavor-anarchic, i.e., if the couplings of the Higgs to the composite fermions does not exhibit any particular flavor structure, the relation Eq. (11.76) implies that the light fermions are mostly elementary states ($\sin\theta_i \ll 1$), while the third generation quarks need to have a sizable degree of compositeness. The partial compositeness paradigm offers an appealing dynamical explanation of the hierarchies in the fermion masses. In fact, assuming the strong sector to be almost conformal above the confinement scale, the low-energy values of the mass-mixing parameters $\lambda_{L,R}$ are determined by the (constant) anomalous dimension of the composite operator they mix with. If the UV scale at which the linear mixings are generated is large, then $\mathcal{O}(1)$ differences in the anomalous dimensions can generate naturally large hierarchies in the fermion masses via renormalization group running [413]. While the introduction of partial compositeness greatly ameliorated the flavor problem of the original composite Higgs models, nevertheless it did not solve the issue completely, at least in the case where the strong sector is assumed to be flavor-anarchic [414]. While the partial compositeness set-up naturally emerges in models built in space-times with extra dimensions, no fully realistic microscopic realization of partial compositeness has been proposed in the literature.

Another nice aspect of the partial compositeness structure is the dynamical generation of the Higgs potential. The Higgs being a pseudo-Nambu–Goldstone boson, its mass does not receive any contribution from the strong sector itself but it is generated at the one-loop level via the couplings of the SM particles to the strong sector since these interactions are breaking the global symmetries under which the Higgs doublet transforms non-linearly. The leading contribution to the potential arises from top loops and it takes the form

$$\begin{aligned} V(H) = & m_\rho^4 \frac{\sin\theta_{tL}\sin\theta_{tR}}{16\pi^2}\,(\alpha\cos(H/f) + \beta\sin^2(H/f) \\ & + \gamma\sin^4(H/f)\Big), \end{aligned} \tag{11.77}$$

where α, β, γ are numbers of order 1 subject to selection rules following the transformation properties of the top quark under the global symmetries of the strong sector[12], and $m_\rho \approx g_\rho f$ is the typical mass scale of the strong sector resonances. The gauge contribution to the potential takes the form (g denotes the SU(2) gauge coupling)

$$m_\rho^4 \frac{g^2/g_\rho^2}{16\pi^2}\sin^2(H/f), \tag{11.78}$$

[12] For instance in the SO(5)/SO(4) composite models, when the top quark is embedded into a spinorial representation of SO(5), then $\gamma = 0$ and when it is part of a **5**, **10** or **14** representation, $\alpha = 0$ as it can be inferred by looking at the structure of the H-dependent invariants built out of these representations [415]. The coefficient γ also generically comes with an extra power of the top compositeness fractions.

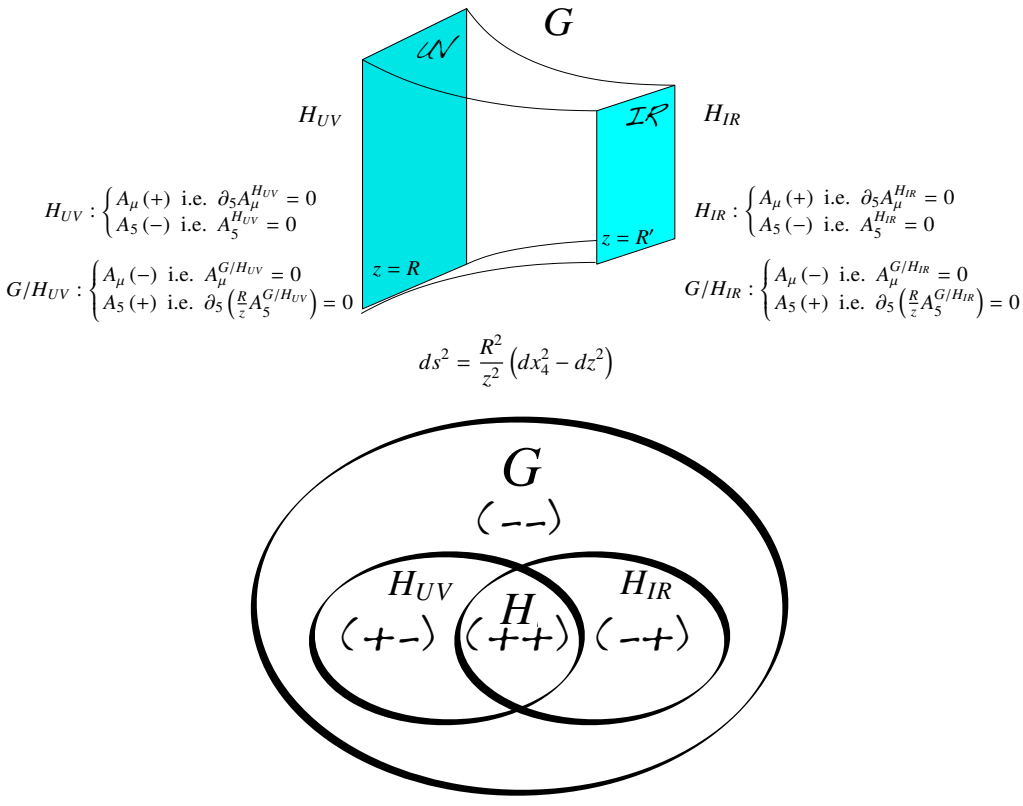

Figure 11.28: Composite models built in five dimensional Anti-de-Sitter space-time and their symmetry breaking pattern interpretation. In 5D, the gauge symmetry in the bulk, G, is broken by suitable boundary conditions to H_{UV} on the UV brane and to H_{IR} on the IR brane. The low energy theory mimics in 4D a strongly interacting sector invariant under a global symmetry G spontaneously broken to H_{IR} at the IR scale with a subgroup H_{UV} which is weakly gauged. The number of Goldstone bosons is equal to $\dim(G/H_{IR})$, $\dim(H_{UV}/H)$ being eaten to give a mass to some gauge bosons ($H = H_{UV} \cap H_{IR}$). The remaining $\dim(G/H_{IR}) - \dim(H_{UV}/H)$ massless Goldstone's are described on the 5D side by the massless modes of the gauge fields along the fifth dimension, A_5^H.

which is parametrically suppressed with respect to the top contribution by $g^2/(g_\rho y_t)$. The gauge term is always positive, and cannot trigger EWSB by itself. When $\alpha = 0$, the minimization condition of the potential simply reads

$$\sin^2 \frac{\langle H \rangle}{f} = -\frac{\beta}{2\gamma}, \tag{11.79}$$

which implies that the natural expectation is that the scale f is generically of the order of the weak scale. Obtaining $v \ll f$, as required phenomenologically, requires some degree of tuning, which scales like $\xi \equiv v^2/f^2$. A mild tuning of the order of 10% ($\xi \approx 0.1$) is typically enough to comply with electroweak precision constraints. This is an

important point: in partial compositeness models, the entire Higgs potential is generated at one loop, therefore the separation between v and f can only be obtained at a price of a tuning. This marks a difference with respect to the Little Higgs models, which realize a parametric hierarchy between the quartic and mass terms through the collective symmetry breaking mechanism. In fact in Little Higgs models, the quartic coupling is a tree-level effect, leading to a potential

$$V(H) \approx \frac{g_{\rm SM}^2}{16\pi^2} m_\rho^2 H^2 + g_{\rm SM}^2 H^4, \tag{11.80}$$

where $g_{\rm SM}$ generically denotes the SM couplings. The minimization condition now reads $v^2/f^2 \sim g_\rho^2/(16\pi^2)$, therefore v is formally loop suppressed with respect to f. This is the major achievement of the Little Higgs constructions, which however comes at the price of the presence of sub-TeV vectors carrying EW quantum numbers and therefore giving rise generically to large oblique corrections to the propagators of the W and the Z gauge bosons.

After minimization, the potential Eq. (11.77) leads to an estimate of the Higgs mass as

$$m_H^2 \approx g_\rho^3\, y_t 2\pi^2 v^2. \tag{11.81}$$

It follows that the limit $f \to \infty$, i.e. $\xi \to 0$, is a true decoupling limit: all the resonances of the strong sector become heavy but the Higgs whose mass is protected by the symmetries of the coset G/H. When compared to the experimentally measured Higgs mass, this estimate puts an upper bound on the strength of the strong interactions: $1 \lesssim g_\rho \lesssim 2$. In this limit of not so large coupling, the Higgs potential receives additional contributions. In particular, the fermionic resonances in the top sector which follow from the global symmetry structure of the new physics sector can help raising the Higgs mass. For instance in the minimal SO(5)/SO(4) model, using some dispersion relation techniques, one obtains [416]

$$m_H^2 \approx \frac{6}{\pi^2}\frac{m_t^2}{f^2}\frac{m_{Q_4}^2 m_{Q_1}^2}{m_{Q_1}^2 - m_{Q_4}^2}\log\left(\frac{m_{Q_1}}{m_{Q_4}}\right) \tag{11.82}$$

where Q_4 and Q_1 are fermionic color resonances transforming as a weak bi-doublet of hypercharge $Y = 1/6$ and $Y = 7/6$ and a weak singlet with hypercharge $Y = -1/3$. Therefore a 125 GeV mass is obtained if at least one of the fermionic resonances is lighter than $\sim 1.4\, f$. As in supersymmetric scenarios, the top sector is playing a crucial role in the dynamics of EWSB and can provide the first direct signs of new physics. The direct searches for these top partners, in particular the ones with exotic electric charges 5/3, are already exploring the natural parameter spaces of these models [417,418,411].

The main physics properties of a pseudo Nambu–Goldstone Higgs boson can be captured in a model-independent way by a few number of higher-dimensional operators. Indeed, the strong dynamics at the origin of the composite Higgs singles out a few operators among the complete list presented earlier in Section IV: these are the operators

that involve extra powers of the Higgs doublets and they are therefore generically suppressed by a factor $1/f^2$ as opposed to the operators that involve extra derivatives or gauge bosons and are suppressed by a factor $1/(g_\rho^2 f^2)$. The relevant effective Lagrangian describing a strongly interacting light Higgs is:

$$\begin{aligned}\mathcal{L}_{\rm SILH} =& \frac{c_H}{2f^2}\left(\partial_\mu\left(\Phi^\dagger\Phi\right)\right)^2 + \frac{c_T}{2f^2}\left(\Phi^\dagger \overleftrightarrow{D}^\mu \Phi\right)^2 - \frac{c_6\lambda}{f^2}\left(\Phi^\dagger\Phi\right)^3 \\ &+ \left(\sum_f \frac{c_f\, y_f}{f^2}\Phi^\dagger\Phi\bar{f}_L\Phi f_R + \text{h.c.}\right).\end{aligned} \tag{11.83}$$

Typically, these new interactions induce deviations in the Higgs couplings that scale like $\mathcal{O}(v^2/f^2)$, hence the measurements of the Higgs couplings can be translated into some constraints on the compositeness scale, $4\pi f$, of the Higgs boson. The peculiarity of these composite models is that, due to the Goldstone nature of the Higgs boson, the direct couplings to photons and gluons are further suppressed and generically the coupling modifiers defined in Section IV scale like

$$\begin{aligned}\kappa_{W,Z,f} &\sim 1 + \mathcal{O}\left(\frac{v^2}{f^2}\right), \\ \kappa_{Z\gamma} &\sim \mathcal{O}\left(\frac{v^2}{f^2}\right), \\ \kappa_{\gamma,g} &\sim \mathcal{O}\left(\frac{v^2}{f^2}\times\frac{y_t^2}{g_\rho^2}\right),\end{aligned} \tag{11.84}$$

where g_ρ denotes the typical coupling strength among the states of the strongly coupled sector and y_t is the top Yukawa coupling, the largest interaction that breaks the Goldstone symmetry. The $\kappa_{Z\gamma,\gamma,g}$ coupling modifiers are not generated by the strong coupling operators of Eq. (11.83) but some subleading form-factor operator generated by loops of heavy resonances of the strong sector. The coupling modifiers also receive additional contributions from the other resonances of the strong sector, in particular the fermionic resonances of the top sector that are required to be light to generate a 125 GeV Higgs mass. Some indirect information on the resonance spectrum could thus be inferred by a precise measurement of the Higgs coupling deviations. However, it was realized [419] that the task is actually complicated by the fact that, in the minimal models, these top partners give a contribution to both κ_t (resulting from a modification of the top Yukawa coupling) and κ_γ and κ_g (resulting from new heavy particles running into the loops) and the structure of interactions are such that the net effect vanishes for inclusive quantities like $\sigma(gg \to H)$ or $\Gamma(H \to \gamma\gamma)$ as a consequence of the Higgs low energy theorem [19,20,182]. So one would need to rely on differential distribution, like the Higgs p_T distribution [420] (for a recent analysis and further references, see Ref. [421]), to *see* the top partner effects in Higgs data [422].

V.7.3. Minimal composite Higgs models

The minimal composite Higgs models (MCHM) are concrete examples of the partial compositeness paradigm. The Higgs doublet is described by the coset space SO(5)/SO(4)

where a subgroup $SU(2)_L \times U(1)_Y$ is weakly gauged under which the four Goldstone bosons transform as a doublet of hypercharge 1. There is some freedom on how the global symmetry is acting on the SM fermions: in MCHM4 [415] the quarks and leptons are embedded into spinorial representations of SO(5), while in MHCM5 [423] they are part of fundamental representations (it might also be interesting phenomenologically to consider larger representations like MCHM14 [424] with the SM fermions inside a representation of dimension 14). The non-linearly realized symmetry acting on the Goldstone bosons leads to general predictions of the coupling of the Higgs boson to the EW gauge bosons. For instance, it can be shown that the quadratic terms in the W and Z bosons read

$$m_W^2(H)\left(W_\mu W^\mu + \frac{1}{2\cos^2\theta_W} Z_\mu Z^\mu\right)$$

with $m_W(H) = \frac{gf}{2}\sin\frac{H}{f}$. Expanding around the EW vacuum, the expression of the weak scale is:

$$v = f\sin(\langle H\rangle/f), \tag{11.85}$$

and the values of the modified Higgs couplings to the W and Z:

$$g_{HVV} = \frac{2m_V^2}{v}\sqrt{1-v^2/f^2}\,, \quad g_{HHVV} = \frac{2m_V^2}{v^2}(1-2v^2/f^2)\,. \tag{11.86}$$

Note that the Higgs couplings to gauge bosons is always suppressed compared to the SM prediction. This is a general result [425] that holds as long as the coset space is compact.

The Higgs couplings to the fermions depend on the representation which the SM fermions are embedded into. For the most commonly used embeddings, they take the following forms

$$\begin{aligned}
\text{MCHM4}: g_{Hff} &= \frac{m_f}{v}\sqrt{1-v^2/f^2}\,,\\
\text{MCHM5}: g_{Hff} &= \frac{m_f}{v}\frac{1-2v^2/f^2}{\sqrt{1-v^2/f^2}}\,,\\
\text{MCHM14}: g_{Hff} &= \frac{m_f}{v}\left(1 + A(M_{1,4,9})\frac{v^2}{f^2} + O(v^4/f^4)\right)\,,\\
&\text{with } A(M_{1,4,9}) = \frac{3M_1M_4 - 11M_1M_9 + 8M_4M_9}{2M_9(M_1-M_4)}\,.
\end{aligned} \tag{11.87}$$

While in MHCM4 and MCHM5, the modifications of the couplings depend only on the Higgs compositeness scale, in MCHM14 the leading corrections do depend also on the mass spectrum of the resonances parametrized by M_1, M_4 and M_9 [424]. This is due to the fact that more than one SO(5) invariant give rise to SM fermion masses.

The (κ_V, κ_f) experimental fit of the Higgs couplings can thus be used to derive a lower bound on the Higgs compositeness scale $4\pi f \gtrsim 9\,\text{TeV}$, which is less stringent than the

indirect bound obtained from EW precision data, $4\pi f \gtrsim 15\,\text{TeV}$ [426], which is however subject to various assumptions [427].

V.8. The Higgs boson as a dilaton

The possibility that the new particle H^0 discovered at the LHC is in fact the Goldstone boson associated to the spontaneous breaking of scale invariance at a scale f attracted some attention [16,17] but is now challenged by the fact that all its properties are in good agreement with those predicted for the SM Higgs. And this scenario now requires rather involved model-building engineering. The first issue is the fact that the observed scalar couplings are close to their SM values. In a generic theory of spontaneously broken scale invariance, order one shifts are possible, and indeed expected in most models. Also, the apparent hierarchy between the light scalar and the cutoff of the dilaton effective theory is not reconcilable with the general walking technicolor (or Higgsless) type scenario unless a tuning is imposed.

The general couplings of a wide class of dilaton models are given (at leading order in a low-energy theorem limit for dilatons) by

$$\begin{aligned}\mathcal{L}_{dilaton} = \frac{\sigma}{f}\left[2M_W^2 W_\mu^\pm W^{\pm\mu} + M_Z^2 Z_\mu Z^\mu + \sum_{ij}\sqrt{m_f^i m_f^j}\,\Gamma^{ij}\bar{\psi}^i\psi^j\right] \\ + \frac{\sigma}{f}\left[\frac{2}{e}\Delta\beta^{\text{em}}F_{\mu\nu}^2 + \frac{2}{g_3}\Delta\beta^{\text{QCD}}G_{\mu\nu}^{a\ 2}\right]\end{aligned} \tag{11.88}$$

where Γ^{ij} is a matrix that depends upon anomalous dimensions of operators in the conformal theory that give rise to fermion masses, and the terms $\Delta\beta$ are the differences in the beta functions of electromagnetism or QCD at scales above and below the scale at which conformal symmetry is spontaneously broken. The SM low energy theorem limit for the standard model Higgs is obtained from this expression by taking

$$f = v, \quad \Gamma^{ij} = I_{3\times 3}, \quad \Delta\beta^{em} = \beta_{top}^{em} + \beta_W^{em}, \quad \Delta\beta^{qcd} = \beta_{top}^{qcd}. \tag{11.89}$$

It is unclear why these relations might be approximately realized in a generic conformal field theory, as must be the case to be consistent with current data and allow for a scalar with mass of about 125 GeV . For example, in warped models of electroweak symmetry breaking (AdS/CFT duals to theories with strongly broken conformal invariance), the ratio v/f is a function of the geometry, and is suppressed when the 5D theory is perturbative, contrary to the experimental result that the v/f ratio should be close to 1.

An additional complication is that the mass of the dilaton is expected to appear, along with many other resonances, around the cutoff scale of the strongly interacting theory responsible for breaking the scale invariance spontaneously. Suppression of the dilation mass either requires a tuning of order $v^2/\Lambda^2 \sim$ percent, or a very special conformal

dynamics where the beta function of the interaction leading to the scale invariance breaking remains small over a large region of couplings [428].

V.9. Searches for signatures of extended Higgs sectors

The measurements described in Section III and Section IV have established the existence of one state of the electroweak symmetry breaking sector, compatible within with a SM Higgs boson, but not that it is the only one.

Various classes of models beyond the Standard Model discussed above require extended Higgs sectors. These models, and in particular the MSSM and the NMSSM serve as guiding principle of the experimental searches for additional scalar states beyond the Standard Model. However these searches are made as model-independent as possible and can be summarized in the following classes: (i) the search for an additional *CP*-even state mostly in the high mass domain decaying to vector bosons, which would correspond to the heavy *CP*-even state in a generic 2HDM where the light state would be the discovered H or a generic additional singlet; (ii) the search for a state in the high mass domain decaying to pairs of fermions, which would correspond a *CP*-odd A and the heavy *CP*-even state H in a generic 2HDM; (iii) the search for charged Higgs bosons, which also appear in generic 2HDMs; (iv) the search for a *CP*-odd state a in the low mass region which appears in the NMSSM; and (v) doubly charged Higgs which are motivated in extensions of the Higgs sector with triplets.

(i) Searches for an additional CP-even state

(a) Exclusion limits from LEP

The negative result of LEP searches for the SM Higgs boson and the absolute lower limit on its mass of 114 GeV strongly disfavors the existence of a lower mass *CP*-even state, but does not exclude it if its couplings are reduced enough with respect to those of the SM Higgs boson. These searches were also interpreted as 95% CL upper bounds on the ratio of the coupling g_{HZZ} to its SM prediction as a function of the Higgs boson mass [107]. Among the MSSM new benchmarks, the low-m_H is one example which is disfavored by these function of the Higgs boson mass [107] searches, and nearly ruled out by current direct constraints and charged Higgs limits from LHC [429]. Another example is the light *CP*-even Higgs boson of the NMSSM, which is constrained to have a strong function of the Higgs boson mass [107] singlet component. An additional motivation for these scenarios is given by the slight excess observed at LEP [107] at a Higgs boson mass hypothesis of approximately 98 GeV. The light *CP*-even Higgs boson h was also searched for in association with the *CP*-odd A, these searches are described in Section III.

(b) Searches at Tevatron and at the LHC

The searches for the Standard Model Higgs boson before the discovery were covering a wide range of mass hypotheses. Until recently the range of investigation at LHC was from 100 GeV to 600 GeV. It has been extended to masses of up to 1 TeV. At the Tevatron this mass range was limited to up to 200 GeV. Since the discovery, the SM Higgs boson

searches are reappraised to search for a heavy *CP*-even state. This state could be the heavy *CP*-even Higgs boson of a 2HDM, or a generic additional singlet. In both cases the natural width of the additional H state can be very different from that of the SM Higgs boson. To preserve unitarity of the longitudinal vector boson scattering and the longitudinal vector boson scattering into fermion pairs, the couplings of the additional *CP*-even Higgs boson to gauge bosons and fermions should not be too large and should constrain the natural width to be smaller than that of a unique Higgs boson at high mass with couplings to fermions and gauge bosons as predicted by the SM (and provided that trilinear and quartic couplings are not too large and that no new state affects the heavy state total width). It is therefore reasonable to consider total widths for the high mass *CP*-even state smaller than the equivalent SM width. For the sake of generality these searches should be done as a function of Higgs boson mass and total width. Until recently only two cases have been investigated: (i) the SM width using the complex pole scheme (CPS), and (ii) the narrow width approximation.

One example of searches for high mass *CP*-even Higgs bosons decaying to a pair of gauge bosons in the narrow width approximation in the $H \to W^{(*)}W^{(*)} \to \ell\nu\ell\nu$ inclusive search channel by the ATLAS collaboration is given in Fig. 11.29. The searches for the Higgs boson in the $H \to \gamma\gamma$ and $H \to W^{(*)}W^{(*)}$ in the $\ell\nu\ell\nu$ and $\ell\nu q\overline{q}$ channels and the $H \to Z^{(*)}Z^{(*)}$ searches in the 4ℓ, $\ell\ell q\overline{q}$ and $\ell\ell\nu\nu$ channels have also been done, but in most cases are simple reinterpretations of the SM Higgs search in the CPS scheme. Recent references are summarized in Table 11.18.

(c) Searches for an additional state with the presence of H

In the post-discovery era, analyses in general need to take into account the presence of the newly discovered state. For searches with sufficiently high resolution of additional states non degenerate in mass, the strength of the observed state and limits on the signal strength of a potential additional state can be set independently as discussed in the next section. However in some cases, such as when a channel does not have a sufficiently fine mass resolution or when the states are nearly degenerate in mass, specific analyses need to be designed. There are two examples of such analyses: (i) the search for an additional state in the $H \to W^{(*)}W^{(*)} \to \ell\nu\ell\nu$ channel in ATLAS and (ii) the search for nearly degenerate states in the $H \to \gamma\gamma$ channel with the CMS detector.

The search, in the $H \to W^{(*)}W^{(*)} \to \ell\nu\ell\nu$ channel, for an additional state is done using boosted decision tree combining several discriminating kinematic characteristics to optimally separate the signal from the background and a high mass signal H from the lower mass state h [430]. A simultaneous fit of the two states h and H is then made to test the presence of an additional state. In this case, the usual null hypothesis of background is generated including the SM signal. The results of this search are shown in Fig. 11.30.

The CMS search for nearly degenerate mass states decaying to a pair of photons [431] is more generic and could for instance apply to *CP*-odd Higgs bosons as well. It consists of a fit to the diphoton mass spectrum using two nearly degenerate mass templates.

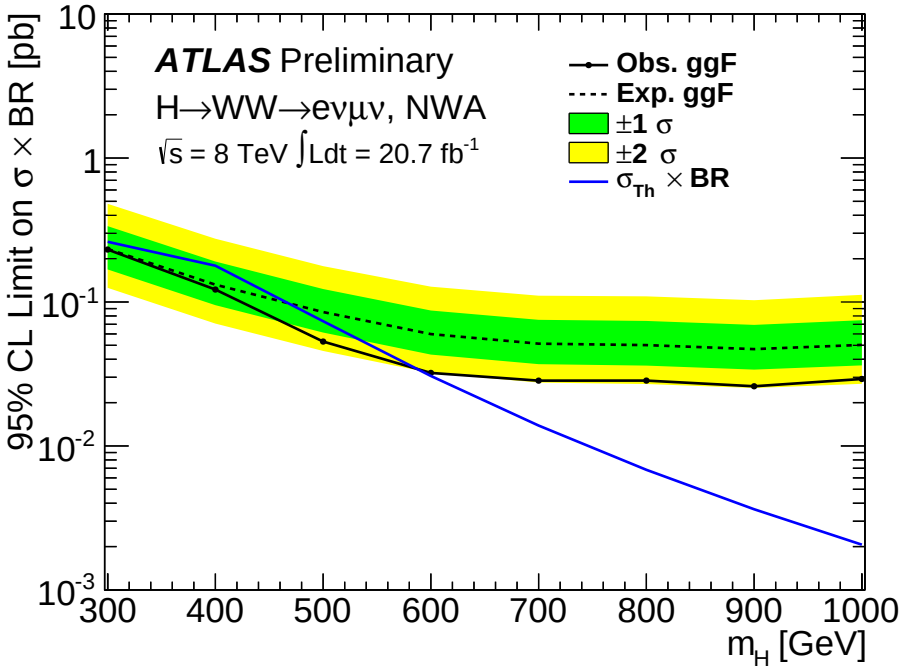

Figure 11.29: The 95% CL upper limits on the Higgs boson production cross section times branching ratio for $H \to W^{(*)}W^{(*)} \to \ell\nu\ell\nu$ for the gluon-fusion process and a Higgs boson with a narrow lineshape (NWA). The green and yellow bands show the 1σ and 2σ uncertainties on the expected limit [478]. The expected cross section times branching ratio for the production of a SM Higgs boson is shown as a blue line.

(d) Type I 2HDM and Fermiophobia

The measurements of coupling properties of H indirectly excludes that the discovered state is fermiophobic. However, the presence of an additional fermiophobic state, as predicted by Type I 2HDMs, is not excluded. Prior to the discovery, ATLAS and CMS have performed searches for a fermiophobic Higgs boson, *i.e.* produced through couplings with vector bosons only (VBF and VH) and decaying in $h_f \to \gamma\gamma$, optimized for fermiophobic signatures in the diphoton channel [432,433]. CMS has further combined these results with searches for $h_f \to W^+W^-$ and $h_f \to ZZ$ assuming fermiophobic production and decay [434]. CMS excludes a fermiophobic Higgs boson in the range $110\,\text{GeV} < m_H < 188\,\text{GeV}$ at the 95% C.L.

(e) Interpretation benchmarks in the light of the discovered Higgs boson

Two specific benchmark scenarios driven by unitarity relations are proposed in Ref. [38], assuming the existence of an additional state h' with coupling scale factors, i.e, deviations from the couplings predicted for the SM Higgs at the same mass, denoted

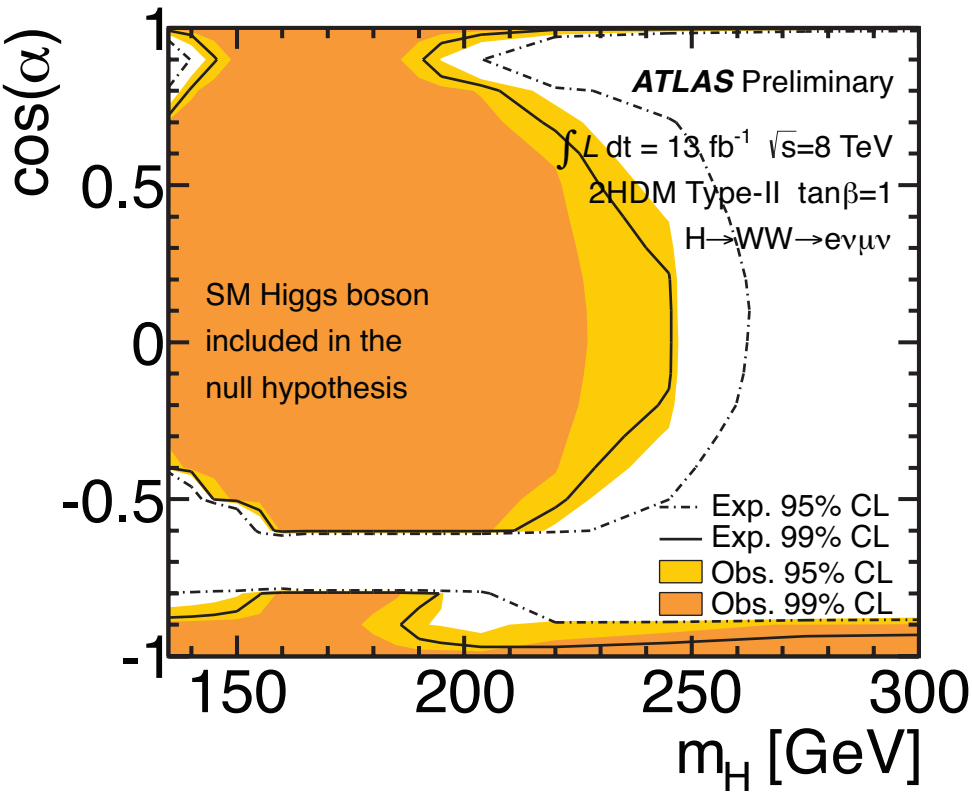

Figure 11.30: The ATLAS 95% CL exclusion contours in the $(\cos\alpha, m_H)$ plane for $\tan\beta = 1$ of the type-II 2HDM [430].

κ'_V and κ'_F for the couplings of h' to vector bosons and fermions respectively. The gauge boson scattering unitarity then yields the following sum rule

$$\kappa_V^2 + \kappa_V'^2 = 1 \tag{11.90}$$

and the unitarization of the gauge boson scattering to fermions yields

$$\kappa_V \cdot \kappa_F + \kappa'_V \cdot \kappa'_F = 1 \tag{11.91}$$

The two benchmark scenarios are then defined as follows: (i) a single coupling scale factor is assumed for the gauge bosons and the fermions, with an additional parameter to take into account decays to new states; (ii) two parameters are used to describe independently the couplings to fermions and the couplings to vector bosons. A direct application of the latter can be done in the *CP*-even sector of the type-I 2HDM.

(ii) Searches for additional states decaying to fermions

(a) Exclusion limits from LEP

In e^+e^- collisions at LEP centre-of-mass energies, the main production mechanisms of the neutral MSSM Higgs bosons were the Higgs-strahlung processes $e^+e^- \to hZ$, HZ and the pair production processes $e^+e^- \to hA$, HA, while the vector boson fusion processes played a marginal role. Higgs boson decays to $b\bar{b}$ and $\tau^+\tau^-$ were used in these searches.

The searches and limits from the four LEP experiments are described in Refs. [435,436]. The combined LEP data did not contain any excess of events which would imply the production of a Higgs boson, and combined limits were derived [437]. For $m_A \gg M_Z$ the limit on m_h is nearly that of the SM searches, as $\sin^2(\beta-\alpha) \approx 1$. For high values of $\tan\beta$ and low m_A ($m_A \leq m_h^{max}$), the $e^+e^- \to hA$ searches become the most important, and the lightest Higgs h is non SM-like. In this region, the 95% CL mass bounds are $m_h > 92.8\,\text{GeV}$ and $m_A > 93.4\,\text{GeV}$. In the m_h-max. scenario, values of $\tan\beta$ from 0.7 to 2.0 are excluded taking $m_t = 174.3\,\text{GeV}$, while a much larger $\tan\beta$ region is excluded for other benchmark scenarios such as the no-mixing one.

Neutral Higgs bosons may also be produced by Yukawa processes $e^+e^- \to f\overline{f}\phi$, where the Higgs particle $\phi \equiv h$, H, A, is radiated off a massive fermion ($f \equiv b$ or $\tau^\pm$). These processes can be dominant at low masses, and whenever the $e^+e^- \to h\text{Z}$ and hA processes are suppressed. The corresponding ratios of the $f\overline{f}h$ and $f\overline{f}A$ couplings to the SM coupling are $\sin\alpha/\cos\beta$ and $\tan\beta$, respectively. The LEP data have been used to search for $b\overline{b}\,b\overline{b}$, $b\overline{b}\tau^+\tau^-$, and $\tau^+\tau^-\,\tau^+\tau^-$ final states [438,439]. Regions of low mass and high enhancement factors are excluded by these searches.

A flavor-independent limit for Higgs bosons in the Higgs-strahlung process at LEP has also been set at 112 GeV [440].

In the case where the Higgs boson does not predominantly decay to a pair of b quarks, the searches for the SM Higgs boson have been performed at LEP. All four collaborations conducted dedicated searches for the Higgs boson with reduced model dependence, assuming it is produced via the Higgs-strahlung process, and not addressing its flavor of decay, a lower limit on the Higgs mass of 112.9 GeV is set by combining the data of all four experiments [440]. Using an effective Lagrangian approach and combining several results sensitive to the $h\gamma\gamma$, $hZ\gamma$ and hZZ couplings, an interpretation of several searches for the Higgs boson was made and set a lower limit of 106.7 GeV on the mass of a Higgs boson that can couple anomalously to photons [440].

(b) Searches at the Tevatron and LHC

The best sensitivity is in the regime with low to moderate m_A and with large $\tan\beta$ which enhances the couplings of the Higgs bosons to down-type fermions. The corresponding limits on the Higgs boson production cross section times the branching ratio of the Higgs boson into down-type fermions can be interpreted in MSSM benchmark scenarios [249]. If $\phi = A, H$ for $m_A > m_h^{\text{max}}$, and $\phi = A, h$ for $m_A < m_h^{\text{max}}$, the most promising channels at the Tevatron are the inclusive $p\overline{p} \to \phi \to \tau^+\tau^-$ process, with

contributions from both $gg \to \phi$ and $b\overline{b}\phi$ production, and $b\overline{b}\phi, \phi \to \tau^+\tau^-$ or $\phi \to b\overline{b}$, with $b\tau\tau$ or three tagged b-jets in the final state, respectively. Although Higgs boson production via gluon fusion has a higher cross section in general than via associated production, it cannot be used to study the $\phi \to b\overline{b}$ decay mode since the signal is overwhelmed by the QCD background.

The CDF and D0 collaborations have searched for neutral Higgs bosons produced in association with bottom quarks and which decay into $b\overline{b}$ [441,442], or into $\tau^+\tau^-$ [443,444]. The most recent searches in the $b\overline{b}\phi$ channel with $\phi \to b\overline{b}$ analyze approximately 2.6 fb^{-1} of data (CDF) and 5.2 fb^{-1} (D0), seeking events with at least three b-tagged jets. The cross section is defined such that at least one b quark not from ϕ decay is required to have $p_T > 20\,\text{GeV}$ and $|\eta| < 5$. The decay widths of the Higgs bosons are assumed to be much smaller than the experimental resolution. The invariant mass of the two leading jets as well as b-tagging variables are used to discriminate the signal from the backgrounds. The QCD background rates and shapes are inferred from data control samples, in particular, the sample with two b-tagged jets and a third, untagged jet. Separate-signal hypotheses are tested and limits are placed on $\sigma(p\overline{p} \to b\overline{b}\phi) \times \text{BR}(\phi \to b\bar{b})$. A local excess of approximately 2.5σ significance has been observed in the mass range of 130–160 GeV, but D0's search is more sensitive and sets stronger limits. The D0 result had an $\mathcal{O}(2\sigma)$ local upward fluctuation in the 110 to 125 GeV mass range. These results have been superseded by the LHC searches and the excess seen in the D0 experiment has not been confirmed elsewhere.

ATLAS and CMS also search for $\phi \to \tau^+\tau^-$ in pp collisions at $\sqrt{s} = 7\,\text{TeV}$. ATLAS seeks tau pairs in 4.7–4.8 fb^{-1} of data [445], and the search by CMS uses the full 4.9 fb^{-1} of 7 TeV data 4.9 fb^{-1} of 8 TeV data [446] and bb [448]. The searches are performed in categories of the decays of the two tau leptons: $e\tau_{\text{had}}$, $\mu\tau_{\text{had}}$, $e\mu$, and $\mu\mu$, where τ_{had} denotes a tau lepton which decays to one or more hadrons plus a tau neutrino, e denotes $\tau \to e\nu\nu$, and μ denotes $\tau \to \mu\nu\nu$. The dominant background comes from $Z \to \tau^+\tau^-$ decays, although $t\overline{t}$, W+jets and Z+jets events contribute as well. Separating events into categories based on the number of b-tagged jets improves the sensitivity in the MSSM. The $b\bar{b}$ annihilation process and radiation of a Higgs boson from a b quark gives rise to events in which the Higgs boson is accompanied by a $b\bar{b}$ pair in the final state. Requiring the presence of one or more b jets reduces the background from Z+jets. Data control samples are used to constrain background rates. The rates for jets to be identified as a hadronically decaying tau lepton are measured in dijet samples, and W+jets samples provide a measurement of the rate of events that, with a fake hadronic tau, can pass the signal selection requirements. Lepton fake rates are measured using samples of unisolated lepton candidates and same-sign lepton candidates. Constraints from the CMS searches for $h \to \tau^+\tau^-$ and $h \to b\overline{b}$ are shown in Fig. 11.31 in the m_h-max benchmark scenario, with $\mu = 200\,\text{GeV}$ and $\mu = -200\,\text{GeV}$ respectively. The neutral Higgs boson searches consider the contributions of both the *CP*-odd and *CP*-even neutral Higgs bosons with enhanced couplings to bottom quarks, as they were for the Tevatron results.

A search for $\phi \to \mu^+\mu^-$ has also been performed by the ATLAS collaboration [445]. The exclusion limits obtained are given in terms of cross section times branching fraction and combined with those of $\phi \to \tau^+\tau^-$ [445].

The LHC has the potential to explore a broad range of SUSY parameter space through the search for non-SM-like Higgs bosons. Nevertheless, Fig. 11.31 shows a broad region with intermediate $\tan\beta$ and large values of m_A that is not tested by present neutral or charged Higgs boson searches, and which cannot be covered completely via these searches, even with much larger data sets. In this region of parameter space it is possible that only the SM-like Higgs boson can be within the LHC's reach. If no other state of the EWSB sector than H is discovered, it may be challenging to determine only from the Higgs sector whether there is a supersymmetric extension of the SM in nature.

(iii) Searches for Charged Higgs bosons $H^\pm$

At e^+e^- colliders charged Higgs bosons can pair produced in the s-channel via γ or Z boson exchange. This process is dominant in the LEP centre-of-mass energies range *i.e.* up to 209 GeV. At higher centre-of-mass energies, other processes can play an important role such as the production in top quark decays via $t \to b + H^+$ if $m_H^\pm < m_t - m_b$ or via the one-loop process $e^+e^- \to W^\pm H^\mp$ [282,283], which allows the production of a charged Higgs boson with $m_H^\pm > \sqrt{s}/2$, even when H^+H^- production is kinematically forbidden. Other single charged Higgs production mechanisms include $t\bar{b}H^-/\,\bar{t}bH^+$ production [90], $\tau^+\nu H^-/\,\tau^-\bar{\nu}H^+$ production [284], and a variety of processes in which $H^\pm$ is produced in association with a one or two other gauge and/or Higgs bosons [285].

At hadron colliders, Charged Higgs bosons can be produced in several different modes. If $m_{H^\pm} < m_t - m_b$, the charged Higgs boson can be produced in decays of the top quark via the decay $t \to bH^\pm$. Relevant QCD and SUSY-QCD corrections to $\mathrm{BR}(t \to H^\pm b)$ have been computed [291–294]. For values of $m_{H^\pm}$ near m_t, width effects are important. In addition, the full $2 \to 3$ processes $pp/p\bar{p} \to H^+\bar{t}b + X$ and $pp/p\bar{p} \to H^-t\bar{b} + X$ must be considered. If $m_{H^\pm} > m_t - m_b$, then charged Higgs boson production occurs mainly through radiation from a third generation quark. Charged Higgs bosons may also be produced singly in association with a top quark via the $2 \to 3$ partonic processes gg, $q\bar{q} \to t\bar{b}H^-$. For charged Higgs boson production cross section predictions for the Tevatron and the LHC, see Refs. [38,10,37]. Charged Higgs bosons can also be produced via associated production with $W^\pm$ bosons through $b\overline{b}$ annihilation and gg-fusion [295] and in pairs via $q\overline{q}$ annihilation [296].

(a) Exclusion limits from LEP

Charged Higgs bosons have been searched for at LEP, where the combined data of the four experiments, ALEPH, DELPHI, L3, and OPAL, were sensitive to masses of up to about 90 GeV [437] in two decay channels, the $\tau\nu$ and $c\overline{s}$. The exclusion limit independent of the admixture of the two above mentioned branching fractions was 78.6 GeV.

(b) Exclusion limits from Tevatron

Compared to the LEP mass domain of searches, Tevatron covered a complementary range of charged Higgs mass hypotheses. The CDF and D0 collaborations have also searched for charged Higgs bosons in top quark decays with subsequent decays to $\tau\nu$ or to $c\bar{s}$ [449–451]. In the $H^+ \to c\bar{s}$, the limits on $\mathrm{BR}(t \to H^+b)$ from CDF and D0 are

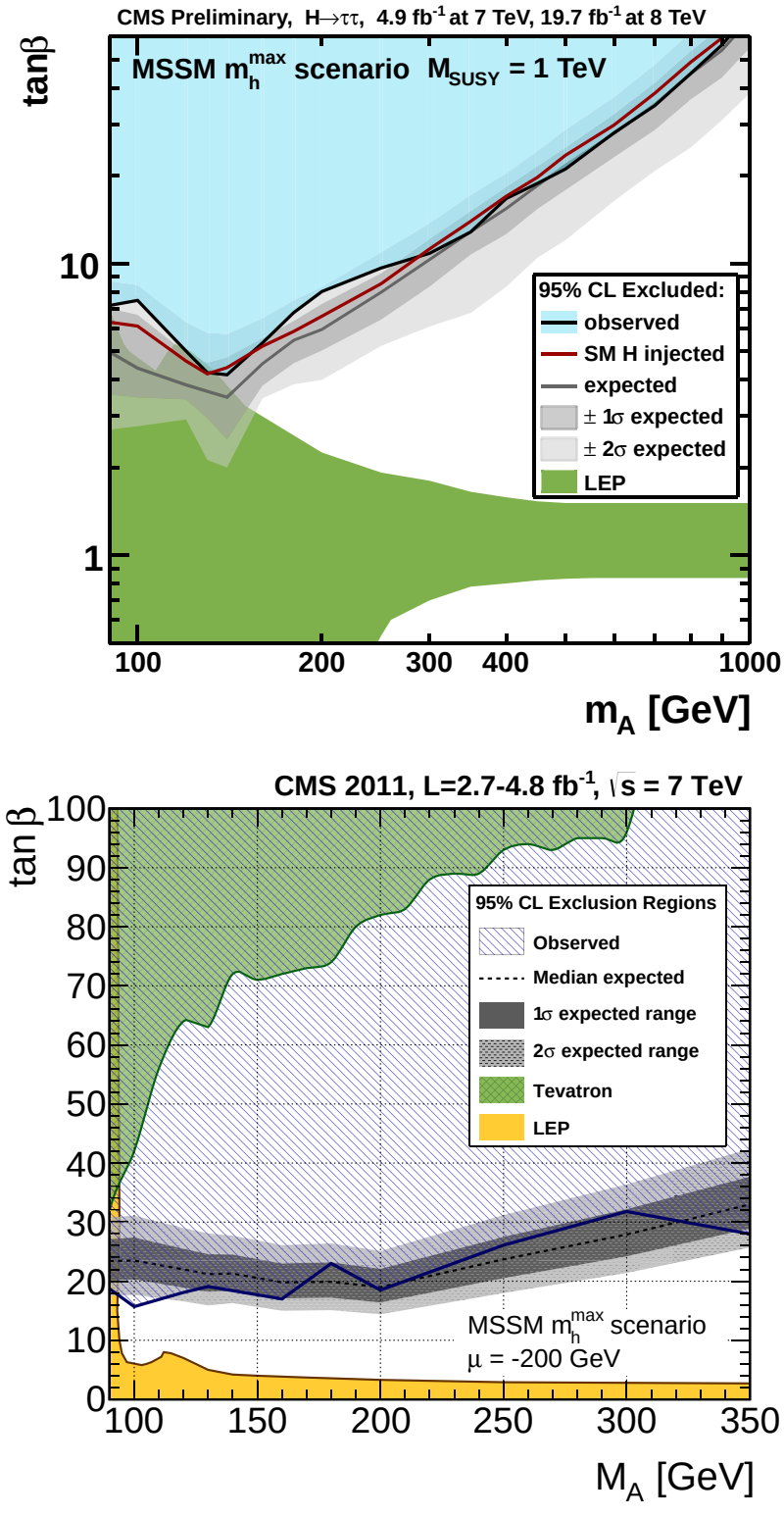

Figure 11.31: The 95% CL exclusion contours in the $(M_A, \tan\beta)$ parameter space for the MSSM mhmax scenario, for the $\tau^+\tau^-$ channel [446] (upper plot) and the $b\overline{b}$ channel [448](lower plot).

$\approx 20\%$ in the mass range $90\,\text{GeV} < m_{H^+} < 160\,\text{GeV}$ and assuming a branching fraction of 100% in this specific final state. $H^+ \to \tau^+\nu_\tau$ channel, D0's limits on $\text{BR}(t \to H^+b)$ are also $\approx 20\%$ in the same mass range and assuming a branching fraction of 100% in this final state. These limits are valid in general 2HDMs, and they have also been interpreted in terms of the MSSM [449–451].

(c) Exclusion limits from LHC

At the LHC the sensitive mass domain is much larger and the variety of search channels wider. Until recently, only the $\tau\nu$ and $c\bar{s}$ final states have been investigated.

The ATLAS and CMS collaborations have searched for charged Higgs bosons produced in the decay of top quarks in $t\bar{t}$ events. ATLAS has searched for the decay $H^+ \to \tau^+\nu_\tau$ in three final state topologies [452]: (i) lepton+jets: with $t\bar{t} \to \bar{b}WH^+ \to b\bar{b}(q\bar{q}')(\tau_{\text{lep}}\nu)$, i.e., the W boson decays hadronically and the tau decays into an electron or a muon, with two neutrinos; (ii) τ +lepton: with $t\bar{t} \to \bar{b}WH^+ \to b\bar{b}(l\nu)(\tau_{\text{had}}\nu)$ i.e., the W boson decays leptonically (with $\ell = e,\ \mu$) and the tau decays hadronically; (iii) τ+jets: $t\bar{t} \to \bar{b}WH^+ \to b\bar{b}(q\bar{q}')(\tau_{\text{had}}\nu)$, i.e., both the W boson and the τ decay hadronically [453]. The latter channel has been recently updated with the full 8 TeV dataset of pp collisions, corresponding to an integrated luminosity of 19.5 fb^{-1} [453]. Assuming $\text{BR}(H^+ \to \tau^+\nu_\tau) = 100\%$, ATLAS sets upper limits on $\text{BR}(t \to H^+b)$ between 0.24% and 2.1% for charged Higgs boson masses between 90 GeV to 160 GeV. When interpreted in the context of the m_h^{max} scenario of the MSSM, these bounds exclude a large fraction of the ($m_{H^\pm}$,$\tan\beta$) plane as illustrated in Fig. 11.32.

The CMS collaboration has searched for the charged Higgs boson in the decay products of top quark pairs: $t\bar{t} \to H^\pm W^\mp b\bar{b}$ and $t\bar{t} \to H^+H^-b\bar{b}$ [454,455] as well. Three types of final states with large missing transverse energy and jets originating from b-quark hadronization have been analyzed: the fully-hadronic channel with a hadronically decaying tau in association with jets, the dilepton channel with a hadronically decaying tau in association with an electron or muon and the dilepton channel with an electron-muon pair. Combining the results of these three analyses and assuming $\text{BR}(H^\pm \to \tau\nu)$=1, the upper limits on $\text{BR}(t \to H^+b)$ are less than 2% to 3% depending on the charged Higgs boson mass in the interval $80\,\text{GeV} < m_{H^+} < 160\,\text{GeV}$.

ATLAS has also searched for charged Higgs bosons in top quark decays assuming $\text{BR}(H^+ \to c\bar{s}) = 100\%$ [456], and sets limits of $\approx 20\%$ on $\text{BR}(t \to H^+b)$ in the $90\,\text{GeV} < m_{H^+} < 160\,\text{GeV}$ mass range.

At the LHC various other channels can be investigated, in particular the challenging search for a heavy charged Higgs decaying to $t\bar{b}$, searches involving additional neutral scalars in particular in WH, WA where A is the pseudo scalar MSSM Higgs boson, and Wa where a is the light CP-odd scalars of the NMSSM.

(iv) Searches for a light CP-odd Higgs boson a

A light pseudoscalar boson a from a two Higgs double model or a model, such as the NMSSM, enhanced with an additional singlet field. The theoretical motivations for singlet extensions of the MSSM are discussed in Section V.2. The main focus of searches

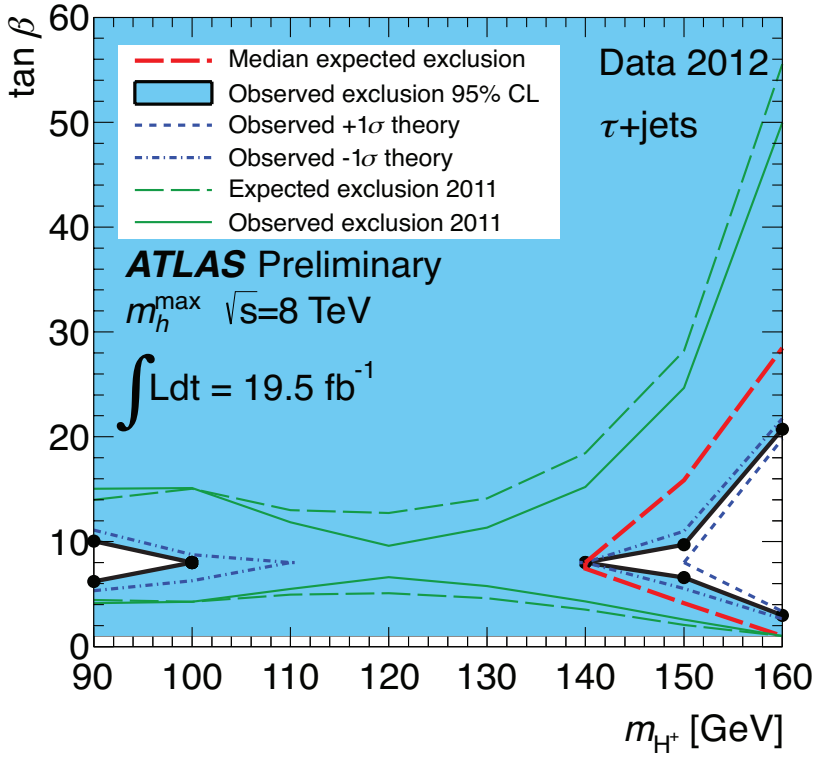

Figure 11.32: ATLAS exclusion limits of the searches of the light $H^{\pm}$, in the context of the MSSM m_h^{max} scenario with $\mu = 200\,\text{GeV}$ [453]. For comparison, the 2011 limits are also indicated.

for signatures of the NMSSM is on low mass pseudo-scalar boson a for several reasons: (i) in the NMSSM, the light pseudo-scalar a boson can, as a pseudo goldstone boson, be a natural candidate for an axion; (ii) scenarios where $m_a > 2m_b$ and a CP-even state h can decay to a pair of a ($m_h > 2m_a$) are excluded by direct searches at LEP in the $4b$ channel [437,457,458]. for Higgs boson decays to $4b$-quarks have been carried out at LEP; (iii) in the pre-discovery era, LEP limits on a CP-even higgs boson resulted in fine tuning MSSM constraints [459], these could be evaded through non standard decays of the Higgs to aa; (iv) an NMSSM CP-odd a boson with a mass in the range 9.2–12 GeV can also account for the difference observed between the measured anomalous muon magnetic moment and its prediction [460]. A scenario that has drawn particular attention was motivated by a small excess of events 2.3σ in the SM Higgs search at LEP at Higgs boson masse of around 98 GeV. Speculative interpretations of this excess as a signal of a Higgs boson with reduced couplings to b-quarks were given [459]. Complete reviews of the NMSSM phenomenology can be found in Refs. [461,458].

The potential benchmark scenarios have changed in the light of the H discovery. The discovered state could be the lightest or the next-to-lightest of the three CP-even states of the NMSSM. Light pseudoscalar scenarios are still very interesting in particular for the potential axion candidate. There are three main types of direct searches for the light a

boson: (i) for masses below the Υ resonance, the search is for radiative decays $\Upsilon \to a\gamma$ at B-factories; (ii) the inclusive search for in high energy pp collisions at the LHC; (iii) the search for decays of a *CP*-even Higgs h boson to a pair of a bosons.

Radiative decays $\Upsilon \to a\gamma$, have been searched for in various colliders, the most recent results are searches for radiative decays of the $\Upsilon(1s)$ to $a\gamma$ with a subsequent decay of the a boson to a pair of taus at CLEO [462] and the radiative decays of the $\Upsilon(1s, 2s, 3s)$ to $a\gamma$ with subsequent decays to a pair of muons or taus by the Babar collaboration [463,464].

Direct inclusive searches for the light pseudo scalar a boson were performed in the $a \to \mu\mu$ channel at the Tevatron by the D0 experiment [465] and by the ATLAS [466] and CMS [467] collaborations at the LHC.

Finally searches for the decays of a *CP*-even Higgs boson to a pair of a bosons where performed with subsequent decays to four photons by the ATLAS experiment [468], in the four muons final state by the CMS and D0 experiments [469,458], in the two muons and two taus final state by the D0 collaboration [458], and in the four taus final state by the ALEPH collaboration at LEP [470].

No significant excess in the searches for a light *CP*-odd a boson were found and limits on the production times branching fractions of the a boson have been set.

(v) Searches for doubly charged Higgs bosons $H^{\pm\pm}$

As discussed in Section V.6.2 the generation of small neutrino masses via the standard EWSB mechanism described in Section II, requires unnaturally small Yukawa couplings, provided that neutrinos are Dirac-type fermions. A Majorana mass term with a see-saw mechanism for neutrinos, would allow for naturally small masses and yield a framework for the appealing scenario of leptogenesis. However within the SM Majorana mass terms correspond to (non-renomalizable) dimension-5 operators. Such effective interactions can be generated via renormalizable interactions with an electroweak triplet of complex scalar fields (corresponding to a type-II see-saw mechanism). Other models such as the Zee–Babu model, with the introduction of two $\mathrm{SU}(2)_L$ singlets, also generate Majorana mass terms. The signature of such models would be the presence of doubly charged Higgs bosons $H^{\pm\pm}$.

The main production mechanisms of $H^{\pm\pm}$ bosons at hadron colliders are the pair production in the s-channel through the exchange of a Z boson or a photon and the associated production with a Charged Higgs boson through the exchange of a W boson.

V.9.1. Standard decays for non-standard processes

The discovery of the H state has also allowed for searches of BSM (beyond the SM) processes involving standard decays of the Higgs boson. One example directly pertaining to the search for additional states of the EWSB sector is the search for Higgs bosons in the cascade decay of a heavy *CP*-even Higgs boson decaying to charged Higgs boson and a W boson, and the charged Higgs boson subsequently decaying to H and another W boson. This search has been performed by the ATLAS collaboration in $b\overline{b}$ decays of the H particle [485].

Another example of searches for non standard processes through the presence of the H particle is the search for large flavor changing neutral current decays of the top quark to

Table 11.18: Summary of references to searches for additional states from extended Higgs sectors, where BBr denotes the BaBar experiment, TeV the Tevatron experiments.

	ATLAS	CMS	Other experiments
CP-even H			
$h, H \to \gamma\gamma$	–	[431]	–
$h, H \to ZZ \to 4\ell$	[471]	[472]	–
$h, H \to ZZ \to \ell\ell\nu\nu$	[473]	[474]	–
$h, H \to ZZ \to \ell\ell q\overline{q}$	[475,476]	[477]	–
$h, H \to WW \to \ell\nu\ell\nu$	[478]	[472]	–
$h, H \to WW \to \ell\nu\ell\nu$ (2HDM)	[430]	[472]	–
$h, H \to WW \to \ell\nu q\overline{q'}$	[479]	[480,481]	–
CP-odd A			
$h, H, A \to \tau^+\tau^-$	[445]	[446]	[443,444]-TeV
			[447]-LHCb
$h, H, A \to \mu^+\mu^-$	[445]	–	–
$h, H, A \to b\overline{b}$	–	[448]	[441,442]-TeV
Charged $H^\pm$			
$H^\pm \to \tau^\pm\nu$	[453]	[455]	–
$H^\pm \to cs$	[482]	–	–
CP-odd NMSSM a			
$a \to \mu^+\mu^-$	[466]	[467]	–
$h \to aa \to 4\mu, 4\tau, 4\gamma$	[468]	[469]	–
$\Upsilon_{1s,3s} \to a\gamma$	–	–	[463,464]-BBr
Doubly Charged $H^\pm$	[483]	[484]	–

H and a charm quark. This search has been performed with the ATLAS experiment in the $H \to \gamma\gamma$ channel [486].

V.9.2. Outlook of searches for additional states

Although the LHC program of searches for additional states covers a large variety of decay channels for additional states, various important topologies are still not covered. In particular when searching for additional states the decays of heavy additional particles such as those of the neutral states decaying to a pair of HH or to ZH are important. Similarly the search for charged Higgs bosons can be extended to include the search for HW and cover the high mass region with $t\overline{b}$ decays. The LHC program for searches of additional scalar states is also rich in other yet to be explored final states such as heavy neutral Higgs bosons decays to a top-quark pair or charged Higgs boson decays to a, AW.

VI. Summary and Outlook

The discovery of the Higgs boson is a milestone in particle physics and an extraordinary success of the LHC machine and the ATLAS and CMS collaborations. The emerging understanding of the nature of this new particle is confirmed by various measurements of its properties, all consistent with the EWSB mechanism and other properties of the Standard Model. The Higgs coupling to gauge bosons has been measured to a precision of nearly 10%. The combination of LHC and Tevatron experiments have accessed couplings to the heavier fermions, although this still needs further confirmation from the LHC experiments. The quantum numbers of the new particle have been probed and show an excellent consistency with $J^{PC} = 0^{++}$. Hints of the direct large Yukawa coupling to the top quark are emerging. Rare decay modes (e.g. $\mu\mu$ and $Z\gamma$) have been searched for, and the experiments will eventually have sensitivity to the expected SM rates. These measurements mark the start of a new era of precision Higgs boson measurements and the use of the Higgs boson as a portal to new physics. Positive or negative, searches for additional states belonging to the EWSB sector will bring invaluable insights on the needed extension(s) of the Standard Model at higher energies.

The Higgs boson couplings are not dictated by gauge symmetries. Thus, in addition to a new particle, the LHC has also discovered a new force, different in nature from the other fundamental interactions since it is non-universal and distinguishes between the three families of quarks and leptons.

Furthermore, the mere existence of the Higgs boson with a mass of approximately 125 GeV, embodies the problem of an unnatural cancellation among the quantum corrections to its mass. The non-observation of additional states which could stabilize the Higgs mass is a challenge for natural scenarios like supersymmetry or models with a new strong interaction in which the Higgs boson is not a fundamental particle. This increasingly pressing paradox starts questioning the principle of naturalness relying on the hypothesis that phenomena at different scales do not influence each others.

The unitarization of the vector boson scattering (VBS) amplitudes, dominated at high energies by their longitudinal polarizations, has been the basis of the *no lose* theorem at the LHC and was one of the main motivations to build the accelerator and the detectors. It motivated the existence of a Higgs boson or the observability of manifestations of strong dynamics at TeV scale. Now that a Higgs boson has been found and that its couplings to gauge bosons follow the SM predictions, perturbative unitarity is preserved to a large amount with the sole exchange of the Higgs boson and without the need for any additional states. It is, however, still an important channel to investigate further in order to better understand the nature of the Higgs sector and the possible completion of the SM at the TeV scale. In association with the double Higgs boson production channel by vector boson fusion, VBS could, for instance, confirm that the Higgs boson is part of a weak doublet and also establish if it is a composite state and whether or not it emerges as a pseudo-Nambu–Goldstone boson from an underlying broken symmetry.

The search for the Higgs boson has occupied the Particle physics community for the last 50 years. Its discovery is now shaping and sharpening the physics programs of future accelerators.

Acknowledgements

We would like to thank many of our colleagues for proofreading parts of the review, for useful criticism and their input in general: W. Altmannshofer, G. Branco, F. Cerutti, R. Contino, J. Conway, J.B. De Vivie, J.R. Espinosa, A. Falkowski, W. Fischer, M. Grazzini, H. Haber, S. Heinemeyer, J. Hubisz, A. Korytov, B. Jäger, H. Ji, T. Junk, P. Langacker, J. Lykken, F. Maltoni, M. Mühlleitner, B. Murray, M. Neubert, G. Perez, G. Petrucciani, A. Pomarol, E. Pontón, D. Rebuzzi, E. Salvioni, N. Shah, G. Shaughnessy, M. Spira, O. Stål, A. Strumia, R. Tanaka, A. Vartak, C. Wagner, and A. Weiler.

We are also most grateful to the ATLAS, CDF, CMS and D0 collaborations for their help with this review.

M.C. is supported by Fermilab, that is operated by Fermi Research Alliance, LLC under Contract No. DE–AC02–07CH11359 with the United States Department of Energy. C.G. is supported by the Spanish Ministry MICINN under contract FPA2010–17747, the European Commission under the ERC Advanced Grant 22637 MassTeV and the contract PITN–GA–2009–237920 UNILHC. M.K. is supported by the ANR HiggsNet grant. V.S. is supported by the grant DE–SC0009919 of the United States Department of Energy.

References

1. G. Aad *et al.*, [ATLAS Collab.], Phys. Lett. **B716**, 1 (2012).
2. S. Chatrchyan *et al.*, [CMS Collab.], CMS Collab., Phys. Lett. **B716**, 30 (2012).
3. F. Englert and R. Brout, Phys. Rev. Lett. **13**, 321 (1964);
   P.W. Higgs, Phys. Rev. Lett. **13**, 508 (1964) and Phys. Rev. **145**, 1156 (1966);
   G.S. Guralnik, C.R. Hagen, and T.W. Kibble, Phys. Rev. Lett. **13**, 585 (1964).
4. S.L. Glashow, Nucl. Phys. **20**, 579 (1961);
   S. Weinberg, Phys. Rev. Lett. **19**, 1264 (1967);
   A. Salam, *Elementary Particle Theory*, eds.: Svartholm, Almquist and Wiksells, Stockholm, 1968;
   S. Glashow, J. Iliopoulos, and L. Maiani, Phys. Rev. **D2**, 1285 (1970).
5. J.M. Cornwall, D.N. Levin, and G. Tiktopoulos, Phys. Rev. Lett. **30**, 1286 (1973) and Phys. Rev. **D10**, 1145 (1974);
   C.H. Llewellyn Smith, Phys. Lett. **B46**, 233 (1973).
6. B.W. Lee, C. Quigg, and H.B. Thacker, Phys. Rev. **D16**, 1519 (1977).
7. K. Wilson, Phys. Rev. D 3,1818(1971);
   G.t'Hooft, in *Proc. of 1979 Cargèse Institute on Recent Developments in Gauge Theories,* p. 135 Press, New York 1980;
   For a recent review, see G.F. Giudice, `arXiv:1307.7879 [hep-ph]` (2013).
8. J. Wess and B. Zumino, Nucl. Phys. **B70**, 39 (1974) and Phys. Lett. **49B**, 52 (1974);
   H.P. Nilles, Phys. Rev. **C110**, 1 (1984);
   S.P. Martin, `arXiv:hep-ph/9709356` (1997);
   P. Fayet, Phys. Lett. **B69**, 489 (1977) Phys. Lett. **B84**, 421 (1979), Phys. Lett. **B86**, 272 (1979) and Nucl. Phys. **B101**, 81 (2001).

9. E. Witten, Nucl. Phys. **B188**, 513 (1981);
R.K. Kaul, Phys. Lett. **B109**, 19 (1982) and Pramana **19**, 183 (1982);
L. Susskind, Phys. Rev. **104**, 181 (1984).
10. H.E. Haber and G.L. Kane, Phys. Rev. **C117**, 75 (1985).
11. P. Fayet, Phys. Lett. **B64**, 159 (1976);
F. Riva, C. Biggio, and A. Pomarol, JHEP **1302**, 081 (2013).
12. J. F. Gunion *et al.*, *The Higgs Hunter's Guide*, Addison-Wesley (1990).
13. S. Weinberg, Phys. Rev. **D13**, 974 (1979) and Phys. Rev. **D19**, 1277 (1979);
L. Susskind, Phys. Rev. **D20**, 2619 (1979);
E. Farhi and L. Susskind, Phys. Rev. **74**, 277 (1981);
R.K. Kaul, Rev. Mod. Phys. **55**, 449 (1983);
C. T. Hill and E. H. Simmons, Phys. Reports **381**, 235 (2003) [E: **390**, 553 (2004)].
14. D. B. Kaplan and H. Georgi, Phys. Lett. **B136**, 183 (1984).
15. C. Csaki *et al.*, Phys. Rev. **D69**, 055006 (2004);
C. Csaki *et al.*, Phys. Rev. Lett. **92**, 101802 (2004);
C. Csaki, J. Hubisz, and P. Meade, `hep-ph/0510275` (2005).
16. C. Csaki *et al.*, Phys. Rev. **D62**, 045015 (2000);
C. Csaki, M. L. Graesser, and G. D. Kribs, Phys. Rev. **D63**, 065002 (2001);
G. F. Giudice, R. Rattazzi, and J. D. Wells, Nucl. Phys. **B595**, 250 (2001);
M. Chaichian *et al.*, Phys. Lett. **B524**, 161 (2002);
D. Dominici *et al.*, Acta Phys. Polon. **B 33**, 2507 (2002);
J. L. Hewett and T. G. Rizzo, JHEP **0308**, 028 (2003);
B. Grzadkowski and J. F. Gunion, `arXiv:1202.5017 [hep-ph]` (2012);
C. Csaki, J. Hubisz, and S. J. Lee, Phys. Rev. **D76**, 125015 (2007);
B. Coleppa, T. Gregoire, and H. Logan, Phys. Rev. **D85**, 055001 (2012).
17. W. D. Goldberger, B. Grinstein, and W. Skiba, Phys. Rev. Lett. **100**, 111802 (2008);
J. Fan *et al.*, Phys. Rev. **D79**, 035017 (2009);
B. Bellazzini *et al.*, Eur. Phys. J. **C73**, 2333 (2013);
Z. Chacko and R. K. Mishra, Phys. Rev. **D87**, 115006 (2013);
Z. Chacko, R. Franceschini, and R. K. Mishra, JHEP **1304**, 015 (2013).
18. T. van Ritbergen and R. G. Stuart, Phys. Rev. Lett. **82**, 488 (1999) and Nucl. Phys. **B564**, 343 (2000);
M. Steinhauser and T. Seidensticker, Phys. Lett. **B467**, 271 (1999);
D. M. Webber *et al.*, [MuLan Collab.], Phys. Rev. Lett. **106**, 041803 (2011).
19. J. Ellis, M.K. Gaillard, and D.V. Nanopoulos, Nucl. Phys. **B106**, 292 (1976).
20. M.A. Shifman *et al.*, Sov. J. Nucl. Phys. **30**, 711 (1979) [Yad. Fiz. **30**, 1368 (1979)].
21. P. Sikivie *et al.*, Nucl. Phys. **B173**, 189 (1980);
H. Georgi, Ann. Rev. Nucl. and Part. Sci. **43**, 209 (1993).
22. M. J. G. Veltman, Nucl. Phys. **B123**, 89 (1977).
23. R. S. Chivukula *et al.*, Ann. Rev. Nucl. and Part. Sci. **45**, 255 (1995).
24. S. Willenbrock, `arXiv:0410370 [hep-ph]` (2008).

25. I. V. Krive and A. D. Linde, Nucl. Phys. **B117**, 265 (1976);
P. Q. Hung, Phys. Rev. Lett. **42**, 873 (1979);
N. Cabibbo *et al.*, Nucl. Phys. **B158**, 295 (1979);
M. Lindner, Z. Phys. **C31**, 295 (1986);
M. Luscher and P. Weisz, Nucl. Phys. **B290**, 25 (1987) and Nucl. Phys. **B295**, 65 (1988);
M. Lindner, M. Sher, and H. W. Zaglauer, Phys. Lett. **B228**, 139 (1989);
M. Sher, Phys. Reports **179**, 273 (1989);
G. Altarelli and G. Isidori, Phys. Lett. **B337**, 141 (1994);
J.A. Casas, J.R. Espinosa, and M. Quiros, Phys. Lett. **B342**, 171 (1995) and Phys. Lett. **B382**, 374 (1996);
T. Hambye and K. Riesselmann, Phys. Rev. **D55**, 7255 (1997).
26. J. Elias-Miro *et al.*, Phys. Lett. **B709**, 222 (2012);
G. Degrassi *et al.*, JHEP **1208**, 098 (2012);
D. Buttazzo *et al.*, `arXiv:1307.3536 [hep-ph]`.
27. J.R. Espinosa and M. Quiros, Phys. Lett. **B353**, 257 (1995);
G. Isidori, G. Ridolfi, and A. Strumia, Nucl. Phys. **B609**, 387 (2001).
28. C. D. Froggatt and H. B. Nielsen, Phys. Lett. **B368**, 96 (1996);
M. Shaposhnikov and C. Wetterich, Phys. Lett. **B683**, 196 (2010);
M. Holthausen, K. S. Lim, and M. Lindner, JHEP **1202**, 037 (2012).
29. F. Bezrukov *et al.*, JHEP **1210**, 140 (2012).
30. F. L. Bezrukov and M. Shaposhnikov, Phys. Lett. **B659**, 703 (2008);
F. L. Bezrukov, A. Magnin, and M. Shaposhnikov, Phys. Lett. **B675**, 88 (2009).
31. A. Salvio, Phys. Lett. **B727**, 234 (2013).
32. B.A. Kniehl, Phys. Reports **240**, 211 (1994).
33. M. Spira, Fortsch. Phys. **46**, 203 (1998).
34. M. Carena and H.E. Haber, Prog. in Part. Nucl. Phys. **50**, 152 (2003).
35. A. Djouadi, Phys. Reports **457**, 1 (2008).
36. S. Dittmaier *et al.*, [LHC Higgs Cross Section Working Group], `arXiv:1101.0593[hep ph]` (2011).
37. S. Dittmaier *et al.*, [LHC Higgs Cross Section Working Group], `arXiv:1201.3084 [hep-ph]` (2012).
38. S. Heinemeyer *et al.*, [LHC Higgs Cross Section Working Group], `arXiv:1307.1347[h ph]` (2013).
39. LHC Higgs Cross Section Working Group, `https://twiki.cern.ch/twiki/bin/view/LHCPhysics/CrossSections`.
40. T. Aaltonen *et al.*, [CDF and D0 Collaborations], Phys. Rev. **D88**, 052014 (2013).
41. H.M. Georgi *et al.*, Phys. Rev. Lett. **40**, 692 (1978).
42. D. Graudenz, M. Spira, and P.M. Zerwas, Phys. Rev. Lett. **70**, 1372 (1993).
43. M. Spira *et al.*, Nucl. Phys. **B453**, 17 (1995).
44. S. Dawson, Nucl. Phys. **B359**, 283 (1991);
A. Djouadi, M. Spira, and P.M. Zerwas, Phys. Lett. **B264**, 440 (1991).

45. R.V. Harlander and W.B. Kilgore, Phys. Rev. Lett. **88**, 201801 (2002);
C. Anastasiou and K. Melnikov, Nucl. Phys. **B646**, 220 (2002);
V. Ravindran, J. Smith, and W.L. van Neerven, Nucl. Phys. **B665**, 325 (2003).
46. R.V. Harlander and K.J. Ozeren, JHEP **0911**, 088 (2009);
A. Pak, M. Rogal, and M. Steinhauser, JHEP **1002**, 025 (2010).
47. A. Djouadi and P. Gambino, Phys. Rev. Lett. **73**, 2528 (1994);
S. Actis *et al.*, Phys. Lett. **B670**, 12 (2008);
U. Aglietti *et al.*, Phys. Lett. **B595**, 432 (2004);
G. Degrassi and F. Maltoni, Phys. Lett. **B600**, 255 (2004).
48. C. Anastasiou, R. Boughezal, and F. Petriello, JHEP **0904**, 003 (2009).
49. S. Catani *et al.*, JHEP **0307**, 028 (2003);
S. Moch and A. Vogt, Phys. Lett. **B631**, 48 (2005);
E. Laenen and L. Magnea, Phys. Lett. **B632**, 270 (2006);
A. Idilbi *et al.*, Phys. Rev. **D73**, 077501 (2006);
V. Ravindran, Nucl. Phys. **B752**, 173 (2006);
V. Ahrens *et al.*, Eur. Phys. J. **C62**, 333 (2009).
50. V. Ahrens *et al.*, Phys. Rev. **D79**, 033013 (2009).
51. V. Ahrens *et al.*, Phys. Lett. **B698**, 271 (2011);
D. de Florian and M. Grazzini, Phys. Lett. **B718**, 117 (2012);
C. Anastasiou *et al.*, JHEP **1204**, 004 (2012).
52. J.C. Collins, D.E. Soper, and G.F. Sterman, Nucl. Phys. **B250**, 199 (1985).
53. D. de Florian *et al.*, JHEP **1111**, 064 (2011);
T. Becher and M. Neubert, Eur. Phys. J. **C71**, 1665 (2011);
J.-Y. Chiu *et al.*, JHEP **1205**, 084 (2012);
J. Wang *et al.*, Phys. Rev. **D86**, 094026 (2012);
T. Becher, M. Neubert, and D. Wilhelm, JHEP **1305**, 110 (2013).
54. S. Catani and M. Grazzini, Eur. Phys. J. **C72**, 2013 (2012) [E: **C72**, 2132 (2012)].
55. W.-Y. Keung and F.J. Petriello, Phys. Rev. **D80**, 01007 (2009);
S. Boehler *et al.*, JHEP **1207**, 115 (2012);
M. Grazzini and H. Sargsyan, JHEP **1309**, 129 (2013).
56. R.V. Harlander, S. Liebler, and H. Mantler, Comp. Phys. Comm. **184**, 1605 (2013).
57. D. de Florian, M. Grazzini, and Z. Kunszt, Phys. Rev. Lett. **82**, 5209 (1999);
X. Liu and F. Petriello, Phys. Rev. **D87**, 014018 (2013).
58. J.M. Campbell, R.K. Ellis, and G. Zanderighi, JHEP **0610**, 028 (2006);
J.M. Campbell, R.K. Ellis, and C. Williams, Phys. Rev. **D81**, 074023 (2010).
59. R. Boughezal *et al.*, JHEP **1306**, 072 (2013).
60. C. F. Berger *et al.*, JHEP **1104**, 092 (2011);
A. Banfi, G.P. Salam, and G. Zanderighi, JHEP **1206**, 159 (2012);
T. Becher and M. Neubert, JHEP **1207**, 108 (2012);
A. Banfi *et al.*, Phys. Rev. Lett. **109**, 202001 (2012);
F. J. Tackmann, J. R. Walsh, and S. Zuberi, Phys. Rev. **D86**, 053011 (2012);
T. Becher, M. Neubert, and L. Rothen, JHEP **1310**, 125 (2013).

61. S. Dawson and R. P. Kauffman, Phys. Rev. Lett. **68**, 2273 (1992);
R. P. Kauffman, S. V. Desai, and D. Risal, Phys. Rev. **D55**, 4005 (1997) [E: **D58**, 119901 (1998)];
V. Del Duca *et al.*, Phys. Rev. Lett. **87**, 122001 (2001);
V. Del Duca *et al.*, Nucl. Phys. **B616**, 367 (2001).
62. R. K. Ellis, W. T. Giele, and G. Zanderighi, Phys. Rev. **D72**, 054018 (2005) [Erratum-ibid. **D74**, 079902 (2006)];
L. J. Dixon and Y. Sofianatos, JHEP **0908**, 058 (2009);
S. Badger *et al.*, JHEP **1001**, 036 (2010);
H. van Deurzen *et al.*, Phys. Lett. **B721**, 74 (2013);
G. Cullen *et al.*, Phys. Rev. Lett. **111**, 131801 (2013).
63. V. D. Barger, R. J. N. Phillips, and D. Zeppenfeld, Phys. Lett. **B346**, 106 (1995);
V. Del Duca *et al.*, JHEP **0610**, 016 (2006).
64. M. Duhrssen *et al.*, Phys. Rev. **D70**, 113009 (2004).
65. T. Han, G. Valencia, and S. Willenbrock, Phys. Rev. Lett. **69**, 3274 (1992);
T. Figy, C. Oleari, and D. Zeppenfeld, Phys. Rev. **D68**, 073005 (2003);
T. Figy and D. Zeppenfeld, Phys. Lett. **B591**, 297 (2004);
E.L. Berger and J. Campbell, Phys. Rev. **D70**, 073011 (2004);
M. Ciccolini, A. Denner, and S. Dittmaier, Phys. Rev. Lett. **99**, 161803 (2007);
Ciccolini, A. Denner, and S. Dittmaier, Phys. Rev. **D77**, 103002 (2008);
A. Denner, S. Dittmaier, and A. Muck, HAWK,
`http://omnibus.uni-freiburg.de/~sd565/programs/hawk/hawk.html`;
K. Arnold *et al.*, VBFNLO, Comp. Phys. Comm. **180**, 1661 (2009);
M. Spira, VV2H, `http://people.web.psi.ch/spira/vv2h` ;
N. Adam *et al.*, `arXiv:0803.1154 [hep-ph]` (2008);
T. Figy, S. Palmer, and G. Weiglein, JHEP **1202**, 105 (2012).
66. P. Nason and C. Oleari, JHEP **1002**, 037 (2010);
S. Frixione, P. Torrielli, and M. Zaro, Phys. Lett. **B726**, 273 (2013);
F. Maltoni, K. Mawatari, and M. Zaro, `arXiv:1311.1829 [hep-ph]` (2013).
67. P. Bolzoni *et al.*, Phys. Rev. Lett. **105**, 011801 (2010).
68. R. V. Harlander, J. Vollinga, and M. M. Weber, Phys. Rev. **D77**, 053010 (2008).
69. S L. Glashow, D.V. Nanopoulos, and A. Yildiz, Phys. Rev. **D18**, 1724 (1978);
T. Han and S. Willenbrock, Phys. Lett. **B273**, 167 (1991);
T. Han, G. Valencia, and S. Willenbrock, Phys. Rev. Lett. **69**, 3274 (1992);
H. Baer, B. Bailey, and J. F. Owens, Phys. Rev. **D47**, 2730 (1993);
J. Ohnemus and W. J. Stirling, Phys. Rev. **D47**, 2722 (1993).
70. A. Stange, W. Marciano, and S. Willenbrock, Phys. Rev. **D49**, 1354 (1994).
71. A. Stange, W. Marciano, and S. Willenbrock, Phys. Rev. **D50**, 4491 (1994).
72. M.L. Ciccolini, S. Dittmaier, and M. Kramer, Phys. Rev. **D68**, 073003 (2003);
A. Denner, S Dittmaier, and S. Kalweit, JHEP **1203**, 075 (2012).
73. R. Hamberg, W. L. van Neerven, and T. Matsuura, Nucl. Phys. **B359**, 343 (1991).

74. O. Brein, A. Djouadi, and R. Harlander, Phys. Lett. **B579**, 149 (2004); L. Altenkamp *et al.*, JHEP **1302**, 078 (2013).
75. O. Brein *et al.*, Eur. Phys. J. **C72**, 1868 (2012).
76. O. Brein, R. V. Harlander, and T. J. Zirke, Comp. Phys. Comm. **184**, 998 (2013).
77. A. Denner *et al.*, JHEP **1203**, 075 (2012).
78. G. Ferrera, M. Grazzini, and F. Tramontano, Phys. Rev. Lett. **107**, 152003 (2011).
79. R. Raitio and W. W. Wada, Phys. Rev. **D19**, 941 (1979); J. N. Ng and P. Zakarauskas, Nucl. Phys. **B247**, 339 (1984); J. F. Gunion, Phys. Lett. **B261**, 510 (1991); W. J. Marciano and F. E. Paige, Phys. Rev. Lett. **66**, 2433 (1991).
80. W. Beenakker *et al.*, Phys. Rev. Lett. **87**, 201805 (2001); L. Reina and S. Dawson, Phys. Rev. Lett. **87**, 201804 (2001); S. Dawson *et al.*, Phys. Rev. **D67**, 071503 (2003); W. Beenakker *et al.*, Nucl. Phys. **B653**, 151 (2003).
81. R. Frederix *et al.*, Phys. Lett. **B701**, 427 (2011); M. Garzelli *et al.*, Europhys. Lett. **96**, 11001 (2011).
82. K.A.Assamagan *et al.*, [Higgs Working Group Collab.], `arXiv:hep-ph/0406152`(2004)
83. R.V. Harlander and W.B. Kilgore, Phys. Rev. **D68**, 013001 (2003); J. M. Campbell *et al.*, Phys. Rev. **D67**, 095002 (2003); S. Dawson *et al.*, Phys. Rev. Lett. **94**, 031802 (2005); S. Dittmaier, M. Kramer, and M. Spira, Phys. Rev. **D70**, 074010 (2004); S. Dawson *et al.*, Phys. Rev. **D69**, 074027 (2004).
84. W.J. Stirling and D.J. Summers, Phys. Lett. **B283**, 411 (1992); F. Maltoni *et al.*, Phys. Rev. **D64**, 094023 (2001).
85. B.L. Ioffe and V.A. Khoze, Sov. J. Nucl. Phys. **9**, 50 (1978).
86. D.R.T. Jones and S. Petcov, Phys. Lett. **B84**, 440 (1979); R.N. Cahn and S. Dawson, Phys. Lett. **B136**, 196 (1984); G.L. Kane, W.W. Repko, and W.B. Rolnick, Phys. Lett. **B148**, 367 (1984); G. Altarelli, B. Mele, and F. Pitolli, Nucl. Phys. **B287**, 205 (1987); W. Kilian, M. Kramer, and P.M. Zerwas, Phys. Lett. **B373**, 135 (1996).
87. B.A. Kniehl, Z. Phys. **C55**, 605 (1992).
88. J. Fleischer and F. Jegerlehner, Nucl. Phys. **B216**, 469 (1983); A. Denner *et al.*, Z. Phys. **C56**, 261 (1992).
89. B.A. Kniehl, Int. J. Mod. Phys. **A17**, 1457 (2002).
90. K.J. Gaemers and G.J. Gounaris, Phys. Lett. **B77**, 379 (1978); A. Djouadi, J. Kalinowski, and P. M. Zerwas, Z. Phys. **C54**, 255 (1992); B.A. Kniehl, F. Madricardo, and M. Steinhauser, Phys. Rev. **D66**, 054016 (2002).
91. S. Dittmaier *et al.*, Phys. Lett. **B441**, 383 (1998); S. Dittmaier *et al.*, Phys. Lett. **B478**, 247 (2000); S. Dawson and L. Reina, Phys. Rev. **D59**, 054012 (1999).
92. S. Dawson *et al.*, `arXiv:1310.8361 [hep-ex]` (2013).
93. D. M. Asner *et al.*, `arXiv:1310.0763 [hep-ph]` (2013).
94. A. Denner *et al.*, Eur. Phys. J. **C71**, 1753 (2011).

95. A. Djouadi, J. Kalinowski, and M. Spira, Comp. Phys. Comm. **108**, 56 (1998);
A. Djouadi *et al.*, `arXiv:1003.1643 [hep-ph]` (2010).

96. S. Gorishnii *et al.*, Mod. Phys. Lett. **A5**, 2703 (1990);
S. Gorishnii *et al.*, Phys. Rev. **D43**, 1633 (1991);
A. L. Kataev and V. T. Kim, Mod. Phys. Lett. **A9**, 1309 (1994);
L. R. Surguladze, Phys. Lett. **B341**, 60 (1994);
S. Larin, T. van Ritbergen, and J. Vermaseren, Phys. Lett. **B362**, 134 (1995);
K. Chetyrkin and A. Kwiatkowski, Nucl. Phys. **B461**, 3 (1996);
K. Chetyrkin, Phys. Lett. **B390**, 309 (1997);
P. A. Baikov, K. G. Chetyrkin, and J. H. Kuhn, Phys. Rev. Lett. **96**, 012003 (2006).

97. J. Fleischer and F. Jegerlehner, Phys. Rev. **D23**, 2001 (1981);
D. Bardin, B. Vilensky, and P. Khristova, Sov. J. Nucl. Phys. **53**, 152 (1991);
A. Dabelstein and W. Hollik, Z. Phys. **C53**, 507 (1992);
B.A. Kniehl, Nucl. Phys. **B376**, 3 (1992);
A. Djouadi *et al.*, *Proceedings e^+e^- collisions at 500 GeV* (1991).

98. T. Inami, T. Kubota, and Y. Okada, Z. Phys. **C18**, 69 (1983);
K.G. Chetyrkin, B.A. Kniehl, and M. Steinhauser, Phys. Rev. Lett. **79**, 353 (1997);
P.A. Baikov and K.G. Chetyrkin, Phys. Rev. Lett. **97**, 061803 (2006).

99. H.-Q. Zheng and D.-D. Wu, Phys. Rev. **D42**, 3760 (1990);
A. Djouadi *et al.*, Phys. Lett. **B257**, 187 (1991);
S. Dawson and R. Kauffman, Phys. Rev. **D47**, 1264 (1993);
A. Djouadi, M. Spira, and P. Zerwas, Phys. Lett. **B311**, 255 (1993);
K. Melnikov and O. I. Yakovlev, Phys. Lett. **B312**, 179 (1993);
M. Inoue *et al.*, Mod. Phys. Lett. **A9**, 1189 (1994).

100. U. Aglietti *et al.*, Phys. Lett. **B595**, 432 (2004);
G. Degrassi and F. Maltoni, Phys. Lett. **B600**, 255 (2004);
S. Actis *et al.*, Phys. Lett. **B670**, 12 (2008);
U. Aglietti *et al.*, Phys. Lett. **B600**, 57 (2004);
G. Degrassi and F. Maltoni, Nucl. Phys. **B724**, 183 (2005);
U. Aglietti *et al.*, `arXiv:hep-ph/0612172` (2006).

101. A. Abbasabadi *et al.*, Phys. Rev. **D55**, 5647 (1997);
A. Abbasabadi and W. W. Repko, Phys. Rev. **D71**, 017304 (2005);
A. Abbasabadi and W. W. Repko, JHEP **0608**, 048 (2006);
D. A. Dicus and W. W. Repko, Phys. Rev. **D87**, 077301 (2013);
L. -B. Chen, C. -F. Qiao, and R. -L. Zhu, Phys. Lett. **B726**, 306 (2013);
Y. Sun, H. -R. Chang, and D. -N. Gao, JHEP **1305**, 061 (2013);
G. Passarino, `arXiv:1308.0422 [hep-ph]` (2013).

102. M. Spira, A. Djouadi, and P. M. Zerwas, Phys. Lett. **B276**, 350 (1992).

103. A. Bredenstein *et al.*, Phys. Rev. **D74**, 013004 (2006);
A. Bredenstein *et al.*, JHEP **0702**, 080 (2007);
A. Bredenstein *et al.*, Prophecy4f: A Monte Carlo generator for a proper description of the Higgs decay into 4 fermions, `http://omnibus.uni-freiburg.de/~sd565/programs/prophecy4f/prophecy4f.html`.

104. A. Ghinculov, Phys. Lett. **B337**, 137 (1994) [E: **B346**, 426 (1995)];
L. Durand, B. A. Kniehl, and K. Riesselmann, Phys. Rev. **D51**, 5007 (1995);
L. Durand, K. Riesselmann, and B. A. Kniehl, Phys. Rev. Lett. **72**, 2534 (1994) [E: **74**, 1699 (1995)].
105. E. Braaten and J.P. Leveille, Phys. Rev. **D22**, 715 (1980);
L. Durand, K. Riesselmann, and B.A. Kniehl, Phys. Rev. Lett. **72**, 2534 (1994);
E. Gross, G. Wolf, and B. A. Kniehl, Z. Phys. **C63**, 417 (1994); [E: *ibid.*, **C66**, 32 (1995)];
A. Ghinculov, Phys. Lett. **B337**, 137 (1994) and Nucl. Phys. **B455**, 21 (1995);
A. Djouadi, M. Spira, and P. M. Zerwas, Z. Phys. **C70**, 427 (1996);
A. Frink *et al.*, Phys. Rev. **D54**, 4548 (1996);
K.G. Chetyrkin and M. Steinhauser, Phys. Lett. **B408**, 320 (1997);
R. Harlander and M. Steinhauser, Phys. Rev. **D56**, 3980 (1997);
A.L. Kataev, Sov. Phys. JETP Lett. **66**, 327 (1997) [*Pis'ma Zh. Éksp. Teor. Fiz.* **66** (1997) 308];
S. Actis *et al.*, Nucl. Phys. **B811**, 182 (2009).
106. J. Erler and A. Freitas, *Electroweak Model and Constraints on New Physics*, review article in this volume.
107. ALEPH, DELPHI, L3, and OPAL Collaborations, The LEP Working Group for Higgs Boson Searches, Phys. Lett. **B565**, 61 (2003).
108. CDF and D0 Collaborations, Phys. Rev. D 88 ,052014 (2013).
109. L. Lyons, *The Annals of Applied Statistics,* Vol. 2, No. 3, 887 (2008).
110. L. Demortier, "P-Values and Nuisance Parameters", *Proceedings of PHYSTAT 2007,* CERN-2008-001, p. 23 (2008).
111. S. Dittmaier and M. Schumacher, Prog. Part. Nucl. Phys. **70**, 1 (2013).
112. ATLAS Collab., ATLAS-CONF-2011-112 (2011).
113. CMS Collab., CMS-HIG-11-011 (2011).
114. G. Aad *et al.*, [ATLAS Collab.], Phys. Rev. **D86**, 032003 (2012).
115. CMS Collab., CMS-HIG-12-008 (2012).
116. ATLAS Collab., ATLAS-CONF-2013-034 (2013).
117. CMS Collab., CMS-HIG-12-045 (2012).
118. M. Vesterinen and T. R. Wyatt, Nucl. Instrum. Methods **A602**, 88 (2012).
119. G. Aad *et al.*, [ATLAS Collab.], Phys. Lett. **B726**, 88 (2013).
120. CMS Collab., CMS-PAS-HIG-13-001 (2013).
121. CMS Collab., CMS-PAS-HIG-13-002 (2013).
122. S. Chatrchyan *et al.*, [CMS Collab.], JHEP **12**, 034 (2012).
123. S. Chatrchyan *et al.*, [CMS Collab.], arXiv:1312.5353 (2013), Submitted to Phys. Rev. (D).
124. CMS Collab., CMS-PAS-HIG-13-005 (2013).
125. CMS Collab., CMS-PAS-HIG-13-016 (2013).
126. ATLAS Collab., ATLAS-CONF-2013-030 (2013).
127. CMS Collab., CMS-PAS-HIG-13-003 (2013).
128. CMS Collab., CMS-PAS-HIG-13-022 (2013).
129. ATLAS Collab., ATLAS-CONF-2013-075 (2013).

130. CMS Collab., CMS-PAS-HIG-13-017 (2013).
131. CMS Collab., CMS-PAS-HIG-13-004 (2013) and CMS-PAS-HIG-12-053 (2013).
132. CMS Collab., arXiv:1401.5041 (2014), Submitted to JHEP.
133. ATLAS Collab., ATLAS-CONF-2013-108 (2013).
134. ATLAS Collab., ATLAS-CONF-2012-160 (2012).
135. CDF and D0 Collaborations, Phys. Rev. Lett. **109**, 071804 (2012).
136. J. M. Butterworth *et al.*, Phys. Rev. Lett. **100**, 242001 (2008).
137. CMS Collab., CMS-PAS-HIG-13-012 (2013).
138. ATLAS Collab., ATLAS-CONF-2013-079 (2013).
139. ATLAS Collab., ATLAS-CONF-2013-080 (2013).
140. CMS Collab., CMS-PAS-HIG-13-015 (2013).
141. ATLAS Collab., ATLAS-CONF-2012-135 (2012).
142. CMS Collab., CMS-PAS-HIG-12-025 (2012).
143. S. Chatrchyan *et al.*, [CMS Collab.], JHEP **1305**, 145 (2013).
144. CMS Collab., CMS-PAS-HIG-13-019 (2013).
145. CMS Collab., CMS-PAS-HIG-13-020 (2013).
146. CMS Collab., CMS-PAS-HIG-13-015 (2013).
147. S. Chatrchyan *et al.*, [CMS Collab.] Phys. Lett. **B726**, 587 (2013).
148. ATLAS Collab., ATLAS-CONF-2013-009 (2013).
149. ATLAS Collab., ATLAS-CONF-2013-010 (2013).
150. CMS Collab., CMS-PAS-HIG-13-007 (2013).
151. C. Delaunay *et al.*, `arXiv:1310.7029 [hep-ph]` (2013).
152. G. T. Bodwin *et al.*, Phys. Rev. **D88**, 053003 (2013).
153. A. Djouadi *et al.*, Eur. Phys. J. **C73**, 2455 (2013).
154. ATLAS Collab., `arXiv:1309.4017 [hep-ex]` (2013).
155. ATLAS Collab., ATLAS-CONF-2013-011 (2013).
156. CMS Collab., CMS-PAS-HIG-13-018 (2013).
157. CMS Collab., CMS-PAS-HIG-13-028 (2013).
158. CMS Collab., CMS-PAS-HIG-13-013 (2013).
159. M. J. Strassler and K. M. Zurek, Phys. Lett. **B651**, 374 (2007).
160. M. J. Strassler and K. M. Zurek, Phys. Lett. **B661**, 263 (2008).
161. T. Han *et al.*, JHEP **0807**, 008 (2008).
162. A. Falkowski *et al.*, JHEP **1005**, 077 (2010) and Phys. Rev. Lett. **105**, 241801 (2010).
163. G. Aad *et al.*, [ATLAS Collab.], New J. Phys. **15**, 043009 (2013).
164. G. Aad *et al.*, [ATLAS Collab.], Phys. Lett. **B721**, 32 (2013).
165. G. Aad *et al.*, [ATLAS Collab.], Phys. Rev. Lett. **108**, 251801 (2012).
166. D. Tucker-Smith and N. Weiner, Phys. Rev. **D64**, 043502 (2001).
167. S. Chatrchyan *et al.*, [CMS Collab.], Phys. Lett. **B726**, 564 (2013).
168. W. Buchmuller and D. Wyler, Nucl. Phys. **B268**, 621 (1986).
169. B. Grzadkowski *et al.*, JHEP **1010**, 085 (2010).
170. G. F. Giudice *et al.*, JHEP **0706**, 045 (2007).
171. R. Contino *et al.*, JHEP **1307**, 035 (2013).
172. J. Elias-Miro *et al.*, `arXiv:1308.1879 [hep-ph]`.

173. K. Hagiwara *et al.*, Phys. Lett. **B283**, 353 (1992);
K. Hagiwara *et al.*, Phys. Rev. **D48**, 2182 (1993);
K. Hagiwara, R. Szalapski, and D. Zeppenfeld, Phys. Lett. **B318**, 155 (1993).
174. A. Pomarol and F. Riva, arXiv:1308.2803 [hep-ph].
175. C. Degrande *et al.*, JHEP **1207**, 036 (2012) J. F. Kamenik, M. Papucci, and A. Weiler, Phys. Rev. **D85**, 071501 (2012).
176. P. Artoisenet *et al.*, JHEP **1311**, 043 (2013);
A. Alloul, B. Fuks, and V. Sanz, arXiv:1310.5150 [hep-ph].
177. CMS Collab., CMS-PAS-HIG-13-005 (2013).
178. ATLAS Collab., ATLAS-CONF-2013-079 (2013).
179. ATLAS Collab., ATLAS-CONF-2012-160 (2012).
180. S. Chatrchyan *et al.*, [CMS Collab.], JHEP **1305**, 145 (2013).
181. A. David *et al.*, [LHC Higgs Cross Section Working Group Collab.], arXiv:1209.0040 [hep-ph] (2012).
182. B. A. Kniehl and M. Spira, Z. Phys. **C69**, 77 (1995).
183. G. Isidori, A. V. Manohar, and M. Trott, arXiv:1305.0663 [hep-ph];
G. Isidori and M. Trott, arXiv:1307.4051 [hep-ph].
184. R. Godbole *et al.*, arXiv:1306.2573 [hep-ph].
185. M. Reece, New J. Phys. **15**, 043003 (2013).
186. S. Biswas, E. Gabrielli, and B. Mele, JHEP **1301**, 088 (2013);
S. Biswas *et al.*, JHEP **07**, 073 (2013).
187. M. Farina *et al.*, JHEP **1305**, 022 (2013).
188. ATLAS Collab., ATLAS-CONF-2013-072 (2013).
189. L. D. Landau, Dokl. Akad. Nauk Ser. Fiz. **60**, 207 (1948);
C. -N. Yang, Phys. Rev. **D77**, 242 (1950).
190. S. Bolognesi *et al.*, Phys. Rev. **D86**, 095031 (2012).
191. A. De Rujula *et al.*, Phys. Rev. **D82**, 013003 (2010).
192. Y. Gao *et al.*, Phys. Rev. **D81**, 075022 (2010).
193. A. L. Read, J. Phys. **G28**, 2693 (2002).
194. J. Ellis *et al.*, JHEP **1211**, 134 (2012).
195. D0 Collab., Note 6387-CONF (2013).
196. D0 Collab., Note 6406-CONF (2013).
197. G. Aad *et al.* [ATLAS Collab.], Phys. Lett. B **726**, 120 (2013).
198. CMS Collab., CMS-PAS-HIG-13-003 (2013).
199. CMS Collab., CMS-PAS-HIG-13-002 (2013).
200. H.E. Haber, *Supersymmetry*, in this volume.
201. L.E. Ibanez and G.G. Ross, Phys. Lett. **B110**, 215 (1982);
L.E. Ibanez, Phys. Lett. **B118**, 73 (1982);
J. Ellis, D.V. Nanopoulos, and K. Tamvakis, Phys. Lett. **B121**, 123 (1983);
L. Alvarez-Gaume, J. Polchinski, and M.B. Wise, Nucl. Phys. **B221**, 495 (1983).
202. L.E. Ibanez and G.G. Ross, Phys. Lett. **B105**, 439 (1981);
S. Dimopoulos, S. Raby, and F. Wilczek, Phys. Rev. **D24**, 1681 (1981);
M.B. Einhorn and D.R.T. Jones, Nucl. Phys. **B196**, 475 (1982);
W.J. Marciano and G. Senjanovic, Phys. Rev. **D25**, 3092 (1982).

203. J. Ellis, S. Kelley, and D.V. Nanopoulos, Phys. Lett. **B249**, 441 (1990);
P. Langacker and M. Luo, Phys. Rev. **D44**, 817 (1991);
U. Amaldi, W. de Boer, and H.Furstenau, Phys. Lett. **B260**, 447 (1991);
P. Langacker and N. Polonsky, Phys. Rev. **D52**, 3081 (1995);
S. Pokorski, Act. Phys. Pol. **B30**, 1759 (1999);
For a recent review, see R.N. Mohapatra, in *Proceedings of the ICTP Summer School in Particle Physics,* Trieste, Italy, 21 June–9 July, 1999, edited by G. Senjanovic and A.Yu. Smirnov. (World Scientific, Singapore, 2000) pp. 336–394.

204. N. Cabibbo, G.R. Farrar, and L. Maiani, Phys. Lett. **B105**, 155 (1981);
H. Goldberg, Phys. Rev. Lett. **50**, 1419 (1983);
J. R. Ellis *et al.*, Nucl. Phys. **B238**, 453 (1984);
G. Bertone, D. Hooper, and J. Silk, Phys. Reports **405**, 279 (2005).

205. A. G. Cohen, D. B. Kaplan, and A. E. Nelson, Ann. Rev. Nucl. and Part. Sci. **43**, 27 (1993);
M. Quiros, Helv. Phys. Acta **67**, 451 (1994);
V. A. Rubakov and M. E. Shaposhnikov, Usp. Fiz. Nauk **166**, 493 (1996) [Phys. Usp. **39**, 461 (1996)];
M. Quiros, `hep-ph/9901312`;
A. Riotto and M. Trodden, Ann. Rev. Nucl. and Part. Sci. **49**, 35 (1999).

206. Y. Okada, M. Yamaguchi, and T. Yanagida, Prog. Theor. Phys. **85**, 1 (1991);
J. Ellis, G. Ridolfi, and F. Zwirner, Phys. Lett. **B257**, 83 (1991).

207. H.E. Haber and R. Hempfling, Phys. Rev. Lett. **66**, 1815 (1991).

208. S.P. Li and M. Sher, Phys. Lett. **B140**, 339 (1984);
R. Barbieri and M. Frigeni, Phys. Lett. **B258**, 395 (1991);
M. Drees and M.M. Nojiri, Phys. Rev. **D45**, 2482 (1992);
J. A. Casas *et al.*, Nucl. Phys. **B436**, 3 (1995) [E: **B439** (1995) 466];
J. Ellis, G. Ridolfi, and F. Zwirner, Phys. Lett. **B262**, 477 (1991);
A. Brignole *et al.*, Phys. Lett. **B271**, 123 (1991) [E: **B273** (1991) 550].

209. R.-J. Zhang, Phys. Lett. **B447**, 89 (1999);
J.R. Espinosa and R.-J. Zhang, JHEP **0003**, 026 (2000);
J.R. Espinosa and R.-J. Zhang, Nucl. Phys. **B586**, 3 (2000);
A. Dedes, G. Degrassi, and P. Slavich, Nucl. Phys. **B672**, 144 (2003).

210. J.F. Gunion and A. Turski, Phys. Rev. **D39**, 2701 (1989), Phys. Rev. **D40**, 2333 (1989);
M.S. Berger, Phys. Rev. **D41**, 225 (1990);
A. Brignole, Phys. Lett. **B277**, 313 (1992), Phys. Lett. **B281**, 284 (1992);
M.A. Diaz and H.E. Haber, Phys. Rev. **D45**, 4246 (1992);
P.H. Chankowski, S. Pokorski, and J. Rosiek, Phys. Lett. **B274**, 191 (1992), Nucl. Phys. **B423**, 437 (1994);
A. Yamada, Phys. Lett. **B263**, 233 (1991), Z. Phys. **C61**, 247 (1994);
A. Dabelstein, Z. Phys. **C67**, 496 (1995);
R. Hempfling and A.H. Hoang, Phys. Lett. **B331**, 99 (1994);
S. Heinemeyer, W. Hollik, and G. Weiglein, Phys. Rev. **D58**, 091701 (1998), Phys. Lett. **B440**, 296 (1998), Eur. Phys. J. **C9**, 343 (1999).

211. D. M. Pierce *et al.*, Nucl. Phys. **B491**, 3 (1997).
212. R. Barbieri, M. Frigeni, and F. Caravaglios, Phys. Lett. **B258**, 167 (1991);
Y. Okada, M. Yamaguchi, and T. Yanagida, Phys. Lett. **B262**, 45 (1991);
J.R. Espinosa and M. Quiros, Phys. Lett. **B266**, 389 (1991);
D.M. Pierce, A. Papadopoulos, and S. Johnson, Phys. Rev. Lett. **68**, 3678 (1992);
R. Hempfling, in *Phenomenological Aspects of Supersymmetry*, edited by W. Hollik, R. Rückl and J. Wess (Springer-Verlag, Berlin, 1992) pp. 260–279;
J. Kodaira, Y. Yasui, and K. Sasaki, Phys. Rev. **D50**, 7035 (1994);
H.E. Haber and R. Hempfling, Phys. Rev. **D48**, 4280 (1993);
M. Carena *et al.*, Phys. Lett. **B355**, 209 (1995).
213. H.E. Haber, R. Hempfling, and A.H. Hoang,Z. Phys. **C75**, 539 (1997).
214. M. Carena *et al.*, Nucl. Phys. **B580**, 29 (2000).
215. M. Carena, M. Quiros, and C.E.M. Wagner, Nucl. Phys. **B461**, 407 (1996).
216. S. Martin, Phys. Rev. **D67**, 095012 (2003);
S. Martin Phys. Rev. **D71**, 016012 (2005);
S. Martin Phys. Rev. **D75**, 055005 (2007).
217. M. Carena, S. Mrenna, and C.E.M. Wagner, Phys. Rev. **D60**, 075010 (1999);
ibid., Phys. Rev. **D62**, 055008 (2000).
218. S. Heinemeyer, W. Hollik, and G. Weiglein, Phys. Lett. **B455**, 179 (1999).
219. J.R. Espinosa and I. Navarro, Nucl. Phys. **B615**, 82 (2001);
G. Degrassi, P. Slavich, and F. Zwirner, Nucl. Phys. **B611**, 403 (2001);
A. Brignole *et al.*, Nucl. Phys. **B631**, 195 (2002);
A. Brignole *et al.*, Nucl. Phys. **B643**, 79 (2002);
S. Heinemeyer *et al.*,.
220. G. Degrassi *et al.*, Eur. Phys. J. **C28**, 133 (2003).
221. U. Ellwanger and C. Hugonie, Mod. Phys. Lett. **A22**, 1581 (2007).
222. J.R. Espinosa and M. Quiros, Phys. Rev. Lett. **81**, 516 (1998).
223. P. Batra *et al.*, JHEP **0402**, 043 (2004).
224. M. Dine, N. Seiberg, and S. Thomas, Phys. Rev. **D76**, 095004 (2007) and references therein.
225. K. Blum, C. Delaunay, and Y. Hochberg, Phys. Rev. **D80**, 075004 (2009).
226. M. Carena *et al.*, Phys. Rev. **D81**, 015001 (2010);
W. Altmannshofer *et al.*, Phys. Rev. **D84**, 095027 (2011).
227. I. Antoniadis *et al.*, Nucl. Phys. **B831**, 133 (2010).
228. T. J. LeCompte and S. P. Martin, Phys. Rev. **D84**, 015004 (2011) and Phys. Rev. **D85**, 035023 (2012).
229. J. Fan, M. Reece, and J. T. Ruderman, JHEP **1111**, 012 (2011) and JHEP **1207**, 196 (2012).
230. R. Barbier *et al.*, `hep-ph/9810232` (1998); R. Barbier *et al.*, Phys. Reports **420**, 1 (2005).
231. C. Smith, `arXiv:0809.3152 [hep-ph]` (2008);
C. Csaki, Y. Grossman, and B. Heidenreich, Phys. Rev. **D85**, 095009 (2012).
232. S. Chatrchyan *et al.*, [CMS Collab.], `arXiv:1301.2175 [hep-ex]` 2013.

233. M. Papucci, J. T. Ruderman, and A. Weiler, JHEP **1209**, 035 (2012);
R. Essig *et al.*, JHEP **1201**, 074 (2012);
Y. Kats *et al.*, JHEP **1202**, 115 (2012);
C. Brust *et al.*, JHEP **1203**, 103 (2012).
234. J. Mrazek, A. Pomarol, R. Rattazzi, M. Redi, J. Serra and A. Wulzer, Nucl. Phys. **B853**, 1 (2011).
235. H. Georgi and D. B. Kaplan, Phys. Lett. **B145**, 216 (1984).
236. D. B. Kaplan, Nucl. Phys. **B365**, 259 (1991).
237. E. Savioni, PhD thesis, 2013
`http://www.infn.it/thesis/thesis_dettaglio.php?tid=8079`.
238. G. Panico *et al.*, JHEP **1303**, 051 (2013).
239. S. Dimopoulos and H. Georgi, Nucl. Phys. **B193**, 150 (1981);
K. Harada and N. Sakai, Prog. Theor. Phys. **67**, 1877 (1982);
K. Inoue *et al.*, Prog. Theor. Phys. **67**, 1889 (1982);
L. Girardello and M.T. Grisaru, Nucl. Phys. **B194**, 65 (1982);
L.J. Hall and L. Randall, Phys. Rev. Lett. **65**, 2939 (1990);
I. Jack and D.R.T. Jones, Phys. Lett. **B457**, 101 (1999).
240. S. Dimopoulos and D.W. Sutter, Nucl. Phys. **B452**, 496 (1995);
D.W. Sutter, Stanford Ph. D. thesis, `hep-ph/9704390` (1997);
H.E. Haber, Nucl. Phys. (Proc. Supp.) **B62A-C**, 469 (1998).
241. A. Djouadi, Phys. Reports **459**, 1 (2008).
242. H.E. Haber and Y. Nir, Nucl. Phys. **B335**, 363 (1990);
A. Dabelstein, Nucl. Phys. **B456**, 25 (1995);
S. Heinemeyer, W. Hollik, and G. Weiglein, Eur. Phys. J. **C16**, 139 (2000);
A. Dobado, M. J. Herrero, and S. Penaranda, Eur. Phys. J. **C17**, 487 (2000);
J.F. Gunion and H.E. Haber, Phys. Rev. **D67**, 075019 (2003).
243. J. F. Gunion and H. E. Haber, Phys. Rev. **D67**, 075019 (2003);
G. C. Branco *et al.*, Phys. Reports **516**, 1 (2012).
244. N. Craig, J. Galloway, and S. Thomas, `arXiv:1305.2424 [hep-ph]` (2013);
D. Asner *et al.*, `arXiv:1310.0763 [hep-ph]` (2013).
245. M. Carena *et al.*, `arXiv:1310.2248 [hep-ph]` (2013).
246. S. P. Martin, Phys. Rev. **D75**, 055005 (2007);
P. Kant *et al.*, JHEP **1008**, 104 (2010);
J. L. Feng *et al.*, Phys. Rev. Lett. **111**, 131802 (2013).
247. M. Carena *et al.*, JHEP **1203**, 014 (2012);
M. Carena *et al.*, JHEP **1207**, 175 (2012).
248. M. Carena *et al.*, Eur. Phys. J. **C26**, 601 (2003);
M. Carena *et al.*, Eur. Phys. J. **C73**, 2552 (2013).
249. M. Carena *et al.*, Eur. Phys. J. **C45**, 797 (2006).
250. S. Heinemeyer *et al.*, JHEP **0808**, 087 (2008).
251. S. Y. Choi, M. Drees, and J. S. Lee, Phys. Lett. **B481**, 57 (2000);
M. Carena *et al.*, Nucl. Phys. **B625**, 345 (2002).
252. A. Pilaftsis and C.E.M. Wagner, Nucl. Phys. **B553**, 3 (1999).

253. A. Arbey *et al.*, Phys. Lett. **B708**, 162 (2012);
A. Arbey *et al.*, JHEP **1209**, 107 (2012).
254. L.J. Hall, D. Pinner, and J.T. Ruderman, JHEP **1204**, 131 (2012).
255. H. Baer, V. Barger, and A. Mustafayev, Phys. Rev. **D85**, 075010 (2012).
256. P. Draper *et al.*, Phys. Rev. **D85**, 095007 (2012).
257. S. Heinemeyer, O. Stal, and G. Weiglein, Phys. Lett. **B710**, 201 (2012).
258. M. Kadastik *et al.*, JHEP **1205**, 061 (2012).
259. ATLAS Collab.,
`https://twiki.cern.ch/twiki/bin/view/AtlasPublic/Publications`;
CMS Collab., `https://twiki.cern.ch/twiki/bin/view/AtlasPublic/CombinedSummaryPlots#Susy DirectStopSummary`.
260. T.D. Lee, Phys. Rev. **D8**, 1226 (1973);
P. Fayet, Nucl. Phys. **B78**, 14 (1974);
R.D. Peccei and H.R. Quinn, Phys. Rev. Lett. **38**, 1440 (1977);
P. Fayet and S. Ferrara, Phys. Reports **32**, 249 (1977);
L.J. Hall and M.B. Wise, Nucl. Phys. **B187**, 397 (1981);
V.D. Barger, J.L. Hewett, and R.J.N. Phillips, Phys. Rev. **D41**, 3421 (1990).
261. A. Dabelstein, Nucl. Phys. **B456**, 25 (1995);
F. Borzumati *et al.*, Nucl. Phys. **B555**, 53 (1999);
H. Eberl *et al.*, Phys. Rev. **D62**, 055006 (2000).
262. J.A. Coarasa, R.A. Jimenez, and J. Sola, Phys. Lett. **B389**, 312 (1996);
R.A. Jimenez and J. Sola, Phys. Lett. **B389**, 53 (1996);
A. Bartl *et al.*, Phys. Lett. **B378**, 167 (1996).
263. S. Heinemeyer, W. Hollik, and G. Weiglein, Eur. Phys. J. **C16**, 139 (2000).
264. H. E. Haber *et al.*, Phys. Rev. **D63**, 055004 (2001).
265. L. Hall, R. Rattazzi, and U. Sarid, Phys. Rev. **D50**, 7048 (1994);
R. Hempfling, Phys. Rev. **D49**, 6168 (1994).
266. M. S. Carena *et al.*, Nucl. Phys. **B426**, 269 (1994).
267. J. Guasch, P. Hafliger, and M. Spira, Phys. Rev. **D68**, 115001 (2003);
D. Noth and M. Spira, Phys. Rev. Lett. **101**, 181801 (2008);
D. Noth and M. Spira, JHEP **1106**, 084 (2011);
L. Mihaila and C. Reisser, JHEP **1008**, 021 (2010).
268. M. S. Carena *et al.*, Phys. Lett. **B499**, 141 (2001).
269. A. Djouadi, J. Kalinowski, and P.M. Zerwas, Z. Phys. **C57**, 569 (1993);
H. Baer *et al.*, Phys. Rev. **D47**, 1062 (1993);
A. Djouadi *et al.*, Phys. Lett. **B376**, 220 (1996);
A. Djouadi *et al.*, Z. Phys. **C74**, 93 (1997);
S. Heinemeyer and W. Hollik, Nucl. Phys. **B474**, 32 (1996).
270. J.F. Gunion, Phys. Rev. Lett. **72**, 199 (1994);
D. Choudhury and D.P. Roy, Phys. Lett. **B322**, 368 (1994);
O.J. Eboli and D. Zeppenfeld, Phys. Lett. **B495**, 147 (2000);
B.P. Kersevan, M. Malawski, and E. Richter-Was, Eur. Phys. J. **C29**, 541 (2003).

271. E. L. Berger *et al.*, Phys. Rev. **D66**, 095001 (2002).
272. A. Brignole *et al.*, Nucl. Phys. **B643**, 79 (2002);
R. Dermisek and I. Low, Phys. Rev. **D77**, 035012 (2008).
273. A. Djouadi, Phys. Lett. **B435**, 101 (1998).
274. M. R. Buckley and D. Hooper, Phys. Rev. **D86**, 075008 (2012);
M. W. Cahill-Rowley *et al.*, Phys. Rev. **D86**, 075015 (2012);
A. Fowlie *et al.*, Phys. Rev. **D86**, 075010 (2012);
F. Brummer, S. Kraml, and S. Kulkarni, JHEP **1208**, 089 (2012);
N. D. Christensen, T. Han, and S. Su, Phys. Rev. **D85**, 115018 (2012);
H. Baer, V. Barger, and A. Mustafayev, JHEP **1205**, 091 (2012);
L. Aparicio, D. G. Cerdeno, and L. E. Ibanez, JHEP **1204**, 126 (2012);
J. Cao *et al.*, Phys. Lett. **B710**, 665 (2012);
M. Kadastik *et al.*, JHEP **1205**, 061 (2012);
H. Baer, V. Barger, and A. Mustafayev, Phys. Rev. **D85**, 075010 (2012).
275. J. -J. Cao *et al.*, JHEP **1203**, 086 (2012);
R. Benbrik *et al.*, Eur. Phys. J. **C72**, 2171 (2012);
Z. Kang, J. Li, and T. Li, JHEP **1211**, 024 (2012);
S. F. King, M. Muhlleitner, and R. Nevzorov, Nucl. Phys. **B860**, 207 (2012);
J. F. Gunion, Y. Jiang, and S. Kraml, Phys. Lett. **B710**, 454 (2012);
U. Ellwanger, JHEP **1203**, 044 (2012).
276. T. Kitahara, JHEP **1211**, 021 (2012);
M. Carena *et al.*, JHEP **1302**, 114 (2013).
277. B. Batell, S. Jung, and C. E. M. Wagner, `arXiv:1309.2297 [hep-ph]` (2013).
278. ATLAS Collab.,
`https://twiki.cern.ch/twiki/bin/view/AtlasPublic/Publications`;
CMS Collab., `https://twiki.cern.ch/twiki/bin/view/CMSPublic/Snowmass2013SUSY`.
279. M. Carena *et al.*, JHEP **1308**, 087 (2013).
280. J. F. Gunion *et al.*, Phys. Rev. **D38**, 3444 (1988).
281. S. Heinemeyer *et al.*, Eur. Phys. J. **C19**, 535 (2001).
282. S.H. Zhu, `hep-ph/9901221` (1999);
S. Kanemura, Eur. Phys. J. **C17**, 473 (2000);
A. Arhrib *et al.*, Nucl. Phys. **B581**, 34 (2000).
283. H.E. Logan and S. Su, Phys. Rev. **D66**, 035001 (2002).
284. A. Gutierrez-Rodriguez and O.A. Sampayo, Phys. Rev. **D62**, 055004 (2000);
A. Gutierrez-Rodriguez, M.A. Hernandez-Ruiz, and O.A. Sampayo, J. Phys. Soc. Jap. **70**, 2300 (2001);
S. Moretti, EPJdirect **C15**, 1 (2002).
285. S. Kanemura, S. Moretti, and K. Odagiri, JHEP **0102**, 011 (2001).
286. R. Raitio and W. W. Wada, Phys. Rev. **D19**, 941 (1979);
J. N. Ng and P. Zakarauskas, Phys. Rev. **D29**, 876 (1984);
Z. Kunszt, Nucl. Phys. **B247**, 339 (1984);
J. F. Gunion and H.E. Haber, Nucl. Phys. **B278**, 449 (1986) [E: **B402**, 567

(1993)];
D. A. Dicus and S. Willenbrock, Phys. Rev. **D39**, 751 (1989);
J. F. Gunion, Phys. Lett. **B261**, 510 (1991);
W. J. Marciano and F. E. Paige, Phys. Rev. Lett. **66**, 2433 (1991);
M. Spira *et al.*, Phys. Lett. **B318**, 347 (1993);
S. Dawson, A. Djouadi, and M. Spira, Phys. Rev. Lett. **77**, 16 (1996);
D. Dicus *et al.*, Phys. Rev. **D59**, 094016 (1999);
C. Balazs, H. -J. He, and C. P. Yuan, Phys. Rev. **D60**, 114001 (1999);
A. Djouadi and M. Spira, Phys. Rev. **D62**, 014004 (2000);
R.V. Harlander and W.B. Kilgore, JHEP **0210**, 017 (2002) and Phys. Rev. **D68**, 013001 (2003);
C. Anastasiou and K. Melnikov, Phys. Rev. **D67**, 037501 (2003);
J. Guasch, P. Hafliger, and M. Spira, Phys. Rev. **D68**, 115001 (2003);
S. Dittmaier, M. Kramer, and M. Spira, Phys. Rev. **D70**, 074010 (2004);
S. Dawson *et al.*, Phys. Rev. **D69**, 074027 (2004);
R.V. Harlander and M. Steinhauser, JHEP **0409**, 066 (2004);
S. Dawson *et al.*, Mod. Phys. Lett. **A21**, 89 (2006);
T. Hahn *et al.*, `arXiv:hep-ph/0607308` (2006);
M. Muhlleitner and M. Spira, Nucl. Phys. **B790**, 1 (2008).

287. D. Dicus *et al.*, Phys. Rev. **D59**, 094016 (1999).
288. C. Balazs, H.-J. He, and C.P. Yuan, Phys. Rev. **D60**, 114001 (1999).
289. E. Boos *et al.*, Phys. Rev. **D66**, 055004 (2002);
E. Boos, A. Djouadi, and A. Nikitenko, Phys. Lett. **B578**, 384 (2004);
E. Boos *et al.*, Phys. Lett. **B622**, 311 (2005);
M. Carena *et al.*, JHEP **1207**, 091 (2012).
290. A. A. Barrientos Bendezu and B. A. Kniehl, Phys. Rev. **D64**, 035006 (2001).
291. J. A. Coarasa Perez *et al.*, Eur. Phys. J. **C2**, 373 (1998);
J. A. Coarasa Perez *et al.*, Phys. Lett. **B425**, 329 (1998).
292. C.S. Li and T.C. Yuan, Phys. Rev. **D42**, 3088 (1990) [E: **D47**, 2156 (1993)];
A. Czarnecki and S. Davidson, Phys. Rev. **D47**, 3063 (1993);
C.S. Li, Y.-S. Wei, and J.-M. Yang, Phys. Lett. **B285**, 137 (1992).
293. J. Guasch, R.A. Jimenez, and J. Sola, Phys. Lett. **B360**, 47 (1995).
294. M. S. Carena *et al.*,Nucl. Phys. **B577**, 88 (2000).
295. A.A. Barrientos Bendezu and B.A. Kniehl, Phys. Rev. **D59**, 015009 (1999), Phys. Rev. **D61**, 015009 (2000) and Phys. Rev. **D63**, 015009 (2001).
296. A.A. Barrientos Bendezu and B.A. Kniehl, Nucl. Phys. **B568**, 305 (2000).
297. A. Krause *et al.*, Nucl. Phys. **B519**, 85 (1998);
O. Brein and W. Hollik, Eur. Phys. J. **C13**, 175 (2000).
298. R.M. Barnett, H.E. Haber, and D.E. Soper, Nucl. Phys. **B306**, 697 (1988);
F. Olness and W.-K. Tung, Nucl. Phys. **B308**, 813 (1988);
F. Borzumati, J.-L. Kneur, and N. Polonsky, Phys. Rev. **D60**, 115011 (1999);
L. G. Jin *et al.*, Eur. Phys. J. **C14**, 91 (2000) and Phys. Rev. **D62**, 053008 (2000);
S. -h. Zhu, Phys. Rev. **D67**, 075006 (2003);
A. Belyaev *et al.*, JHEP **0206**, 059 (2002);

G. -p. Gao *et al.*, Phys. Rev. **D66**, 015007 (2002);
M. Guchait and S. Moretti, JHEP **0201**, 001 (2002);
H. Baer *et al.*, Phys. Rev. **D65**, 031701 (2002);
G. Gao *et al.*, Phys. Rev. **D66**, 015007 (2002);
T. Plehn, Phys. Rev. **D67**, 014018 (2003);
S.-H. Zhu, Phys. Rev. **D67**, 075006 (2005);
E. L. Berger *et al.*, Phys. Rev. **D71**, 115012 (2005);
S. Dittmaier *et al.*, Phys. Rev. **D83**, 055005 (2011).
299. K. Blum, R. T. D'Agnolo, and J. Fan, JHEP **1301**, 057 (2013);
A. Azatov *et al.*, Phys. Rev. **D86**, 075033 (2012);
J. R. Espinosa *et al.*, JHEP **1212**, 077 (2012);
R. S. Gupta, M. Montull, and F. Riva, JHEP **1304**, 132 (2013);
R. T. D'Agnolo, PhD thesis, Scuola Normale Superiore, Pisa, 2013.
300. C. F. Berger *et al.*, JHEP **0902**, 023 (2009);
S. S. AbdusSalam *et al.*, Phys. Rev. **D81**, 095012 (2010);
P. Bechtle *et al.*, Eur. Phys. J. **C73**, 2354 (2013);
P. Bechtle *et al.*, `arXiv:1305.1933 [hep-ph]` (2013).
301. G. D'Ambrosio *et al.*, Nucl. Phys. **B645**, 155 (2002);
R. S. Chivukula and H. Georgi, Phys. Lett. **B188**, 99 (1987);
L. J. Hall and L. Randall, Phys. Rev. Lett. **65**, 2939 (1990);
A. J. Buras *et al.*, Phys. Lett. **B500**, 161 (2001).
302. A Arbey, M Battaglia, and F. Mahmoudi, Phys. Rev. **D88**, 015007 (2013).
303. S. Bertolini *et al.*, Nucl. Phys. **B353**, 591 (1991);
T. Goto, Y. Okada, and Y. Shimizu, Phys. Rev. **D58**, 094006 (1998);
G. Isidori and P. Paradisi, Phys. Lett. **B639**, 499 (2006);
W. Altmannshofer, A. J. Buras, and D. Guadagnoli, JHEP **0711**, 065 (2007);
F. Domingo and U. Ellwanger, JHEP **0712**, 090 (2007);
W. Altmannshofer and D. M. Straub, JHEP **1009**, 078 (2010).
304. M. S. Carena *et al.*, Phys. Rev. **D74**, 015009 (2006).
305. J. R. Ellis *et al.*, JHEP **0708**, 083 (2007).
306. E. Lunghi, W. Porod, and O. Vives, Phys. Rev. **D74**, 075003 (2006).
307. A. Arbey *et al.*, JHEP **1209**, 107 (2012).
308. U. Haisch and F. Mahmoudi JHEP **1301**, 061 (2013);
J. Cao *et al.*, JHEP **1210**, 079 (2012).
309. W. Altmannshofer *et al.*, JHEP **1301**, 160 (2013).
310. G. Buchalla, A.J. Buras, and M.E. Lautenbacher, Rev. Mod. Phys. **68**, 1125 (1996).
311. A. Dedes and A. Pilaftsis, Phys. Rev. **D67**, 015012 (2003).
312. A. J. Buras *et al.*, Phys. Lett. **B546**, 96 (2002).
313. A. J. Buras *et al.*, Nucl. Phys. **B659**, 2 (2003).
314. S. R. Choudhury and N. Gaur, Phys. Lett. B **451**, 86 (1999);
G. Isidori and A. Retico, JHEP **0111**, 001 (2001);
K.S. Babu and C.F. Kolda, Phys. Rev. Lett. **84**, 228 (2000).
315. R. Aaij *et al.*, [LHCb Collab.], Phys. Rev. Lett. **111**, 101805 (2013);
CMS Collab., Phys. Rev. Lett. **111**, 101804 (2013).

316. A. G. Akeroyd, F. Mahmoudi, and D. Martinez Santos, JHEP **1112**, 088 (2011);
A. Arbey, M. Battaglia, and F. Mahmoudi, Eur. Phys. J. **C72**, 1906 (2012);
A. Arbey *et al.*, Phys. Lett. **B720**, 153 (2013).
317. M. Misiak *et al.*, Phys. Rev. Lett. **98**, 022002 (2007) and references therein.
318. T. Becher and M. Neubert, Phys. Rev. Lett. **98**, 022003 (2007);
M. Benzke *et al.*, JHEP **1008**, 099 (2010).
319. Heavy Flavor Averaging Group (HFAG), `arXiv:1207.1158 [hep-ex]` (2012).
320. T. Hermann, M. Misiak, and M. Steinhauser, JHEP **1211**, 036 (2012).
321. I. Adachi *et al.*, [Belle Collab.], Phys. Rev. Lett. **110**, 131801 (2013);
K. Hara *et al.*, [Belle Collab.], Phys. Rev. **D82**, 071101 (2010).
322. J. P. Lees *et al.*, [BaBar Collab.], Phys. Rev. **D88**, 031102 (2013);
B. Aubert *et al.*, [BaBar Collab.], Phys. Rev. **D81**, 051101 (2010).
323. M. Bona *et al.*, [UTfit Collab.], Phys. Lett. B **687**, 61 (2010).
324. G. Isidori and P. Paradisi, Phys. Lett. **B639**, 499 (2006).
325. M. Tanaka, Z. Phys. **C67**, 321 (1995);
U. Nierste, S. Trine, and S. Westhoff, Phys. Rev. **D78**, 015006 (2008);
J. F. Kamenik and F. Mescia, Phys. Rev. **D78**, 014003 (2008);
S. Fajfer, J. F. Kamenik, and I. Nisandzic, Phys. Rev. **D85**, 094025 (2012);
D. Becirevic, N. Kosnik, and A. Tayduganov, Phys. Lett. **B716**, 208 (2012);
J. A. Bailey *et al.*, Phys. Rev. Lett. **109**, 071802 (2012).
326. J. P. Lees *et al.*, [BaBar Collab.], Phys. Rev. Lett. **109**, 101802 (2012).
327. A. Bozek *et al.*, [Belle Collab.], Phys. Rev. **D82**, 072005 (2010).
328. M. Carena, A. Menon, and C.E.M. Wagner, Phys. Rev. **D79**, 075025 (2009).
329. J. R. Ellis *et al.*, Phys. Lett. **B653**, 292 (2007).
330. A. Djouadi and Y. Mambrini, JHEP **0612**, 001 (2006).
331. M. Carena, D. Hooper, and A. Vallinotto, Phys. Rev. **D75**, 055010 (2007).
332. J. R. Ellis, K.A. Olive, and Y. Santoso, Phys. Rev. **D71**, 095007 (2005).
333. C. Boehm *et al.*, JHEP **1306**, 113 (2013).
334. T. Han, Z. Liu, and A. Natarajan, JHEP **1311**, 008 (2013).
335. L. J. Hall, J. Lykken, and S. Weinberg, Phys. Rev. **D27**, 2359 (1983);
J. E. Kim and H. P. Nilles, Phys. Lett. **B138**, 150 (1984);
G. F. Giudice and A. Masiero, Phys. Lett. **B206**, 480 (1988);
E. J. Chun, J. E. Kim, and H. P. Nilles, Nucl. Phys. **B370**, 105 (1992);
I. Antoniadis *et al.*, Nucl. Phys. **B432**, 187 (1994).
336. R. D. Peccei and H. R. Quinn, Phys. Rev. Lett. **38**, 1440 (1977).
337. P. Fayet, Phys. Lett. **B90**, 104 (1975);
H.-P. Nilles, M. Srednicki, and D. Wyler, Phys. Lett. **B120**, 346 (1983);
J.-M. Frere, D.R.T. Jones, and S. Raby, Nucl. Phys. **B222**, 11 (1983);
J.-P. Derendinger and C.A. Savoy, Nucl. Phys. **B237**, 307 (1984);
B.R. Greene and P.J. Miron, Phys. Lett. **B168**, 226 (1986);
J. R. Ellis *et al.*, Phys. Lett. **B176**, 403 (1986);
L. Durand and J.L. Lopez, Phys. Lett. **B217**, 463 (1989);
M. Drees, Int. J. Mod. Phys. **A4**, 3635 (1989);
U. Ellwanger, Phys. Lett. **B303**, 271 (1993);

U. Ellwanger, M. Rausch de Taubenberg, and C.A. Savoy, Phys. Lett. **B315**, 331 (1993), Z. Phys. **C67**, 665 (1995) and Phys. Lett. **B492**, 21 (1997);
P.N. Pandita, Phys. Lett. **B318**, 338 (1993) and Z. Phys. **C59**, 575 (1993);
T. Elliott, S.F. King, and P.L.White, Phys. Lett. **B305**, 71 (1993), Phys. Lett. **B314**, 56 (1993), Phys. Rev. **D49**, 2435 (1994) and Phys. Lett. **B351**, 213 (1995);
K.S. Babu and S.M. Barr, Phys. Rev. **D49**, R2156 (1994);
S.F. King and P.L. White, Phys. Rev. **D52**, 4183 (1995);
N. Haba, M. Matsuda, and M. Tanimoto, Phys. Rev. **D54**, 6928 (1996);
F. Franke and H. Fraas, Int. J. Mod. Phys. **A12**, 479 (1997);
S.W. Ham, S.K. Oh, and H.S. Song, Phys. Rev. **D61**, 055010 (2000);
D.A. Demir, E. Ma, and U. Sarkar, J. Phys. **G26**, L117 (2000);
R. B. Nevzorov and M. A. Trusov, Phys. Atom. Nucl. **64**, 1299 (2001);
U. Ellwanger and C. Hugonie, Eur. Phys. J. **C25**, 297 (2002);
U. Ellwanger *et al.*, `arXiv:hep-ph/0305109` (2003);
D.J. Miller and S. Moretti, `arXiv:hep-ph/0403137` (2004).

338. Y. B. Zeldovich, I. Y. Kobzarev, and L. B. Okun, Zh. Eksp. Teor. Fiz. **67**, 3 (1974);
A. Vilenkin, Phys. Reports **121**, 263 (1985).

339. H. P. Nilles, M. Srednicki, and D. Wyler, Phys. Lett. **B124**, 337 (1983);
A. B. Lahanas, Phys. Lett. **B124**, 341 (1983);
U. Ellwanger, Phys. Lett. **B133**, 187 (1983);
J. Bagger and E. Poppitz, Phys. Rev. Lett. **71**, 2380 (1993);
J. Bagger, E. Poppitz, and L. Randall, Nucl. Phys. **B426**, 3 (1994);
V. Jain, Phys. Lett. **B351**, 481 (1995);
S. A. Abel, Nucl. Phys. **B480**, 55 (1996);
C. F. Kolda, S. Pokorski, and N. Polonsky, Phys. Rev. Lett. **80**, 5263 (1998).

340. C. Panagiotakopoulos and K. Tamvakis, Phys. Lett. **B469**, 145 (1999);
A. Dedes *et al.*, Phys. Rev. **D63**, 055009 (2001);
A. Menon, D. Morrissey, and C.E.M. Wagner, Phys. Rev. **D70**, 035005, (2004).

341. M. Cvetic *et al.*, Phys. Rev. **D56**, 2861 (1997) [E: **D58**, 119905 (1998)];
P. Langacker and J. Wang, Phys. Rev. **D58**, 115010 (1998) and references therein.

342. J. Erler, P. Langacker, and T. j. Li, Phys. Rev. **D66**, 015002 (2002);
T. Han, P. Langacker and B. McElrath, Phys. Rev. **D70**, 115006 (2004);
V. Barger *et al.*, Phys. Rev. **D73**, 115010 (2006).

343. V. Barger *et al.*, Phys. Rev. **D73**, 115010 (2006);
V. Barger, P. Langacker, and G. Shaughnessy, Phys. Rev. **D75**, 055013 (2007).

344. E. Accomando, *et al.*, hep-ph/0608079 (2006).

345. M. Pietroni, Nucl. Phys. **B402**, 27 (1993);
A. T. Davies, C. D. Froggatt, and R. G. Moorhouse, Phys. Lett. **B372**, 88 (1996);
S. J. Huber *et al.*, Nucl. Phys. **A785**, 206 (2007);
S. J. Huber *et al.*, Nucl. Phys. **B757**, 172 (2006);
A. Menon, D. E. Morrissey, and C. E. M. Wagner, Phys. Rev. **D70**, 035005 (2004).

346. B. A. Dobrescu, G. L. Landsberg, and K. T. Matchev, Phys. Rev. **D63**, 075003 (2001).
347. R. Dermisek and J. F. Gunion, Phys. Rev. Lett. **95**, 041801 (2005).
348. M. Carena *et al.*, JHEP **0804**, 092 (2008).
349. O. J. P. Eboli and D. Zeppenfeld, Phys. Lett. **B495**, 147 (2000);
H. Davoudiasl, T. Han, and H. E. Logan, Phys. Rev. **D71**, 115007 (2005).
350. L. Wang and X. -F. Han, Phys. Rev. **D87**, 015015 (2013);
K. Schmidt-Hoberg and F. Staub, JHEP **1210**, 195 (2012);
H. An, T. Liu, and L. -T. Wang, Phys. Rev. **D86**, 075030 (2012);
D. A. Vasquez *et al.*, Phys. Rev. **D86**, 035023 (2012);
S. F. King, M. Muhlleitner, and R. Nevzorov, Nucl. Phys. **B860**, 207 (2012).
351. P. Batra *et al.*, JHEP **0406**, 032 (2004);
A. Maloney, A. Pierce, and J. G. Wacker, JHEP **0606**, 034 (2006);
Y. Zhang *et al.*, Phys. Rev. **D78**, 011302 (2008);
C. W. Chiang *et al.*, Phys. Rev. **D81**, 015006 (2010);
A. D. Medina, N. R. Shah, and C. E. M. Wagner, Phys. Rev. **D80**, 015001 (2009);
M. Endo *et al.*, Phys. Rev. **D85**, 095006 (2012);
C. Cheung and H. L. Roberts, `arXiv:1207.0234 [hep-ph]` (2012).
352. R. Huo *et al.*, Phys. Rev. **D87**, 055011 (2013).
353. R. T. D'Agnolo, E. Kuflik, and M. Zanetti, JHEP **1303**, 043 (2013).
354. A. Azatov and J. Galloway, Int. J. Mod. Phys. **A28**, 1330004 (2013).
355. N. Craig and A. Katz, JHEP **1305**, 015 (2013).
356. T. -F. Feng *et al.*, Nucl. Phys. **B871**, 223 (2013).
357. A. D. Sakharov, Sov. Phys. JETP Lett. **5**, 24 (1967);
M. B. Gavela *et al.*, Nucl. Phys. **B430**, 382 (1994).
358. J. R. Ellis, J. S. Lee, and A. Pilaftsis, JHEP **0810**, 049 (2008);
Y. Li, S. Profumo, and M. Ramsey-Musolf, JHEP **1008**, 062 (2010);
M. Pospelov and A. Ritz, Ann. Phys. **318**, 119 (2005).
359. S. Dimopoulos and S. Thomas, Nucl. Phys. **B465**, 23, (1996);
S. Thomas, Int. J. Mod. Phys. **A13**, 2307 (1998).
360. M. S. Carena *et al.*, Nucl. Phys. **B586**, 92 (2000).
361. A. Pilaftsis, Phys. Rev. **D58**, 096010 (1998) and Phys. Lett. **B435**, 88 (1998);
K. S. Babu *et al.*, Phys. Rev. **D59**, 016004 (1999).
362. G.L. Kane and L.-T. Wang, Phys. Lett. **B488**, 383 (2000);
S.Y. Choi, M. Drees, and J.S. Lee, Phys. Lett. **B481**, 57 (2000);
S.Y. Choi and J.S. Lee, Phys. Rev. **D61**, 015003 (2000);
S.Y. Choi, K. Hagiwara, and J.S. Lee, Phys. Rev. **D64**, 032004 (2001) and Phys. Lett. **B529**, 212 (2002);
T. Ibrahim and P. Nath, Phys. Rev. **D63**, 035009 (2001);
T. Ibrahim, Phys. Rev. **D64**, 035009 (2001);
S. Heinemeyer, Eur. Phys. J. **C22**, 521 (2001);
S. W. Ham *et al.*, Phys. Rev. **D68**, 055003 (2003).

363. M. Frank *et al.*, JHEP **0702**, 047 (2007);
S. Heinemeyer *et al.*, Phys. Lett. **B652**, 300 (2007);
T. Hahn *et al.*, `arXiv:0710.4891` (2007).
364. D.A. Demir, Phys. Rev. **D60**, 055006 (1999);
S. Y. Choi, M. Drees, and J. S. Lee, Phys. Lett. **B481**, 57 (2000);
K. E. Williams, H. Rzehak, and G. Weiglein, Eur. Phys. J. **C71**, 1669 (2011).
365. E. Christova *et al.*, Nucl. Phys. **B639**, 263 (2002) [E: Nucl. Phys. **B647**, 359 (2002)].
366. S.L. Glashow and S. Weinberg, Phys. Rev. **D15**, 1958 (1977);
E.A. Paschos, Phys. Rev. **D15**, 1966 (1977);
H. Georgi, Hadronic J. **1,** 1227 (1978);
H. Haber, G Kane, and T Sterling, Nucl. Phys. **B161**, 493 (1979);
A. G. Akeroyd, Phys. Lett. **B368**, 89 (1996);
A.G. Akeroyd, Nucl. Phys. **B544**, 557 (1999);
A. G. Akeroyd, A. Arhrib, and E. Naimi, Eur. Phys. J. **C20**, 51 (2001).
367. N.G. Deshpande and E. Ma Phys. Rev. **D18**, 2574 (1978);
R. Barbieri, L.J. Hall, and V. Rychkov Phys. Rev. **D74**, 015007 (2006);
L. Lopez Honorez *et al.*, JCAP **0702**, 028 (2007);
E. Lundstrom, M. Gustafsson, and J. Edsjo, Phys. Rev. D **79**, 035013 (2009);
E. Dolle *et al.*, Phys. Rev. **D8**, 035003 (2010);
X. Miao, S. Su, and B. Thomas, Phys. Rev. **D82**, 035009 (2010);
L. Lopez-Honorez and C.Yaguna, JCAP **1101**, 002 (2011).
368. A. Arhrib, R. Benbrik, and N. Gaur, Phys. Rev. D **85**, 095021 (2012);
B. Swiezewska and M. Krawczyk, Phys. Rev. D **88**, 035019 (2013);
A. Goudelis, B. Herrmann, and O. Stoel, JHEP **1309**, 106 (2013).
369. V. Barger, H. E. Logan, and G. Shaughnessy, Phys. Rev. **D79**, 115018 (2009).
370. D. O'Connell, M. J. Ramsey-Musolf, and M. B. Wise, Phys. Rev. **D75**, 037701 (2007);
V. Barger *et al.*, Phys. Rev. **D77**, 035005 (2008);
V. Barger *et al.*, Phys. Rev. **D79**, 015018 (2009).
371. H.E. Haber, *Proceedings of the 1990 Theoretical Advanced Study Institute in Elementary Particle Physics,* edited by M. Cvetič and Paul Langacker (World Scientific, Singapore, 1991) pp. 340–475 and references therein.
372. S. Glashow and S. Weinberg, Phys. Rev. **D15**, 1958 (1977).
373. G. C. Branco, W. Grimus, and L. Lavoura, Phys. Lett. **B380**, 119 (1996);
F. J. Botella, G. C. Branco, M. N. Rebelo Phys. Lett. **B687**, 194 (2010).
374. N. Craig and S. Thomas, JHEP **1211**, 083 (2012).
375. G. C. Branco *et al.*, Phys. Reports **516**, 1 (2012).
376. C. -Y. Chen, S. Dawson, and M. Sher, Phys. Rev. **D88**, 015018 (2013).
377. B. Swiezewska and M. Krawczyk, Phys. Rev. **D88**, 035019 (2013).
378. N. Craig, J. Galloway, and S. Thomas, `arXiv:1305.2424 [hep-ph]` (2013).
379. J. Schechter and J. W. F. Valle, Phys. Rev. **D22**, 2227 (1980).
380. T. P. Cheng and L. -F. Li, Phys. Rev. **D22**, 2860 (1980).
381. H. Georgi and M. Machacek, Nucl. Phys. **B262**, 463 (1985).

382. M. S. Chanowitz and M. Golden, Phys. Lett. **B165**, 105 (1985).
383. J. F. Gunion, R. Vega, and J. Wudka, Phys. Rev. **D42**, 1673 (1990).
384. H. E. Logan and M. -A. Roy, Phys. Rev. **D82**, 115011 (2010).
385. H. E. Haber and H. E. Logan, Phys. Rev. **D62**, 015011 (2000).
386. A. G. Akeroyd, M. Aoki, and H. Sugiyama, Phys. Rev. **D77**, 075010 (2008).
387. P. Nath *et al.*, Nucl. Phys. (Proc. Supp.) **B200**, 185 (2010).
388. J. Garayoa and T. Schwetz, JHEP **0803**, 009 (2008).
389. J. F. Gunion, R. Vega, and J. Wudka, Phys. Rev. **D43**, 2322 (1991).
390. S. Kanemura and K. Yagyu, Phys. Rev. **D85**, 115009 (2012).
391. I. Low and J. Lykken, JHEP **1010**, 053 (2010).
392. C. Englert, E. Re, and M. Spannowsky, Phys. Rev. **D87**, 095014 (2013).
393. I. Low, J. Lykken, and G. Shaughnessy, Phys. Rev. **D86**, 093012 (2012).
394. A. Falkowski, S. Rychkov, and A. Urbano, JHEP **1204**, 073 (2012).
395. B. A. Dobrescu and J. D. Lykken, JHEP **1302**, 073 (2013).
396. D. Carmi *et al.*, JHEP **1210**, 196 (2012).
397. C. -W. Chiang and K. Yagyu, JHEP **1301**, 026 (2013).
398. G. Belanger *et al.*, Phys. Rev. **D88**, 075008 (2013).
399. C. Englert, E. Re, and M. Spannowsky, Phys. Rev. **D88**, 035024 (2013).
400. N. Arkani-Hamed *et al.*, JHEP **0207**, 034 (2002).
401. N. Arkani-Hamed, A. G. Cohen, and H. Georgi, Phys. Lett. **B513**, 232 (2001).
402. N. Arkani-Hamed *et al.*, JHEP **0208**, 021 (2002).
403. M. Schmaltz, JHEP **0408**, 056 (2004).
404. M. Schmaltz, D. Stolarski, and J. Thaler, JHEP **1009**, 018 (2010).
405. M. Perelstein, Prog. in Part. Nucl. Phys. **58**, 247 (2007).
406. M. Schmaltz and D. Tucker-Smith, Ann. Rev. Nucl. and Part. Sci. **55**, 229 (2005).
407. J. A. Casas, J. R. Espinosa, and I. Hidalgo, JHEP **0503**, 038 (2005).
408. H. -C. Cheng and I. Low, JHEP **0309**, 051 (2003).
409. M. S. Carena *et al.*, Phys. Rev. **D75**, 091701 (2007).
410. ATLAS Collab., ATLAS-CONF-2012-147, ATLAS-CONF-2012-109 and ATLAS-CONF-2013-024;
    CMS Collab., CMS-PAS-EXO-12-048 and CMS-SUS-12-028.
411. CMS Collab., CMS-PAS-B2G-12-015;
    ATLAS Collab., ATLAS-CONF-2013-060.
412. R. S. Chivukula, M. Narain, and J. Womersley, *Dynamical Electroweak Symmetry Breaking*, in this volume.
413. H. Georgi, A. E. Nelson, and A. Manohar, Phys. Lett. **B126**, 169 (1983);
    A. E. Nelson and M. J. Strassler, JHEP **0009**, 030 (2000);
    S. Davidson, G. Isidori, and S. Uhlig, Phys. Lett. **B663**, 73 (2008).
414. C. Csaki, A. Falkowski, and A. Weiler, JHEP **0809**, 008 (2008);
    B. Keren-Zur *et al.*, Nucl. Phys. **B867**, 429 (2013).
415. K. Agashe, R. Contino, and A. Pomarol, Nucl. Phys. **B719**, 165 (2005).
416. O. Matsedonskyi, G. Panico, and A. Wulzer, JHEP **1301**, 164 (2013);
    M. Redi and A. Tesi, JHEP **1210**, 166 (2012);

D. Marzocca, M. Serone, and J. Shu, JHEP **1208**, 013 (2012);
A. Pomarol and F. Riva, JHEP **1208**, 135 (2012).
417. R. Contino and G. Servant, JHEP **0806**, 026 (2008);
J. Mrazek and A. Wulzer, Phys. Rev. **D81**, 075006 (2010).
418. A. De Simone *et al.*, JHEP **1304**, 004 (2013) A. Azatov *et al.*, `arXiv:1308.6601 [hep-ph]` (2013).
419. A. Falkowski, Phys. Rev. **D77**, 055018 (2008);
I. Low and A. Vichi, Phys. Rev. **D84**, 045019 (2011);
A. Azatov and J. Galloway, Phys. Rev. **D85**, 055013 (2012);
C. Delaunay, C. Grojean, and G. Perez, JHEP **1309**, 090 (2013).
420. R.K. Ellis *et al.*, Nucl. Phys. **B297**, 221 (1988);
U. Baur and E.W.N. Glover, Nucl. Phys. **B339**, 38 (1990);
O. Brein and W. Hollik, Phys. Rev. **D68**, 095006 (2003);
U. Langenegger *et al.*, JHEP **0606**, 035 (2006).
421. M. Grazzini and H. Sargsyan, JHEP **1309**, 129 (2013).
422. A. Banfi, A. Martin, and V. Sanz, `arXiv:1308.4771 [hep-ph]` (2013);
A. Azatov and A. Paul, `arXiv:1309.5273 [hep-ph]` (2013);
C. Grojean *et al.*, `arXiv:1312.3317 [hep-ph]` (2013).
423. R. Contino, L. Da Rold, and A. Pomarol, Phys. Rev. **D75**, 055014 (2007).
424. D. Pappadopulo, A. Thamm, and R. Torre, JHEP **1307**, 058 (2013);
M. Montull *et al.*, `arXiv:1308.0559 [hep-ph]` (2013).
425. I. Low, R. Rattazzi, and A. Vichi, JHEP **1004**, 126 (2010).
426. M. Ciuchini *et al.*, JHEP **1308**, 106 (2013).
427. C. Grojean, O. Matsedonskyi, and G. Panico, `arXiv:1306.4655 [hep-ph]` (2013).
428. B. Bellazzini *et al.*, `arXiv:1305.3919 [hep-th]` (2013);
F. Coradeschi *et al.*, JHEP **1311**, 057 (2013).
429. M. Carena, S. Heinemeyer, G. Weiglein, and C. Wagner, private communication.
430. ATLAS Collab., ATLAS-CONF-2013-027 (2013).
431. CMS Collab., CMS-PAS-HIG-13-016 (2013).
432. ATLAS Collab., ATLAS-CONF-2012-013 (2012).
433. CMS Collab., CMS-PAS-HIG-12-002 (2012).
434. CMS Collab., CMS-HIG-12-013 (2013), CERN-PH-EP/2013-011.
435. ALEPH Collab., Phys. Lett. **B526**, 191 (2002).
436. L3 Collab., Phys. Lett. **B545**, 30 (2002).
437. S. Schael *et al.*, [ALEPH, DELPHI, L3 and OPAL Collaborationsand LEP Working Group for Higgs Boson Searches], Eur. Phys. J. **C47**, 547 (2006).
438. OPAL Collab., Eur. Phys. J. **C23**, 397 (2002).
439. DELPHI Collab., Eur. Phys. J. **C38**, 1 (2004).
440. M. M. Kado and C. G. Tully, Ann. Rev. Nucl. and Part. Sci. **52**, 65 (2002).
441. V.M. Abazov *et al.*, [D0 Collab.], Phys. Lett. **B698**, 97 (2011).
442. T. Aaltonen *et al.*, [CDF Collab.], Phys. Rev. **D85**, 032005 (2012).
443. V.M. Abazov *et al.*, [D0 Collab.], Phys. Rev. Lett. **104**, 151801 (2010).
444. D0 Collab., D0 Note 5974-CONF (2011).

445. ATLAS Collab., ATLAS-CONF-2012-094 (2012).
446. CMS Collab., CMS-PAS-HIG-13-021 (2013).
447. RAaij *et al.*, [LHCb Collab.], JHEP **1305**, 132 (2013).
448. S. Chatrchyan *et al.*, [CMS Collab.], Phys. Lett. **B722**, 207 (2013).
449. B. Abbott *et al.*, [D0 Collab.], Phys. Rev. Lett. **82**, 4975 (1999).
450. A. Abulencia *et al.*, [CDF Collab.], Phys. Rev. Lett. **96**, 042003 (2006).
451. V.M. Abazov *et al.*, [D0 Collab.], Phys. Lett. **B682**, 278 (2009).
452. ATLAS Collab., JHEP **1206**, 039 (2012).
453. ATLAS Collab., ATLAS-CONF-2012-090 (2013).
454. CMS Collab., CMS-PAS-HIG-11-019.
455. S. Chatrchyan *et al.*, [CMS Collab.], JHEP **1207**, 143 (2012).
456. ATLAS Collab., ATLAS-CONF-2011-094 (2011).
457. J. Abdallah *et al.*, [DELPHI Collab.], Eur. Phys. J. **C54**, 1 (2008) [E: **C56**, 165 (2008)].
458. V. M. Abazov *et al.*, [D0 Collab.], Phys. Rev. Lett. **103**, 061801 (2009).
459. R. Dermisek, Mod. Phys. Lett. **A24**, 1631 (2009).
460. J. F. Gunion, JHEP **0908**, 032 (2009).
461. U. Ellwanger, Eur. Phys. J. **C71**, 1782 (2011).
462. W. Love *et al.*, [CLEO Collab.], Phys. Rev. Lett. **101**, 151802 (2008).
463. B. Aubert *et al.*, [BaBar Collab.], Phys. Rev. Lett. **103**, 081803 (2009).
464. B. Aubert *et al.*, [BaBar Collab.], Phys. Rev. Lett. **103**, 181801 (2009).
465. V. M. Abazov *et al.*, [D0 Collab.], Phys. Rev. Lett. **103**, 061801 (2009).
466. ATLAS Collab., ATLAS-CONF-2011-020 (2011).
467. S. Chatrchyan *et al.*, [CMS Collab.], Phys. Rev. Lett. **109**, 121801 (2012).
468. ATLAS Collab., ATLAS-CONF-2011-020 (2011).
469. CMS Collab., CMS-PAS-HIG-13-010 (2013).
470. S. Schael *et al.*, [ALEPH Collab.], JHEP **1005**, 049 (2010).
471. ATLAS Collab., ATLAS-CONF-2013-013 (2013).
472. S. Chatrchyan *et al.*, [CMS Collab.], Eur. Phys. J. **C73**, 2469 (2013).
473. ATLAS Collab., ATLAS-CONF-2012-016 (2012).
474. CMS Collab., CMS-PAS-HIG-13-014 (2013).
475. ATLAS Collab., ATLAS-CONF-2012-017 (2012).
476. ATLAS Collab., ATLAS-CONF-2012-163 (2012).
477. CMS Collab., CMS-PAS-HIG-12-024 (2012).
478. ATLAS Collab., ATLAS-CONF-2013-067 (2013).
479. ATLAS Collab., ATLAS-CONF-2012-018 (2012).
480. CMS Collab., CMS-PAS-HIG-13-008 (2013).
481. CMS Collab., CMS-PAS-HIG-12-046 (2012).
482. ATLAS Collab., ATLAS-CONF-2012-010 (2012).
483. G. Aad *et al.*, [ATLAS Collab.], Eur. Phys. J. **C72**, 2244 (2012).
484. S. Chatrchyan *et al.*, [CMS Collab.], Eur. Phys. J. **C72**, 2189 (2012).
485. ATLAS Collab., CERN-PH-EP-2013-172 (2013).
486. ATLAS Collab., ATLAS-CONF-2013-081 (2013).